NUWC-NPT Technical Report 10,199
25 November 1992

Forced Harmonic Vibration of the Generally Orthotropic Cylindrical Shell With Inner and Outer Fluid Loading

Mark S. Peloquin
Submarine Sonar Department

Naval Undersea Warfare Center Detachment
New London, Connecticut

PREFACE

The research presented in this report was prepared under the *Acoustic Array Technology Project* as part of the Submarine/Surface Ship USW Surveillance Program sponsored by the Antisubmarine Warfare/Undersea Technology Directorate of the Office of Naval Technology: Program Element 0602314N; ONT Block Program UN3B; Project No. RJ14R3; NUWC Job Order No. A60010; NUWC Principal Investigator, D. A. Hurdis (Code 2141); Program Director, G. C. Connolly (Code 2192). The sponsoring activity's Technology Area Manager for Undersea Target Surveillance is T. G. Goldsberry (ONT 231).

The technical reviewer for this report was Andrew Hull (Code 2141).

REVIEWED AND APPROVED: 25 November 1992

F. V. Kingsbury

F. J. Kingsbury
Head, Submarine Sonar Department

REPORT DOCUMENTATION PAGE

Form Approved
OMB No. 0704-0188

1. AGENCY USE ONLY (Leave blank)	2. REPORT DATE	3. REPORT TYPE AND DATES COVERED
	25 November 1992	Progress

4. TITLE AND SUBTITLE

Forced Harmonic Vibration of the Generally Orthotropic Cylindrical Shell With Inner and Outer Fluid Loading

5. FUNDING NUMBERS

PE 0602314N
PR RJ14R3

6. AUTHOR(S)

Mark S. Peloquin

7. PERFORMING ORGANIZATION NAME(S) AND ADDRESS(ES)

Naval Undersea Warfare Center
Detachment New London
New London, CT 06320

8. PERFORMING ORGANIZATION REPORT NUMBER

TR 10,199

9. SPONSORING/MONITORING AGENCY NAME(S) AND ADDRESS(ES)

Office of Naval Technology
Arlington, VA 22217-5000

10. SPONSORING/MONITORING AGENCY REPORT NUMBER

11. SUPPLEMENTARY NOTES

12a. DISTRIBUTION/AVAILABILITY STATEMENT

Approved for public release; distribution is unlimited.

12b. DISTRIBUTION CODE

13. ABSTRACT *(Maximum 200 words)*

This report describes a modeled system comprised of an infinite shell with both inner and outer fluids subject to forced harmonic vibration in the longitudinal (x) and circumferential (θ) directions. Two excitations are applied to the outer shell surface: normal pressure, P_o, and longitudinal shear stress, P_x. The equations of motion are derived, from first principles, for an elastic shell, including a full treatment of bending and rotatory inertia. The fluids are treated as linearly elastic, inviscid media and are subject to the wave equation in three dimensions. The stress-strain relationship for the shell is formulated to enable the treatment of isotropic, specially orthotropic, and generally orthotropic composite materials undergoing plane stress.

Two solutions are presented for the equations of motion. The first is a harmonic standing wave in θ and a traveling wave in x, and the second is a

14. SUBJECT TERMS

Anisotropic
Closed Form Solution
Cylindrical Shell
Harmonic
Mode of Propagation
Orthotropic
Structural Damping
Wave Motion
Wavenumber

15. NUMBER OF PAGES

144

16. PRICE CODE

17. SECURITY CLASSIFICATION OF REPORT	18. SECURITY CLASSIFICATION OF THIS PAGE	19. SECURITY CLASSIFICATION OF ABSTRACT	20. LIMITATION OF ABSTRACT
UNCLASSIFIED	UNCLASSIFIED	UNCLASSIFIED	SAR

13. ABSTRACT (Cont'd)

harmonic traveling wave in θ and x. Modes of propagation are designated by mode number, n, which defines the number of wavelengths around the circumference of the shell. Each mode of propagation consists of components from the radial, longitudinal, and circumferential (w,u,v) degrees of freedom in the shell. Although the system is capable of supporting an infinite number of modes of propagation, only the first four (beginning with n = 0) are analyzed here.

A three-dimensional rendering of the mode shapes provides an understanding of the deformed shape of the shell. The closed form solution for the magnitude of the response is then evaluated for three specific shells in the wavenumber-frequency plane. Results are presented in the form of transfer surfaces (i.e., magnitude as a function of wavenumber and frequency for a particular mode number) for the following cases:

- Interior fluid pressure at radial position r normalized by excitation pressure P_o,
- Strain in the shell wall at position z in the wall normalized by excitation pressure P_o, and
- Interior fluid pressure at radial position r normalized by excitation stress P_x.

These transfer surfaces, displayed as grey scale images, illustrate the dispersion, as well as cutoff frequency, group velocity, and phase velocity, of the branches for each mode of propagation.

The problem of the compliant core that partially fills the cross section is solved for the n = 0 mode, and these results are also presented in the form of transfer surfaces.

TABLE OF CONTENTS

TABLE OF CONTENTS (Cont'd)

TABLE OF CONTENTS (Cont'd)

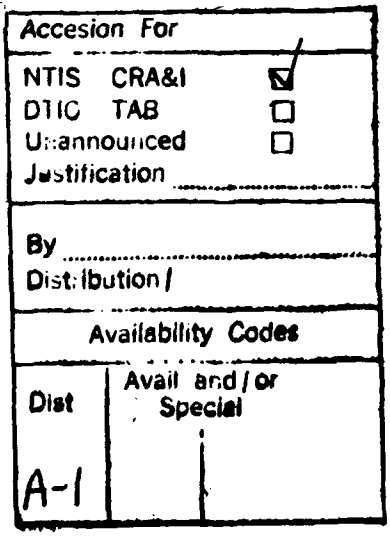

LIST OF ILLUSTRATIONS

LIST OF ILLUSTRATIONS (Cont'd)

LIST OF ILLUSTRATIONS (Cont'd)

LIST OF ILLUSTRATIONS (Cont'd)

LIST OF ILLUSTRATIONS (Cont'd)

NOMENCLATURE

Shell

A = Total cross-sectional area of the shell
A_m = Cross-sectional area of the matrix material
A_f = Cross-sectional area of the reinforcing fiber
a = Mean radius
a_i = Inner radius
a_o = Outer radius
c_l = Extensional wave speed
r = Radial coordinate
x = Axial coordinate
θ = Angular coordinate
E = Young's modulus for an isotropic shell
E_m = Young's modulus of the matrix material
E_f = Young's modulus of the reinforcing fiber
E_1 = Composite Young's modulus, 1 direction
E_2 = Composite Young's modulus, 2 direction
ζ = Structural loss factor
ζ_m = Structural loss factor for the matrix material
ζ_f = Structural loss factor for the reinforcing fiber
ϕ = Reinforcement wrap angle relative to the longitudinal x-axis
ψ = Angular coordinate for strain or displacement calculated in the shell wall relative to the longitudinal x-axis of the shell
φ = Angle formed by the curvature of the shell in the r, x plane
G_{12} = Composite shear modulus
ν = Isotropic Poisson ratio
ν_m = Poisson ratio of the matrix material
ν_f = Poisson ratio of the reinforcing fiber
ν_{12} = Poisson ratio (strain in the 2 direction when stressed in the 1 direction)
ν_{21} = Poisson ratio (strain in the 1 direction when stressed in the 2 direction)
h = Shell thickness
I_x = Mass moment of inertia about the x-axis
I_θ = Mass moment of inertia about the θ-axis
k_a = Fiber misalignment factor
ρ = Shell density
m = Mass of the shell element
n = Number of wavelengths around the circumference
N_{ij} = Shell forces
σ_{ij} = Stress components
ε_{ij} = Strain components
ε_{ij} = $(i \neq j)$ Represents tensor shear strain
γ_{ij} = $(i \neq j)$ Represents engineering shear strain
T = Static tension per unit length of circumference
u,v,w = Displacement of a point in the middle surface of the shell in the axial, tangential, and radial directions (field quantity)
U,V,W = Components of the amplitude of shell motion in the axial, tangential, and radial directions

Fluid

β = Bulk modulus
c_f = Speed of sound in a fluid
c_i = Speed of sound in the inner fluid
c_o = Speed of sound in the outer fluid
$\dot{w}_s$ = Particle velocity in the outer fluid due to the structure-induced pressure field
$\dot{w}_f$ = General fluid particle velocity
$\dot{w}_i$ = Inner fluid particle velocity
ρ_f = General fluid density
ρ_i = Inner fluid density
ρ_o = Outer fluid density
k_r = Radial wavenumber
φ_f = General fluid velocity potential
φ_i = Inner fluid velocity potential
φ_s = Outer fluid velocity potential
p_o = Normal pressure excitation field
p_x = Axial shear stress excitation field
p_θ = Circumferential shear stress excitation field
P_o = Amplitude of the normal pressure field
P_x = Amplitude of the axial shear stress field
p_i = Internal fluid pressure field
p_s = External fluid pressure field
λ_f = Lame constant
μ_f = Lame constant (shear modulus)
J_n = Bessel function of the first kind
Y_n = Bessel function of the first kind
I_n = Modified Bessel function
H_n^1 = Hankel function of the first kind
K_n = Modified Hankel function
p = Pressure field for a general fluid
τ_{ij} = Stress tensor for the fluid
ε_{kk} = Strain tensor for the fluid
δ_{ij} = Kronecker delta
$D, \bar{E}, G, H, M$ = Fluid velocity potential field constants

NOMENCLATURE

Shell & Fluid

c	=	Wave speed
c_b	=	Breathing wave speed
ω	=	Angular frequency
t	=	Time
k	=	Axial wavenumber ($2\pi/L$)
L	=	Axial wavelength
i	=	$\sqrt{-1}$
T_r	=	Transfer function with respect to radial excitation
T_x	=	Transfer function with respect to axial excitation

Core

σ_r	=	Stress in the radial direction
σ_θ	=	Stress in the circumferential direction
ε_r	=	Strain in the radial direction
ε_θ	=	Strain in the circumferential direction
ν_c	=	Poisson ratio
λ_c	=	Lame constant
E_c	=	Young's modulus
u_c	=	Radial displacement
$\dot{u}_c$	=	Radial velocity
r_c	=	Core radius

FORCED HARMONIC VIBRATION OF THE GENERALLY ORTHOTROPIC CYLINDRICAL SHELL WITH INNER AND OUTER FLUID LOADING

INTRODUCTION

The analysis of wave propagation in the system comprised of an infinite elastic cylindrical shell with both inner and outer fluids has a history dating back to the beginning of the 19th century. Thomas Young[1] (after whom Young's modulus is named) derived the first expression for the phase velocity of long wavelength pressure pulses propagating in the fluid contained within the elastic shell. Korteweg (as described by Skalak[2]) and Lamb[3] followed with similar analyses as efforts were made to understand the circulatory system of the human body and, in particular, pressure pulse propagation in blood flow.

The phase velocity, c_b (given in this report by equation (72)) is often referred to as the Moens-Korteweg velocity. This early work was concerned with what we term the w component of the circumferential ($n = 0$) mode of propagation. These first analyses considered only the axisymmetric excitation and response of the shell/fluid system.

Warburton[4] derived the response of the isotropic shell with a limited consideration of bending for axisymmetric and nonaxisymmetric excitation. He solved for the resonant frequencies and wavenumbers for varying shell thickness-to-radius ratios and for various circumferential mode numbers. Additionally, the isotropic shell/fluid system has been studied by Gazis[5] and Greenspon.[6]

In this work, we are interested in the axisymmetric and nonaxisymmetric response of the shell that is "generally orthotropic," which means that the principal material directions are not aligned to the shell axes. Within the plane stress case considered here, the shell is also anisotropic. Thus, in this study, generally orthotropic and anisotropic descriptions of the material are the same. The spirally wrapped composite tubes widely used in commercial products are examples of generally orthotropic shells.

The shell is treated within the assumptions of plane stress, where the stress in the r direction is assumed negligible. A full treatment of bending, transverse shear, and rotatory inertia is addressed in the shell development. In the formulation of the stress resultants, the varying circumferential length of the hoop fibers is retained. Fluid loads are calculated at the inner and outer shell radii rather than at the middle surface. Every attempt has been made to retain all the physics that are possible within the scope of shell theory to keep the solutions valid for as large a value of thickness-to-radius ratio as possible.

The solutions for the displacements of the middle surface of the shell allow for the calculation of the pressure fields in the inner and outer fluids as well as the stresses and strains in the shell wall.

THE PHYSICAL MODEL

The model derived for the dynamic response of the system to harmonic excitation in both time and space will consist of an elastic cylinder that is expressed as a membrane or bending shell of infinite length, which contains an inner fluid and is immersed in an outer fluid.

Three forcing functions are applied to the cylinder: p_o, p_x, and p_θ. These forcing functions exist as pressure fields in the outer fluid. As the surface of the cylinder is set into motion by the forcing functions, pressure fields p_i and p_s are generated in the inner and outer fluids, respectively.

In the formulation of the structure-induced pressure fields p_i and p_s, the fluids will be modeled as compressible, inviscid media that will not support a shear stress. Since p_x and p_θ can only be imparted to the cylinder by a real fluid with nonzero viscosity, this approach will define them as given harmonic functions at the outset.

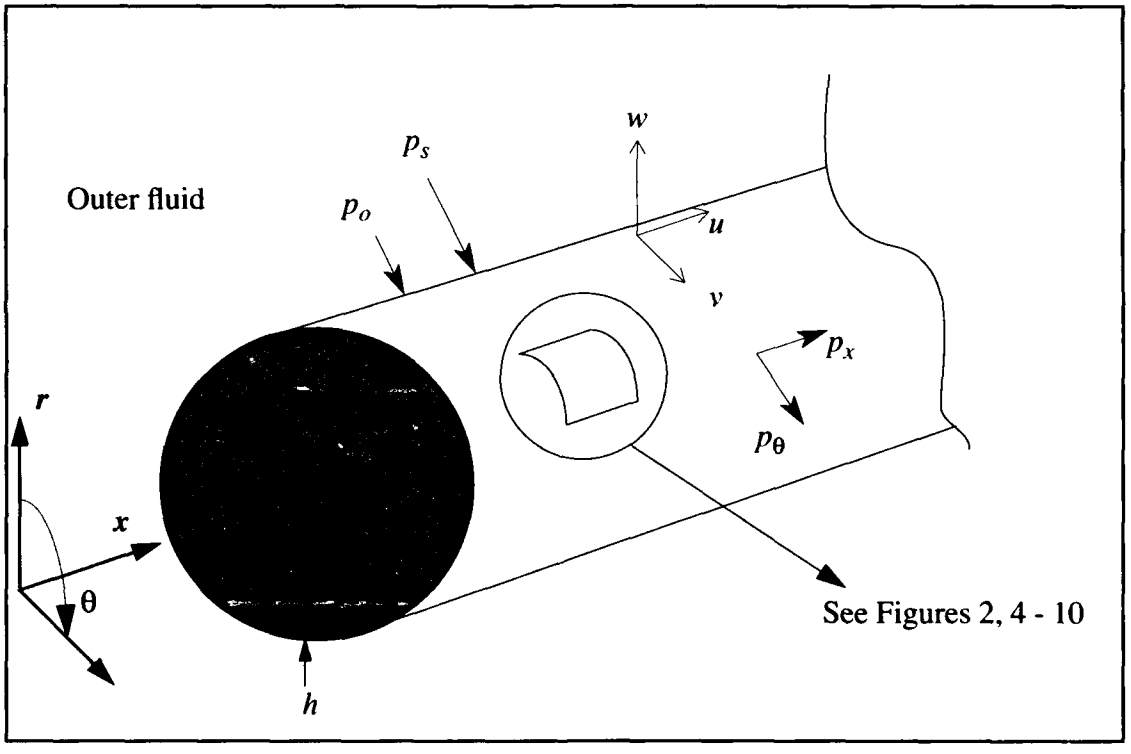

Figure 1. Physical Model Diagram

First, we desire to know the deformation of an arbitrary point of the cylinder having coordinates x, θ and distance z from the middle surface. However, this solution requires an answer to the three-dimensional elasticity problem. The elasticity problem can become the simpler shell problem if simple kinematic relationships are established between an arbitrary point in the shell and the corresponding point on the middle surface with the same x, θ coordinates. When progressing from full elasticity to the shell equations, we are simplifying the elastic behavior in the radial direction. The following assumptions are used in deriving the kinematic relationships:[7]

1. All points lying on one normal to the middle surface before deformation will remain the same after deformation.

2. For all kinematic relations, the distance z of a point from the middle surface may be considered as unaffected by the deformation of the shell.

3. The stress, σ_{rr}, in the r direction may be considered negligible compared with the longitudinal stress, σ_{xx}, and the circumferential stress, $\sigma_{\theta\theta}$.

4. All displacements are small (negligible compared with the radii of curvature of the middle surface), and their first derivatives (the slopes) are small compared with unity.

With the assumptions stated above, we have simplified the elasticity problem to a consideration of the eight stress resultants shown in equation (1).

$$
\begin{aligned}
N_{xx} &= \int_{-\frac{h}{2}}^{\frac{h}{2}} \sigma_{xx}\left(1+\frac{z}{a}\right) dz, \\
N_{x\theta} &= \int_{-\frac{h}{2}}^{\frac{h}{2}} \sigma_{x\theta}\left(1+\frac{z}{a}\right) dz, \\
M_{xx} &= -\int_{-\frac{h}{2}}^{\frac{h}{2}} \sigma_{xx}\left(1+\frac{z}{a}\right) z dz, \\
M_{x\theta} &= -\int_{-\frac{h}{2}}^{\frac{h}{2}} \sigma_{x\theta}\left(1+\frac{z}{a}\right) z dz, \\
N_{\theta\theta} &= \int_{-\frac{h}{2}}^{\frac{h}{2}} \sigma_{\theta\theta} dz, \\
N_{\theta x} &= \int_{-\frac{h}{2}}^{\frac{h}{2}} \sigma_{\theta x} dz, \\
M_{\theta\theta} &= -\int_{-\frac{h}{2}}^{\frac{h}{2}} \sigma_{\theta\theta} z dz, \\
M_{\theta x} &= -\int_{-\frac{h}{2}}^{\frac{h}{2}} \sigma_{\theta x} z dz \, .
\end{aligned}
\tag{1}
$$

BENDING SHELL

From the shell element depicted in figure 2, the stress resultants (both the force and moments) are derived in equation (1) on a per-unit length basis.

Bending stresses arise when the normal and shear stresses are not distributed uniformly across the shell thickness, h. When this condition occurs, a moment results about the middle surface of the shell. The $1 + z/a$ term in the stress resultants reflects the fact that hoop fibers of different radii have various lengths. Accounting for a shell cross section that is trapezoidal in shape causes $N_{x\theta} \neq N_{\theta x}$ and $M_{x\theta} \neq M_{\theta x}$ in this development. The stress tensor is unchanged and is, as usual, symmetric.

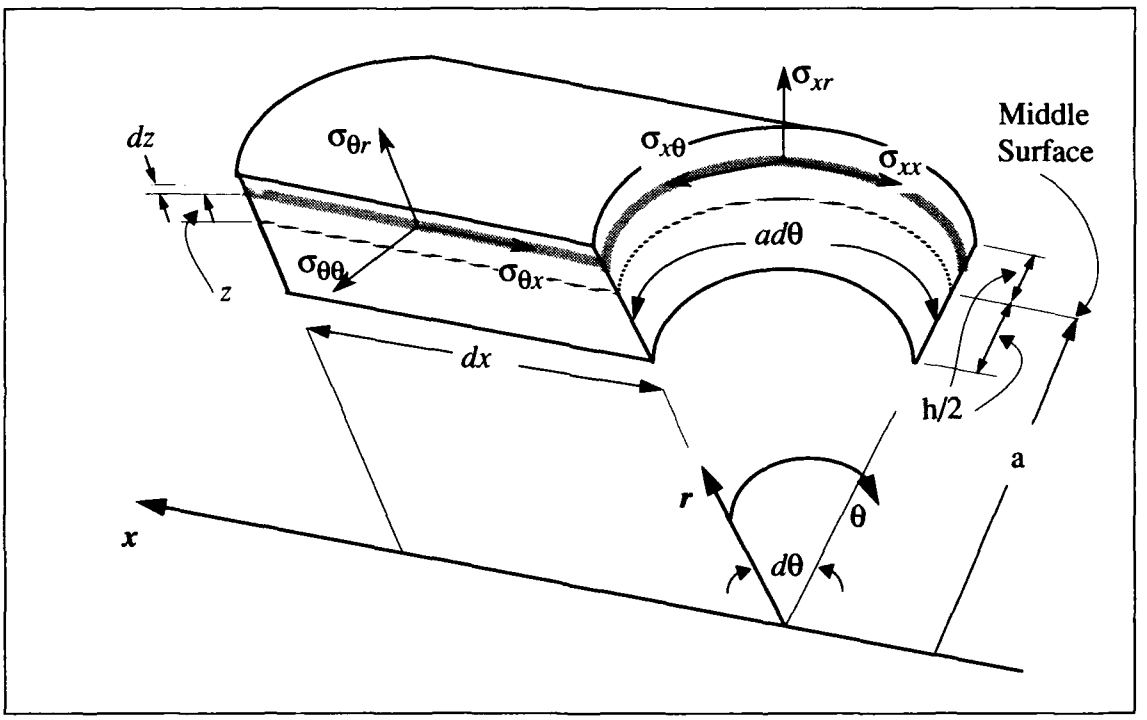

Figure 2. Stress-Resultant Free Body Diagram (FBD)

MEMBRANE SHELL

When we choose to neglect bending and twisting moments, the shell is referred to as a membrane. The membrane forces at a point in the shell represent a state of plane stress in a tangent plane to the middle surface.[8] Three stress resultants remain from equation (1): N_{xx}, $N_{\theta\theta}$, and $N_{x\theta}$. In the membrane case, we find $N_{x\theta} = N_{\theta x}$ due to the requirement that the stress resultants lie in the plane of the middle surface. The trapezoidal shape of the cross section is neglected, which means that the z/a term is dropped from equation (1). When this is done, it is clearly seen that $N_{\theta x} = N_{x\theta}$. Equation (2) gives the relationship between the actual stress and the N_{ij} for the membrane shell:

$$\sigma_{ij} = \frac{N_{ij}}{h} . \tag{2}$$

STRESS-STRAIN RELATIONS

A shell without reinforcement is by definition homogeneous and isotropic. Such a material has the simplest stress-strain relationship and can be defined by two material property constants. Often an axial reinforcement is embedded in the shell to provide an increase in strength. When the principal material directions are aligned with the axes of the structure, the material is termed "specially orthotropic." A specially orthotropic composite obeys the second simplest constitutive law, and four independent material constants are required. In the specially orthotropic case, the normal stresses do not depend on the shear strain as we can be observe by inspecting the Q matrix in equation (3) and noting the location of the zeros. If the principal material directions are not aligned with the coordinate axes of the structure, we would then have a fully populated Q matrix. Such a case would be represented by a spirally wound reinforcement. This situation, where the principal material property axes are not aligned with the coordinate axes of the shell (figure 3), results in the "generally orthotropic" lamina.

MEMBRANE SHELL

Specially Orthotropic

Equation (3) gives the desired relation between stress and strain for the specially orthotropic case of plain stress:[9]

$$\begin{bmatrix} \sigma_{xx} \\ \sigma_{\theta\theta} \\ \sigma_{x\theta} \end{bmatrix} = \begin{bmatrix} Q_{11} & Q_{12} & 0 \\ Q_{12} & Q_{22} & 0 \\ 0 & 0 & Q_{66} \end{bmatrix} \begin{bmatrix} \varepsilon_{xx} \\ \varepsilon_{\theta\theta} \\ \gamma_{x\theta} \end{bmatrix}. \tag{3}$$

Using equation (2) and noting that $C_{ij} = hQ_{ij}$, we rewrite equation (3) in the following form:

$$\begin{bmatrix} N_{xx} \\ N_{\theta\theta} \\ N_{x\theta} \end{bmatrix} = \begin{bmatrix} C_{11} & C_{12} & 0 \\ C_{12} & C_{22} & 0 \\ 0 & 0 & C_{66} \end{bmatrix} \begin{bmatrix} \varepsilon_{xx} \\ \varepsilon_{\theta\theta} \\ \gamma_{x\theta} \end{bmatrix},$$

$$C_{11} = \frac{hE_1}{1-\nu_{12}\nu_{21}}, \quad C_{22} = \frac{hE_2}{1-\nu_{12}\nu_{21}}, \quad C_{12} = \frac{h\nu_{12}E_2}{1-\nu_{12}\nu_{21}}, \quad C_{66} = hG_{12}. \tag{4}$$

Isotropic

Equation (3) will collapse to the isotropic result when we set $\nu_{12} = \nu_{21} = \nu$ and $E_1 = E_2 = E$:

$$\begin{bmatrix} \sigma_{xx} \\ \sigma_{\theta\theta} \\ \sigma_{x\theta} \end{bmatrix} = \begin{bmatrix} \frac{E}{1-\nu^2} & \frac{\nu E}{1-\nu^2} & 0 \\ \frac{\nu E}{1-\nu^2} & \frac{E}{1-\nu^2} & 0 \\ 0 & 0 & \frac{E}{2(1+\nu)} \end{bmatrix} \begin{bmatrix} \varepsilon_{xx} \\ \varepsilon_{\theta\theta} \\ \gamma_{x\theta} \end{bmatrix}. \tag{5}$$

A connection between strain and displacement is required within the shell. Flugge[10] provides a detailed development of the strain displacement relations, which are

$$\varepsilon_{xx} = \frac{\partial u}{\partial x}, \qquad \varepsilon_{\theta\theta} = \frac{1}{a}\left(\frac{\partial v}{\partial \theta} + w\right), \qquad \gamma_{x\theta} = \frac{\partial v}{\partial x} + \frac{1}{a}\frac{\partial u}{\partial \theta}. \tag{6}$$

Caution should be exercised when we work with the tensor representation of shear strain. There is a difference between engineering shear strain and tensor shear strain, where $\gamma_{ij} = 2\varepsilon_{ij}$. The use of one over the other will change the terms in the stiffness matrix Q. The values of the indices (i.e., 11, 12, 16, 26, and 66) relate to the position in the full 6,6 tensor representation.

Generally Orthotropic

The stress-strain relations for the generally orthotropic lamina are obtained by rotating the stresses from the specially orthotropic case through the angle, ϕ. The resulting relations are given by equation (7)[11] as

$$\begin{bmatrix} \sigma_{xx} \\ \sigma_{\theta\theta} \\ \sigma_{x\theta} \end{bmatrix} = \begin{bmatrix} \bar{Q}_{11} & \bar{Q}_{12} & \bar{Q}_{16} \\ \bar{Q}_{12} & \bar{Q}_{22} & \bar{Q}_{26} \\ \bar{Q}_{16} & \bar{Q}_{26} & \bar{Q}_{66} \end{bmatrix} \begin{bmatrix} \varepsilon_{xx} \\ \varepsilon_{\theta\theta} \\ \gamma_{x\theta} \end{bmatrix}. \tag{7}$$

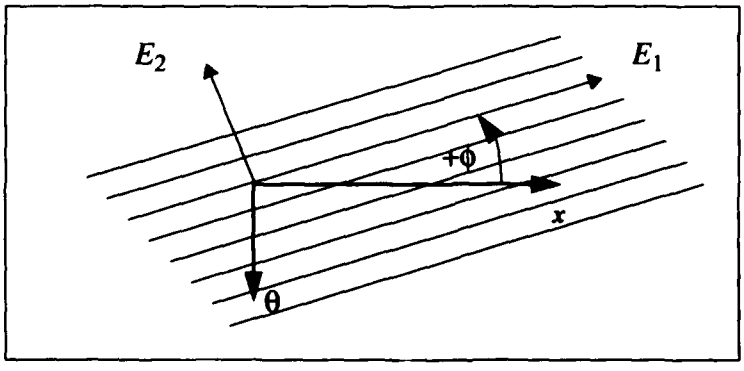

Figure 3. Material Property Versus Shell Coordinate System

In equation (7), the bar over the $\bar{Q}_{ij}$ indicates transformed stiffnesses, given below as

$$\bar{Q}_{11} = Q_{11}\cos^4\phi + 2(Q_{12} + 2Q_{66})\sin^2\phi\cos^2\phi + Q_{22}\sin^4\phi,$$

$$\bar{Q}_{12} = (Q_{11} + Q_{22} - 4Q_{66})\sin^2\phi\cos^2\phi + Q_{12}(\sin^4\phi + \cos^4\phi),$$

$$\bar{Q}_{22} = Q_{11}\sin^4\phi + 2(Q_{12} + 2Q_{66})\sin^2\phi\cos^2\phi + Q_{22}\cos^4\phi,$$

$$\bar{Q}_{16} = (Q_{11} - Q_{12} - 2Q_{66})\sin\phi\cos^3\phi + (Q_{12} - Q_{22} + 2Q_{66})\sin^3\phi\cos\phi,$$

$$\bar{Q}_{26} = (Q_{11} - Q_{12} - 2Q_{66})\sin^3\phi\cos\phi + (Q_{12} - Q_{22} + 2Q_{66})\sin\phi\cos^3\phi,$$

$$\bar{Q}_{66} = (Q_{11} + Q_{22} - 2Q_{12} - 2Q_{66})\sin^2\phi\cos^2\phi + Q_{66}(\sin^4\phi + \cos^4\phi),$$

$$Q_{11} = \frac{E_1}{1 - \nu_{12}\nu_{21}}, \qquad Q_{22} = \frac{E_2}{1 - \nu_{12}\nu_{21}}, \qquad Q_{12} = \frac{\nu_{12}E_2}{1 - \nu_{12}\nu_{21}},$$

$$Q_{66} = G_{12}, \qquad \frac{\nu_{12}}{E_1} = \frac{\nu_{21}}{E_2}. \tag{8}$$

From equation (2) for the membrane shell, we write equation (7) in the following form noting that $\bar{C}_{ij} = h\bar{Q}_{ij}$:

$$\begin{bmatrix} N_{xx} \\ N_{\theta\theta} \\ N_{x\theta} \end{bmatrix} = \begin{bmatrix} \bar{C}_{11} & \bar{C}_{12} & \bar{C}_{16} \\ \bar{C}_{12} & \bar{C}_{22} & \bar{C}_{26} \\ \bar{C}_{16} & \bar{C}_{26} & \bar{C}_{66} \end{bmatrix} \begin{bmatrix} \varepsilon_{xx} \\ \varepsilon_{\theta\theta} \\ \gamma_{x\theta} \end{bmatrix}. \tag{9}$$

BENDING SHELL

Generally Orthotropic

As will soon be seen, deriving the stress resultants for a bending shell is considerably more involved than for the membrane shell. Beginning with the assumptions governing the kinematics of the shell (stated in the beginning of this section), we arrive at the following strain displacement relations:[12]

$$\varepsilon_{xx} = \frac{\partial u}{\partial x} - z\frac{\partial^2 w}{\partial x^2},$$

$$\varepsilon_{\theta\theta} = \frac{1}{a}\frac{\partial v}{\partial \theta} - \frac{z}{a}\frac{1}{(a+z)}\frac{\partial^2 w}{\partial \theta^2} + \frac{w}{a+z},$$

$$\gamma_{x\theta} = \frac{1}{a+z}\frac{\partial u}{\partial \theta} + \frac{a+z}{a}\frac{\partial v}{\partial x} - \frac{\partial^2 w}{\partial x \partial \theta}\left(\frac{z}{a} + \frac{z}{a+z}\right). \tag{10}$$

We use, as before, equation (7) for the stress-strain relationship for the rotated system:

$$\begin{bmatrix}\sigma_{xx}\\ \sigma_{\theta\theta}\\ \sigma_{x\theta}\end{bmatrix} = \begin{bmatrix}\bar{Q}_{11} & \bar{Q}_{12} & \bar{Q}_{16}\\ \bar{Q}_{12} & \bar{Q}_{22} & \bar{Q}_{26}\\ \bar{Q}_{16} & \bar{Q}_{26} & \bar{Q}_{66}\end{bmatrix}\begin{bmatrix}\varepsilon_{xx}\\ \varepsilon_{\theta\theta}\\ \gamma_{x\theta}\end{bmatrix}. \tag{11}$$

Deriving expressions for the stress resultants in terms of the displacements u, v, w, and their derivatives, we substitute equation (10) into (11) and then into equation (1). Now the integrations can be performed, and we arrive at equation (13), where the stress resultants are in the required form. The rigidities are grouped together in equation (12) and the stress resultants are listed in equation (13):

$$D_{11} = \bar{Q}_{11}h, \qquad D_{12} = \bar{Q}_{12}h, \qquad K_{11} = \frac{\bar{Q}_{11}h^3}{12}, \qquad K_{12} = \frac{\bar{Q}_{12}h^3}{12},$$

$$D_{22} = \bar{Q}_{22}h, \qquad D_{26} = \bar{Q}_{26}h, \qquad K_{22} = \frac{\bar{Q}_{22}h^3}{12}, \qquad K_{26} = \frac{\bar{Q}_{26}h^3}{12},$$

$$D_{16} = \bar{Q}_{16}h, \qquad D_{66} = \bar{Q}_{66}h, \qquad K_{16} = \frac{\bar{Q}_{16}h^3}{12}, \qquad K_{66} = \frac{\bar{Q}_{66}h^3}{12}, \tag{12}$$

and

$$N_{xx} = D_{11}\frac{\partial u}{\partial x} + \frac{D_{12}}{a}\left(\frac{\partial v}{\partial \theta} + w\right) - \frac{K_{11}}{a}\frac{\partial^2 w}{\partial x^2} + \frac{D_{16}}{a}\left(\frac{\partial u}{\partial \theta} + a\frac{\partial v}{\partial x}\right) + \frac{K_{16}}{a^2}\left(\frac{\partial v}{\partial x} - \frac{\partial^2 w}{\partial x \partial \theta}\right),$$

$$N_{\theta\theta} = D_{12}\frac{\partial u}{\partial x} + \frac{D_{22}}{a}\left(\frac{\partial v}{\partial \theta} + w\right) + \frac{D_{26}}{a}\left(\frac{\partial u}{\partial \theta} + a\frac{\partial v}{\partial x}\right) + \frac{K_{22}}{a^3}\left(\frac{\partial^2 w}{\partial \theta^2} + w\right) + \frac{K_{26}}{a^3}\left(\frac{\partial u}{\partial \theta} + a\frac{\partial^2 w}{\partial x \partial \theta}\right),$$

$$N_{x\theta} = D_{16}\frac{\partial u}{\partial x} + \frac{D_{26}}{a}\left(\frac{\partial v}{\partial \theta} + w\right) + \frac{D_{66}}{a}\left(\frac{\partial u}{\partial \theta} + a\frac{\partial v}{\partial x}\right) - \frac{K_{16}}{a}\frac{\partial^2 w}{\partial x^2} + \frac{K_{66}}{a^2}\left(\frac{\partial v}{\partial x} - \frac{\partial^2 w}{\partial x \partial \theta}\right),$$

$$N_{\theta x} = D_{16}\frac{\partial u}{\partial x} + \frac{D_{26}}{a}\left(\frac{\partial v}{\partial \theta} + w\right) + \frac{D_{66}}{a}\left(\frac{\partial u}{\partial \theta} + a\frac{\partial v}{\partial x}\right) + \frac{K_{26}}{a^3}\left(\frac{\partial^2 w}{\partial \theta^2} + w\right) + \frac{K_{66}}{a^3}\left(\frac{\partial u}{\partial \theta} + a\frac{\partial^2 w}{\partial x \partial \theta}\right),$$

$$M_{xx} = \frac{K_{11}}{a}\left(a\frac{\partial^2 w}{\partial x^2} - \frac{\partial u}{\partial x}\right) + \frac{K_{12}}{a^2}\left(\frac{\partial^2 w}{\partial \theta^2} - \frac{\partial v}{\partial \theta}\right) + \frac{2K_{16}}{a}\left(\frac{\partial^2 w}{\partial x \partial \theta} - \frac{\partial v}{\partial x}\right),$$

$$M_{\theta\theta} = K_{12}\frac{\partial^2 w}{\partial x^2} + \frac{K_{22}}{a^2}\left(\frac{\partial^2 w}{\partial \theta^2} + w\right) + \frac{K_{26}}{a^2}\left(2a\frac{\partial^2 w}{\partial x \partial \theta} + \frac{\partial u}{\partial \theta} - a\frac{\partial v}{\partial x}\right),$$

$$M_{x\theta} = \frac{K_{16}}{a}\left(a\frac{\partial^2 w}{\partial x^2} - \frac{\partial u}{\partial x}\right) + \frac{K_{26}}{a^2}\left(\frac{\partial^2 w}{\partial \theta^2} - \frac{\partial v}{\partial \theta}\right) + \frac{2K_{66}}{a}\left(\frac{\partial^2 w}{\partial x \partial \theta} - \frac{\partial v}{\partial x}\right),$$

$$M_{\theta x} = K_{16}\frac{\partial^2 w}{\partial x^2} + \frac{K_{26}}{a^2}\left(\frac{\partial^2 w}{\partial \theta^2} + w\right) + \frac{K_{66}}{a^2}\left(2a\frac{\partial^2 w}{\partial x \partial \theta} + \frac{\partial u}{\partial \theta} - a\frac{\partial v}{\partial x}\right). \tag{13}$$

Appendix A provides one complete example of stress-resultant integration along with a discussion of the simplifying assumptions that were necessary to arrive at the final form of equation (13).

EQUATIONS OF MOTION

MEMBRANE SHELL

Figure 1 is the physical model diagram for the infinite shell of thickness h and midradius a. The displacements, u, v, and w are in the x, θ, and r directions; p_o is the excitation pressure; and p_s and p_i are pressure fields that result from the motion of the shell. Consider the incremental volume of a shell that is dx long by $ad\theta$ wide with thickness h (see figure 4). The equations of motion for the system are determined by summing forces and setting the result equal to the mass times the acceleration in the three principal directions. The N_{ij} are forces per unit length. The pressure loads p_o, p_s, and p_i have units of force per unit area.

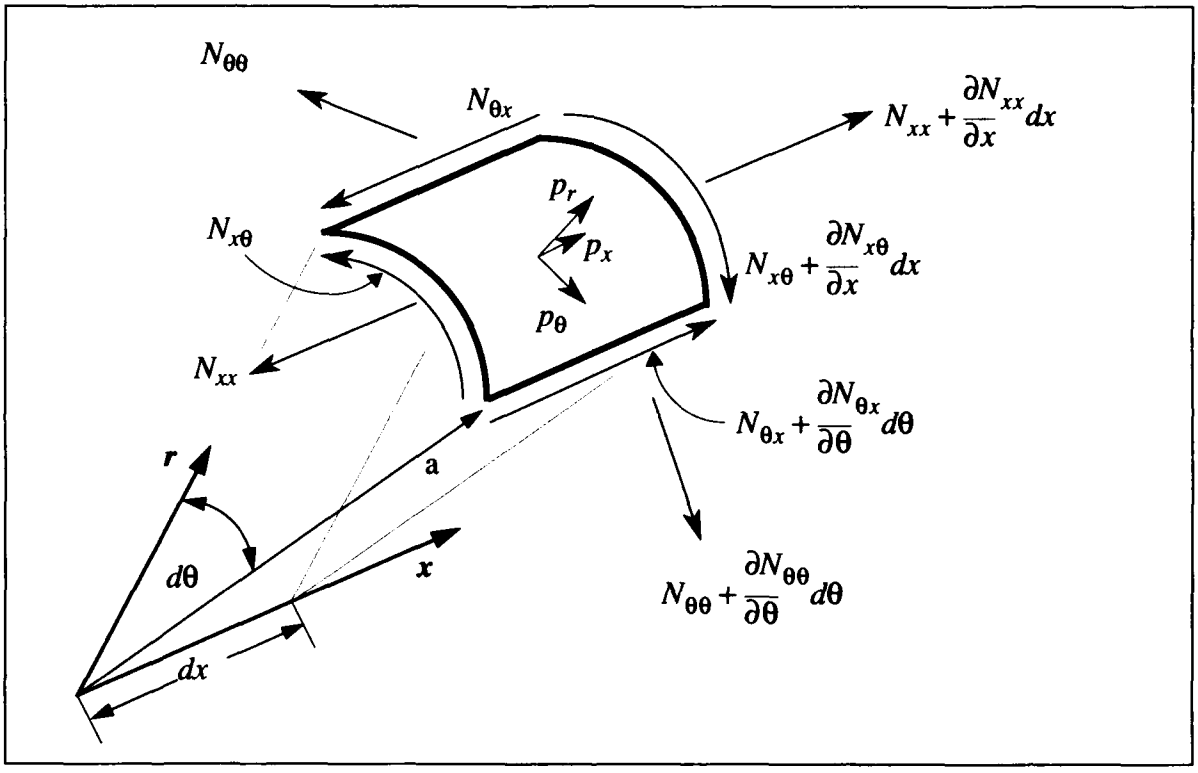

Figure 4. Membrane Shell Element FBD

From first principles, the equations of motion are derived for the shell. Summing forces in the x direction gives

$$\xrightarrow{+} \quad \sum F_x = m\frac{\partial^2 u}{\partial t^2}, \qquad m = \rho a h dx d\theta,$$

$$-N_{\theta x}dx + \left(N_{\theta x} + \frac{\partial N_{\theta x}}{\partial \theta} d\theta\right) dx - N_{xx} a d\theta + \left(N_{xx} + \frac{\partial N_{xx}}{\partial x} dx\right) a d\theta + p_x a d\theta dx = \rho a h dx d\theta \frac{\partial^2 u}{\partial t^2},$$

which can be reduced to

$$\frac{1}{a}\frac{\partial N_{\theta x}}{\partial \theta} + \frac{\partial N_{xx}}{\partial x} + p_x = \rho h \frac{\partial^2 u}{\partial t^2}. \tag{14}$$

Figure 5 illustrates the membrane shell element in the r, θ plane. When we sum the forces acting in the radial direction, $N_{\theta\theta}$ and the static tension, T, in the axial direction must be considered. In the undeformed state, the shell is parallel to the x-axis with no component of T in the radial direction. However, when the shell undergoes deformation, as shown in figure 6, a component of force resulting from the static tension arises in the radial direction. This static tension, T, is much larger than the forces resulting from the applied acoustic pressure loads and may therefore have a significant effect on the structure, depending on its relative magnitude as compared with the other forces involved in the radial direction. For this reason, static tension must be included in the formulation.

$N_{\theta\theta}$ must be separated into components in order to sum forces in the radial direction. Small angle approximations will be used because θ is small; therefore,

$$\cos\theta \approx 1, \qquad \sin\theta \approx \theta \cdot$$

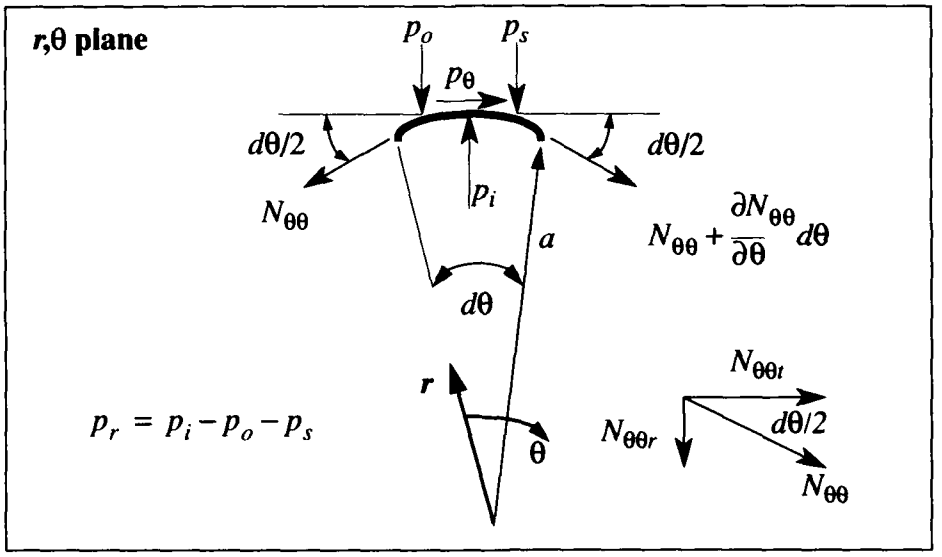

Figure 5. Membrane Shell Element FBD in the r, θ Plane

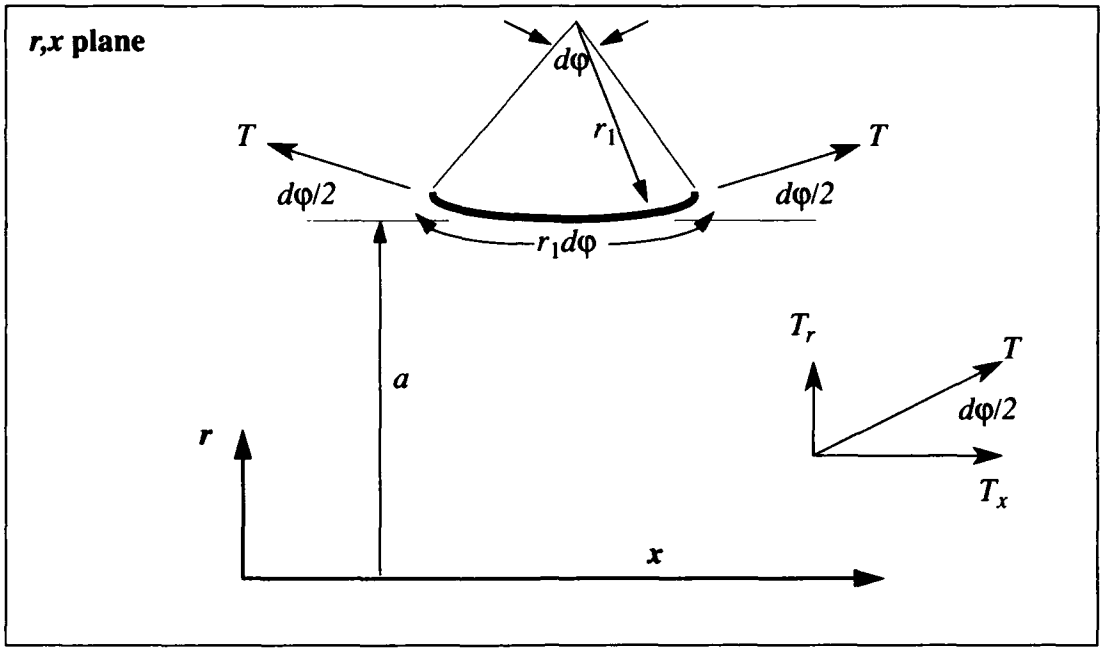

Figure 6. Membrane Shell Element FBD in the *r, x* Plane

Thus, we find, that $N_{\theta\theta r} = N_{\theta\theta} d\theta/2$ and $T_r = T d\varphi/2$. The elemental length in the axial x-direction is equal to $r_1 d\varphi$. Summing forces in the radial direction while referring to figures 5 and 6 yields

$$+\uparrow \qquad \sum F_r = m\frac{\partial^2 w}{\partial t^2}, \qquad m = \rho r_1 d\varphi a d\theta h,$$

$$(p_i - p_o - p_s)\, a d\theta r_1 d\varphi - N_{\theta\theta}\frac{d\theta}{2} r_1 d\varphi - (N_{\theta\theta} + \frac{\partial N_{\theta\theta}}{\partial\theta} d\theta)\frac{d\theta}{2} r_1 d\varphi + (T\frac{d\varphi}{2} + T\frac{d\varphi}{2})\, a d\theta =$$

$$\rho r_1 d\varphi a d\theta h \frac{\partial^2 w}{\partial t^2},$$

which becomes

$$(p_i - p_o - p_s)\, a d\theta r_1 d\varphi - N_{\theta\theta} d\theta r_1 d\varphi - \frac{\partial N_{\theta\theta} d\theta^2 r_1 d\varphi}{\partial\theta\ 2} + T d\varphi a d\theta = \rho r_1 d\varphi a d\theta h \frac{\partial^2 w}{\partial t^2}.$$

Assuming that the slope of the surface is small, the following form for the radius of curvature is used: $\frac{1}{r_1} = \frac{\partial^2 w}{\partial x^2}$. Neglecting the higher order term $\frac{\partial N_{\theta\theta} d\theta^2 r_1 d\varphi}{\partial\theta\ 2}$, we have the following equation of motion in the radial direction:

$$p_i - p_o - p_s - \frac{N_{\theta\theta}}{a} + T\frac{\partial^2 w}{\partial x^2} = h\rho\frac{\partial^2 w}{\partial t^2}. \qquad (15)$$

Summing forces in the θ direction, we have

$$\curvearrowright_{+} \qquad \sum F_\theta = m\frac{\partial^2 v}{\partial t^2}, \qquad m = \rho a h dx d\theta,$$

$$-N_{\theta\theta}dx + (N_{\theta\theta} + \frac{\partial N_{\theta\theta}}{\partial \theta}d\theta)\,dx + p_\theta dx a d\theta - N_{x\theta}a d\theta + (N_{x\theta} + \frac{\partial N_{x\theta}}{\partial x}dx)\,a d\theta = \rho a h dx d\theta \frac{\partial^2 v}{\partial t^2},$$

which can be reduced to

$$\frac{1}{a}\frac{\partial N_{\theta\theta}}{\partial \theta} + \frac{\partial N_{x\theta}}{\partial x} + p_\theta = \rho h \frac{\partial^2 v}{\partial t^2}. \tag{16}$$

Summarizing the equations of motion in the three directions, we obtain

$$\frac{1}{a}\frac{\partial N_{\theta x}}{\partial \theta} + \frac{\partial N_{xx}}{\partial x} + p_x = \rho h \frac{\partial^2 u}{\partial t^2}, \tag{17}$$

$$\frac{1}{a}\frac{\partial N_{\theta\theta}}{\partial \theta} + \frac{\partial N_{x\theta}}{\partial x} + p_\theta = \rho h \frac{\partial^2 v}{\partial t^2}, \tag{18}$$

$$p_i - p_o - p_s - \frac{N_{\theta\theta}}{a} + T\frac{\partial^2 w}{\partial x^2} = \rho h \frac{\partial^2 w}{\partial t^2}. \tag{19}$$

Equations (17) through (19) give relationships between the applied pressures and the corresponding displacements and stress resultants. We will proceed in a direction that gives three equations, where the only unknowns are *u*, *v*, *w*, and their derivatives. By means of equations (17), (18), (19), (6), and (9), we can now write three second-order linear partial differential equations for the displacements of the cylinder.

The first step substitutes equation (6) into (9):

$$N_{xx} = \bar{C}_{11}\frac{\partial u}{\partial x} + \bar{C}_{12}\frac{1}{a}(\frac{\partial v}{\partial \theta} + w) + \bar{C}_{16}(\frac{\partial v}{\partial x} + \frac{1}{a}\frac{\partial u}{\partial \theta}),$$

$$N_{\theta\theta} = \bar{C}_{12}\frac{\partial u}{\partial x} + \bar{C}_{22}\frac{1}{a}(\frac{\partial v}{\partial \theta} + w) + \bar{C}_{26}(\frac{\partial v}{\partial x} + \frac{1}{a}\frac{\partial u}{\partial \theta}),$$

$$N_{x\theta} = \bar{C}_{16}\frac{\partial u}{\partial x} + \bar{C}_{26}\frac{1}{a}(\frac{\partial v}{\partial \theta} + w) + \bar{C}_{66}(\frac{\partial v}{\partial x} + \frac{1}{a}\frac{\partial u}{\partial \theta}). \tag{20}$$

Differentiating equation (20) where needed yields

$$\frac{\partial N_{xx}}{\partial x} = \bar{C}_{11}\frac{\partial^2 u}{\partial x^2} + \bar{C}_{12}\frac{1}{a}\left(\frac{\partial^2 v}{\partial\theta\partial x} + \frac{\partial w}{\partial x}\right) + \bar{C}_{16}\left(\frac{\partial^2 v}{\partial x^2} + \frac{1}{a}\frac{\partial^2 u}{\partial\theta\partial x}\right),$$

$$\frac{\partial N_{\theta\theta}}{\partial\theta} = \bar{C}_{12}\frac{\partial^2 u}{\partial x\partial\theta} + \bar{C}_{22}\frac{1}{a}\left(\frac{\partial^2 v}{\partial\theta^2} + \frac{\partial w}{\partial\theta}\right) + \bar{C}_{26}\left(\frac{\partial^2 v}{\partial x\partial\theta} + \frac{1}{a}\frac{\partial^2 u}{\partial\theta^2}\right),$$

$$\frac{\partial N_{x\theta}}{\partial\theta} = \bar{C}_{16}\frac{\partial^2 u}{\partial x\partial\theta} + \bar{C}_{26}\frac{1}{a}\left(\frac{\partial^2 v}{\partial\theta^2} + \frac{\partial w}{\partial\theta}\right) + \bar{C}_{66}\left(\frac{\partial^2 v}{\partial x\partial\theta} + \frac{1}{a}\frac{\partial^2 u}{\partial\theta^2}\right),$$

$$\frac{\partial N_{x\theta}}{\partial x} = \bar{C}_{16}\frac{\partial^2 u}{\partial x^2} + \bar{C}_{26}\frac{1}{a}\left(\frac{\partial^2 v}{\partial\theta\partial x} + \frac{\partial w}{\partial x}\right) + \bar{C}_{66}\left(\frac{\partial^2 v}{\partial x^2} + \frac{1}{a}\frac{\partial^2 u}{\partial\theta\partial x}\right). \tag{21}$$

Substituting equation (21) into equations (17), (18), and (19) gives

$$\frac{1}{a}\bar{C}_{16}\frac{\partial^2 u}{\partial x\partial\theta} + \bar{C}_{26}\frac{1}{a^2}\left(\frac{\partial^2 v}{\partial\theta^2} + \frac{\partial w}{\partial\theta}\right) + \frac{1}{a}\bar{C}_{66}\left(\frac{\partial^2 v}{\partial x\partial\theta} + \frac{1}{a}\frac{\partial^2 u}{\partial\theta^2}\right) + \bar{C}_{11}\frac{\partial^2 u}{\partial x^2} +$$

$$\bar{C}_{12}\frac{1}{a}\left(\frac{\partial^2 v}{\partial\theta\partial x} + \frac{\partial w}{\partial x}\right) + \bar{C}_{16}\left(\frac{\partial^2 v}{\partial x^2} + \frac{1}{a}\frac{\partial^2 u}{\partial\theta\partial x}\right) + p_x = \rho h\frac{\partial^2 u}{\partial t^2}, \tag{22}$$

$$\bar{C}_{12}\frac{1}{a}\frac{\partial^2 u}{\partial x\partial\theta} + \bar{C}_{22}\frac{1}{a^2}\left(\frac{\partial^2 v}{\partial\theta^2} + \frac{\partial w}{\partial\theta}\right) + \bar{C}_{26}\frac{1}{a}\left(\frac{\partial^2 v}{\partial x\partial\theta} + \frac{1}{a}\frac{\partial^2 u}{\partial\theta^2}\right) + \bar{C}_{16}\frac{\partial^2 u}{\partial x^2} +$$

$$\bar{C}_{26}\frac{1}{a}\left(\frac{\partial^2 v}{\partial\theta\partial x} + \frac{\partial w}{\partial x}\right) + \bar{C}_{66}\left(\frac{\partial^2 v}{\partial x^2} + \frac{1}{a}\frac{\partial^2 u}{\partial\theta\partial x}\right) + p_\theta = \rho h\frac{\partial^2 v}{\partial t^2}, \tag{23}$$

$$p_i - p_o - p_s - \bar{C}_{12}\frac{1}{a}\frac{\partial u}{\partial x} - \bar{C}_{22}\frac{1}{a^2}\left(\frac{\partial v}{\partial\theta} + w\right) - \bar{C}_{26}\frac{1}{a}\left(\frac{\partial v}{\partial x} + \frac{1}{a}\frac{\partial u}{\partial\theta}\right) + T\frac{\partial^2 w}{\partial x^2} = \rho h\frac{\partial^2 w}{\partial t^2}. \tag{24}$$

The following harmonic excitation will be applied to the shell in the r and x-directions

$$p_o = P_o\cos n\theta e^{i(kx-\omega t)}, \qquad p_x = P_x\cos n\theta e^{i(kx-\omega t)}. \tag{25}$$

Normal to the surface is the pressure field p_o and, in the longitudinal direction, the shear stress p_x. Both P_o and P_x are, in general, functions of wavenumber and frequency; however, they have been expressed here in a simpler form as constants since all the results presented will be normalized by P_o or P_x and only the structures response to a unit pressure excitation is considered. It should also be noted that P_o and P_x are amplitudes of the components of each mode of propagation and are in general different for each mode n.

The solutions to equations (22), (23), and (24) are

$$u = U\cos(n\theta)\, e^{i(kx-\omega t)}, \qquad v = V\sin(n\theta)\, e^{i(kx-\omega t)}, \qquad w = W\cos(n\theta)\, e^{i(kx-\omega t)}. \tag{26}$$

BENDING SHELL

Figure 7 depicts the forces acting on an elemental area of the shell. In this case, we include the transverse shear forces that can now be supported by the bending shell model. Proceeding as before, we sum forces in the three coordinate directions to obtain three equations of motion for the middle surface of the shell.

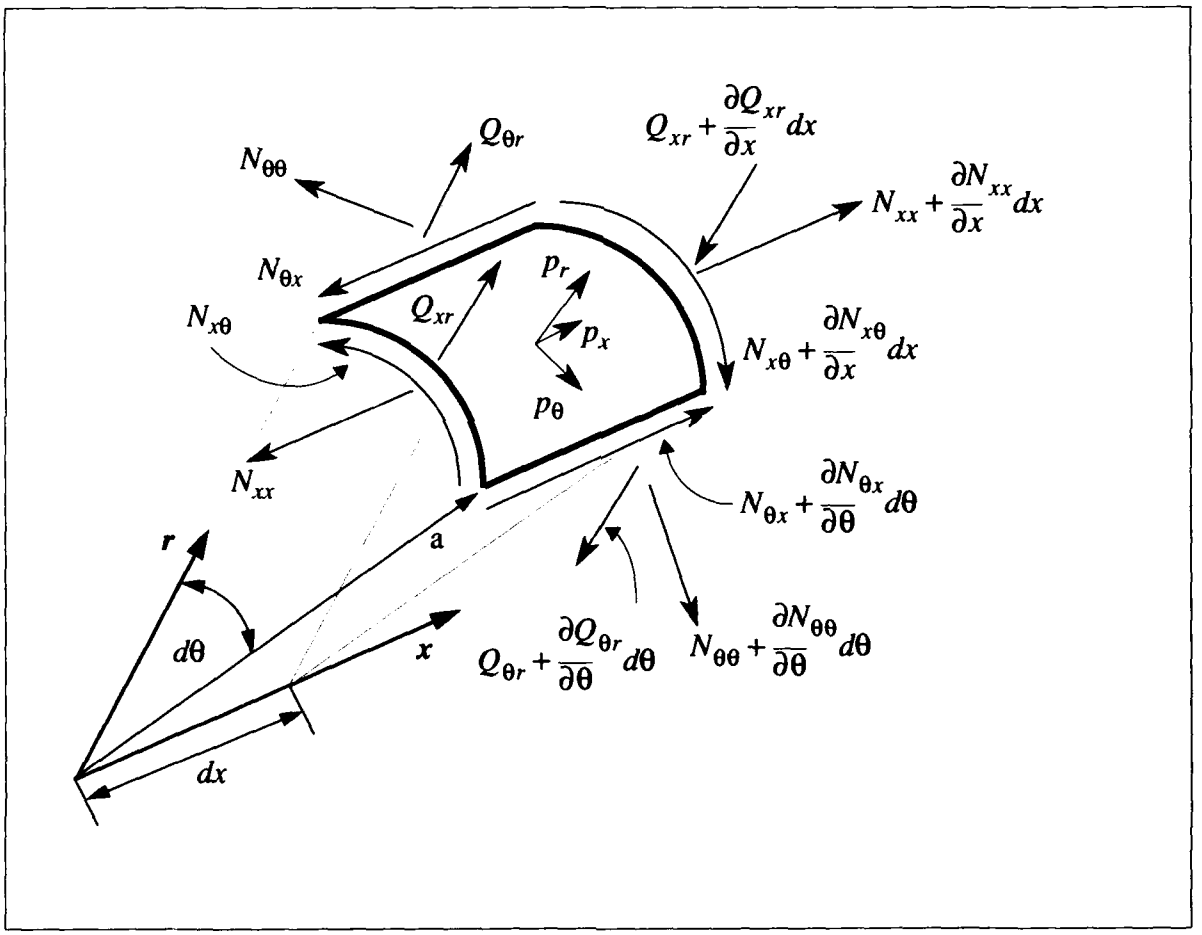

Figure 7. Bending Shell Element FBD Forces Only

Starting with the r direction, we have

$$+\uparrow \qquad \sum F_r = m\frac{\partial^2 w}{\partial t^2}, \qquad m = \rho a h dx d\theta,$$

$$(Q_{\theta r} - Q_{\theta r} - \frac{\partial Q_{\theta r}}{\partial \theta} d\theta)\, dx + (Q_{xr} - Q_{xr} - \frac{\partial Q_{xr}}{\partial x} dx)\, a d\theta - N_{\theta\theta}\frac{d\theta}{2} dx - (N_{\theta\theta} + \frac{\partial N_{\theta\theta}}{\partial \theta} d\theta)\frac{d\theta}{2} dx$$

$$+ p_r a d\theta dx = \rho a h dx d\theta \frac{\partial^2 w}{\partial t^2}. \tag{27}$$

As in the membrane case, we neglect the higher order term $\frac{\partial N_{\theta\theta} d\theta^2 dx}{\partial \theta 2}$. The influence of static tension will be incorporated as in the earlier membrane case by a consideration of the deformed shape of the shell and the radial component that occurs due to the deformation (see figure 6). All other dynamic forces are summed from an undeformed shell element. Therefore, the $T\frac{\partial^2 w}{\partial x^2}$ term is added to the force sum of equation (27), resulting in

$$T\frac{\partial^2 w}{\partial x^2} - \frac{1}{a}\frac{\partial Q_{\theta r}}{\partial \theta} - \frac{\partial Q_{xr}}{\partial x} - \frac{N_{\theta\theta}}{a} + p_r = \rho h \frac{\partial^2 w}{\partial t^2}. \tag{28}$$

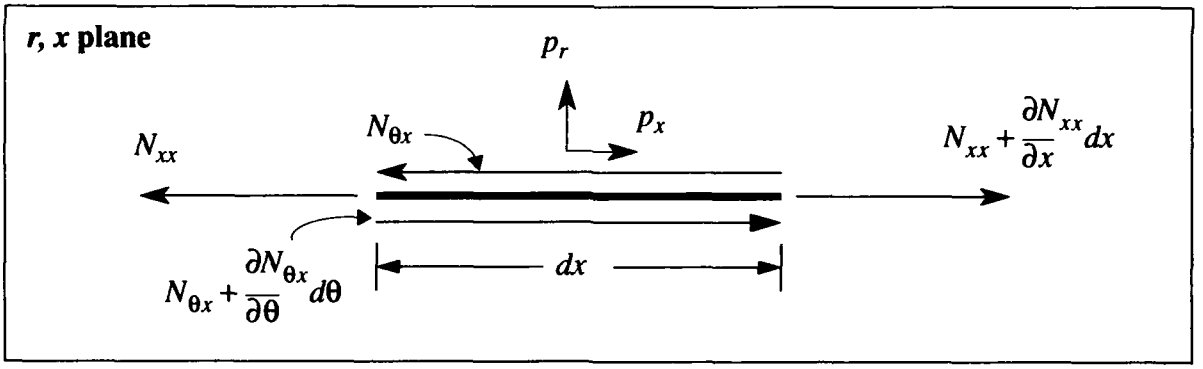

Figure 8. Bending Shell Element FBD Forces Only in the r, x Plane

Summing forces in the longitudinal x-direction in figures 7 and 8 yields

$$\xrightarrow{+} \qquad \sum F_x = m\frac{\partial^2 u}{\partial t^2}, \qquad m = \rho a h dx d\theta,$$

$$(-N_{xx} + N_{xx} + \frac{\partial N_{xx}}{\partial x} dx)\, a d\theta + (-N_{\theta x} + N_{\theta x} + \frac{\partial N_{\theta x}}{\partial \theta} d\theta)\, dx + p_x a d\theta dx = \rho a h dx d\theta \frac{\partial^2 u}{\partial t^2},$$

which can be expressed as

$$\frac{\partial N_{xx}}{\partial x} + \frac{1}{a}\frac{\partial N_{\theta x}}{\partial \theta} + p_x = \rho h \frac{\partial^2 u}{\partial t^2}. \tag{29}$$

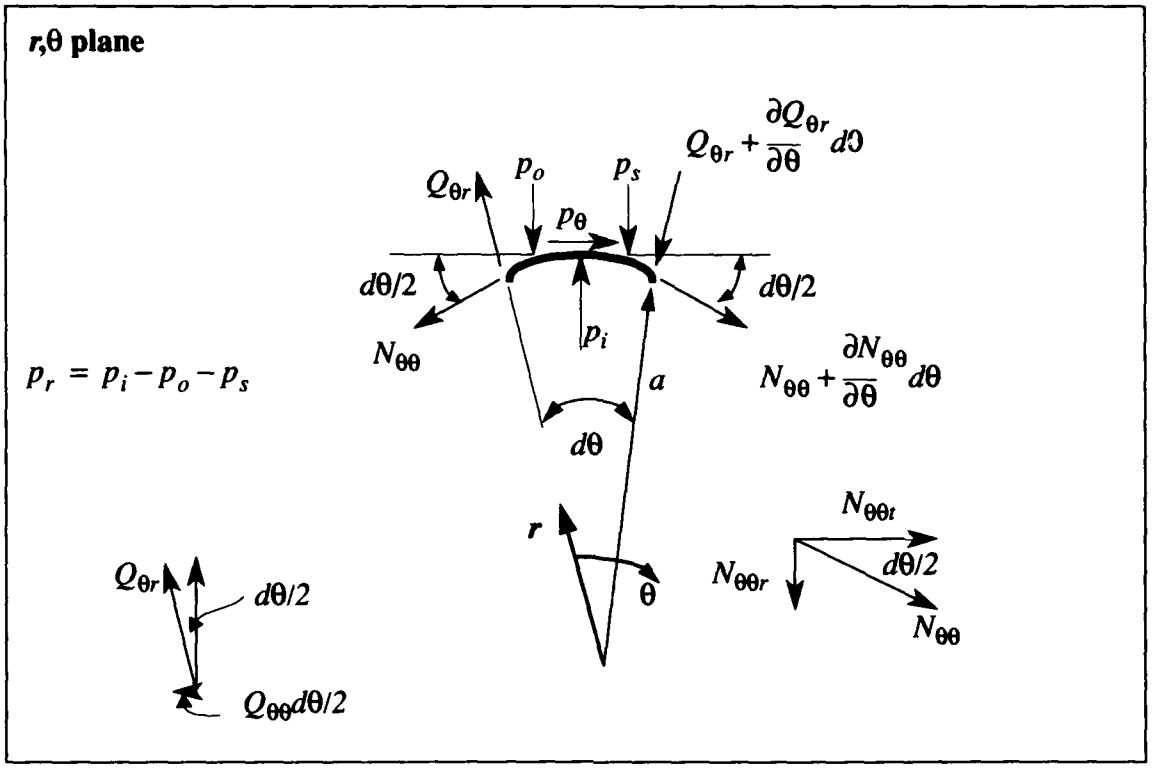

Figure 9. Bending Shell Element FBD Forces Only in the *r*, θ Plane

Referring back to figures 7 and 9 and considering the forces acting in the circumferential direction, we must now consider the circumferential component of the shear force $Q_{\theta r}$:

$$\circlearrowleft_{+} \qquad \sum F_\theta = m\frac{\partial^2 v}{\partial t^2}, \qquad m = \rho a h dx d\theta,$$

$$(-N_{\theta\theta} + N_{\theta\theta} + \frac{\partial N_{\theta\theta}}{\partial \theta} d\theta)\, dx + (-Q_{\theta r} - (Q_{\theta r} + \frac{\partial Q_{\theta r}}{\partial \theta} d\theta))\, \frac{d\theta}{2} dx$$

$$+ (-N_{x\theta} + N_{x\theta} + \frac{\partial N_{x\theta}}{\partial x} dx)\, a d\theta + p_\theta a d\theta dx = \rho a h dx d\theta \frac{\partial^2 v}{\partial t^2},$$

which becomes

$$\frac{\partial N_{x\theta}}{\partial x} + \frac{1}{a}\frac{\partial N_{\theta\theta}}{\partial \theta} - \frac{Q_{\theta r}}{a} + p_\theta = \rho h \frac{\partial^2 v}{\partial t^2}. \tag{30}$$

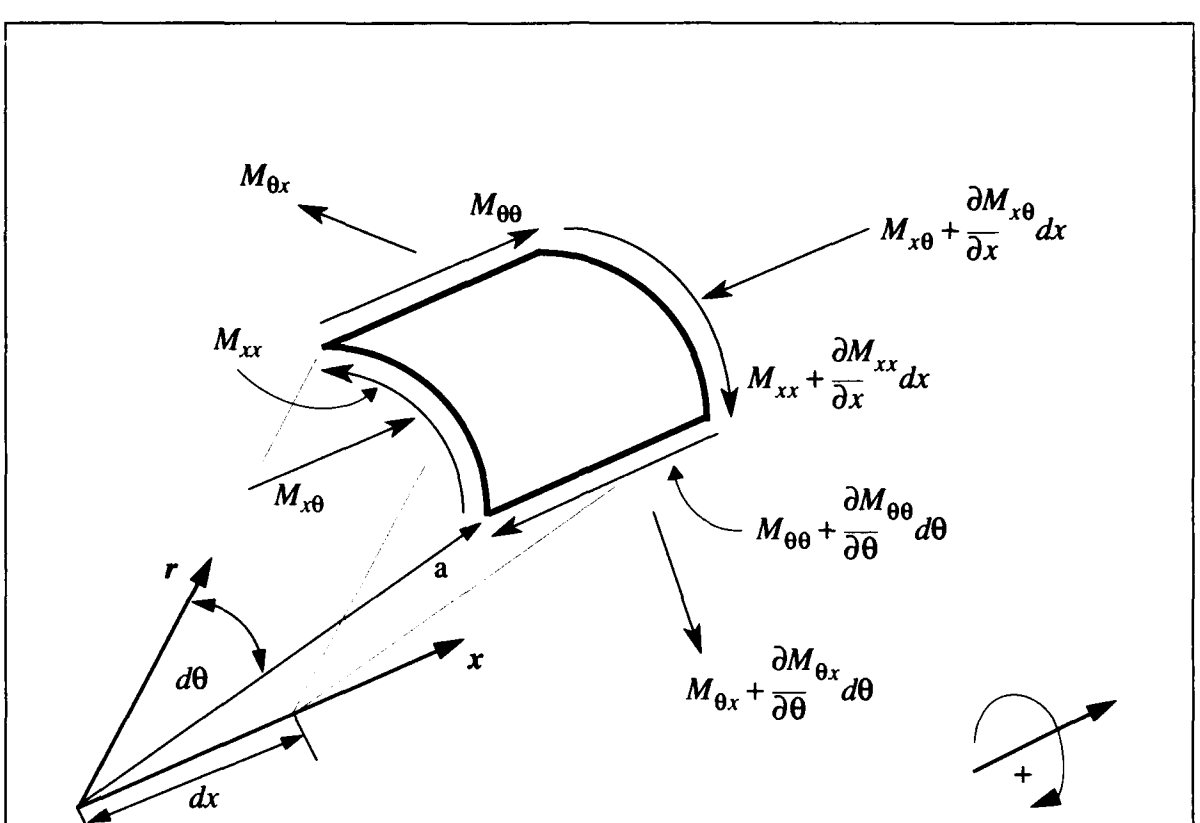

Figure 10. Bending Shell Element FBD Moments Only

We now consider the moments acting on the shell element. Referring to figures 7 and 10, we begin by summing moments about the x- and θ-axes, setting the sum equal to the mass moment of inertia times the angular acceleration about the respective axis. The angular momentum is a small quantity and could have been neglected by setting the moment sum equal to zero; however, to be complete, it has been included in the derivation. The positive direction for a moment is defined as clockwise about the moment vector when we are looking down the axis in the positive direction (figure 10). Beginning with the moments about the x-axis, we have the transverse shear force $Q_{\theta r}$ acting at a distance of $ad\theta/2$ from the centroid of the shell element, along with $M_{x\theta}$ and $M_{\theta\theta}$ yielding the following equation:

$$\circlearrowright_{+} \qquad \sum M_x = I_x \frac{1}{a} \frac{\partial^3 w}{\partial \theta \partial t^2}, \qquad I_x = \frac{mh^2}{12}, \qquad m = \rho a h dx d\theta,$$

$$\left(M_{x\theta} - \left(M_{x\theta} + \frac{\partial M_{x\theta}}{\partial x} dx\right)\right) ad\theta + \left(M_{\theta\theta} - \left(M_{\theta\theta} + \frac{\partial M_{\theta\theta}}{\partial \theta} d\theta\right)\right) dx$$

$$+ \left(Q_{\theta r} + \left(Q_{\theta r} + \frac{\partial Q_{\theta r}}{\partial \theta} d\theta\right)\right) dx \frac{ad\theta}{2} = \frac{\rho h^3 dx d\theta}{12} \frac{\partial^3 w}{\partial \theta \partial t^2}.$$

Simplifying the above equation, we have

$$-\frac{\partial M_{x\theta}}{\partial x}-\frac{1}{a}\frac{\partial M_{\theta\theta}}{\partial\theta}+Q_{\theta r}=\frac{\rho h^3}{12a}\frac{\partial^3 w}{\partial\theta\partial t^2}. \tag{31}$$

The slope of the shell element about the x-axis is expressed as $\frac{1}{a}\frac{\partial w}{\partial\theta}$, and the slope of the shell element about the θ-axis is $\frac{\partial w}{\partial x}$.

About the θ-axis, we have the transverse shear force Q_{xr}, acting through a distance of $dx/2$ on the centroid of the element, along with M_{xx} and $M_{\theta x}$ yielding

$$\curvearrowleft + \qquad \sum M_\theta = I_\theta\frac{\partial^3 w}{\partial x\partial t^2}, \qquad I_\theta=\frac{mh^2}{12}, \qquad m=\rho a h dx d\theta,$$

$$\left(-Q_{xr}-\left(Q_{xr}+\frac{\partial Q_{xr}}{\partial x}dx\right)\right)ad\theta\frac{dx}{2}+\left(-M_{xx}+M_{xx}+\frac{\partial M_{xx}}{\partial x}dx\right)ad\theta$$

$$+\left(-M_{\theta x}+M_{\theta x}+\frac{\partial M_{\theta x}}{\partial\theta}d\theta\right)dx=\frac{\rho a h^3 dx d\theta}{12}\frac{\partial^3 w}{\partial x\partial t^2}.$$

Simplifying the above expression gives

$$-Q_{xr}+\frac{\partial M_{xx}}{\partial x}+\frac{\partial M_{\theta x}}{\partial\theta}\frac{1}{a}=\frac{\rho h^3}{12}\frac{\partial^3 w}{\partial x\partial t^2}. \tag{32}$$

From equations (31) and (32), the transverse shears can be expressed in terms of the moments, thus reducing the number of stress resultants from ten to eight and simplifying the equations of motion (equations (28) through (30)) as follows:

$$\frac{\partial N_x}{\partial x}+\frac{1}{a}\frac{\partial N_{\theta x}}{\partial\theta}+p_x=\rho h\frac{\partial^2 u}{\partial t^2},$$

$$\frac{\partial N_{x\theta}}{\partial x}+\frac{1}{a}\frac{\partial N_{\theta\theta}}{\partial\theta}-\frac{1}{a}\frac{\partial M_{x\theta}}{\partial x}-\frac{1}{a^2}\frac{\partial M_{\theta\theta}}{\partial\theta}+p_\theta=\rho h\left(\frac{\partial^2 v}{\partial t^2}+\frac{h^2}{12a^2}\frac{\partial^3 w}{\partial\theta\partial t^2}\right),$$

$$T\frac{\partial^2 w}{\partial x^2}-\frac{1}{a}\frac{\partial^2 M_{x\theta}}{\partial x\partial\theta}-\frac{1}{a^2}\frac{\partial^2 M_{\theta\theta}}{\partial\theta^2}-\frac{\partial^2 M_{xx}}{\partial x^2}-\frac{1}{a}\frac{\partial^2 M_{\theta x}}{\partial\theta^2}-\frac{N_{\theta\theta}}{a}+p_r=\rho h\left(\frac{\partial^2 w}{\partial t^2}+\frac{h^2}{12a^2}\frac{\partial^4 w}{\partial\theta^2\partial t^2}-\frac{h^2}{12}\frac{\partial^4 w}{\partial x^2\partial t^2}\right),$$

$$p_r=p_i-p_o-p_s. \tag{33}$$

We have not yet discussed p_i or p_s. Let us now turn our attention to the inner and outer fluids appearing in equations (24) and (33), which present a loading on the shell. We will derive expressions for these pressure fields in terms of the shell motion by applying boundary conditions at the fluid shell interface. Once we have expressions for p_i and p_s in terms of W, we will be able to solve for the shell motion and subsequently the interior pressure field. Lastly, the ratio of $p_i(r)/P_o$ will give us an expression for the transfer function of pressure in terms of wavenumber, frequency, and the physical properties of the shell.

FLUIDS AND THE VELOCITY FIELD POTENTIAL

As the surface of the shell is set into motion by the excitation pressure wave, denoted by p_o, a pressure field, p_s, is generated in the outer fluid by the shell surface. When the wavenumber associated with the vibration of the shell surface is smaller than ω/c_o, the pressure radiated into the outer fluid is in the form of a propagating wave. If the wavenumber of the shell vibration is greater than ω/c_o, the pressure field decays exponentially from the surface of the shell in the $+r$ direction. A similar situation exists for the inner fluid for p_i based on ω/c_i. We will model the fluid as an ideal (nonviscous) linearly elastic media that cannot sustain shear stress, even when it is in motion.[13] The equation of state is then

$$\tau_{ij} = -p\delta_{ij},$$

whose components are given by Hooke's law while we set $\mu_f = 0$:

$$\tau_{11} = \tau_{22} = \tau_{33} = \lambda_f \varepsilon_{kk} = -p$$

and

$$\tau_{12} = \tau_{13} = \tau_{23} = 0. \tag{34}$$

The following scalar velocity potential describes the dynamic motion of the fluid[14] in cylindrical coordinates:

$$\nabla^2 \varphi_f = \frac{1}{c_f^2}\frac{\partial^2 \varphi_f}{\partial t^2}, \tag{35}$$

where

$$\nabla^2 = \frac{\partial^2}{\partial r^2} + \frac{1}{r}\frac{\partial}{\partial r} + \frac{1}{r^2}\frac{\partial^2}{\partial \theta^2} + \frac{\partial^2}{\partial z^2}.$$

In the case of fluids, $c_f = \sqrt{\frac{\lambda_f}{\rho_f}}$, which is equivalent to $c_f = \sqrt{\frac{\beta}{\rho_f}}$, where β is the bulk modulus of the fluid. The particle velocity and the pressure in the fluid can be expressed in terms of the velocity potential as follows:

$$\frac{\partial w_f}{\partial t} = \nabla \varphi_f \tag{36}$$

and

$$p = -\rho_f \frac{\partial \varphi_f}{\partial t}. \tag{37}$$

The general solution to equation (35) is given by

$$\varphi_f = F_f(r)\cos(n\theta)\,e^{i(kx-\omega t)} \qquad \text{or} \qquad \varphi_f = F_f(r)\,e^{i(kx+n\theta-\omega t)}, \tag{38}$$

where

$$F_f(r) = DJ_n(k_1 r) + \bar{E}Y_n(k_1 r), \qquad k_1^2 = \frac{\omega^2}{c_f^2} - k^2 \qquad \text{for} \qquad \frac{\omega^2}{c_f^2} > k^2, \tag{39}$$

and

$$F_f(r) = GI_n(k_2 r) + HK_n(k_2 r), \qquad k_2^2 = k^2 - \frac{\omega^2}{c_f^2} \qquad \text{for} \qquad k^2 > \frac{\omega^2}{c_f^2}. \tag{40}$$

At this point, let us temporarily reduce the scope of our study and consider only the axisymmetric zeroth order response ($n = 0$) in equations (38) through (40).

OUTER FLUID VELOCITY FIELD POTENTIAL

For an outgoing wave described by $e^{i(k_r r-\omega t)}$, the field in the outer fluid is physically a radiation from the surface of the cylinder. The radial dependence $F(r)$ takes on the form of a Hankel function of the first kind;[15] i.e., $H^1{}_o(gr) = J_o(gr) + iY_o(gr)$. Therefore, the radial function in the outer fluid is given by

$$F_s(r) = MH_o^1(gr), \qquad g^2 = \frac{\omega^2}{c_o^2} - k^2 \qquad \text{for} \qquad \frac{\omega^2}{c_o^2} > k^2. \tag{41}$$

When $k^2 > \frac{\omega^2}{c_o^2}$, we use the following relationship, substituting a modified Hankel function of real argument:[16]

$$K_n(x) = \frac{\pi}{2} i^{n+1} H_n^1(ix).$$

The velocity potential, φ, must approach 0 as $r \to \infty$; therefore, I_o is not an appropriate choice because it approaches infinity as $r \to \infty$. Of the two possible Bessel functions in equation (40), only the K_o Bessel function provides the necessary bounded solution to this problem. Consequently, we use the following form for the radial dependence of the velocity potential:

$$F_s(r) = HK_o(fr), \qquad f^2 = k^2 - \frac{\omega^2}{c_o^2} \qquad \text{for} \qquad k^2 > \frac{\omega^2}{c_o^2}. \tag{42}$$

The pressure component for the radiated field is obtained with equations (37) and (38) while we substitute an appropriate form for $F(r)$, depending on the value for k:

$$p_s(r) = i\omega\rho_o F_s(r)\,e^{i(kx-\omega t)}. \tag{43}$$

From equation (36), we can write an expression for the particle velocity in the fluid:

$$\frac{\partial w_s}{\partial t} = \frac{\partial}{\partial r} F_s(r)\,e^{i(kx-\omega t)}. \tag{44}$$

INNER FLUID VELOCITY FIELD POTENTIAL

Next, when considering the behavior of the field at $r = 0$, we make the observation that Y_o and K_o approach infinity as the argument of the functions approaches zero. However, because the interior pressure field must be finite at $r = 0$, these solutions are inappropriate and must be discarded. Bessel functions J_o and I_o will be retained for describing the velocity potentials in the inner fluid. Bessel function I_o replaces J_o as the argument becomes imaginary:[17]

$$I_n(x) = i^{-n} J_n(ix),$$

$$F_i(r) = DJ_o(lr), \qquad l^2 = \frac{\omega^2}{c_i^2} - k^2 \qquad \text{for} \qquad \frac{\omega^2}{c_i^2} > k^2 \tag{45}$$

$$F_i(r) = GI_o(mr), \qquad m^2 = k^2 - \frac{\omega^2}{c_i^2} \qquad \text{for} \qquad k^2 > \frac{\omega^2}{c_i^2}. \tag{46}$$

Similar to equations (43) and (44), the pressure and velocity in the inner fluid are

$$p_i(r) = i\omega\rho_i F_i(r)\, e^{i(kx - \omega t)}, \qquad \frac{\partial w_i}{\partial t} = \frac{\partial}{\partial r} F_i(r)\, e^{i(kx - \omega t)}. \tag{47}$$

The derivatives of the Bessel functions needed for the fluid velocity expressions of equations (44) and (47) are

$$\frac{\partial}{\partial r} H_o^1(gr) = -gH_1^1(gr), \qquad \frac{\partial}{\partial r} J_o(lr) = -lJ_1(lr),$$

$$\frac{\partial}{\partial r} K_o(fr) = -fK_1(fr), \qquad \frac{\partial}{\partial r} I_o(mr) = mI_1(mr). \tag{48}$$

SHELL/FLUID BOUNDARY INTERACTION

AXISYMMETRIC DEVELOPMENT

Returning to the shell/fluid interaction, we calculate the fluid pressures in terms of the shell motion. This will allow for the solution of the shell displacements, which are now the only unknowns. We will distinguish between inner and outer shell radii when calculating the fluid velocities. This distinction provides a more accurate value for the fluid velocities and pressure loadings than does the use of the shell midradius for fluid calculations. The first step equates the shell velocity with the outer fluid velocity at the shell outer radius, a_o, and thereby solves for the constants M and H. The second step sets the shell velocity equal to the inner fluid velocity at $r = a_i$. Inserting the expressions from equation (48) that correspond to the outer fluid into equation (44) gives the fluid particle velocity as

$$\frac{\partial w_s}{\partial t} = \nabla \varphi_s = -gMH_1^1(gr)\, e^{i(kx-\omega t)},$$

$$\frac{\partial w_s}{\partial t} = \nabla \varphi_s = -fHK_1(fr)\, e^{i(kx-\omega t)} . \tag{49}$$

Differentiating equation (26) to obtain the shell velocity in the radial direction and then equating the shell and outer fluid velocity at $r = a_o$ while suppressing the exponential term yields

$$\frac{\partial w}{\partial t} = \left.\frac{\partial w_s}{\partial t}\right|_{r=a_o}, \qquad -i\omega W = -gMH_1^1(ga_o), \qquad \therefore M = \frac{i\omega W}{gH_1^1(ga_o)},$$

$$-i\omega W = -fHK_1(fa_o), \qquad \therefore H = \frac{i\omega W}{fK_1(fa_o)} . \tag{50}$$

In a similar fashion, we equate the shell velocity with the inner fluid particle velocity at $r = a_i$ and solve for the constants D and G as

$$\frac{\partial w}{\partial t} = \left.\frac{\partial w_s}{\partial t}\right|_{r=a_i}, \qquad -i\omega W = -lDJ_1(la_i), \qquad \therefore D = \frac{i\omega W}{lJ_1(la_i)},$$

$$-i\omega W = mGI_1(ma_i), \qquad \therefore G = -\frac{i\omega W}{mI_1(ma_i)} . \tag{51}$$

The constants in the expressions for the fluid pressure fields can be eliminated, and the following simplified results are obtained using equations (41), (42), (43), and (50) for p_s and equations (45), (46), (47), and (51) for p_i:

Outer Fluid **Inner Fluid**

$$p_s(r) = \frac{-\omega^2 \rho_o W H_o^1(gr)\, e^{i(kx-\omega t)}}{g H_1^1(g a_o)} \qquad p_i(r) = \frac{-\omega^2 \rho_i W J_o(lr)\, e^{i(kx-\omega t)}}{l J_1(l a_i)}$$

$$p_s(r) = \frac{-\omega^2 \rho_o W K_o(fr)\, e^{i(kx-\omega t)}}{f K_1(f a_o)} \qquad p_i(r) = \frac{\omega^2 \rho_i W I_o(mr)\, e^{i(kx-\omega t)}}{m I_1(m a_i)} \,. \tag{52}$$

The internal and external pressure fields have been expressed in terms of the radial motion of the shell, *W*. Let us make the following simplifications to equation (52) and evaluate the pressure at the required radii, then we will return to the shell equations of motion:

$$p_s(a_o) = \alpha_s(a_o)\, W e^{i(kx-\omega t)} \qquad \alpha_s(a_o) = \frac{-\omega^2 \rho_o H_o^1(g a_o)}{g H_1^1(g a_o)} \quad \text{for} \quad \frac{\omega^2}{c_o^2} > k^2,$$

$$\alpha_s(a_o) = \frac{-\omega^2 \rho_o K_o(f a_o)}{f K_1(f a_o)} \quad \text{for} \quad k^2 > \frac{\omega^2}{c_o^2} \,. \tag{53}$$

$$p_i(r) = \alpha_i(r)\, W e^{i(kx-\omega t)} \qquad \alpha_i(r) = \frac{-\omega^2 \rho_i J_o(lr)}{l J_1(l a_i)} \quad \text{for} \quad \frac{\omega^2}{c_i^2} > k^2,$$

$$\alpha_i(r) = \frac{\omega^2 \rho_i I_o(mr)}{m I_1(m a_i)} \quad \text{for} \quad k^2 > \frac{\omega^2}{c_i^2} \,. \tag{54}$$

$$p_i(a_i) = \alpha_i(a_i)\, W e^{i(kx-\omega t)} \qquad \alpha_i(a_i) = \frac{-\omega^2 \rho_i J_o(l a_i)}{l J_1(l a_i)} \quad \text{for} \quad \frac{\omega^2}{c_i^2} > k^2,$$

$$\alpha_i(a_i) = \frac{\omega^2 \rho_i I_o(m a_i)}{m I_1(m a_i)} \quad \text{for} \quad k^2 > \frac{\omega^2}{c_i^2} \,. \tag{55}$$

AXISYMMETRIC RESPONSE

MEMBRANE SHELL

Let us simplify the problem and consider only zeroth order axisymmetric excitation in the radial direction. Pressure fields will be symmetric with respect to θ; therefore, we will simplify the equations with the following conditions and eliminate the p_x excitation:

$$\frac{\partial}{\partial\theta} = 0, \qquad v = 0, \qquad p_\theta = 0, \qquad \text{and} \qquad p_x = 0 \cdot$$

The specially orthotropic stress-strain relations are used, which are represented by the unbarred quantities. Under these simplifications, equations (22) through (24) reduce to

$$C_{11}\frac{\partial^2 u}{\partial x^2} + C_{12}\frac{1}{a}\frac{\partial w}{\partial x} = \rho h\frac{\partial^2 u}{\partial t^2}, \tag{56}$$

$$p_i(a_i) - p_o - p_s(a_o) - \frac{1}{a}C_{12}\frac{\partial u}{\partial x} + -C_{22}\frac{1}{a^2}w + T\frac{\partial^2 w}{\partial x^2} = \rho h\frac{\partial^2 w}{\partial t^2}\cdot \tag{57}$$

The excitation pressure field, p_o, and the solution for the displacement response are

$$p_o = P_o e^{i(kx-\omega t)},$$

$$u = Ue^{i(kx-\omega t)}, \qquad w = We^{i(kx-\omega t)}. \tag{58}$$

Using the derivatives

$$\frac{\partial u}{\partial x} = ikUe^{i(kx-\omega t)}, \qquad \frac{\partial^2 w}{\partial x^2} = -k^2 We^{i(kx-\omega t)},$$

$$\frac{\partial^2 u}{\partial x^2} = -k^2 Ue^{i(kx-\omega t)}, \qquad \frac{\partial^2 u}{\partial t^2} = -\omega^2 Ue^{i(kx-\omega t)},$$

$$\frac{\partial w}{\partial x} = ikWe^{i(kx-\omega t)}, \qquad \frac{\partial^2 w}{\partial t^2} = -\omega^2 We^{i(kx-\omega t)}, \tag{59}$$

we write the equations of motion, equations (56) and (57), as

$$-C_{11}k^2U + \frac{C_{12}ikW}{a} = -\rho h\omega^2 U, \tag{60}$$

$$-\frac{C_{12}ikU}{a} - \frac{C_{22}W}{a^2} + \alpha_i(a_i)W - P_o - \alpha_s(a_o)W - Tk^2W = -\rho h\omega^2 W. \tag{61}$$

Assembling equations (60) and (61) in matrix form, we now have the system described in terms of a combined dynamic stiffness and mass matrix times a displacement vector equal to a forcing vector:

$$\begin{bmatrix} \dfrac{-C_{12}ik}{a} & \rho h\omega^2 - \dfrac{C_{22}}{a^2} + \alpha_i(a_i) - \alpha_s(a_o) - Tk^2 \\ \rho h\omega^2 - C_{11}k^2 & \dfrac{C_{12}ik}{a} \end{bmatrix} \begin{bmatrix} U \\ W \end{bmatrix} = \begin{bmatrix} P_o \\ 0 \end{bmatrix}. \tag{62}$$

The solution for W is

$$W = \frac{P_o}{\rho h\omega^2 - \dfrac{C_{22}}{a^2} - \dfrac{C_{12}^2 k^2}{a^2(\rho h\omega^2 - C_{11}k^2)} + \alpha_i(a_i) - \alpha_s(a_o) - Tk^2}. \tag{63}$$

By substitution of $c_{ll}^2 = \dfrac{C_{11}}{\rho h}$, equation (63) can be rearranged into a form commonly seen in some of the literature. When the denominator is multiplied by $1/C_{11}/1/C_{11}$, equation (63) then becomes

$$W = \frac{P_o}{\rho h\omega^2 - \dfrac{1}{a^2}\left(C_{22} - \dfrac{\dfrac{C_{12}^2}{C_{11}}k^2}{k^2 - k_{ll}^2}\right) + \alpha_i(a_i) - \alpha_s(a_o) - Tk^2}. \tag{64}$$

Transfer Functions and Wave Speeds

We can now proceed directly to an expression for the transfer function between the internal pressure and the applied external pressure excitation. The pressure field in the internal fluid can be written directly from equations (54) and (64) as

$$p_i(r) = \frac{\alpha_i(r) P_o e^{i(kx - \omega t)}}{\rho h\omega^2 - \dfrac{1}{a^2}\left(C_{22} - \dfrac{\dfrac{C_{12}^2}{C_{11}}k^2}{k^2 - k_{ll}^2}\right) + \alpha_i(a_i) - \alpha_s(a_o) - Tk^2}. \tag{65}$$

The magnitude squared of the transfer function can be expressed as

$$|T_r|^2 = \left|\frac{p_i(r)}{P_o}\right|^2 = \left|\frac{\alpha_i(r)}{\rho h\omega^2 - \frac{1}{a^2}\left(C_{22} - \frac{\frac{C_{12}^2}{C_{11}}k^2}{k^2 - k_{ll}^2}\right) + \alpha_i(a_i) - \alpha_s(a_o) - Tk^2}\right|^2 . \tag{66}$$

The wave speeds in the system can be analyzed by setting the determinant of the system matrix, equation (62), equal to zero and rearranging the resulting expression in terms of $c = \omega/k$. Even for this relatively simple system of a membrane shell with inner and outer fluids, we would have to resort to numerical techniques to determine the behavior of the wave speeds.

We can gain insight into the free wave speeds of the structure by working with the denominator of equation (64) for a limited domain of wavenumber and frequency. At a resonant wavenumber and frequency corresponding to the free wave speed of the system, W will reach a maximum when the denominator equals zero. We will limit our domain of interest to a wavenumber range that corresponds to a small argument approximation for the Bessel functions. This range is not necessarily "low wavenumber," as in the acoustic use of the word. The region will also be one of low frequency. The effects of the outer fluid and the static tension will be considered negligible. We will arrive at simple expressions for the breathing wave and extensional wave speeds.

For the region $k^2 > \frac{\omega^2}{c_i^2}$, we make an approximation for p_i by assuming that

$$k \gg \frac{\omega}{c_i} \qquad \therefore \quad m \sim k,$$

$$I_o(ka_i) \sim 1, \qquad I_1(ka_i) \sim \frac{ka_i}{2}, \tag{67}$$

which results in

$$\frac{I_o}{I_1} \sim \frac{2}{ka_i} \qquad \text{and} \qquad \alpha_i(a_i) \sim \frac{2\omega^2\rho_i}{k^2 a_i} \sim \frac{2\rho_i c^2}{a_i} .$$

We set $T = 0$ and consider $\rho h\omega^2$ to be small compared with the other terms because we restrict ourselves to low frequency. We find the denominator of equation (64) simplified to

$$-\frac{1}{a^2}\left(C_{22} - \frac{\frac{C_{12}^2}{C_{11}}k^2}{k^2 - k_{ll}^2}\right) + \alpha_i(a_i) = 0 . \tag{68}$$

For wavenumbers larger than k_{II}, equation (68) reduces to

$$-\frac{1}{a^2}\left(C_{22}-\frac{C_{12}^2}{C_{11}}\right)+\frac{2\rho_i c^2}{a_i}=0. \tag{69}$$

Solving equation (69) for c, we find the simplified expression for the breathing wave speed, c_b, given as a function of the stiffness matrix coefficients where

$$c_b=\sqrt{\frac{a_i}{2\rho_i a^2}\left(C_{22}-\frac{C_{12}^2}{C_{11}}\right)}. \tag{70}$$

The simplest expression for the breathing wave speed is obtained with an isotropic shell, where the material properties are the same in the three coordinate directions. Such a shell is termed an unreinforced shell. Multiplying the elements of the stiffness matrix, equation (5), by h would then give us the stiffness coefficients needed for equation (70):

$$C_{11}=\frac{hE}{1-\nu^2},\qquad C_{22}=\frac{hE}{1-\nu^2},\qquad C_{12}=\frac{\nu hE}{1-\nu^2}. \tag{71}$$

For the isotropic shell, with all the simplifying assumptions previously mentioned, equation (70) reduces to the following expression:

$$c_b=\sqrt{\frac{hEa_i}{2\rho_i a^2}}. \tag{72}$$

The compliance coefficients exhibit a symmetry property that results in

$$\frac{\nu_{12}}{E_1}=\frac{\nu_{21}}{E_2}. \tag{73}$$

The specially orthotropic stiffness matrix in equation (4) simplifies to the following expression when it is substituted into equation (70), making use of the symmetry property of equation (73) as follows

$$c_b=\sqrt{\frac{hE_2a_i}{2\rho_i a^2}}. \tag{74}$$

The breathing wave speeds given by equations (72) and (74) are not affected by the axial properties of the shell. This condition is a direct result of the simplifying assumption that $k > k_{II}$. In general, the breathing wave is affected by the axial shell properties; however, the effect cannot be observed from the simple expressions.

If the fluids and static tension are ignored in the denominator of equation (64), the velocity for the second wave that the shell will propagate is given by equation (75). Two terms with ω^2 have been set to zero since they are small compared with other terms. Therefore, equation (75) has been linearized with respect to frequency. This second wave is commonly referred to as the extensional wave, because its primary displacement is in the longitudinal direction, representing a stretching and contraction of the shell, as given by

$$c_l = \sqrt{\frac{E_1}{\rho}} \qquad \text{Specially Orthotropic}$$

and

$$c_l = \sqrt{\frac{E}{\rho}} \qquad \text{Isotropic.} \tag{75}$$

NONAXISYMMETRIC RESPONSE

MEMBRANE SHELL

Specially Orthotropic

Returning to the full system description seen in equations (22) through (26), we will not make the simplifying assumptions that reduce the problem to the zeroth order axisymmetric response. In keeping the variation with respect to θ, we will analyze the response of the structure to nonaxisymmetric excitation. Working with the response (equation (26)) allows the following derivatives to be formed:

$$u = U\cos(n\theta)\,e^{i(kx-\omega t)}, \quad v = V\sin(n\theta)\,e^{i(kx-\omega t)}, \quad w = W\cos(n\theta)\,e^{i(kx-\omega t)}, \tag{76}$$

$$\frac{\partial^2 u}{\partial x^2} = -k^2 U\cos(n\theta)\,e^{i(kx-\omega t)},$$

$$\frac{\partial u}{\partial x} = ikU\cos(n\theta)\,e^{i(kx-\omega t)},$$

$$\frac{\partial^2 u}{\partial \theta^2} = -n^2 U\cos(n\theta)\,e^{i(kx-\omega t)},$$

$$\frac{\partial^2 u}{\partial \theta \partial x} = -iknU\sin(n\theta)\,e^{i(kx-\omega t)},$$

$$\frac{\partial^2 v}{\partial \theta \partial x} = iknV\cos(n\theta)\,e^{i(kx-\omega t)},$$

$$\frac{\partial^2 v}{\partial x^2} = -k^2 V\sin(n\theta)\,e^{i(kx-\omega t)},$$

$$\frac{\partial v}{\partial \theta} = nV\cos(n\theta)\,e^{i(kx-\omega t)},$$

$$\frac{\partial^2 v}{\partial \theta^2} = -n^2 V\sin(n\theta)\,e^{i(kx-\omega t)},$$

$$\frac{\partial w}{\partial x} = ikW\cos(n\theta)\,e^{i(kx-\omega t)},$$

$$\frac{\partial^2 w}{\partial x^2} = -k^2 W\cos(n\theta)\,e^{i(kx-\omega t)},$$

and

$$\frac{\partial w}{\partial \theta} = -nW\sin(n\theta)\,e^{i(kx-\omega t)}. \tag{77}$$

Equations (53) through (55) will be modified with the addition of the $cos(n\theta)$ term, as shown in equation (38), along with the generalization of the Bessel function to order n:

$$p_s(a_o) = \alpha_s(a_o)\cos(n\theta)\,We^{i(kx-\omega t)} \qquad \alpha_s(a_o) = \frac{\omega^2\rho_o H_n^1(ga_o)}{H_n^{1\prime}(ga_o)} \quad \text{for} \quad \frac{\omega^2}{c_o^2} > k^2,$$

$$\alpha_s(a_o) = \frac{\omega^2\rho_o K_n(fa_o)}{K_n'(fa_o)} \quad \text{for} \quad k^2 > \frac{\omega^2}{c_o^2}. \tag{78}$$

$$p_i(r) = \alpha_i(r)\cos(n\theta)\,We^{i(kx-\omega t)} \qquad \alpha_i(r) = \frac{\omega^2\rho_i J_n(lr)}{J_n'(la_i)} \quad \text{for} \quad \frac{\omega^2}{c_i^2} > k^2,$$

$$\alpha_i(r) = \frac{\omega^2\rho_i I_n(mr)}{I_n'(ma_i)} \quad \text{for} \quad k^2 > \frac{\omega^2}{c_i^2}. \tag{79}$$

$$p_i(a_i) = \alpha_i(a_i)\cos(n\theta)\,We^{i(kx-\omega t)} \qquad \alpha_i(a_i) = \frac{\omega^2\rho_i J_n(la_i)}{J_n'(la_i)} \quad \text{for} \quad \frac{\omega^2}{c_i^2} > k^2,$$

$$\alpha_i(a_i) = \frac{\omega^2\rho_i I_n(ma_i)}{I_n'(ma_i)} \quad \text{for} \quad k^2 > \frac{\omega^2}{c_i^2}. \tag{80}$$

The prime used with the Bessel functions in equations (78) through (80) indicates differentiation with respect to r, according to the following example

$$H_n^{1\prime}(ga_o) = \frac{\partial}{\partial r}(H_n^1(gr))\Big|_{r=a_o}.$$

Equations (77) through (80) and equation (25) are substituted into equations (22) through (24). The circumferential shear stress, p_θ, will be assumed to be equal to zero. Retaining p_x allows for the study of the system response to harmonic axial shear stress excitation. We arrive at the three equations in the x, θ, and r directions:

$$-C_{11}k^2U + \frac{C_{12}}{a}(iknV + ikW) + \frac{C_{66}}{a}(iknV - \frac{1}{a}n^2U) + P_x = -\rho h\omega^2 U,$$

$$-\frac{C_{12}}{a}iknU - \frac{C_{22}}{a^2}(n^2V + nW) - C_{66}k^2V - iknU\frac{C_{66}}{a} = -\rho h\omega^2 V,$$

$$(\alpha_i(a_i) - \alpha_s(a_o))W - P_o - \frac{C_{12}}{a}ikU - \frac{C_{22}}{a^2}(nV + W) - Tk^2W = -\rho h\omega^2 W. \tag{81}$$

Rearranging equation (81), we have the following system description in matrix form:

$$\begin{bmatrix} \rho h\omega^2 - C_{11}k^2 - \dfrac{C_{66}n^2}{a^2} & \dfrac{(C_{12}+C_{66})\,ikn}{a} & \dfrac{ikC_{12}}{a} \\ -\dfrac{(C_{12}+C_{66})\,ikn}{a} & \rho h\omega^2 - \dfrac{n^2}{a^2}C_{22} - k^2C_{66} & \dfrac{-n}{a^2}C_{22} \\ -\dfrac{C_{12}ik}{a} & \dfrac{-C_{22}n}{a^2} & \alpha_i(a_i) - \alpha_s(a_o) + \rho h\omega^2 - \dfrac{C_{22}}{a^2} - Tk^2 \end{bmatrix} \begin{bmatrix} U \\ V \\ W \end{bmatrix} = \begin{bmatrix} -P_x \\ 0 \\ P_o \end{bmatrix}. \tag{82}$$

Solution of equation (82) for W will give us a description of the interior fluid field and the transfer function between applied outer normal pressure and interior fluid pressure at radial position r, which is

$$W = \frac{(AB - N^2)\,P_o + -i\left(\dfrac{kn^2\,(C_{12}+C_{66})\,C_{22}}{a^3} + \dfrac{kC_{12}B}{a}\right)P_x}{O\,(AB - N^2) - \dfrac{n^2}{a^4}\,(2k^2\,(C_{12}+C_{66})\,C_{22}C_{12} + C_{22}^2A) - \dfrac{k^2C_{12}B}{a^2}},$$

where

$$A = \rho h\omega^2 - k^2C_{11} + -\frac{n^2}{a^2}C_{66},$$

$$B = \rho h\omega^2 - k^2C_{66} + -\frac{n^2}{a^2}C_{22},$$

$$N = \frac{kn}{a}\,(C_{12}+C_{66}),$$

and

$$O = \alpha_i(a_i) - \alpha_s(a_o) + \rho h\omega^2 - \frac{C_{22}}{a^2} - Tk^2. \tag{83}$$

The pressure in the internal fluid can be written from equations (79) and (83) as

$$p_i(r) = \alpha_i(r)\,\frac{(AB - N^2)\,P_o + -i\left(\dfrac{kn^2\,(C_{12}+C_{66})\,C_{22}}{a^3} + \dfrac{kC_{12}B}{a}\right)P_x}{O\,(AB - N^2) - \dfrac{n^2}{a^4}\,(2k^2\,(C_{12}+C_{66})\,C_{22}C_{12} + C_{22}^2A) - \dfrac{k^2C_{12}B}{a^2}} \times \cos(n\theta)\,e^{i(kx - \omega t)}. \tag{84}$$

Let us separate equation (84) into two expressions that individually show the effect of outer normal pressure on internal fluid pressure and the effect of shear stress on internal fluid pressure. Equation (85) is an expression for the magnitude squared of the transfer function between pressure in the internal fluid and the applied normal pressure excitation:

$$|T_r|^2 = \left|\frac{p_i(r)}{P_o}\right|^2 = \left|\frac{\alpha_i(r)\,(AB-N^2)}{O\,(AB-N^2) - \frac{n^2}{a^4}\left(2k^2\,(C_{12}+C_{66})\,C_{22}C_{12} + C_{22}^2A\right) - \frac{k^2C_{12}B}{a^2}}\right|^2. \tag{85}$$

The magnitude squared of the transfer function between pressure in the internal fluid and the applied shear stress in the longitudinal x-direction is

$$|T_x|^2 = \left|\frac{p_i(r)}{P_x}\right|^2 = \left|\left(\frac{-\alpha_i(r)\left(\frac{kn^2\,(C_{12}+C_{66})\,C_{22}}{a^3} + \frac{kC_{12}B}{a}\right)}{O\,(AB-N^2) - \frac{n^2}{a^4}\left(2k^2\,(C_{12}+C_{66})\,C_{22}C_{12} + C_{22}^2A\right) - \frac{k^2C_{12}B}{a^2}}\right)\right|^2. \tag{86}$$

BENDING SHELL

Generally Orthotropic

Returning to the bending shell, we want to solve equation (33) for the displacement magnitude W as was done in the last section for the membrane shell. The excitation pressure fields, p_o and p_x, and the solution to equation (33) are given by the following expressions:

$$p_o = P_o e^{i(kx+n\theta-\omega t)}, \qquad p_x = P_x e^{i(kx+n\theta-\omega t)},$$

$$u = Ue^{i(kx+n\theta-\omega t)}, \qquad v = Ve^{i(kx+n\theta-\omega t)}, \qquad w = We^{i(kx+n\theta-\omega t)}. \tag{87}$$

The interior pressure fields from equations (78) through (80) are modified accordingly as

$$p_s(a_o) = \alpha_s(a_o)\,We^{i(kx+n\theta-\omega t)},$$

$$p_i(r) = \alpha_i(r)\,We^{i(kx+n\theta-\omega t)},$$

$$p_i(a_i) = \alpha_i(a_i)\,We^{i(kx+n\theta-\omega t)}. \tag{88}$$

The solution proceeds as follows. The displacements, equation (87), are differentiated as required and substituted into the equations for the stress resultants, equation (13). The stress resultants are then differentiated as required and substituted into the equations of motion, equation (33), along with the forms for the pressure fields p_i and p_s given by equation (88). Terms are collected and the following dynamic system matrix results:

$$\begin{bmatrix} S_{11} & S_{12} & S_{13} \\ S_{21} & S_{22} & S_{23} \\ S_{31} & S_{32} & S_{33} \end{bmatrix} \begin{bmatrix} U \\ V \\ W \end{bmatrix} = \begin{bmatrix} P_x \\ 0 \\ P_o \end{bmatrix} . \tag{89}$$

The elements of the system matrix S are

$$S_{11} = D_{11}k^2 + 2D_{16}k\frac{n}{a} + D_{66}\frac{n^2}{a^2} + K_{66}\frac{n^2}{a^4} + -\rho h\omega^2,$$

$$S_{12} = D_{12}k\frac{n}{a} + D_{16}k^2 + D_{26}\frac{n^2}{a^2} + D_{66}k\frac{n}{a} + K_{16}\frac{k^2}{a^2},$$

$$S_{13} = i\left(-D_{12}\frac{k}{a} - D_{26}\frac{n}{a^2} - K_{11}\frac{k^3}{a} - K_{16}k^2\frac{n}{a^2} - K_{26}\frac{(n-n^3)}{a^4} + K_{66}k\frac{n^2}{a^3}\right),$$

$$S_{21} = -D_{12}k\frac{n}{a} - D_{26}\frac{n^2}{a^2} - D_{16}k^2 - D_{66}k\frac{n}{a} + -K_{16}\frac{k^2}{a^2},$$

$$S_{22} = -D_{22}\frac{n^2}{a^2} - 2D_{26}k\frac{n}{a} - D_{66}k^2 - 3K_{66}\frac{k^2}{a^2} + \rho h\omega^2 + -2K_{26}k\frac{n}{a^3},$$

$$S_{23} = i\left(D_{22}\frac{n}{a^2} + D_{26}\frac{k}{a} + 2K_{16}\frac{k^3}{a} + 3K_{66}k^2\frac{n}{a^2} + K_{12}k^2\frac{n}{a^2} + 2K_{26}k\frac{n^2}{a^3} + \frac{\rho h^3\omega^2}{12}\frac{n}{a^2}\right),$$

$$S_{31} = i\left(-D_{12}\frac{k}{a} - D_{26}\frac{n}{a^2} - K_{11}\frac{k^3}{a} - K_{16}k^2\frac{n}{a^2} + K_{26}\frac{(n^3-n)}{a^4} + K_{66}k\frac{n^2}{a^3}\right),$$

$$S_{32} = i\left(-D_{22}\frac{n}{a^2} - D_{26}\frac{k}{a} - K_{12}k^2\frac{n}{a^2} - 2K_{16}\frac{k^3}{a} - 2K_{26}k\frac{n^2}{a^3} - 3K_{66}k^2\frac{n}{a^2}\right),$$

$$S_{33} = \left(\rho h\omega^2 - \frac{D_{22}}{a^2} + \alpha_i(a_i) - \alpha_s(a_o) + K_{22}\frac{(-n^4+2n^2-1)}{a^4} - K_{11}k^4 - 2K_{12}k^2\frac{n^2}{a^2}\right.$$
$$\left. + K_{26}\left(\frac{2kn-4kn^3}{a^3}\right) - 4K_{66}k^2\frac{n^2}{a^2} - 4K_{16}k^3\frac{n}{a} + \frac{\rho h^3\omega^2}{12}\left(-\frac{n^2}{a^2} + k^2\right) - Tk^2\right) . \tag{90}$$

We will solve equation (89) for W twice, first using P_o as the excitation with $P_x = 0$ and then with P_x as the excitation, with $P_o = 0$, resulting in

$$W_r = \frac{(S_{11}S_{22} - S_{21}S_{12})P_o}{det[S]}, \qquad W_x = \frac{(S_{21}S_{32} - S_{31}S_{22})P_x}{det[S]}. \tag{91}$$

The corresponding transfer function, magnitude squared, between pressure in the inner fluid and the applied external pressure P_o or P_x can be written as follows:

$$|T_r|^2 = \left|\frac{p_i(r)}{P_o}\right|^2 = \left|\frac{W_r\alpha_i(r)}{P_o}\right|^2 \tag{92}$$

and

$$|T_x|^2 = \left|\frac{p_i(r)}{P_x}\right|^2 = \left|\frac{W_x\alpha_i(r)}{P_x}\right|^2. \tag{93}$$

RESULTS

Let us now apply the dynamic model derived thus far by considering the behavior of specific shells. We will examine the deformed shape of the structure for the first four modes of vibration (i.e., n = 0, 1, 2, and 3) for the two solutions previously discussed. The first case consists of a standing wave in the circumferential θ-direction accompanied by a traveling wave in the longitudinal x-direction; the second case consists of a traveling wave solution in θ and x.

Next, using the solutions represented by equations (92) and (93), we shall examine the system response as a function of longitudinal wavenumber and frequency for each elastic model at each of the first four modes of propagation. Effects of fluid loading and reinforcement wrap angle ϕ will be explored as well as the effects of an internal core for the $n = 0$ mode.

We will then explore the strain in an air-backed shell as developed by the normal pressure excitation. With this structure, we shall increase the stiffness of the shell and observe the effects on the magnitude of the strain response as a function of longitudinal wavenumber and frequency.

MODE SHAPES

The mode number n is defined as the number of wavelengths of oscillation that a quantity undergoes with respect to the circumferential direction at a constant x-location. Figure 11 depicts how the displacement u, v, or w would vary with respect to the circumference of the shell. We note that the $n = 0$ shape is such that all points on the circumference move in phase with one another for a given x-location. For n = 1, we observe one wavelength around the circumference. As the mode number increases (i.e., n = 1, 2, 3...), more wavelengths are added within the circumferential length πd. In this report, two solutions to the equations of motion for the shell and

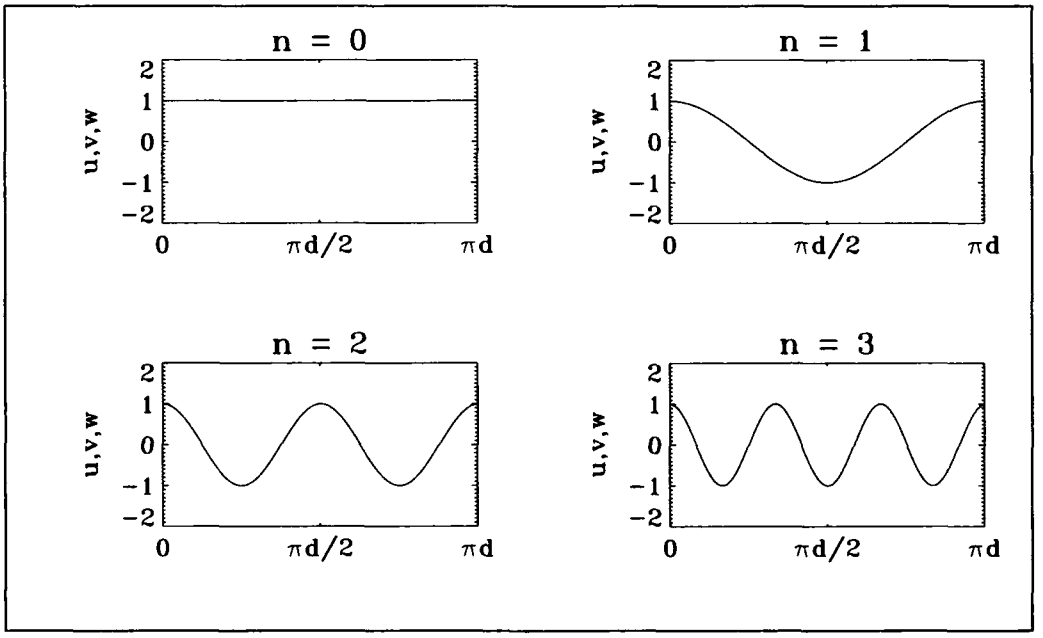

Figure 11. Circumferential Variation of Mode Shapes

fluid are given by equations (26) and (87). Both equations have been applied to depict the deformation of a shell at a given instance in time. Remember that these solutions are for an infinite cylinder; therefore the mode shapes are constructed with a length of shell equal to two wavelengths in order to visualize the displacement that the shell is undergoing. This length is arbitrarily chosen at two wavelengths. Although another length would have been equally correct, it would not necessarily be as instructive for visualizing the mode shapes.

Standing Wave

Figures 12 through 28 have been created from equation (26) for the displacements. As stated before, equation (26) represents a standing wave solution in θ. The mode shape results from a wave traveling in the clockwise and counterclockwise directions. Referring to figure 13, the net result of these pressure fields on the shell is a vibration occurring in the x, $\theta = 0$ plane. The w component of mode 1 causes a translation of the circumference of the shell from the center, resulting in a flexural mode of vibration.

Figure 12 depicts the classic breathing wave, as all points around the circumference at a given x location move in phase in the radial direction. Figures 14 and 15 depict two and then three wavelengths of variation in w around the circumference. The extensional wave, which is the u component of the $n = 0$ mode of propagation, is shown in figure 16, with the higher order modes of u shown in figures 17 through 19. The zeroth order mode in v results in zero tangential displacement as seen from equation (26) and figure 20. Figures 21 through 23 show the effects of the higher modes of v on the shell.

The effects of all three components of displacement (w, u, and v) are imposed on the shell for each mode in figures 24 through 27. To visualize the effects of the combined displacements, the magnitudes of w, u, and v have been arbitrarily chosen to be equal to one another. Actually, the amplitudes U and V are much smaller than W for a radial pressure excitation, which we will consider later. If the actual amplitudes had been displayed for the radial pressure excitation in the correct proportion in figures 24 through 27, only the w mode shape would be visible. Furthermore, the exact proportion of the displacements W/W, V/W, and U/W are functions of the shell and fluid and will be different for each shell model (i.e., isotropic, specially orthotropic, generally orthotropic). These proportions also depend on the magnitude of the elastic constants. We emphasize, therefore, that figures 24 through 27 provide qualitative, not quantitative, information.

Figure 28 is an animation of the w component of the $n = 2$ mode, showing the mode shape for six snapshots in time for the wave propagating in the $+x$-direction. Careful inspection of the figure indicates that the displacement wave is propagating to the left, or positive x-direction.

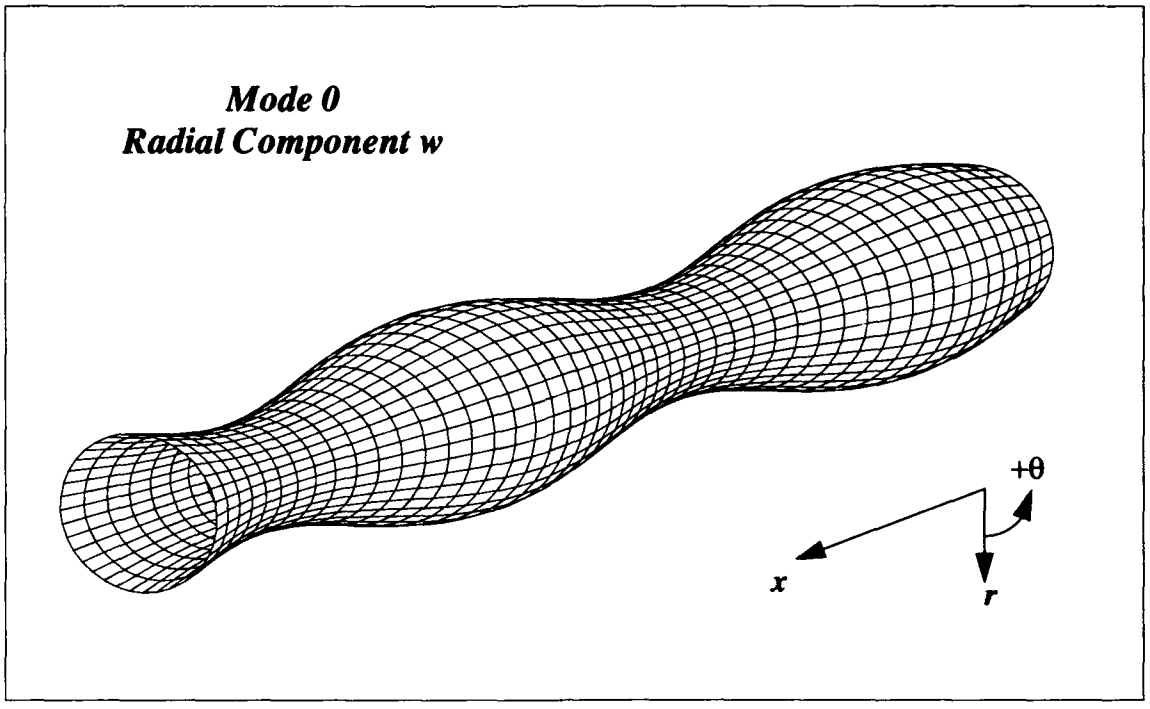

Figure 12. θ Standing Wave Mode Shape; n = 0, w Component

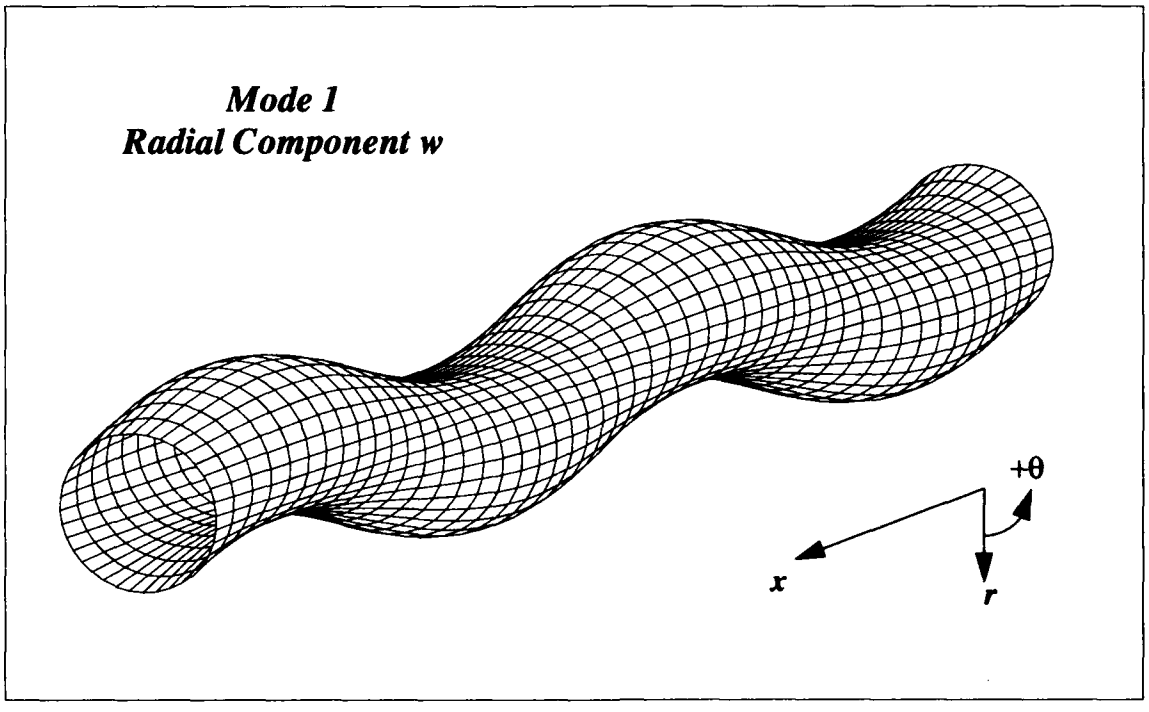

Figure 13. θ Standing Wave Mode Shape; n = 1, w Component

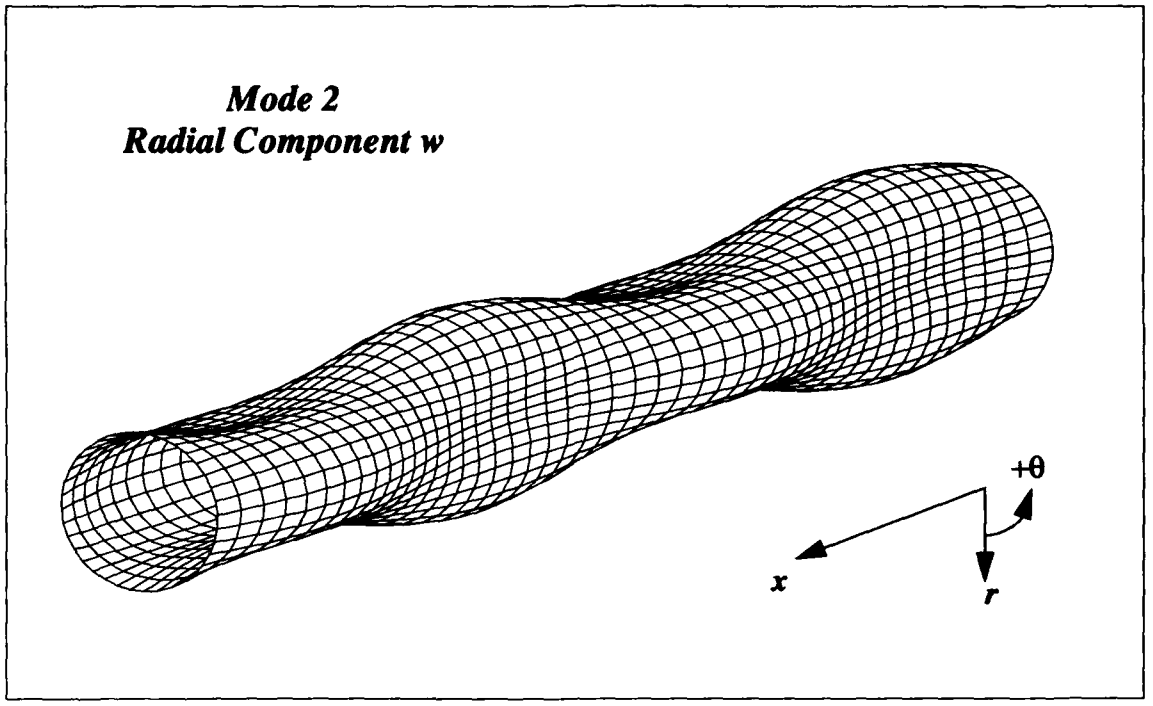

Figure 14. θ Standing Wave Mode Shape; n = 2, w Component

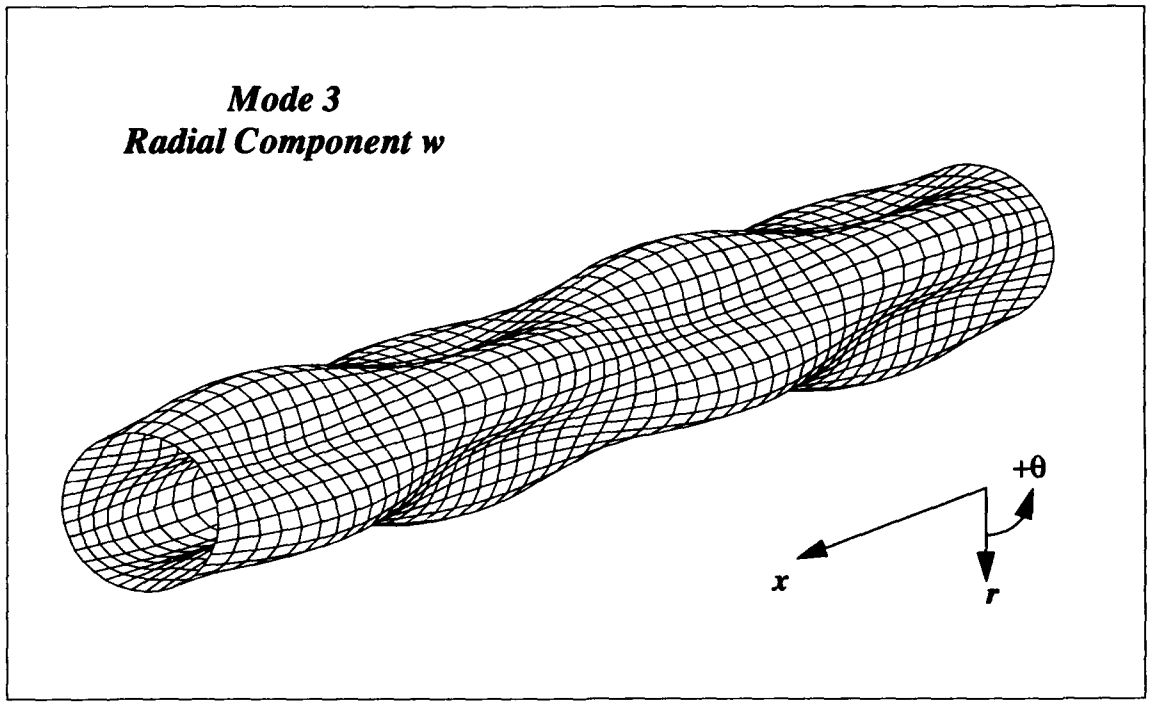

Figure 15. θ Standing Wave Mode Shape; n = 3, w Component

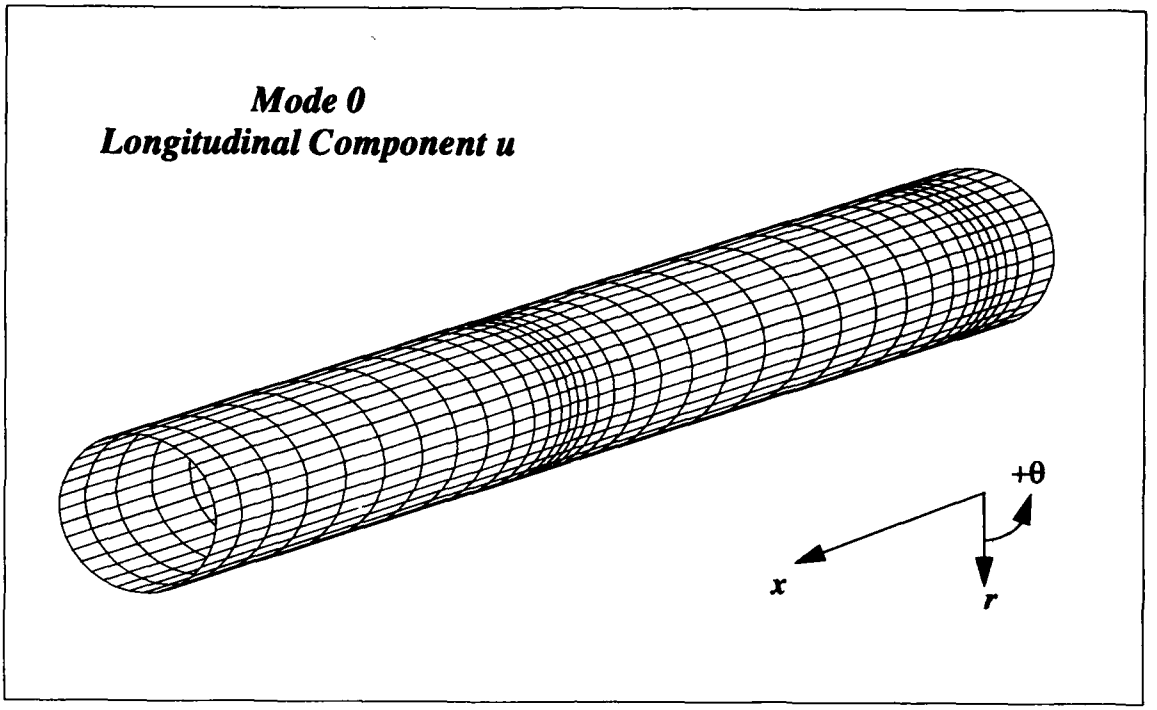

Figure 16. θ Standing Wave Mode Shape; n = 0, u Component

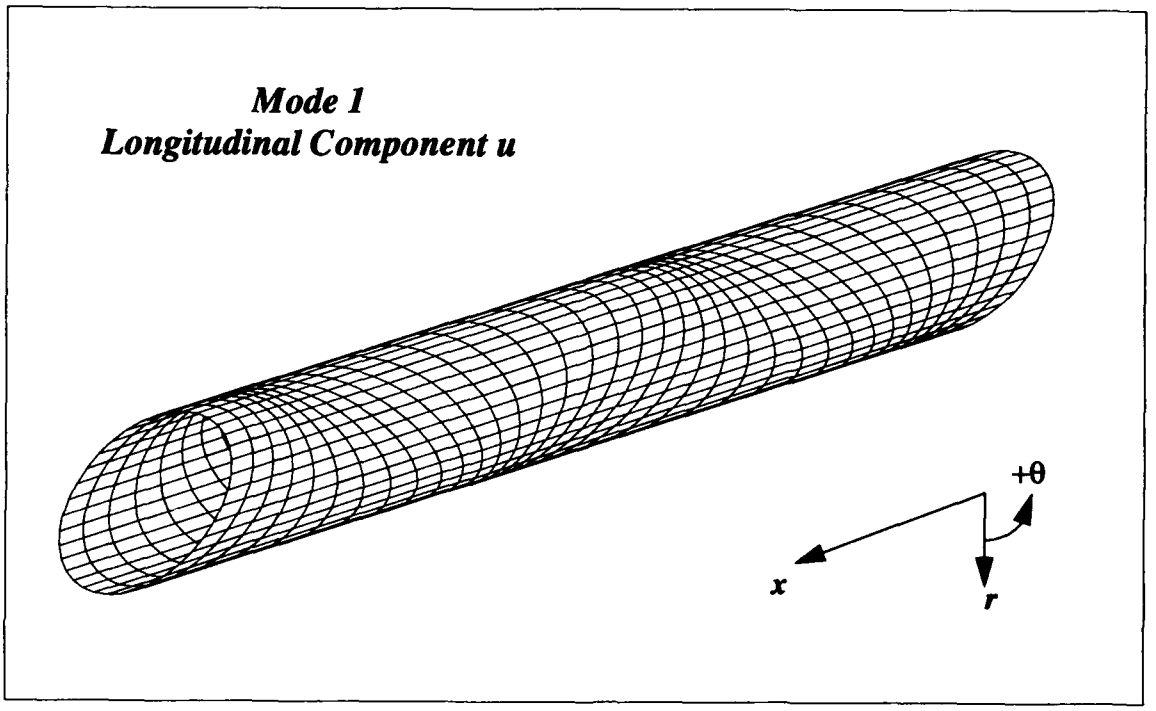

Figure 17. θ Standing Wave Mode Shape; n = 1, u Component

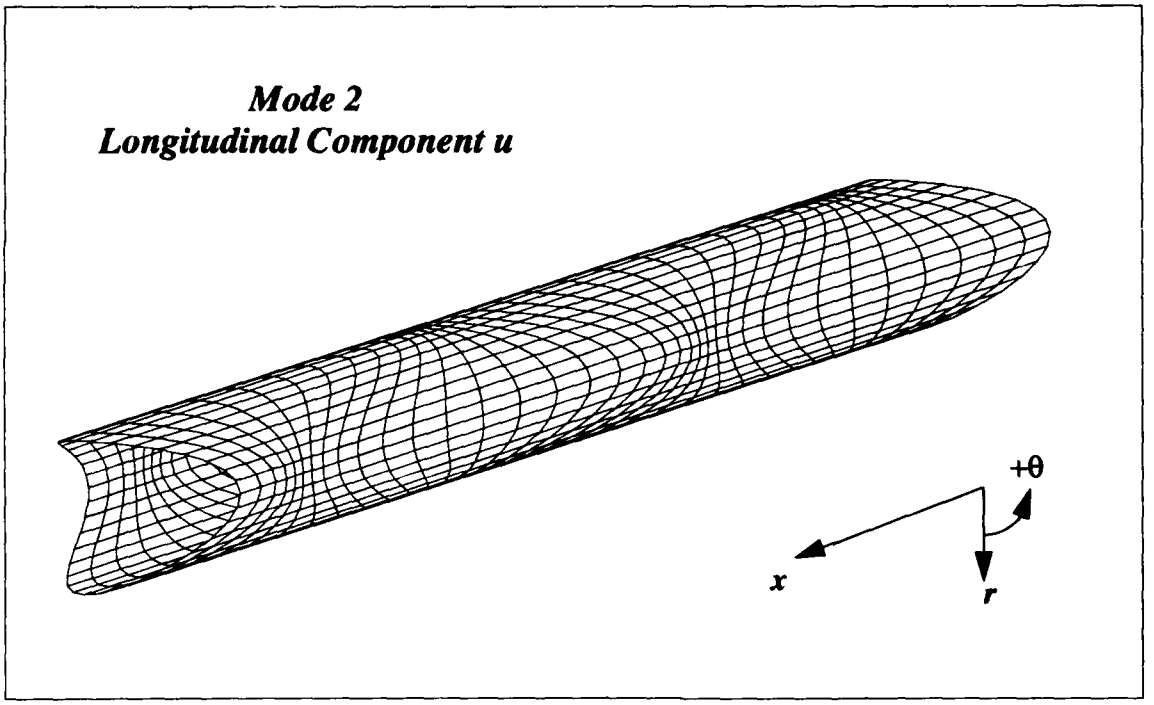

Figure 18. θ Standing Wave Mode Shape; n = 2, u Component

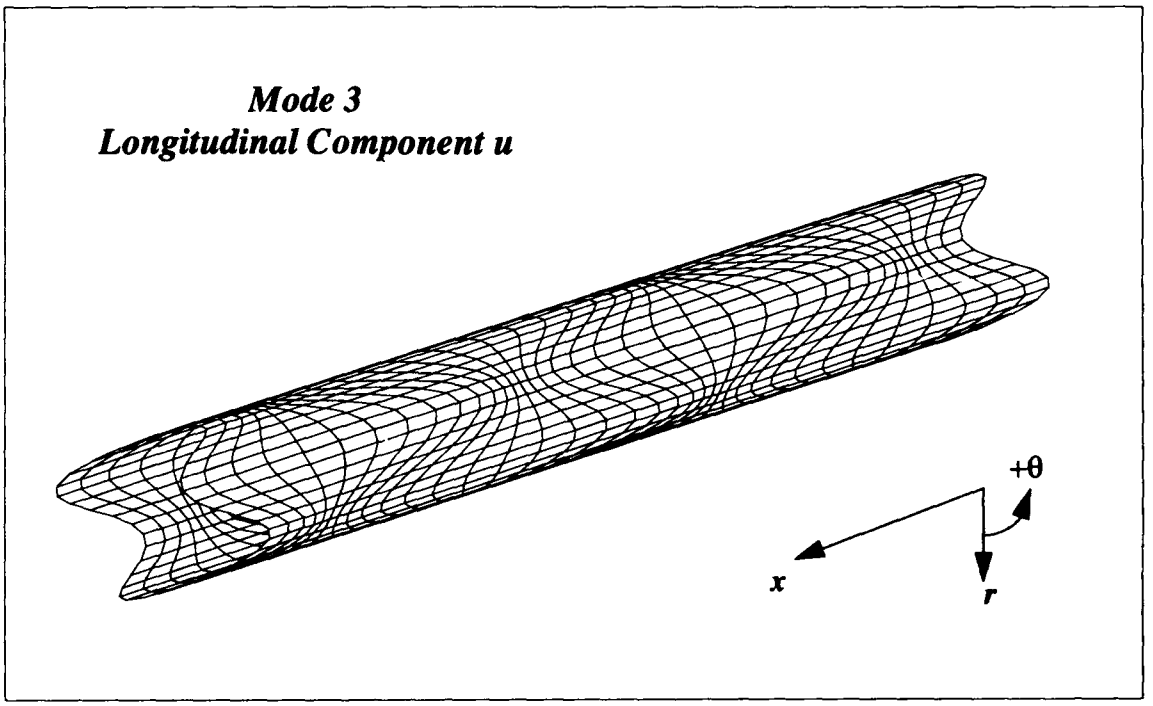

Figure 19. θ Standing Wave Mode Shape; n = 3, u Component

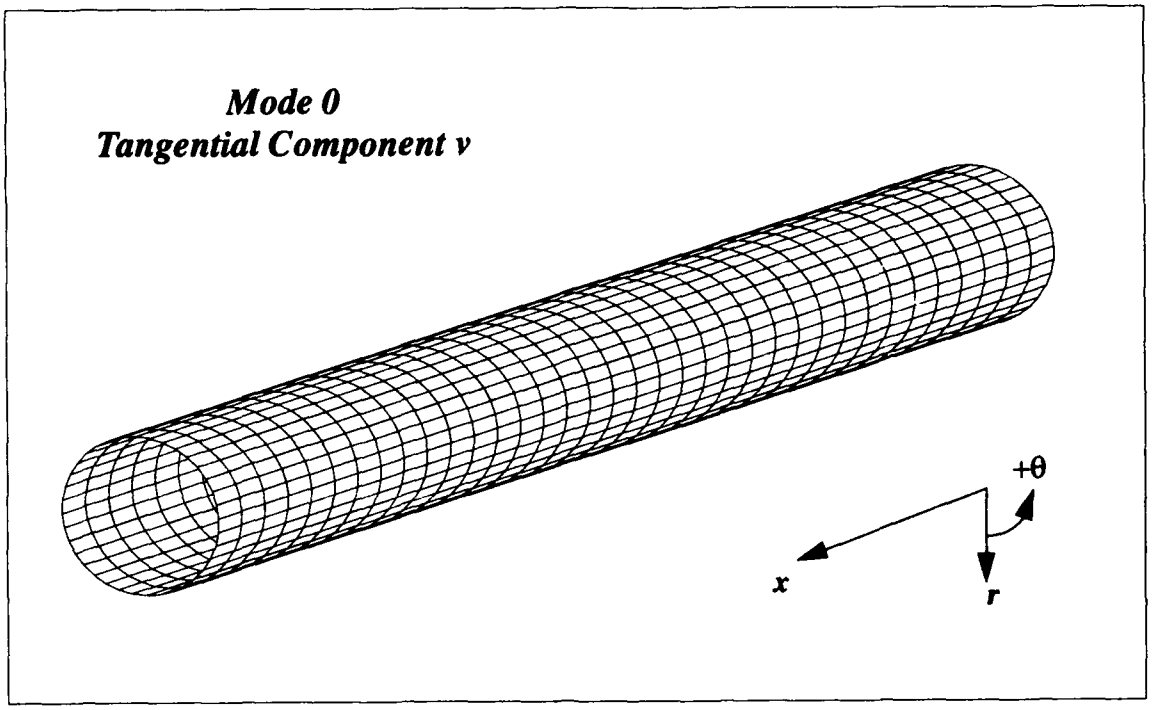

Figure 20. θ Standing Wave Mode Shape; n = 0, v Component

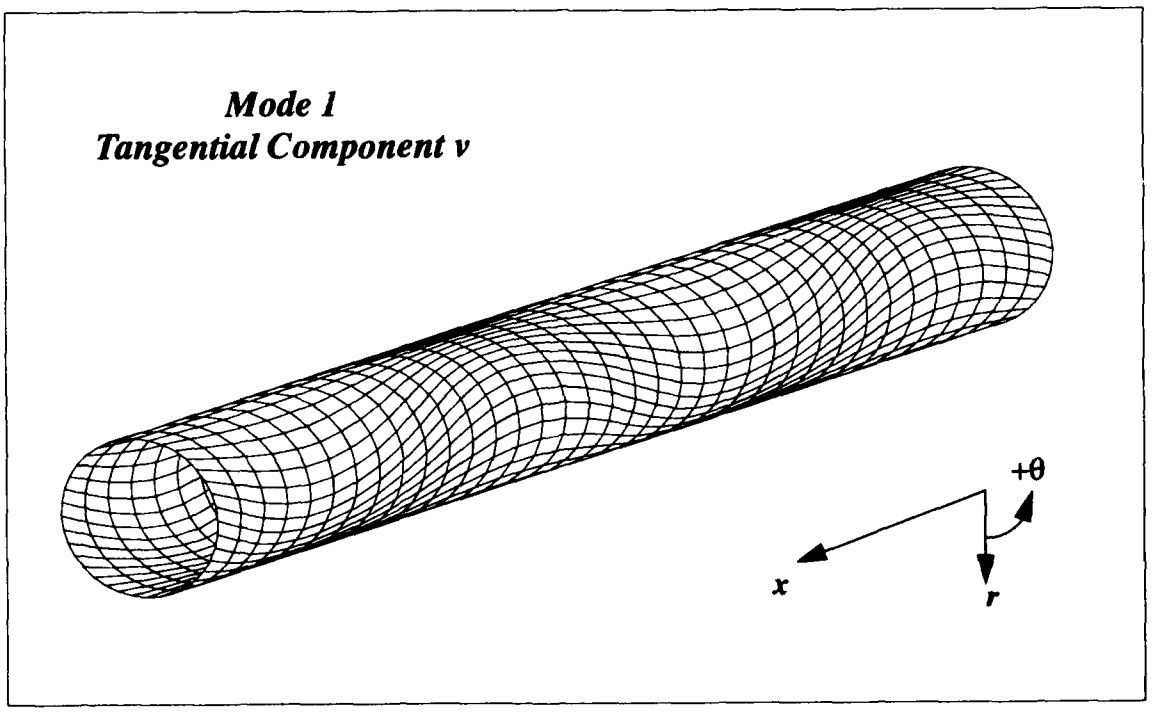

Figure 21. θ Standing Wave Mode Shape; n = 1, v Component

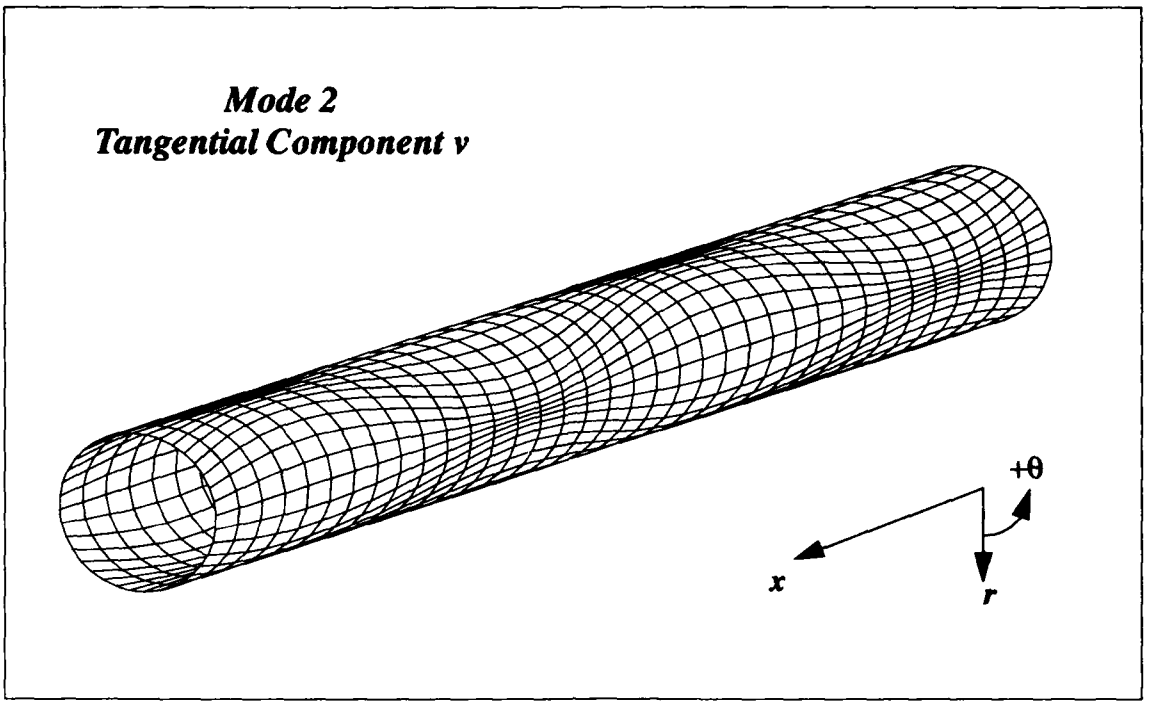

Figure 22. θ Standing Wave Mode Shape; n = 2, v Component

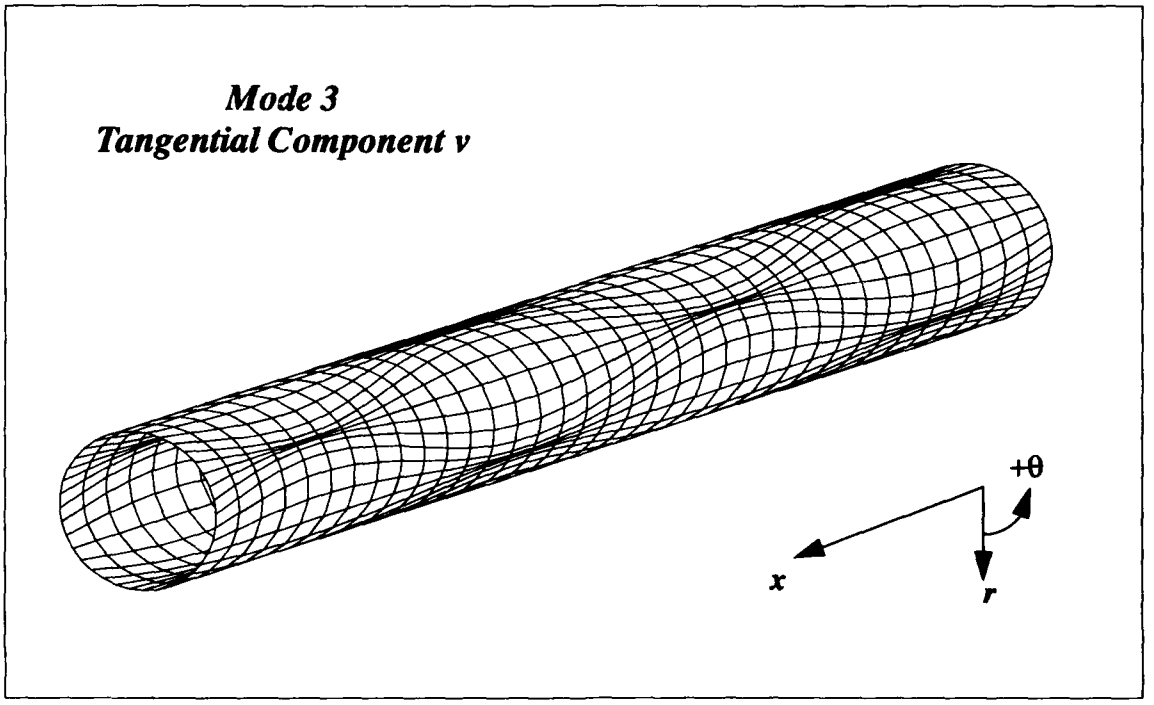

Figure 23. θ Standing Wave Mode Shape; n = 3, v Component

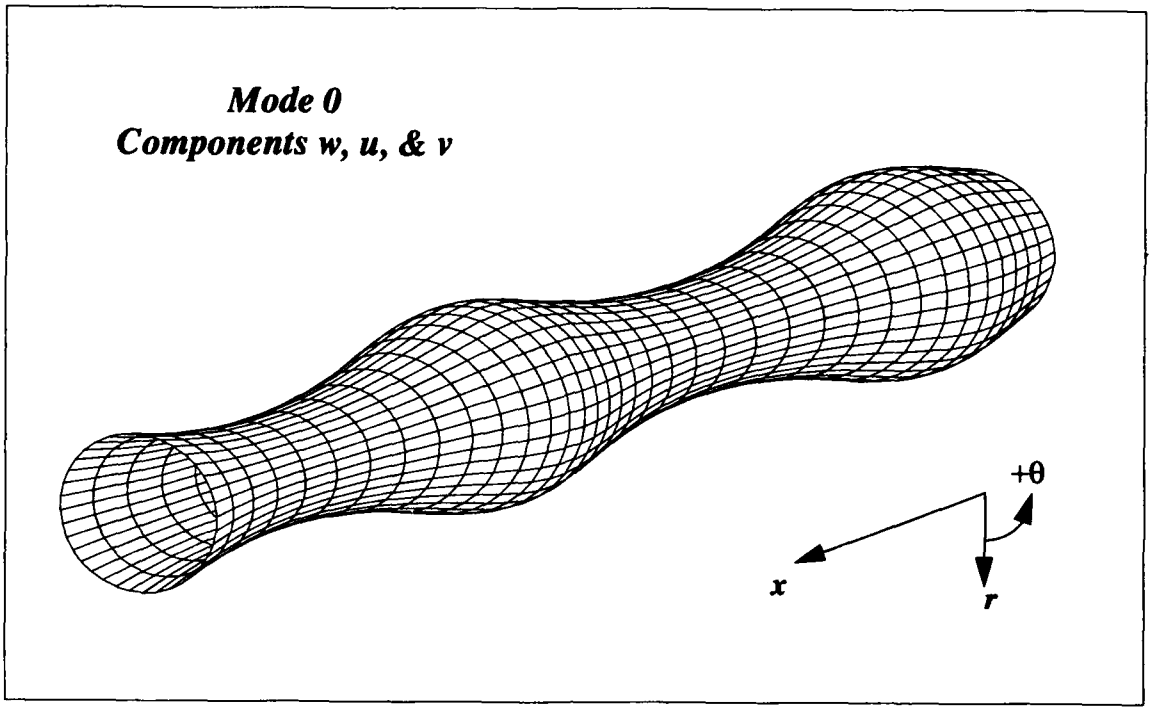

Figure 24. θ Standing Wave Mode Shape; n = 0 for w, u, and v Components

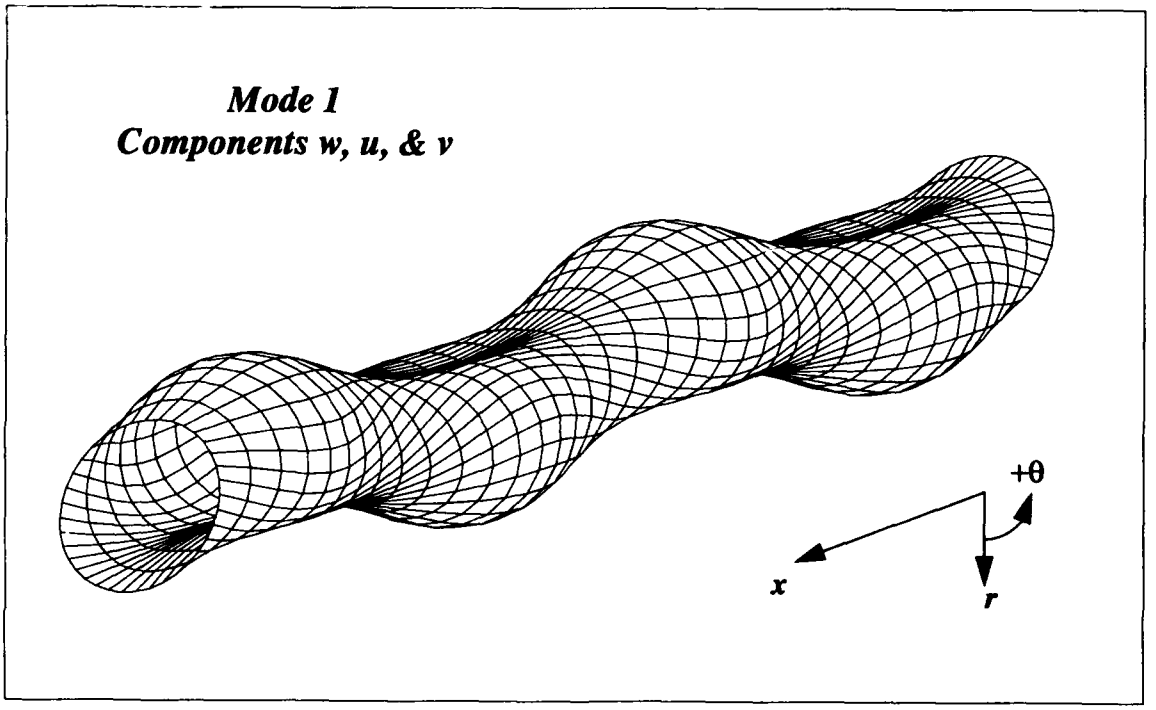

Figure 25. θ Standing Wave Mode Shape; n = 1 for w, u, and v Components

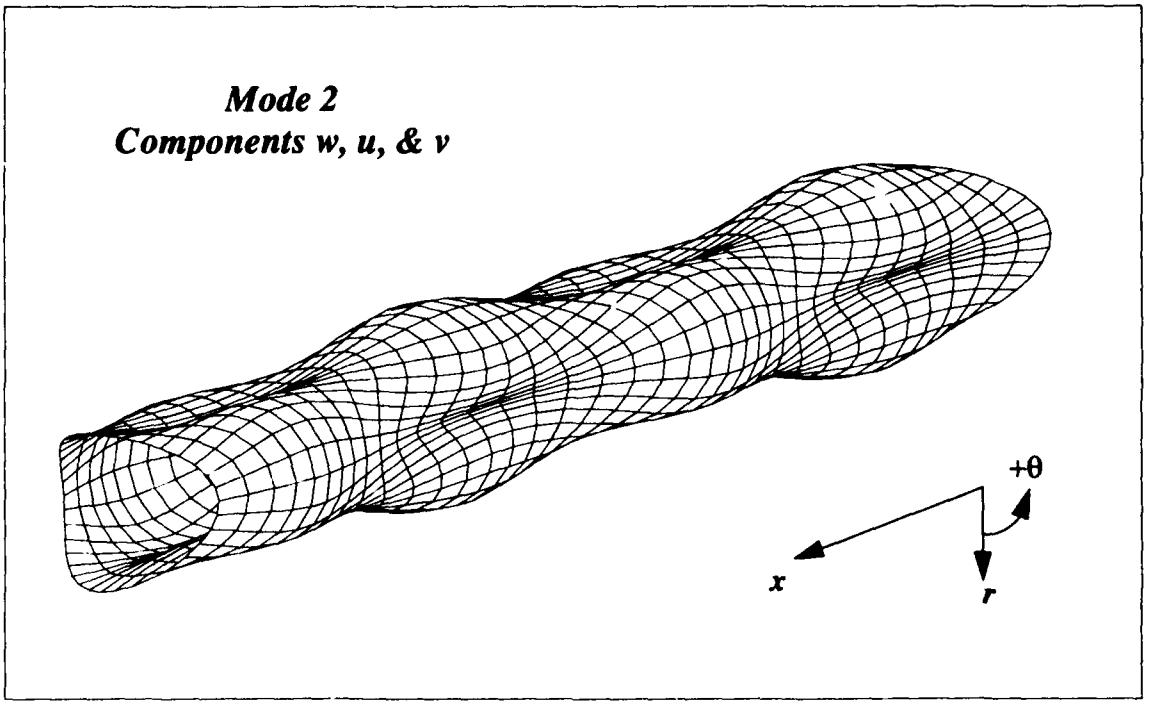

Figure 26. θ Standing Wave Mode Shape; n = 2 for w, u, and v Components

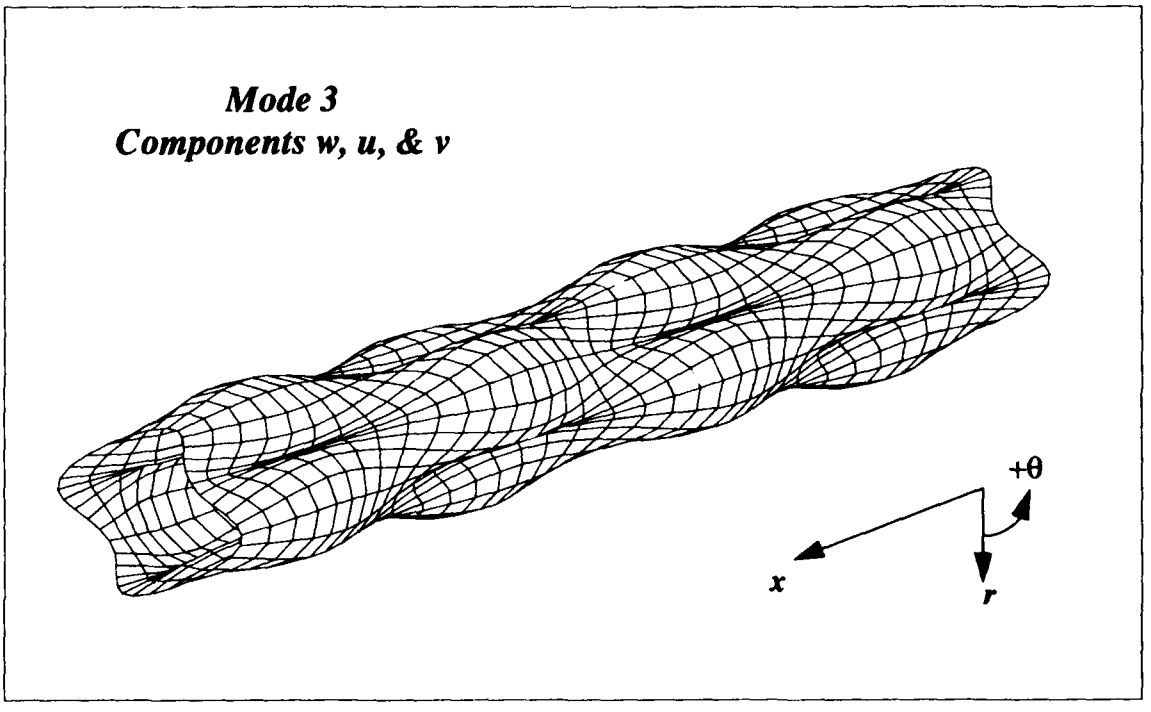

Figure 27. θ Standing Wave Mode Shape; n = 3 for w, u, and v Components

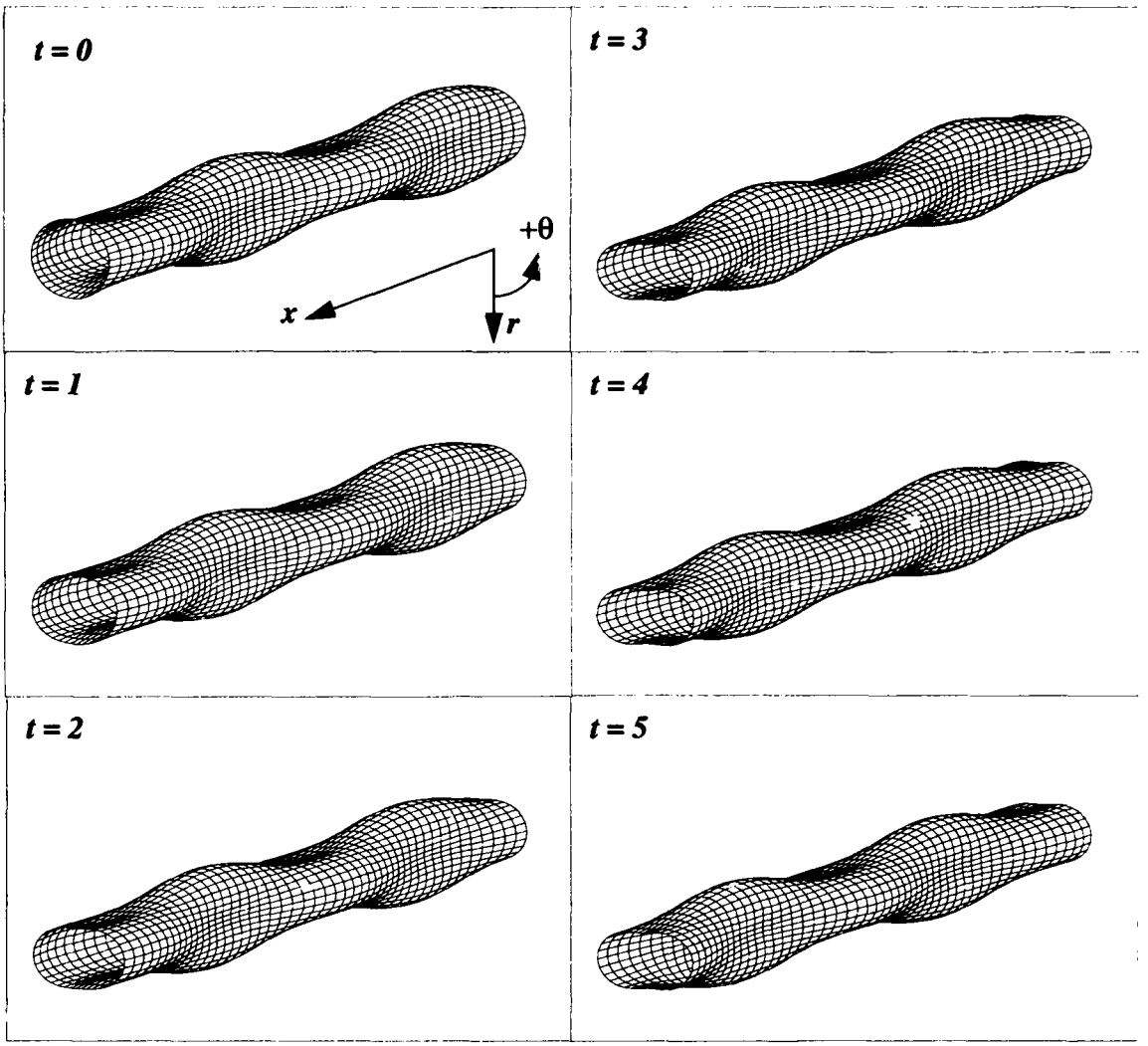

Figure 28. Animation of θ Standing Wave Mode Shape; n = 2, w Component

Traveling Wave

Similar to the previous section, figures 29 through 45 have been created, from equation (87) and depict mode shapes for the first four modes of a traveling wave excitation in x and θ. The direction of propagation is in the $+x$- and $+\theta$-directions.

It is noteworthy that the mode shapes spiral around the circumference of the shell in the $+\theta$-direction as the wave progresses in the $+x$-direction. The w component of mode 1 becomes a bending vibration that causes a corkscrewing of the shell rather than an in-plane vibration as occurs in figure 13 for the standing wave mode shape.

Special attention is warranted for the v component of mode $n = 0$ seen in figure 37. As was stated in the section on Axisymmetric Response Membrane Shell, $v = 0$; this condition is true for isotropic and specially orthotropic formulations for the shell. The only time that v is not equal to zero for the zeroth mode $n=0$ is in the generally orthotropic case. Therefore, figure 37 corresponds to a generally orthotropic shell only. Isotropic and specially orthotropic shells are depicted by figure 20 for the traveling wave case.

The combined effects of the three components of the displacement are shown in figures 41 through 44 (where the displacement magnitudes are equal, as in the standing wave case) only to allow for visualization of the effects of displacement. The traveling wave animation sequence is displayed in figure 45; the wave is traveling in the $+x$- and $+\theta$-directions.

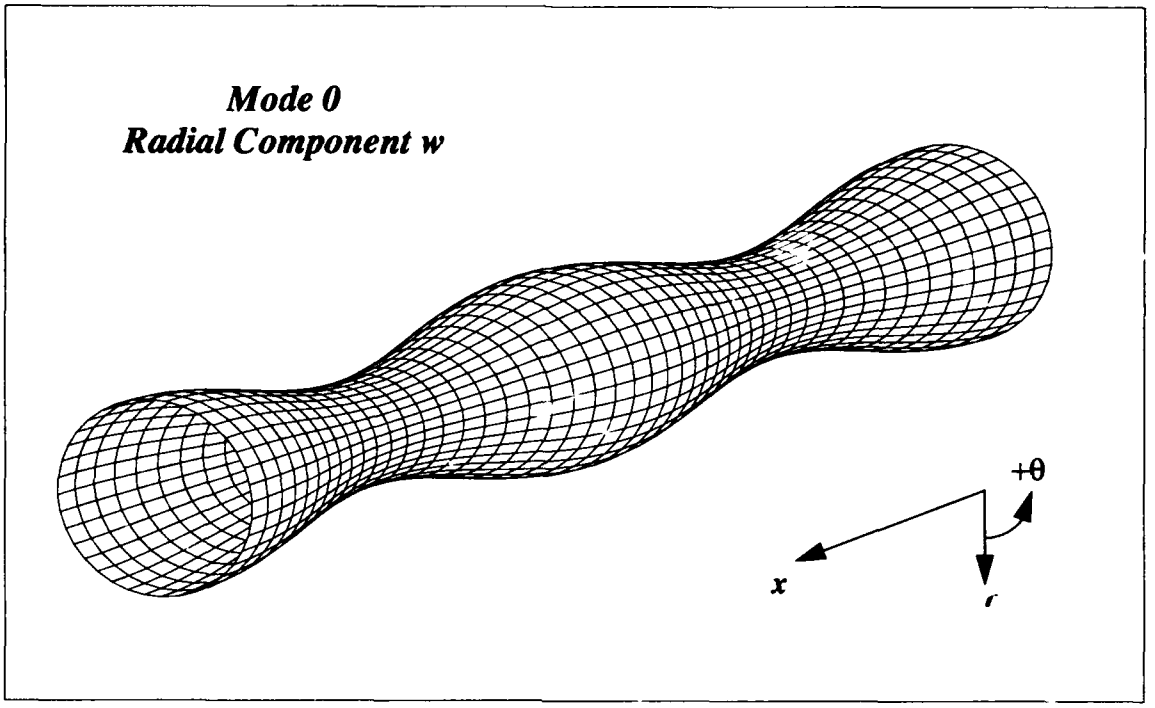

Figure 29. θ Traveling Wave Mode Shape; n = 0, w Component

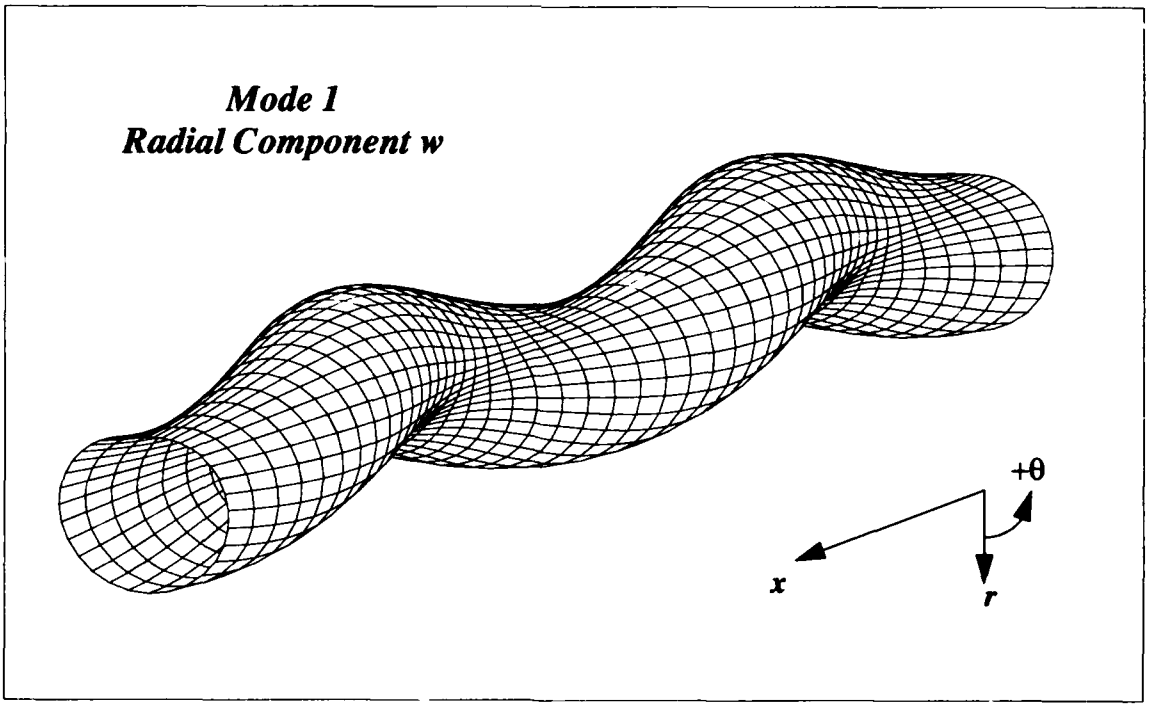

Figure 30. θ Traveling Wave Mode Shape; n = 1, w Component

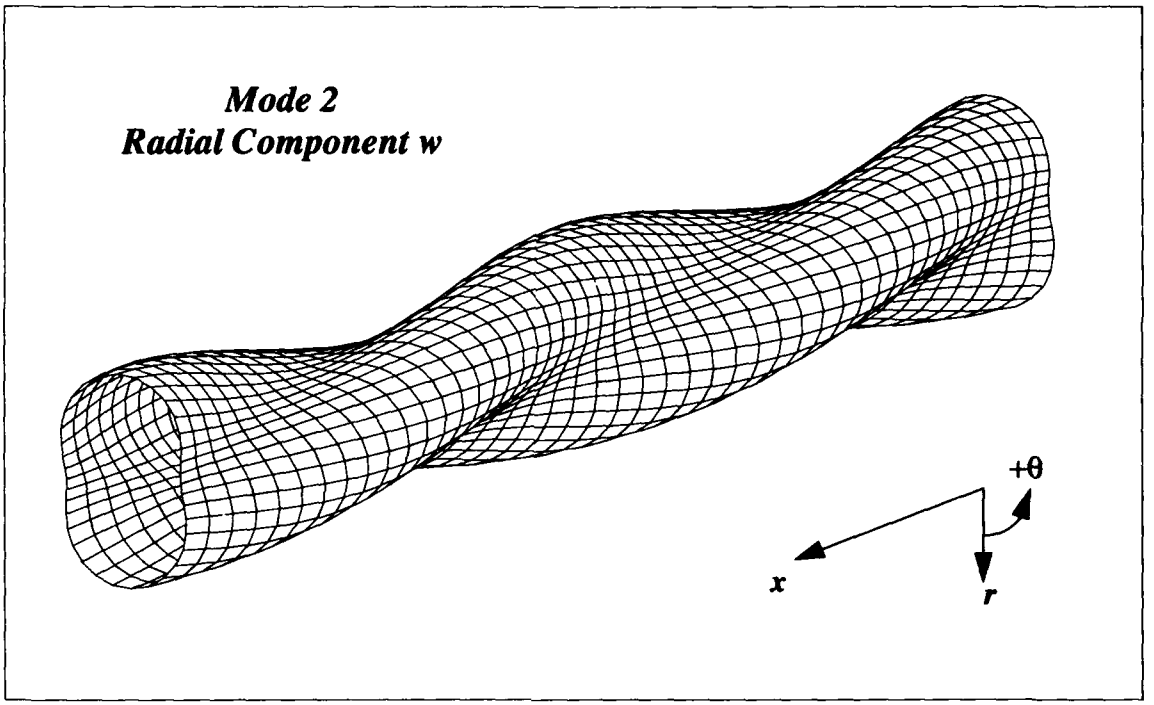

Figure 31. θ Traveling Wave Mode Shape; n = 2, w Component

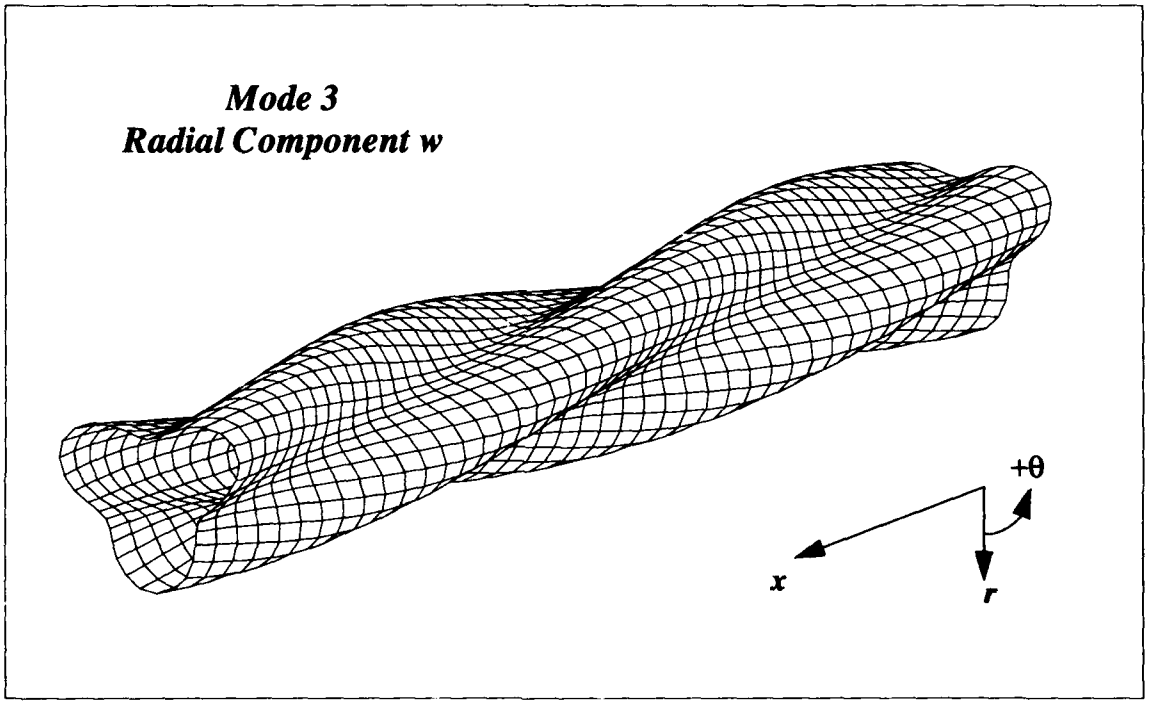

Figure 32. θ Traveling Wave Mode Shape; n = 3, w Component

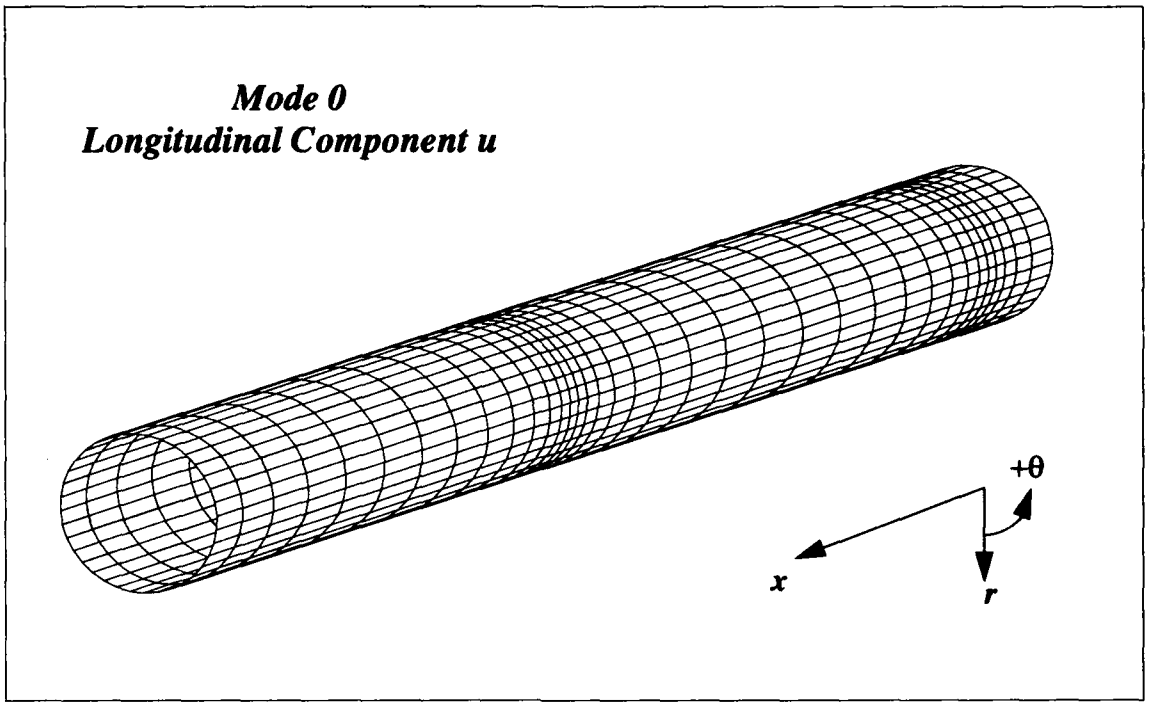

Figure 33. θ Traveling Wave Mode Shape; $n = 0$, u Component

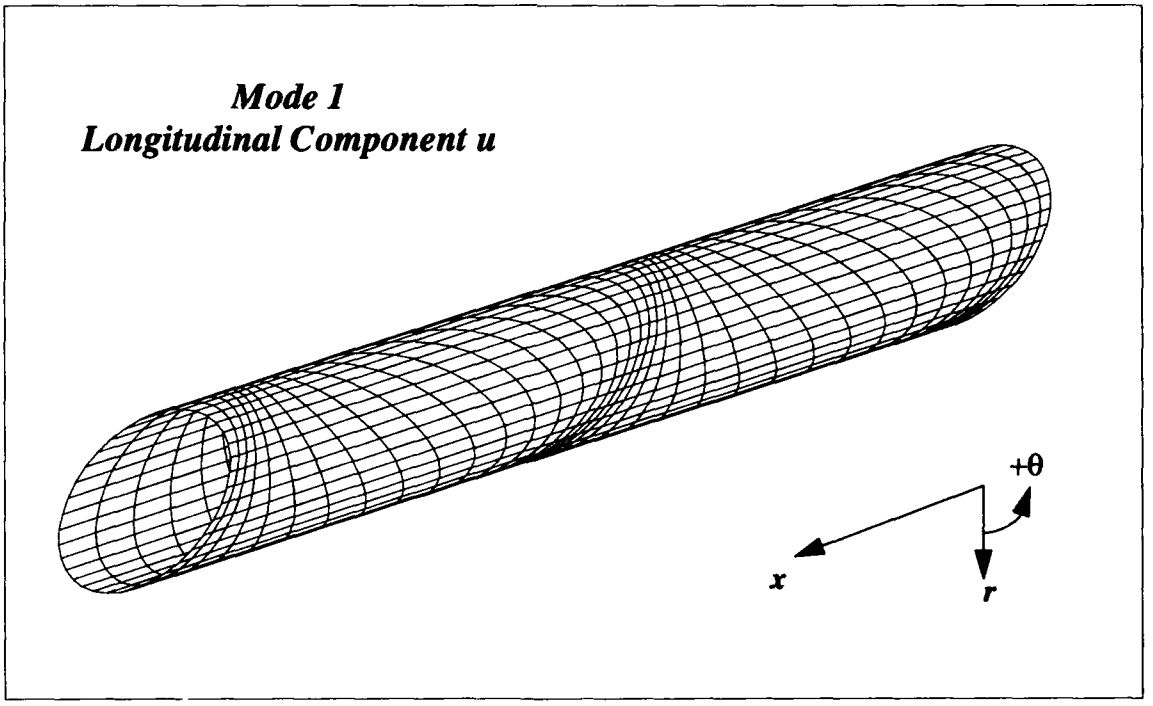

Figure 34. θ Traveling Wave Mode Shape; $n = 1$, u Component

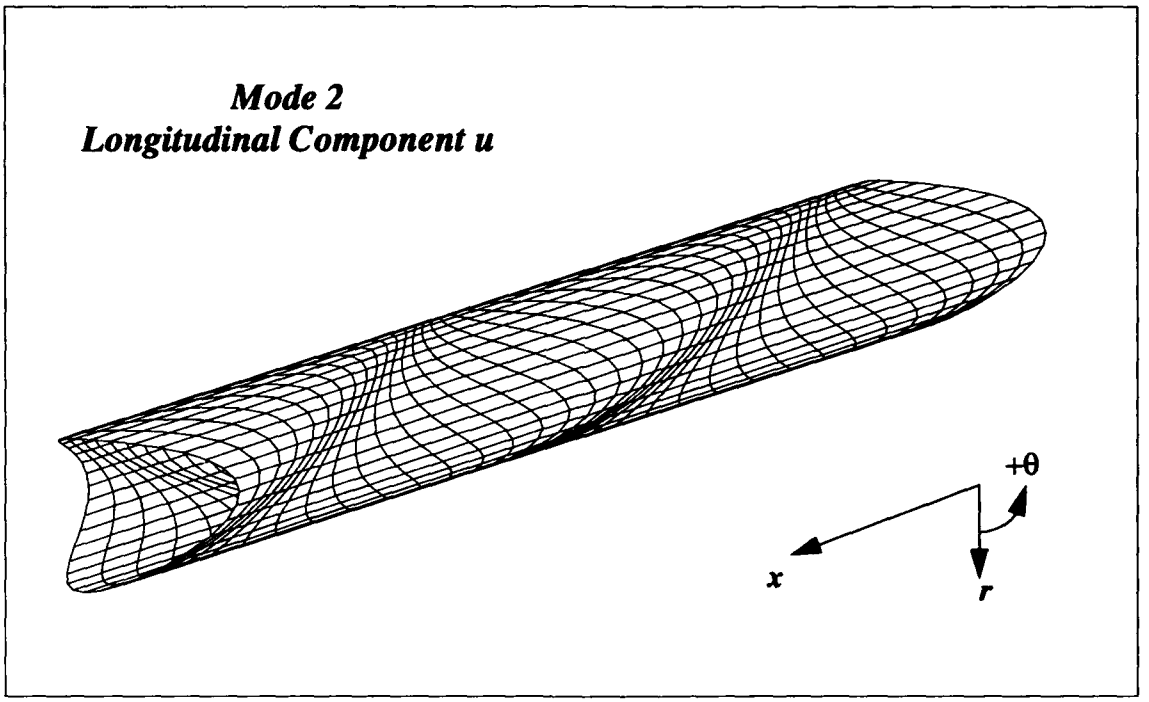

Figure 35. θ Traveling Wave Mode Shape; *n* = 2, *u* Component

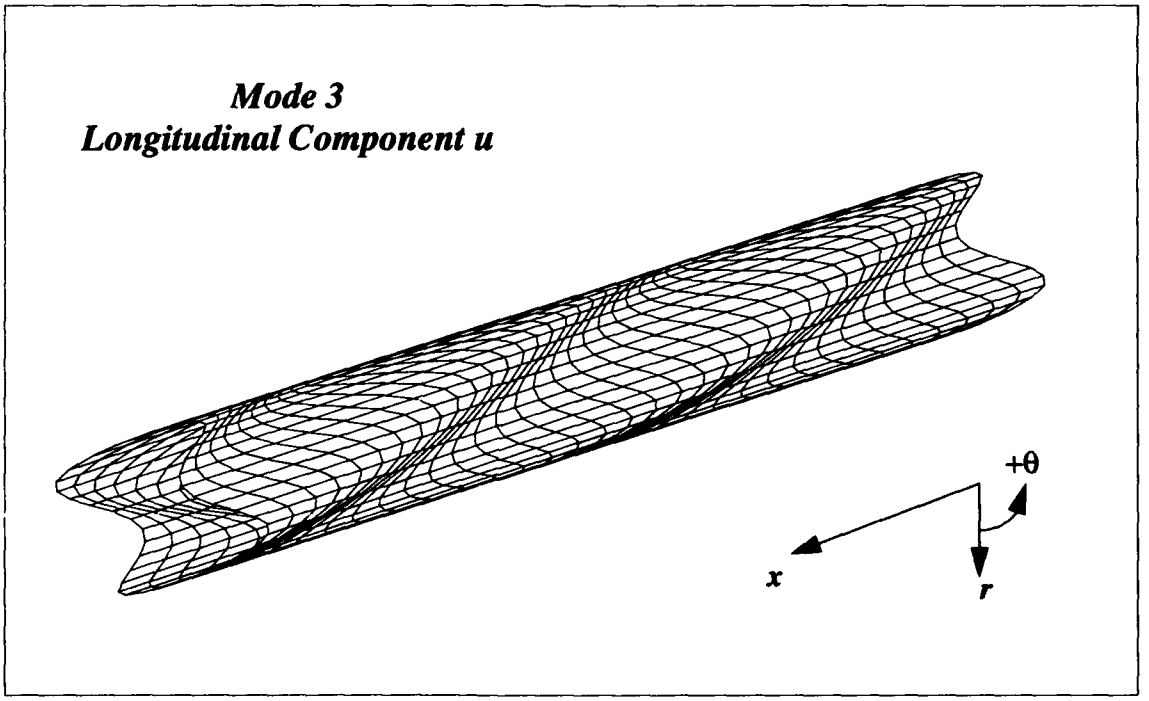

Figure 36. θ Traveling Wave Mode Shape; *n* = 3, *u* Component

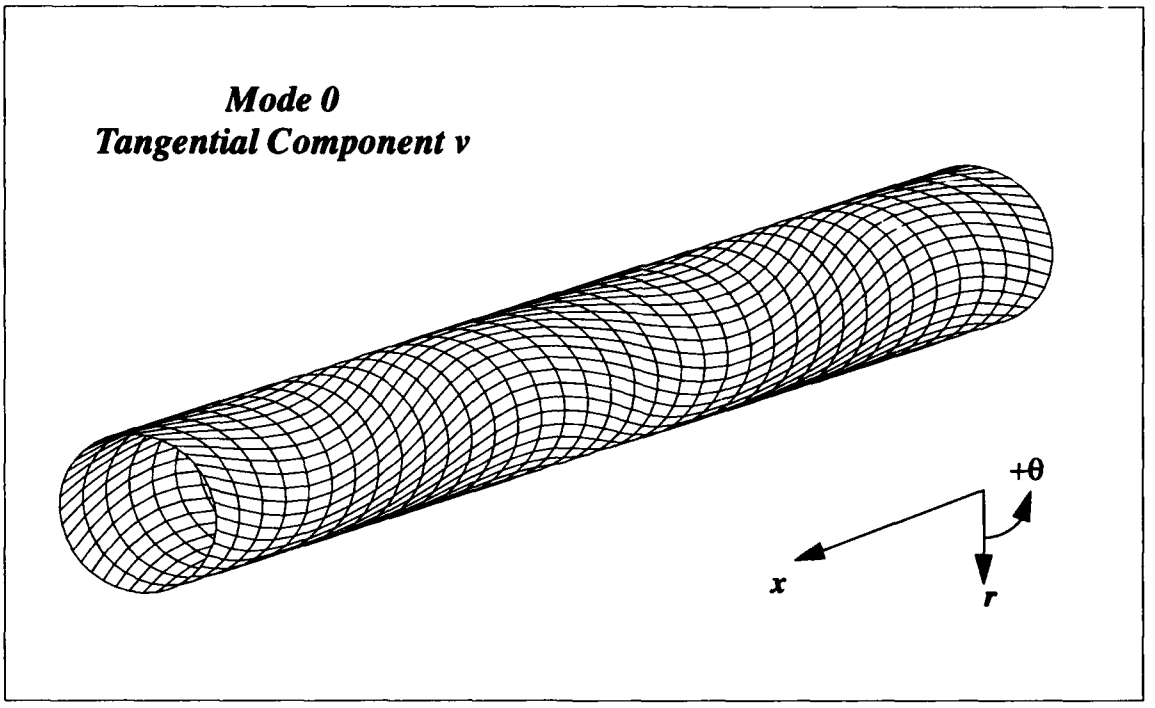

Figure 37. θ Traveling Wave Mode Shape; n = 0, v Component

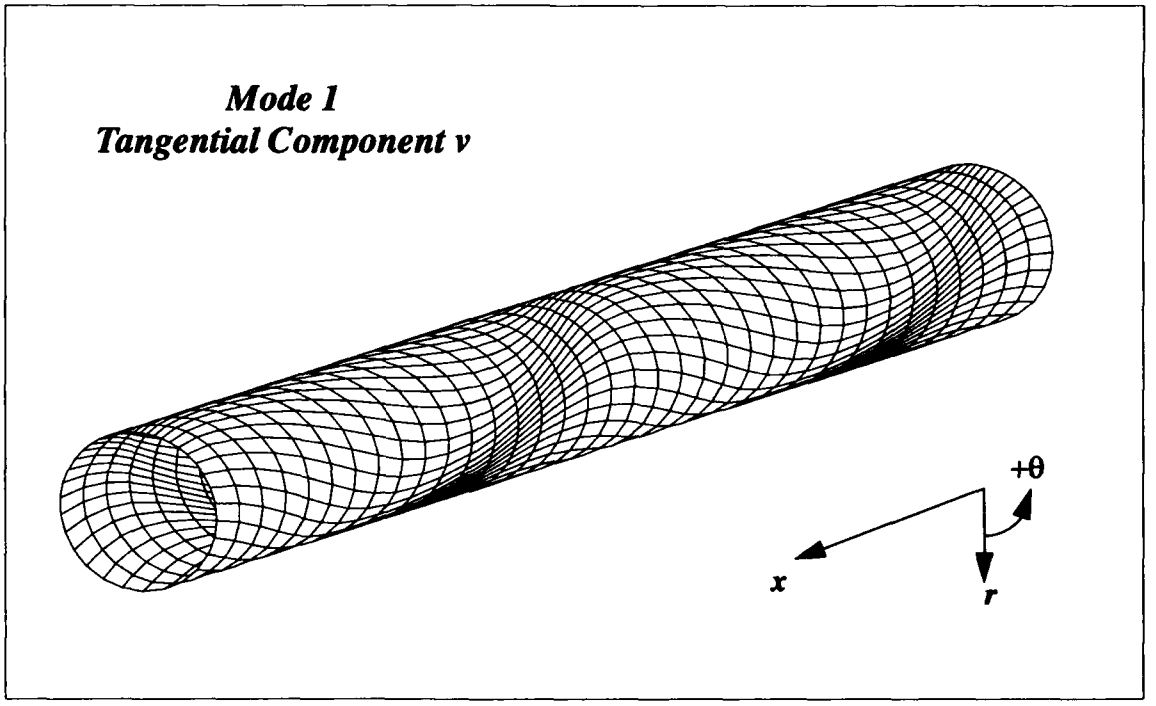

Figure 38. θ Traveling Wave Mode Shape; n = 1, v Component

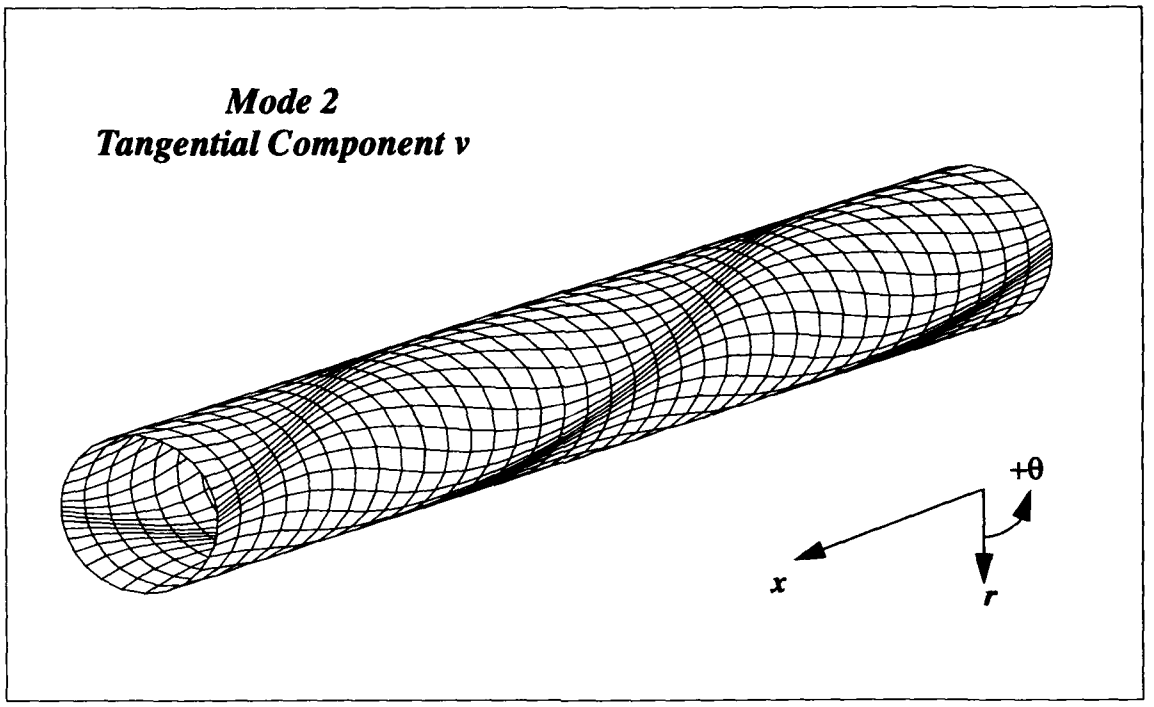

Figure 39. θ Traveling Wave Mode Shape; n = 2, v Component

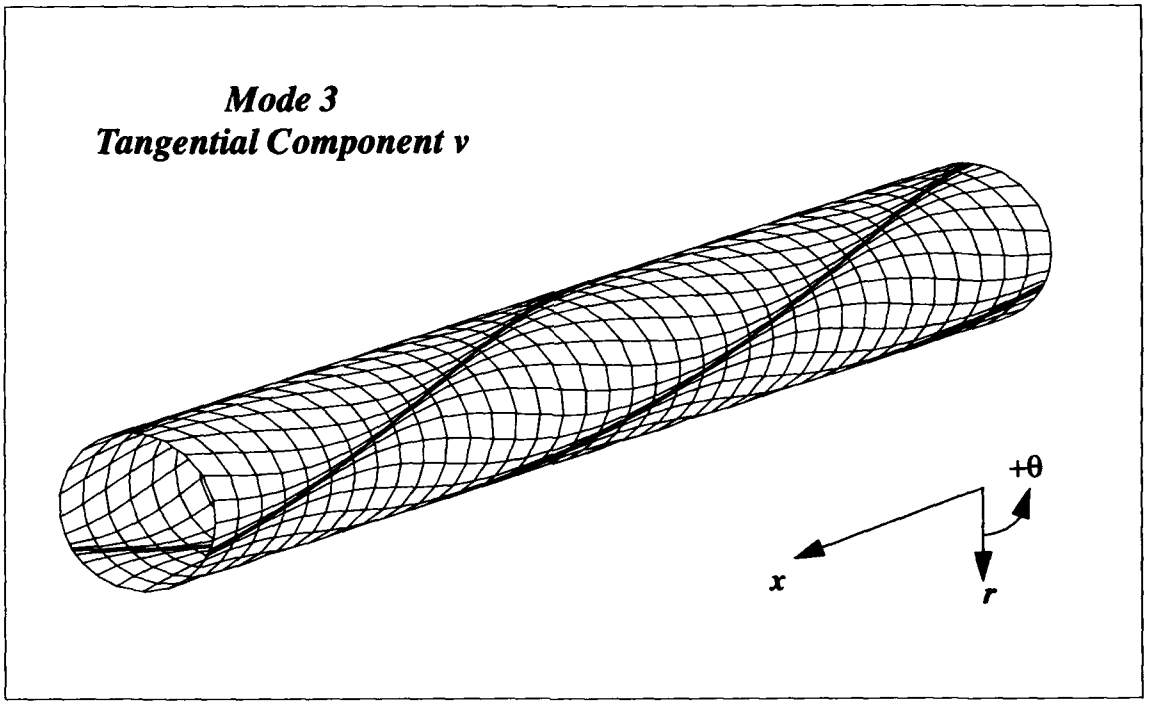

Figure 40. θ Traveling Wave Mode Shape; n = 3, v Component

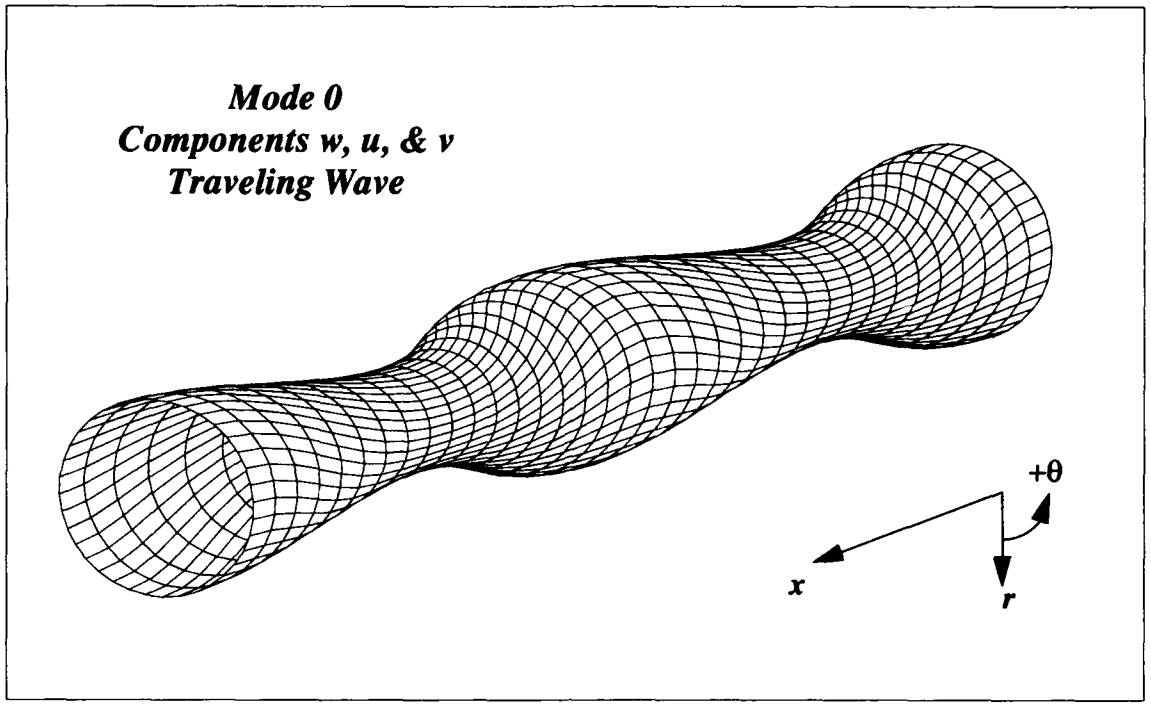

Figure 41. θ Traveling Wave Mode Shape; *n* = 0 for *w*, *u*, and *v* Components

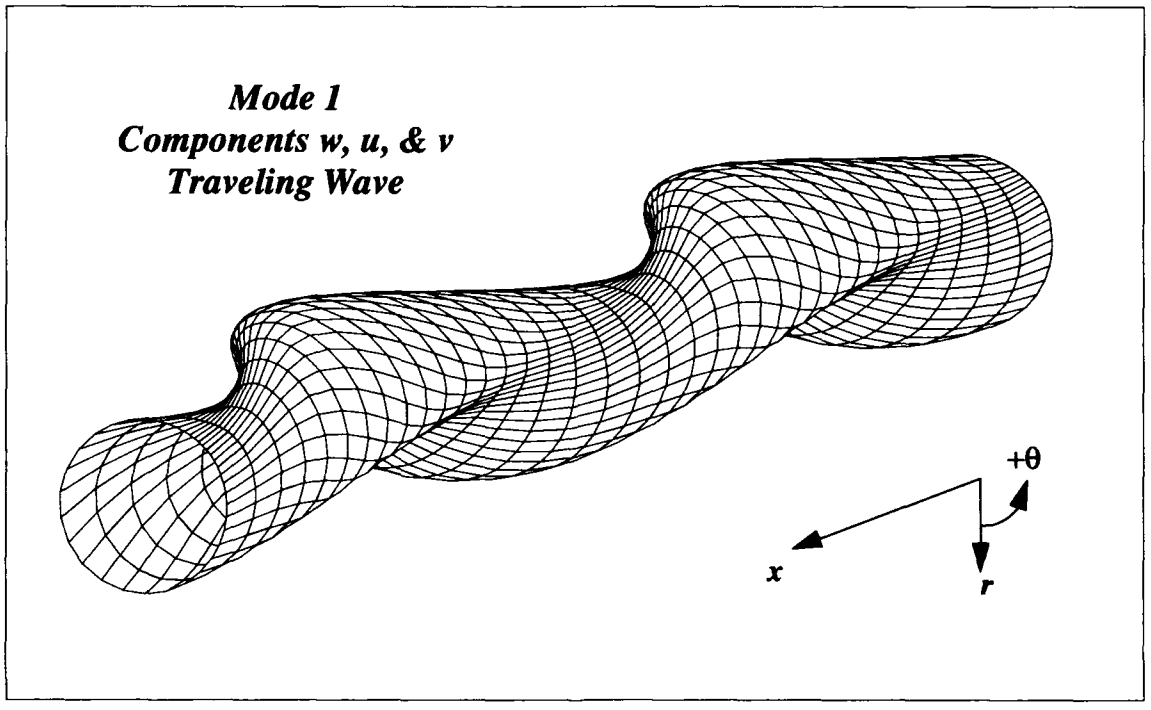

Figure 42. θ Traveling Wave Mode Shape; *n* = 1 for *w*, *u*, and *v* Components

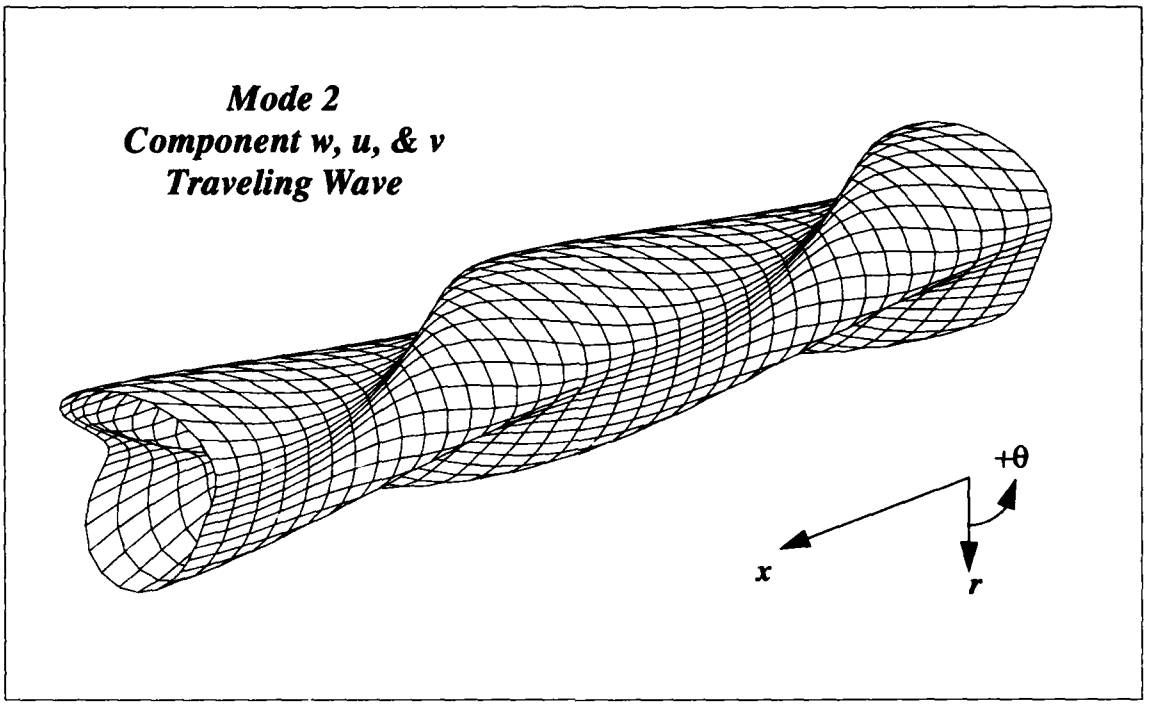

Figure 43. θ Traveling Wave Mode Shape; n = 2 for w, u, and v Components

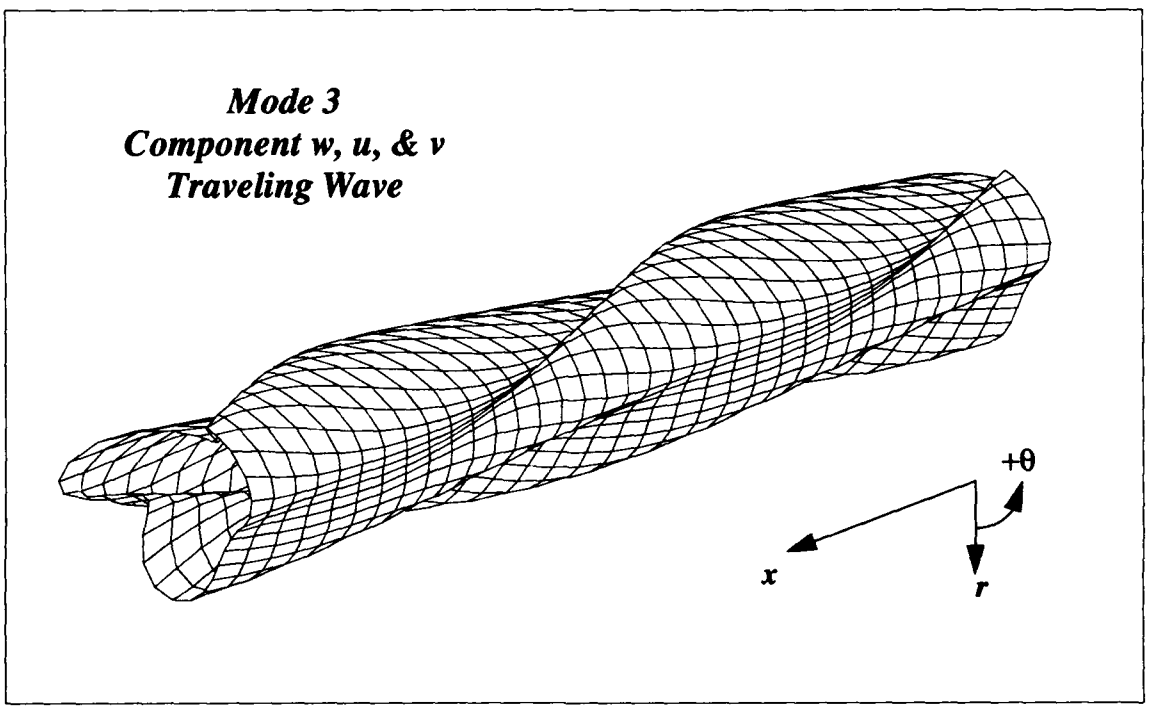

Figure 44. θ Traveling Wave Mode Shape; n = 3 for w, u, and v Components

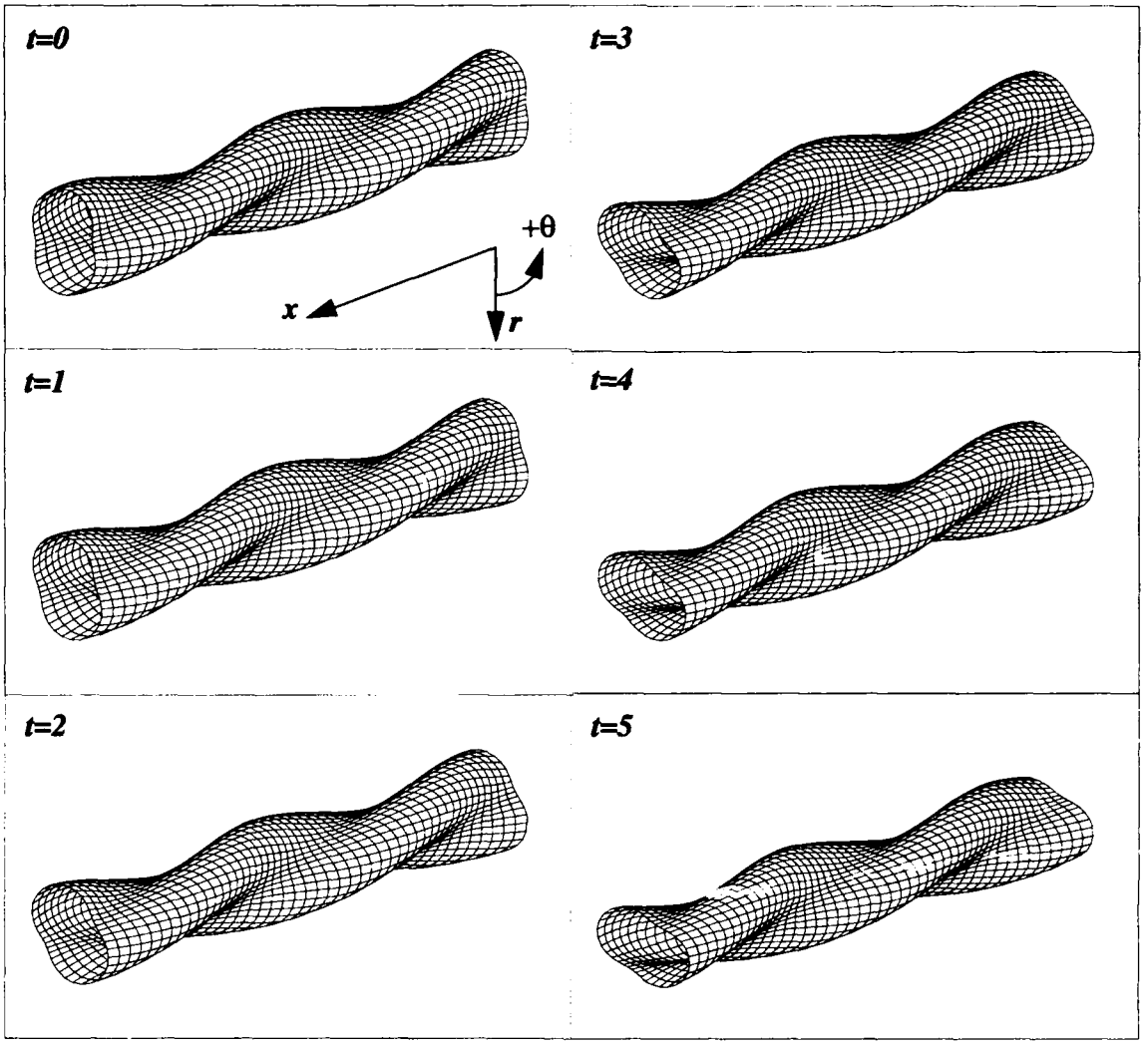

Figure 45. Animation of θ Traveling Wave Mode Shape; n = 2, w Component

MAGNITUDE OF THE SHELL RESPONSE

Now that we have examined the deformation of the shell, let us consider the magnitude (*W*, *U*, and *V*) of the shell response, normalized by the excitation pressure or stress, as a function of wavenumber and frequency.

Urethane Shell Parameters

We will proceed by using material properties that approximate an ordinary garden hose for the first set of numerical results. In subsequent sets, only the parameters that are changed will be described as the other parameters will remain the same.

Matrix

$E_m = 1.5 \times 10^7$ Pa $\qquad \zeta_m = 0.01$

$\nu_m = 0.45$ dimensionless

$\rho_s = 1000 \quad$ kg/m^3

Reinforcing Fiber

$E_f = 1.5 \times 10^9$ Pa $\qquad \zeta_f = 0.0$

$\nu_f = 0.15$ dimensionless

0.9907×10^{-3} meters (0.039 inches) outer diameter each strand

12 strands

Shell

$a = 0.01270$ meters (0.5 inches)

$h = 0.00317$ meters (0.125 inches)

Fluids

$\rho_i = 1000$ kg/m^3 $\qquad c_i = 1500$ m/s

$\rho_o = 1000$ kg/m^3 $\qquad c_o = 1500$ m/s

Structural Damping

We have not yet discussed loss within the structure. The well-known structural damping model will best describe the dissipation of energy within the shell. Structural damping introduces a complex modulus of elasticity where E_m and E_f become

$$E_m = E_m(1 + \zeta_m i),$$

$$E_f = E_f(1 + \zeta_f i).$$

The loss tangent or structural loss factor, ζ, is defined as the ratio of the in-phase to out-of-phase components of the modulus. The loss factor is determined experimentally for the material of interest. Such experiments usually involve excitation of a specimen with a harmonically applied force and measurement of the in-phase and out-of-phase displacement responses with respect to the applied force.

Based on the previously described material properties, the rule of mixtures has been applied (appendix B) to calculate the composite properties for the reinforced shell. Where a plot or image is labelled isotropic, the calculation is performed without reinforcement. When labeled specially orthotropic, the reinforcing fibers are included. The angle ϕ will always be 0 for the isotropic and specially orthotropic case. The generally orthotropic case has an angle that is formed between the reinforcement and the longitudinal axis of the shell (ϕ), as seen in figure 3.

Displacement Response

In figure 46, displacements W, U, and V have been obtained from equation (89), which illustrates an isotropic case, normalized by P_o with $P_x = 0$ at $k = 58.3$ rad/m. At the first resonance (210 Hz), the amplitude of W is the largest among the three amplitude components W, U, and V. There are corresponding displacements in U and V due to the 210-Hz resonance in W, but they are lower in amplitude. The resonance, therefore, corresponds to the w component of the $n = 2$ mode of propagation. The W response couples into the U and V displacements, but at a lower amplitude. Similar behavior occurs at the second resonance, 2000 Hz, which corresponds to the u component of the $n = 2$ mode of propagation. Coupled responses are found in the W and V displacements as well. The v component of mode $n = 2$ occurs at approximately 4000 Hz, causing both U and W coupled displacement responses.

The antiresonances are caused by a difference in phase between the displacement of a given component of the $n = 2$ mode (w for example) and the coupling from the u and v components of the $n = 2$ mode into w. In figure 46, two antiresonances observed in the W response occur under the U and V resonant peaks, at 2000 and 4000 Hz, respectively.

The frequencies and wavenumbers corresponding to the peak values of each component of the $n = 2$ mode are members of branches. Branches will be discussed in a later section where we observe a surface formed from the W response. We will be able to discuss all three branches of the $n = 2$ mode from considering a single transfer surface due to coupling.

Now let us turn our attention to the *W* response in the 100- to 1500-Hz region (figure 46). This region can be divided into three parts, from low to high frequency. The first region is a flat, straight-line stiffness controlled region, which would become increasingly flat if the next decade below 100 Hz was displayed. The second region is marked by the resonance with increasing amplitude and phase difference. The third is a straight, but sloping, region where the response of the system is controlled by its mass.

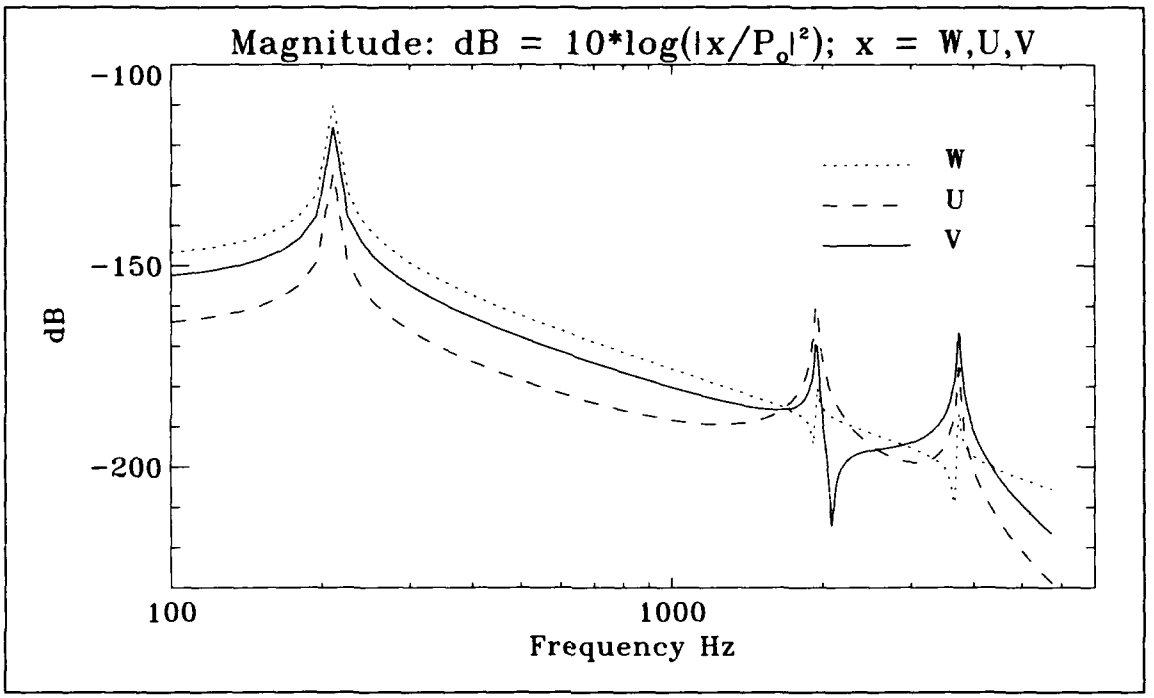

Figure 46. Three Components of Mode $n = 2$ at $k = 58.3$ rad/m

An interesting comparison to the field of modal analysis can be made here. Individually, the modes of a receptance frequency response function (FRF), displayed as a log, log plot, are subject to the same three regions applied to figure 46. Furthermore, the antiresonances appear in the receptance FRF due to a phase difference between adjacent modes. Mode numbering is different in modal analysis. In modal analysis, the resonances, or modes, are numbered with respect to increasing frequency, apart from a consideration of the mode of wave propagation. Therefore, several modes of wave propagation could be supported by a structure. The subsequent numbering of modes in the modal analysis would not necessarily correspond to the numbering of the modes of wave propagation as discussed in this work. Figure 46 depicts the situation for a mode of wave propagation, ($n = 2$) that the structure and fluids will support.

From figure 46, the frequencies of vibration for the various components of the mode shapes can be determined from the resonant peaks. The correct displacement amplitudes are also available in this figure. We see from the first resonance in *W* that corresponding displacement magnitudes in *U* and *V* are some 3 and 10 dB lower, respectively. Therefore, at approximately 220 Hz, which corresponds to the *w* component of mode $n = 2$, we would also observe the *u* and *v* components of mode $n = 2$ occurring with appropriately reduced amplitudes of vibration. Simultaneously seen on the structure, but at 2000 Hz, is the *U* resonance, but it is some 55 dB

lower than the value of the amplitude for the resonance in *W*.

We see that the amplitude ratios depend on the physical properties of the structure. This is why the displacement amplitudes were arbitrarily chosen to be equal in displaying the mode shapes; several of the modes would not be observable if the amplitudes were unequal.

TRANSFER SURFACES IN THE k,ω PLANE

When equation (92) is evaluated over a range of wavenumbers and frequencies, we have the wavenumber-frequency plane shown in figure 47, where the color white indicates maximum amplitude and black indicates minimum amplitude.

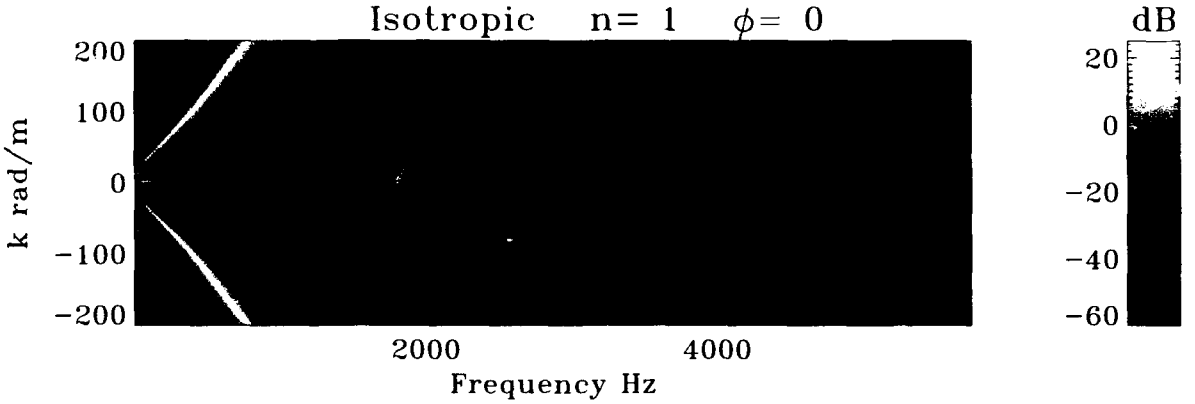

Figure 47. Bending Shell Transfer Surface (Image); dB = 10log($(P_i(a/2)/P_0)^2$)

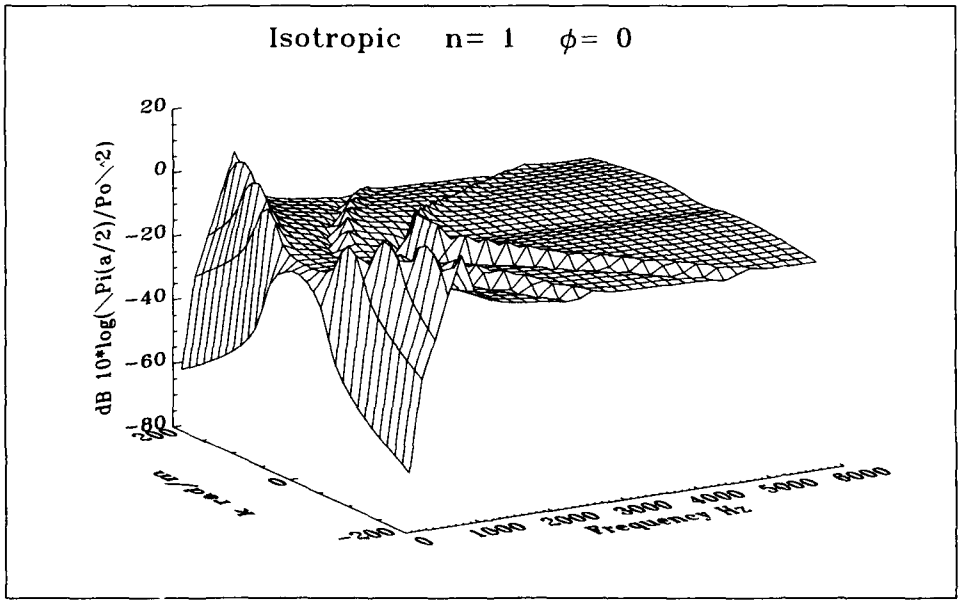

Figure 48. Bending Shell Transfer Surface (Wire Frame); dB = 10log($(P_i(a/2)/P_0)^2$)

The image shown in figure 47 is illustrated as a wire frame surface in figure 48 to help the reader visualize the three-dimensional nature of the response. The transfer surfaces in the remaining figures will be shown as the grey scale image seen in figure 47. The reader should refer to this pair of figures to interpret surfaces in later figures.

Branches

In figure 47, we see three approximately v, or horseshoe-shaped, curves or ridges symmetric about $k = 0$. The peak values along a given ridge line make up the collection of points that comprise a branch. Both the positive and negative wavenumber halves will be considered members of the same branch. Therefore, any reference made to a branch means both halves. A branch displays the relationship between the wavenumber and frequency for a particular mode of propagation. Thus, from left to right, the branches are associated with the w, u, and v components of the mode of propagation $n = 1$. Mode shapes shown in figures 13, 17, and 21 correspond to these three branches, respectively. Strictly speaking, a branch is one set of roots belonging to the determinant of the dynamic system matrix of equation (89). The transfer surfaces have been taken one step further than just a display of the roots of the equation. Here, the magnitude of the displacement has been calculated, as mentioned earlier. Velocity information is still, nonetheless, obtainable from the transfer surfaces when we consider the peak values of the transfer surface ridges as representing the collection of points that comprise the branches. When reference is made to branches, henceforth, the peak value of the ridges is meant.

Phase Velocity

The inverse of the slope calculated by use of the two points consisting of the origin of the k,ω plane and any point on a branch is called the phase velocity. If the phase velocity does not depend on wavenumber, but is rather a constant, the branches are given by straight lines in the k,ω plane and are termed nondispersive. If the phase velocity is a function of wavenumber, the branch describes a dispersive form of wave propagation.

Group Velocity

The quantity $\frac{d\omega}{dk}$ calculated at a point on a branch is called the group velocity for the particular point. The group velocity defines the rate at which energy propagates in the particular mode. For nondispersive modes, the phase and group velocities are equal. Therefore, energy propagates at a constant velocity for all wavenumber and frequency pairs along the nondispersive branch.

All three branches in figure 47 are dispersive. The least dispersion is exhibited by the first branch, which is the farthest left. This branch actually becomes nondispersive for sufficiently high wavenumbers.

Cutoff Frequency

Cylindrical shells have a finite circumferential length. It is the restriction of a spatial dimension that causes the shell to become a waveguide. Waveguides exhibit cutoff frequencies below which particular modes will not propagate. This behavior is most clearly seen in figure 47

for the second and third branches of the $n = 1$ mode. A layer of finite thickness is also a waveguide that exhibits similar behavior.

At the cutoff frequency, the group velocity equals zero, and energy does not propagate along the longitudinal axis of the shell. Along the branch, as the frequency is increased beyond the cutoff frequency, the group velocity increases from zero, and energy begins to propagate down the longitudinal axis of the shell.

We have been considering propagating excitations and responses of the form

$$\cos(n\theta)\, e^{i(kx-\omega t)}, \qquad e^{i(kx+n\theta-\omega t)}. \tag{94}$$

When a branch displays a cutoff frequency, we find that the behavior of the structure can be observed below cutoff frequency by considering imaginary wavenumbers. Inserting ik into equation (94) gives

$$\cos(n\theta)\, e^{-kx} e^{-i\omega t}, \qquad e^{-kx} e^{i(n\theta-\omega t)}. \tag{95}$$

The imaginary wavenumber turns equation (95) into an inhomogeneous vibration whose amplitude is decaying with increasing x. In this case, k is actually an attenuation factor, not a spatial frequency as in the propagating wave case. In the θ-direction of equation (95), we first have a standing wave and then a traveling wave. The amplitude of the response is shown in figures 49 and 50 for a shell only. The effects of the fluids have been removed.

In further discussions, we will explore the effects of various parameters on the cutoff frequencies as well as on the general behavior of the transfer surfaces.

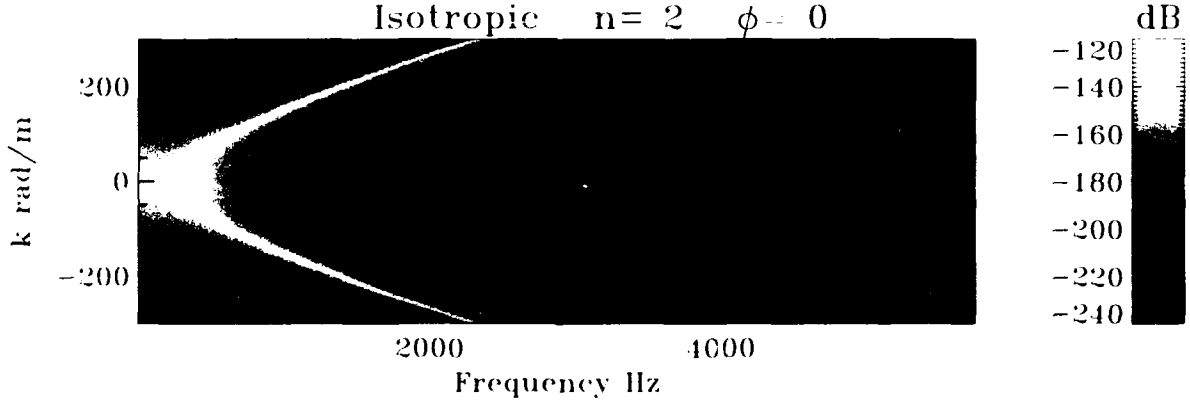

Figure 49. Transfer Surface (Real Wavenumber); dB = 10log($(W/P_0)^2$)

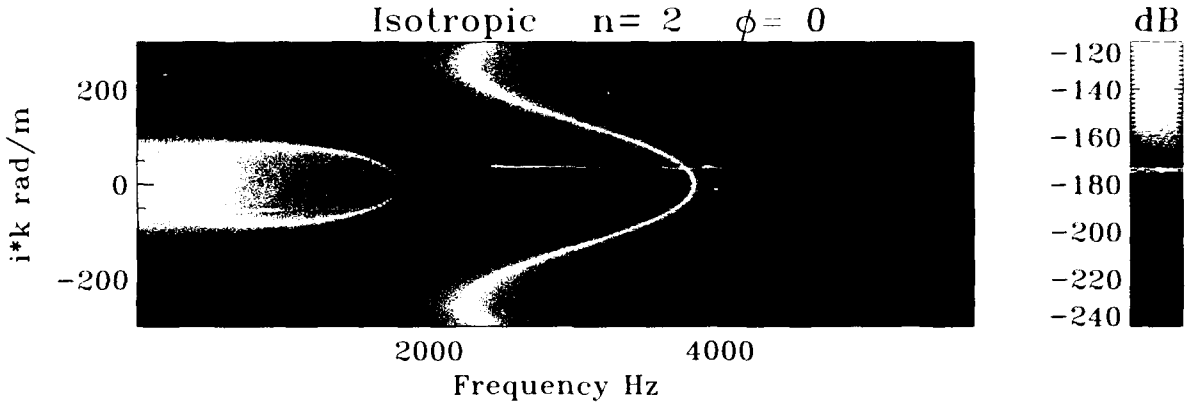

Figure 50. Transfer Surface (Imaginary Wavenumber); dB = 10log($(W/P_0)^2$)

RADIAL PRESSURE TRANSFER SURFACES

Membrane Shell

Figures 51 through 55 describe the membrane shell dynamic response. Figure 52(a) contains two branches. The major and lowest speed branch corresponds to the w component of mode $n = 0$, whose shape is displayed in figure 12. This branch describes a mode of propagation referred to as the breathing wave. The u component of mode $n = 0$, whose displacement shape is seen in figure 16, is faintly visible in figure 52(a) at a higher phase velocity. This u component is referred to as an extensional wave. From figure 52(a), it is clear that the radial P_o excitation does not generate a significant extensional wave level.

Observing mode $n = 1$, we can see the effect of longitudinal stiffness on all three branches, most visibly on the second and third. The group velocity is increased for the third branch and over most of the second branch as well (figure 53(b)).

The branches of the generally orthotropic surfaces exhibit very interesting behavior. For the first time, we observe an asymmetry about $k = 0$. Figure 51 depicts the resultant propagation directions that correspond to the plus and minus wavenumber half planes. For the plus wavenumber half plane, the $+x$, $+\theta$ propagation direction rotates into the direction aligned with the E_2 material property. Arriving from the $-x$, $+\theta$ direction (the negative wavenumber half plane), the propagation is principally in the E_1 material property direction. For the generally orthotropic case, $E_2 \neq E_1$; therefore, different stiffness is presented by the structure to the excitation, and an asymmetry results. It is interesting to note that changing the sign of n from positive to negative will flip the surface 180 degrees about the $k = 0$ axis, as would be expected from the preceding discussion.

Looking at mode $n = 2$, figure 54(a) -(c), we see that the first branch does not exhibit a cutoff frequency. This behavior will be contrasted in the next section on the bending shell, where the first branch of the second mode exhibits a cutoff frequency.

In general, for a given branch of the membrane shell and shell stiffness type (i.e., isotropic), the cutoff frequency increases with increasing mode number, and for a given wavenumber, the group velocity slows down with increasing mode number.

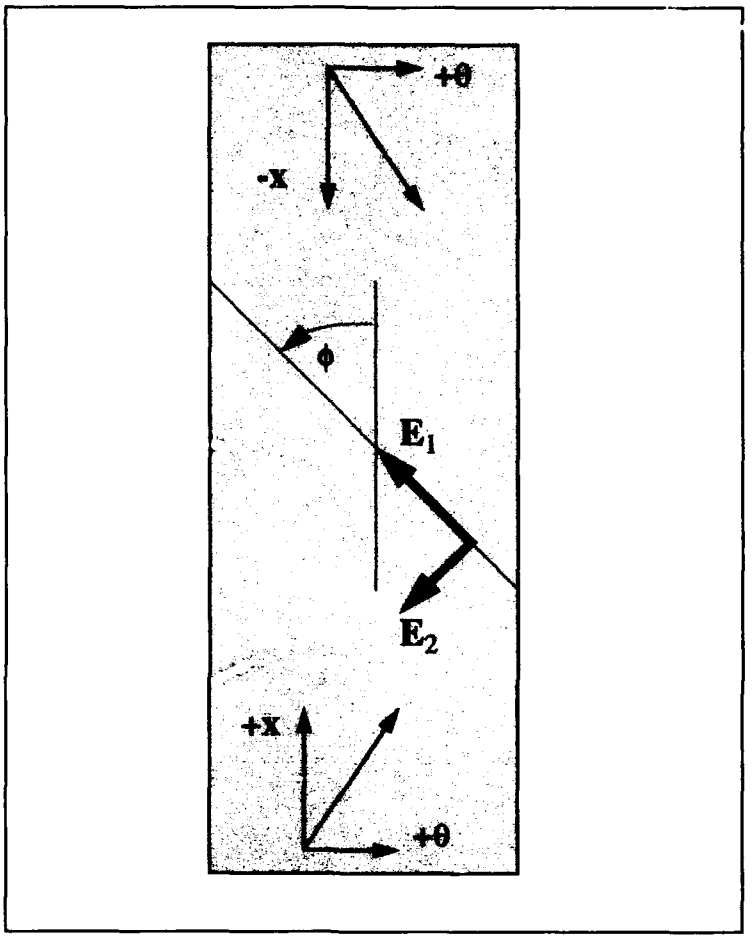

Figure 51. Generally Orthotropic Shell Schematic, Propagation Directions

Bending Shell

Figures 56(a) through 62 correspond to the bending shell dynamic response. Two major differences are observed in the bending shell surfaces. The first concerns the breathing wave, which is the w component of mode $n = 0$ (see figure 56(a)-(c)). At high wavenumbers, the group velocity increases, in contrast to the membrane case where group velocity slows with increasing wavenumber.

The w component of mode $n = 2$, exhibits a cutoff frequency (see figure 58(a)-(c)). We observe, therefore, the importance of bending stiffness on this particular branch.

As in the membrane case, cutoff frequency increases with increasing mode number for a given branch. For the u and v components of the modes, we see the group velocity decreasing with increasing mode number for all dispersive branches.

Membrane Shell Sequence

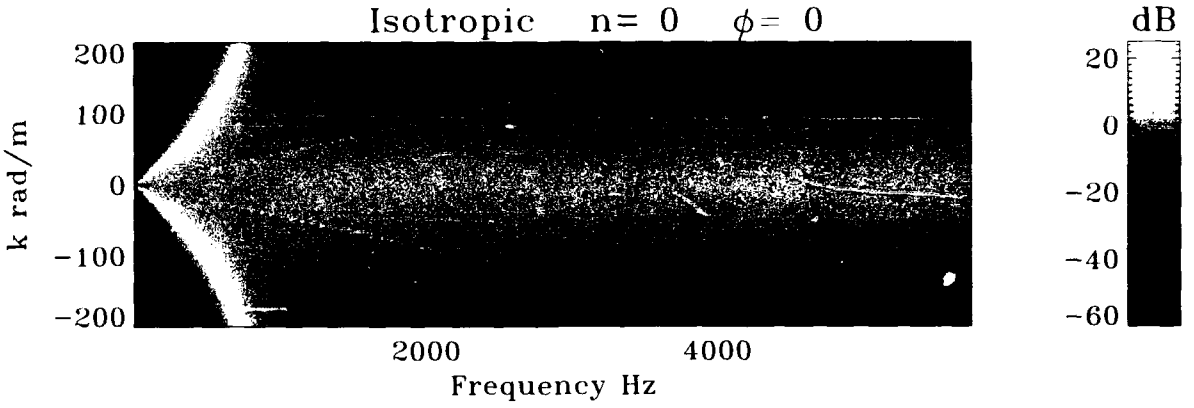

(a)

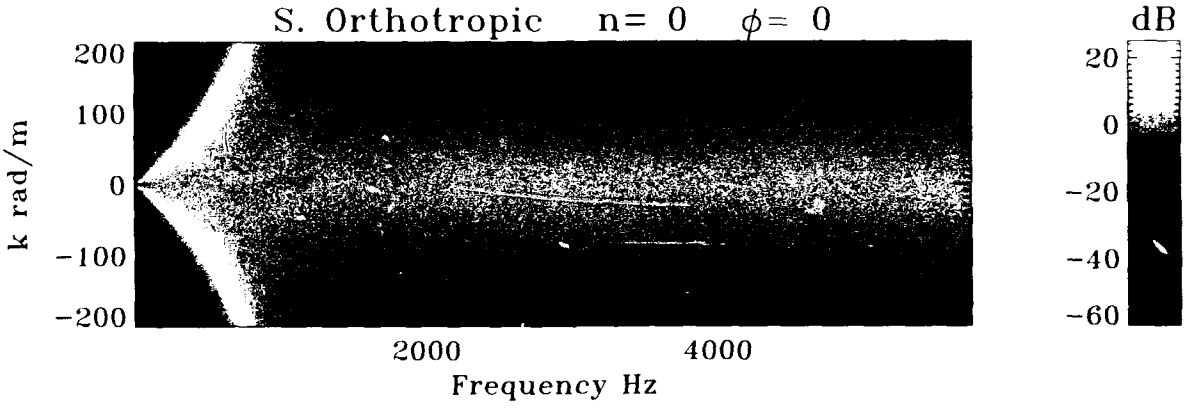

(b)

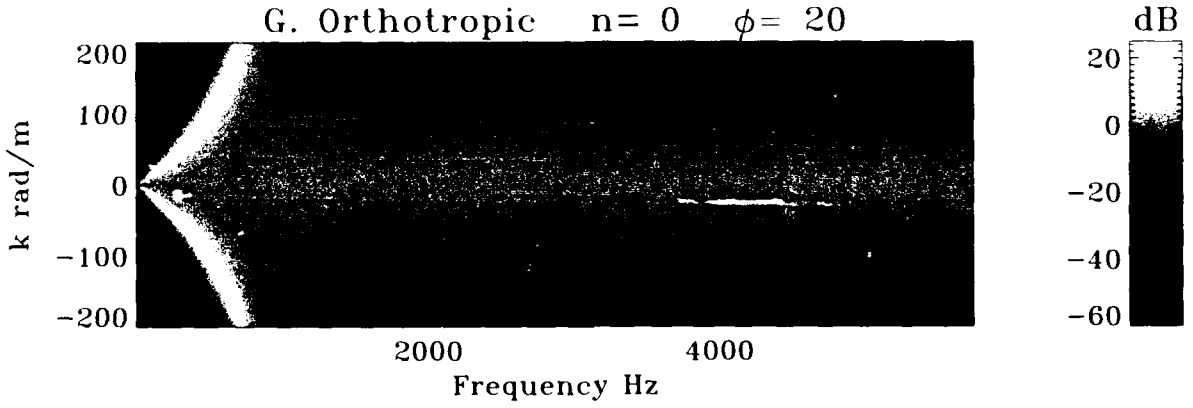

(c)

Figure 52. Membrane Shell Transfer Surface (n = 0); dB = $10\log((P_t(a/2)/P_o)^2)$

Membrane Shell Sequence Continued

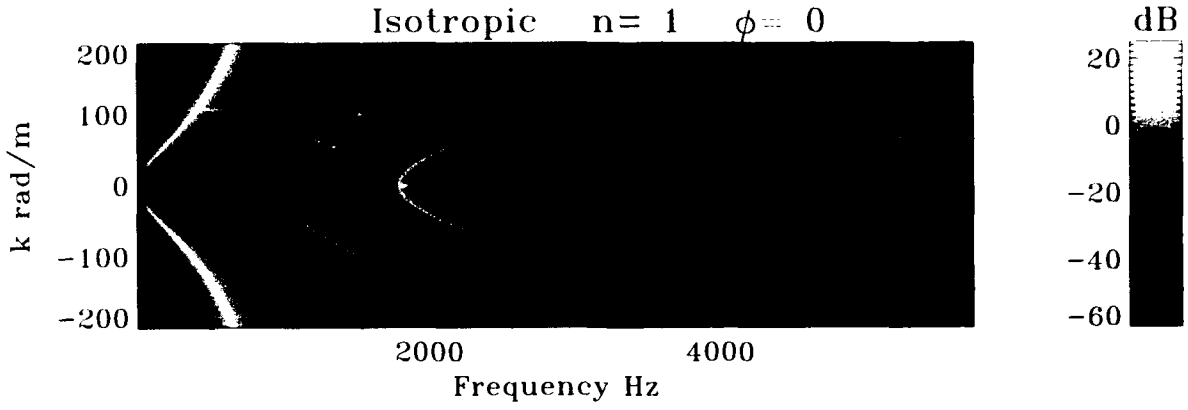

(a)

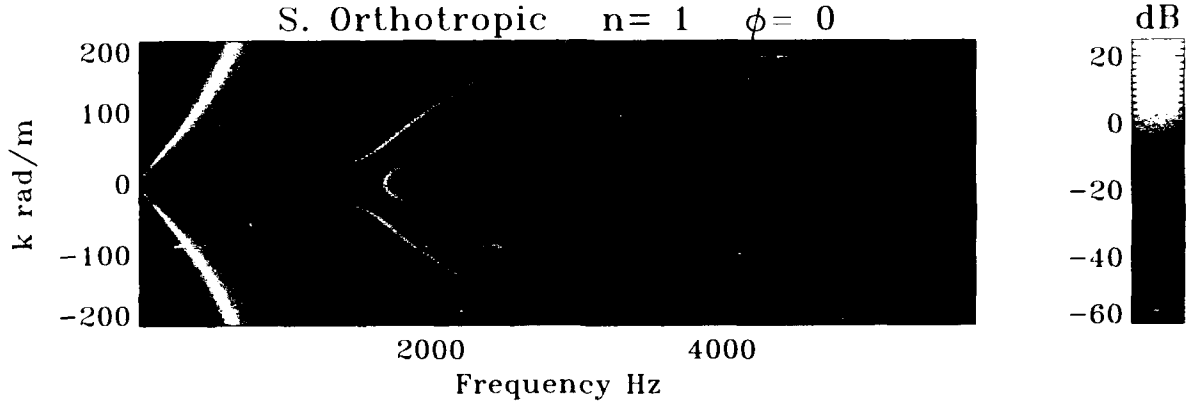

(b)

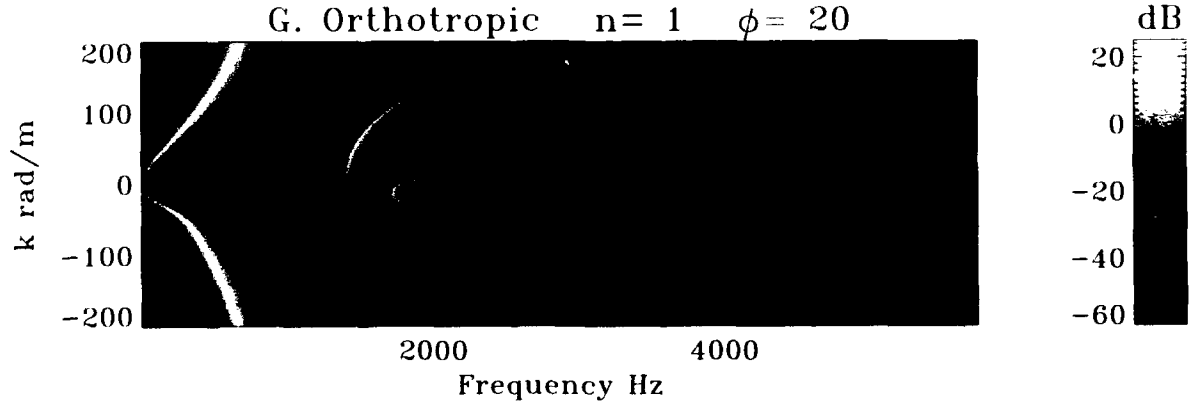

(c)

Figure 53. Membrane Shell Transfer Surface (n = 1); dB = $10\log((P_i(a/2)/P_0)^2)$

Membrane Shell Sequence Continued

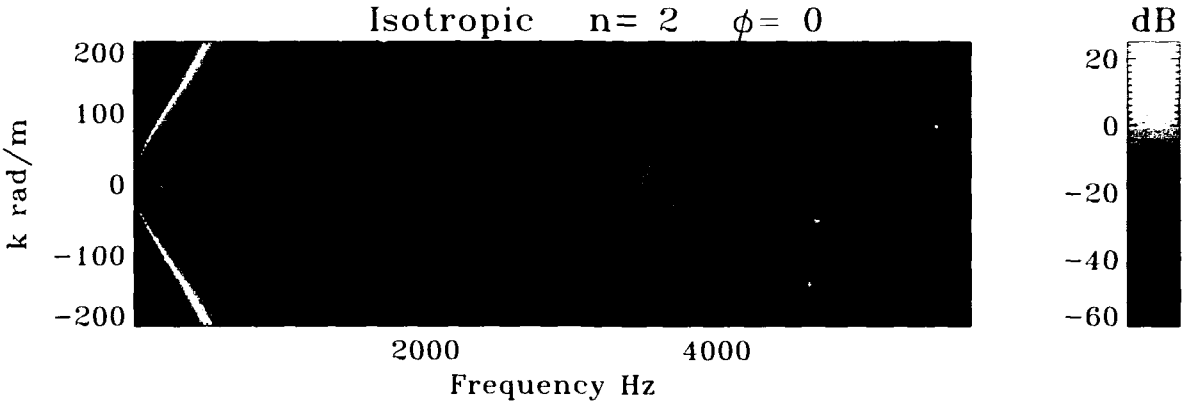

(a)

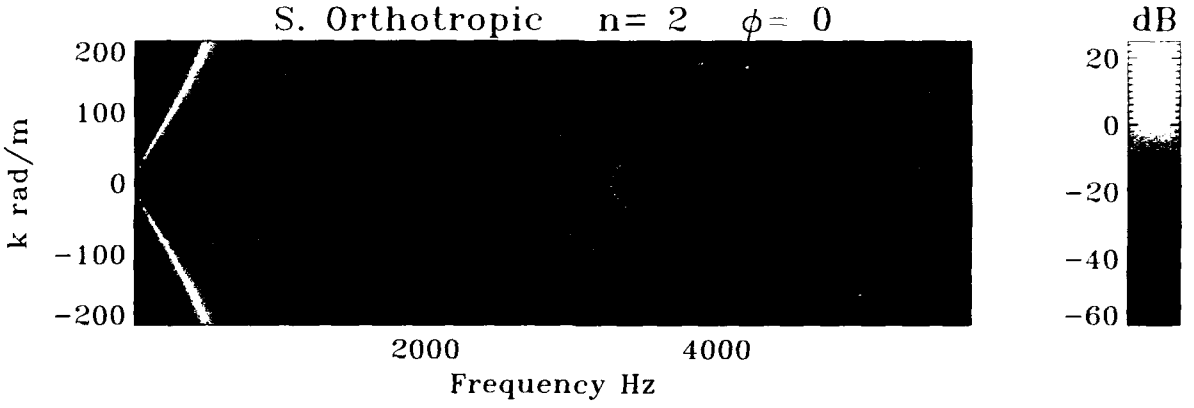

(b)

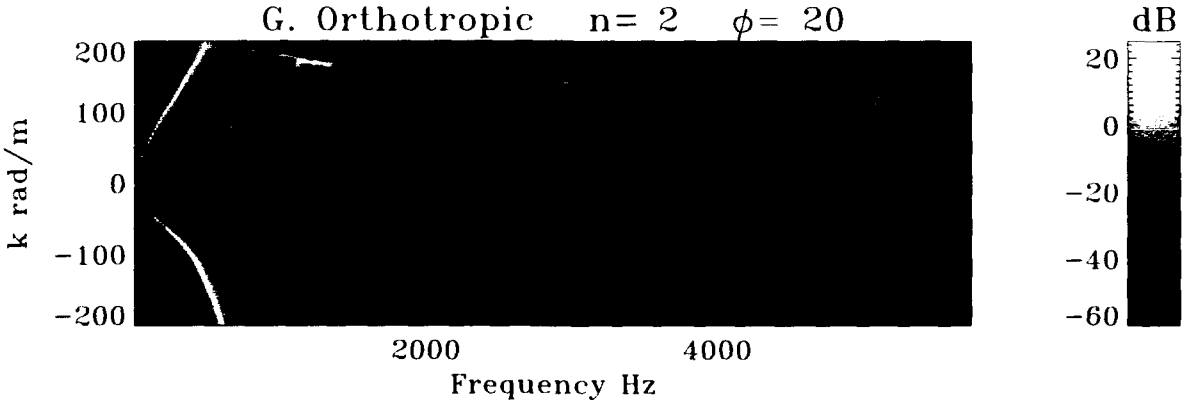

(c)

Figure 54. Membrane Shell Transfer Surface (n = 2); dB = $10\log((P_i(a/2)/P_o)^2)$

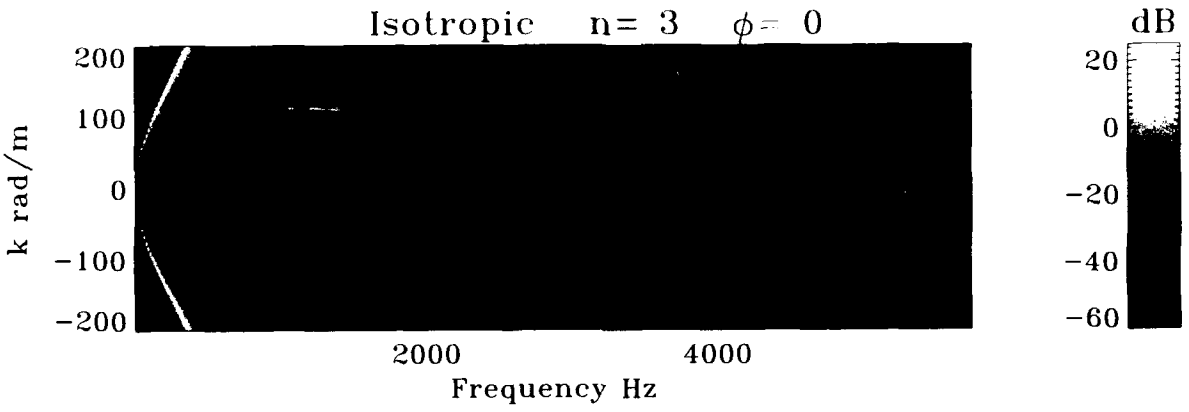

(a)

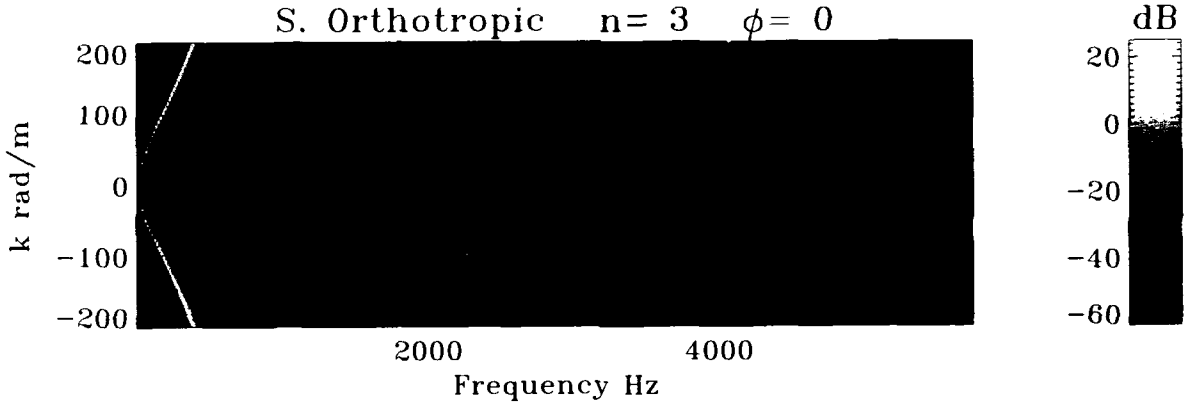

(b)

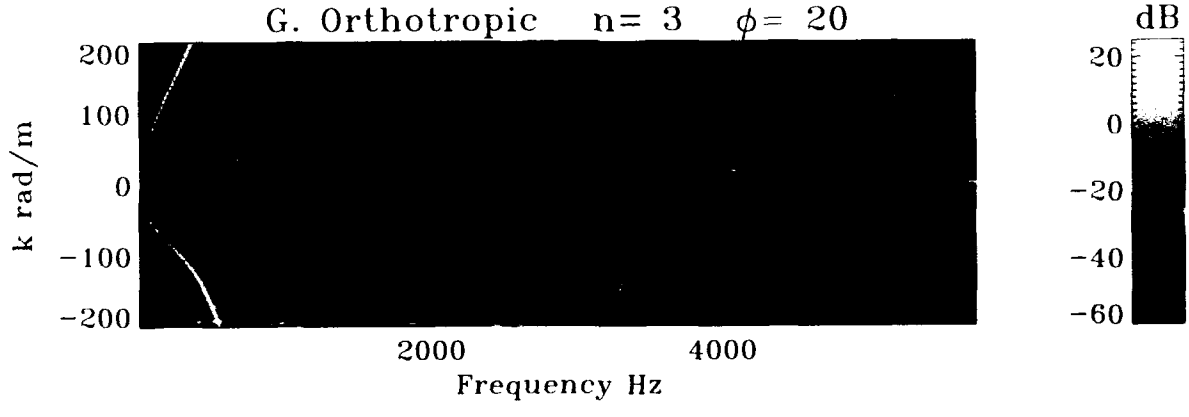

(c)

Figure 55. Membrane Shell Transfer Surface (n = 3); dB = 10log($((P_t(a/2)/P_o)^2)$)

Bending Shell Sequence

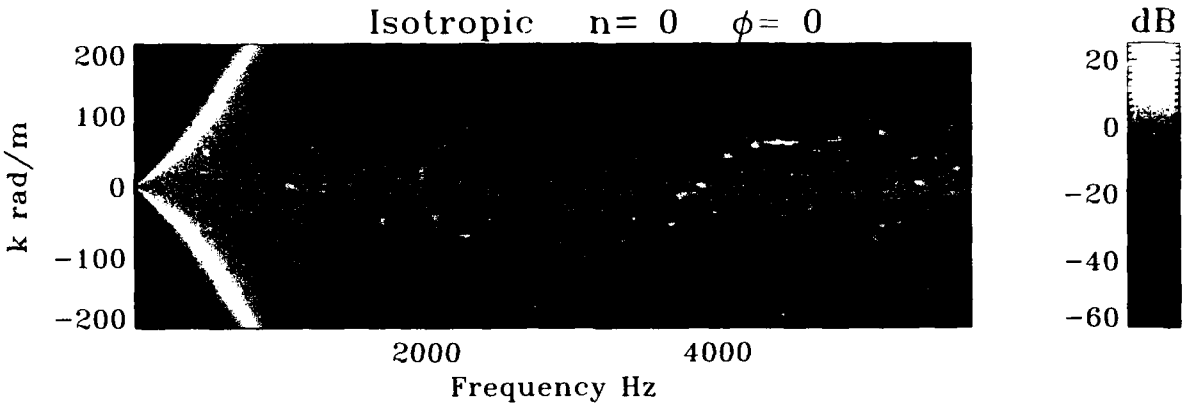

(a)

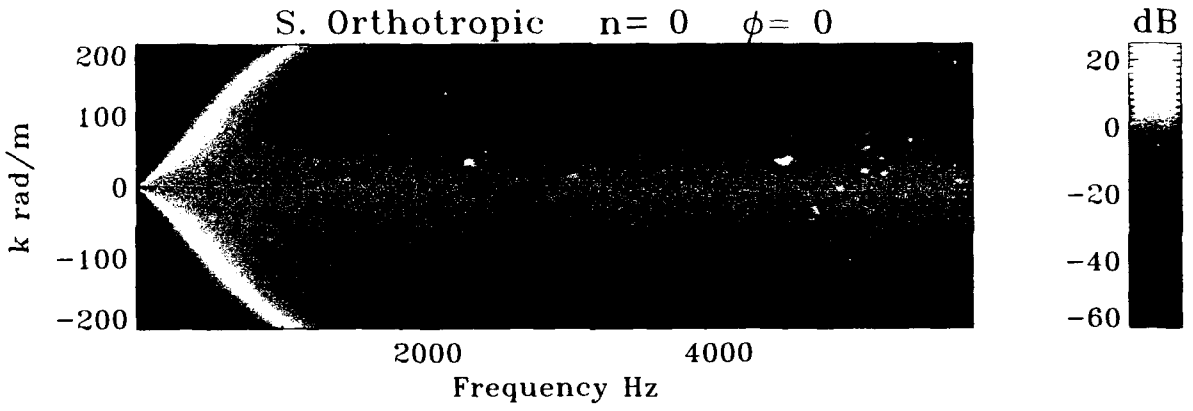

(b)

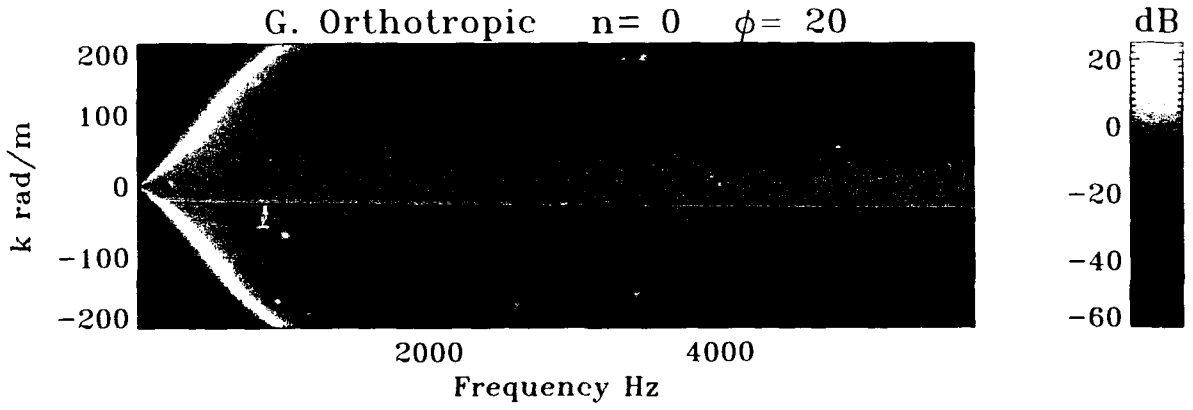

(c)

Figure 56. Bending Shell Transfer Surface (n = 0); dB = 10log($((P_i(a/2)/P_o)^2)$)

Bending Shell Sequence Continued

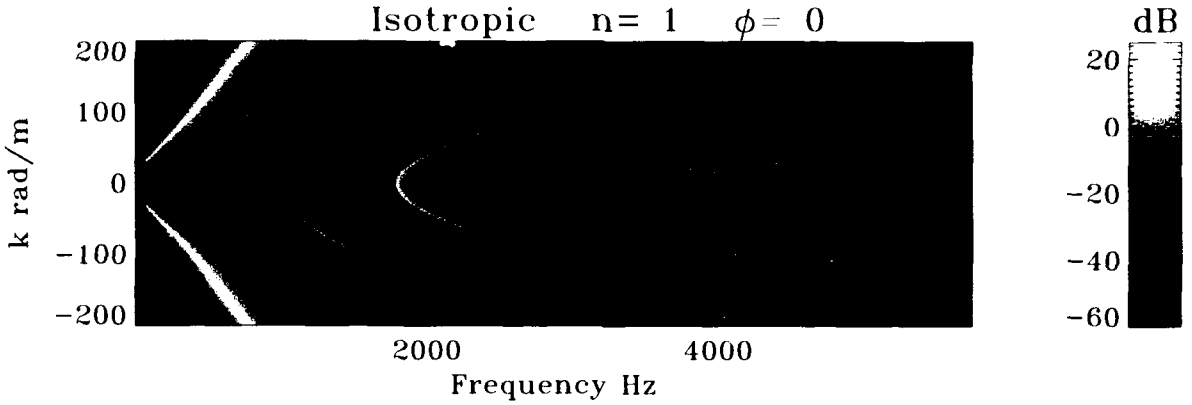

(a)

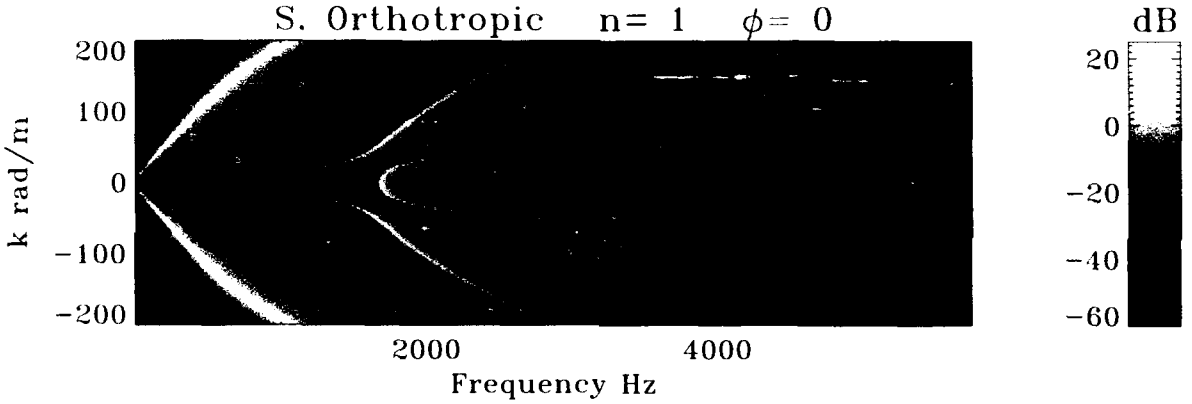

(b)

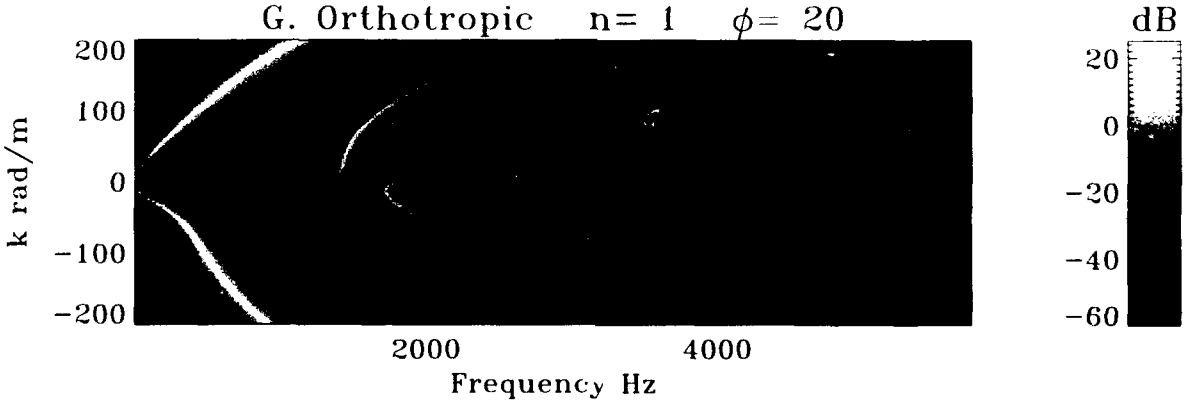

(c)

Figure 57. Bending Shell Transfer Surface (n = 1); dB = 10log($(P_i(a/2)/P_0)^2$)

Bending Shell Sequence Continued

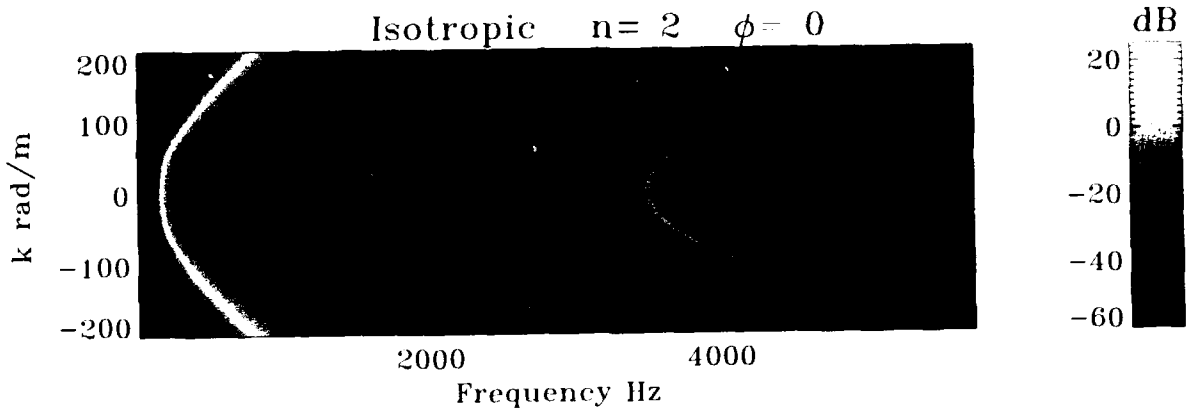

(a)

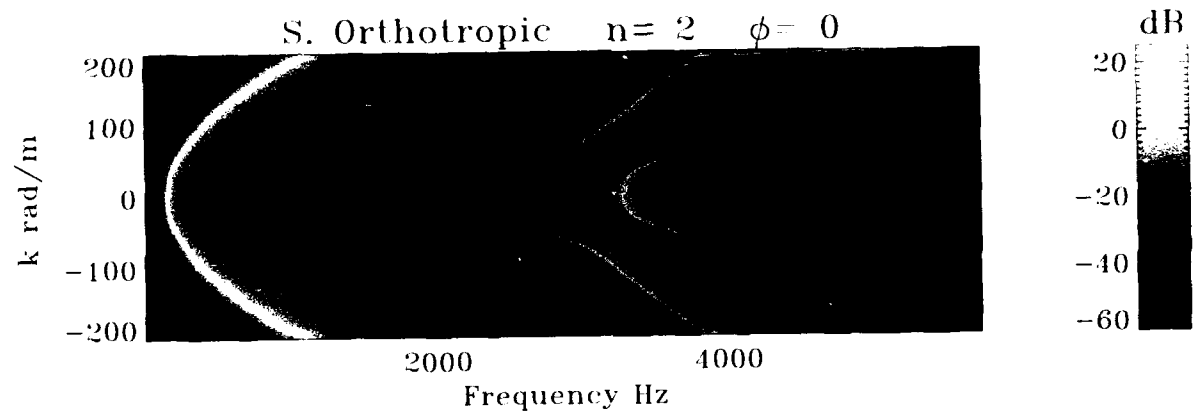

(b)

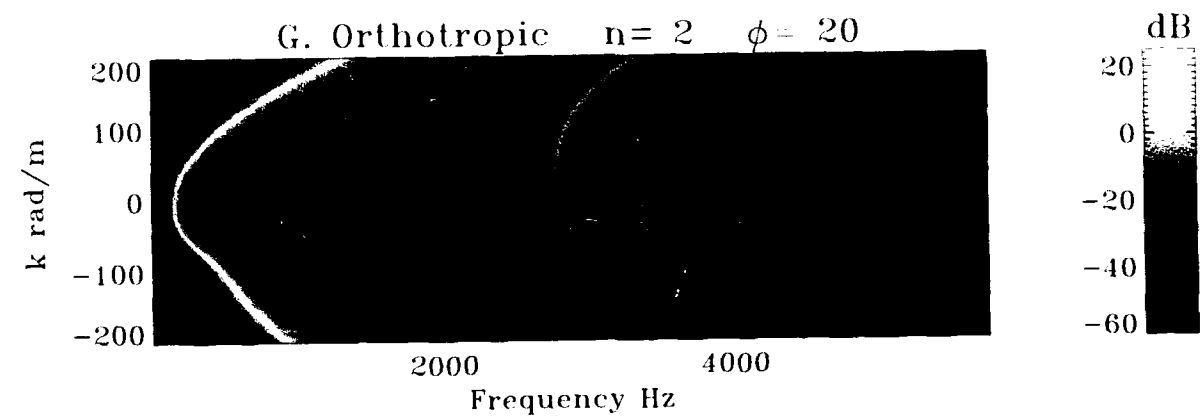

(c)

Figure 58. Bending Shell Transfer Surface (n = 2); dB = $10\log((P_i(a/2)/P_o)^2)$

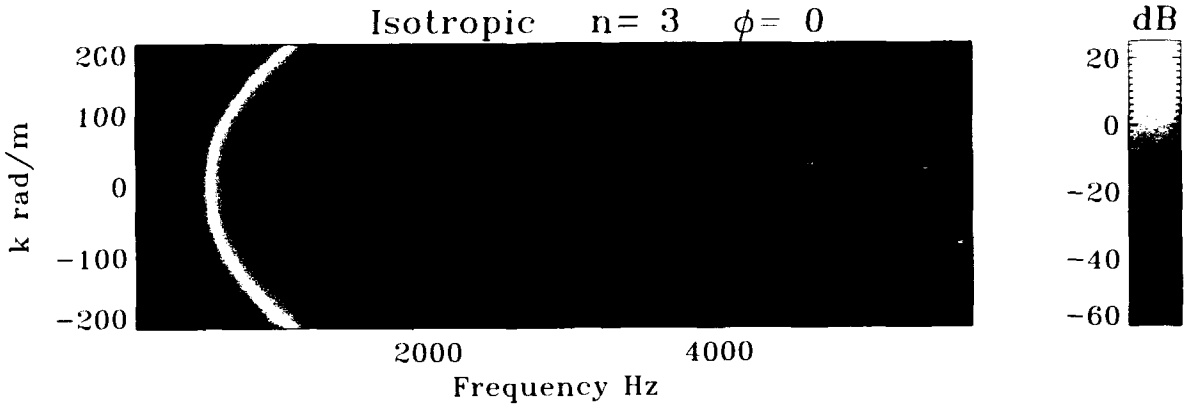

(a)

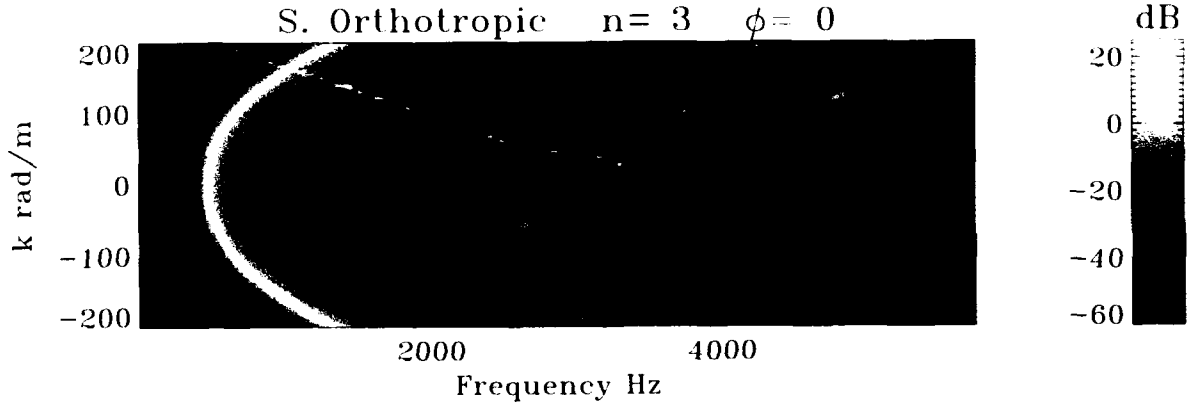

(b)

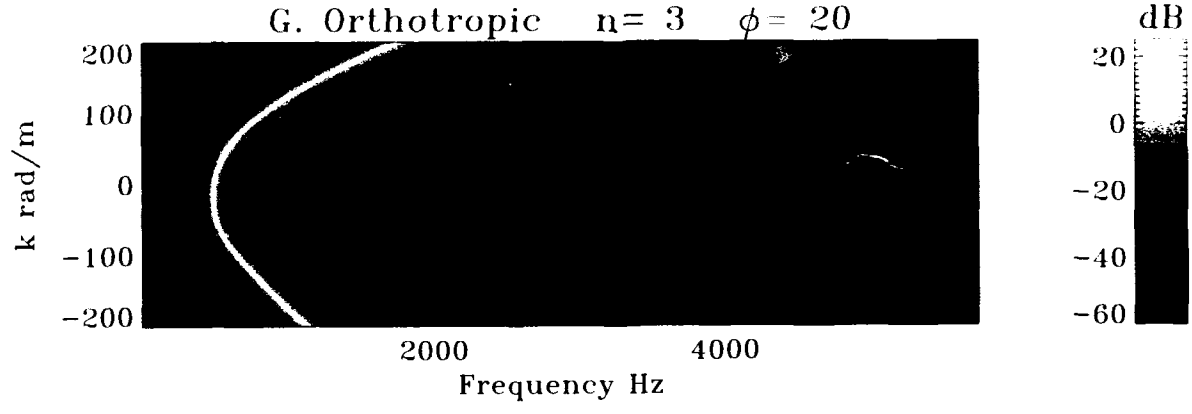

(c)

Figure 59. Bending Shell Transfer Surface (n = 3); dB = 10log($(P_i(a/2)/P_0)^2$)

Outer Fluid Effects on the w Component of the n = 2 Mode

In figures 60 through 62, we see the effects of the outer fluid loading on the w component of mode $n = 2$. The presence of the outer fluid has reduced the cutoff frequency from approximately 200 Hz in the inner-fluid-only case to approximately 150 Hz with both fluids. It should be remembered that both the fluids and the shell have the same density, approximately that of water (1000 kg/m^3). Figure 62 is a comparison of a slice through both surfaces at $k = 0$. The peak value corresponds to a point on the branch and the cutoff frequency for that branch.

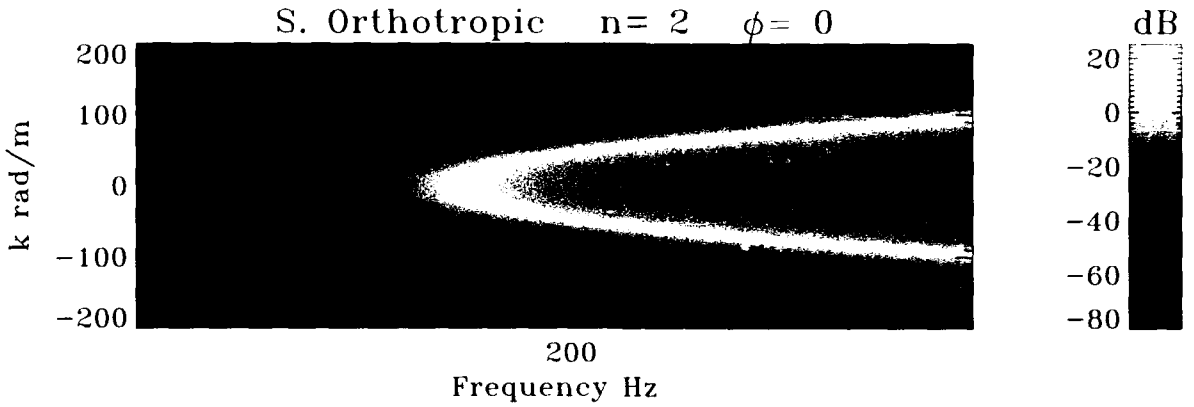

Figure 60. Transfer Surface; dB = 10log(($P_i(a/2)/P_0$)^2), With Outer Fluid Loading

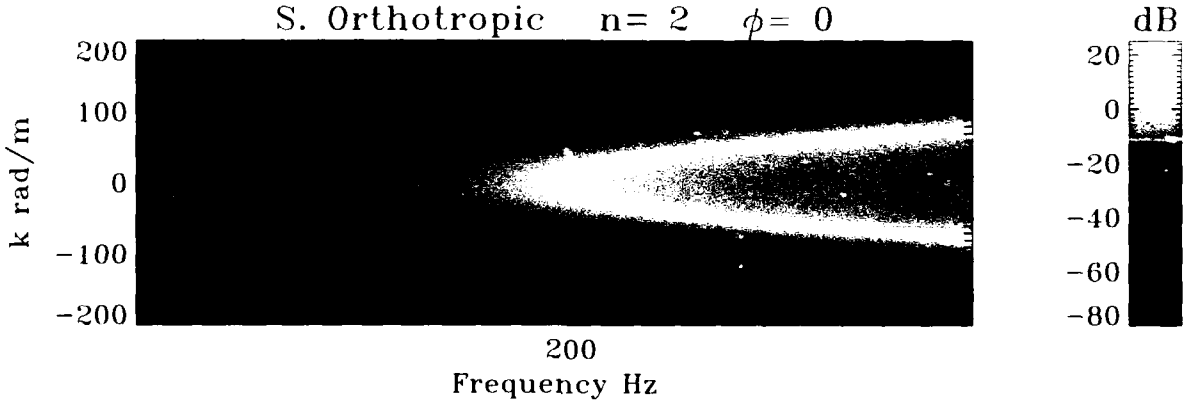

Figure 61. Transfer Surface; dB = 10log(($P_i(a/2)/P_0$)^2), Without Outer Fluid Loading

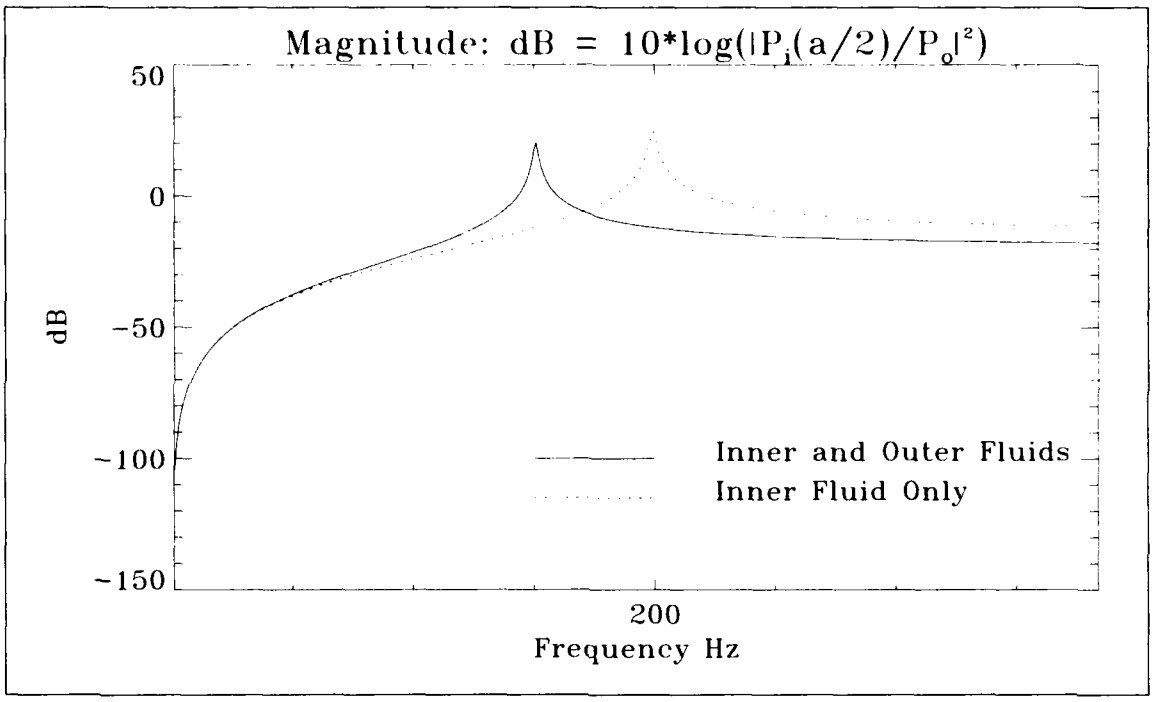

Figure 62. Comparison of Levels at $k = 0$ From Figures 60 and 61

Effects of Wrap Angle ϕ on the n = 2 Mode

Figure 63 displays the effects of increasing the wrap angle from 0 to 90 degrees. The asymmetry introduced by this angle disappears again at $\phi = 90$ degrees, where the structure becomes once again specially orthotropic.

The cutoff frequency for the first branch has increased at $\phi = 90$ degrees because of the increased stiffness in the circumferential direction. The third branch, the v component of mode $n = 2$, is moving in the direction of increasing frequency for the same reason and actually moves out of the range displayed in the k,ω plane.

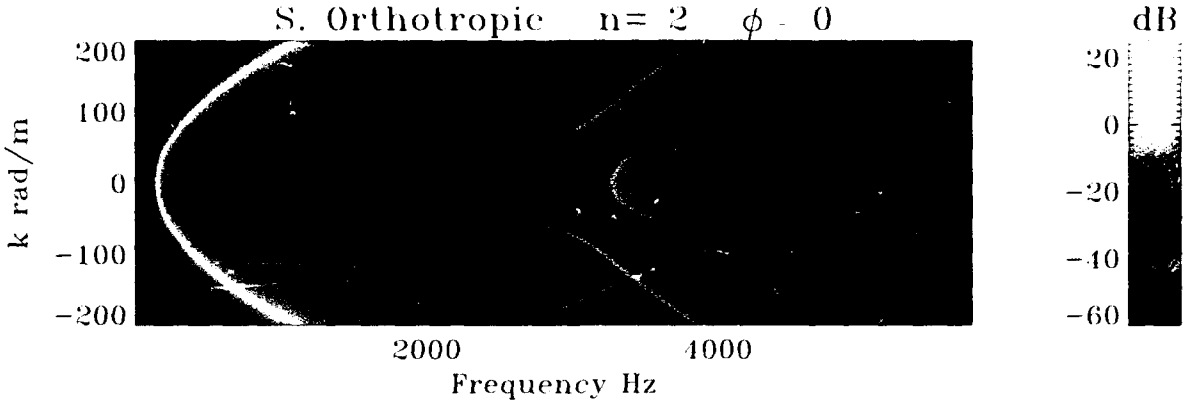

(a)

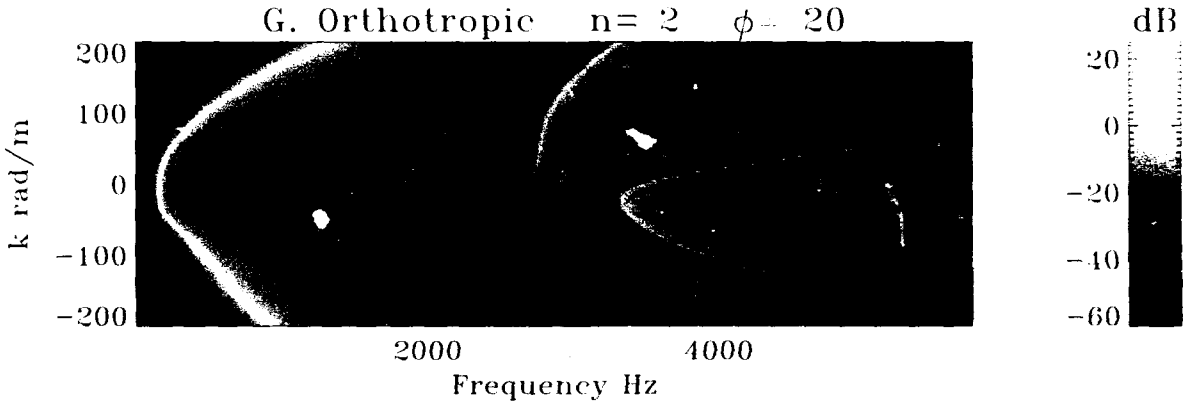

(b)

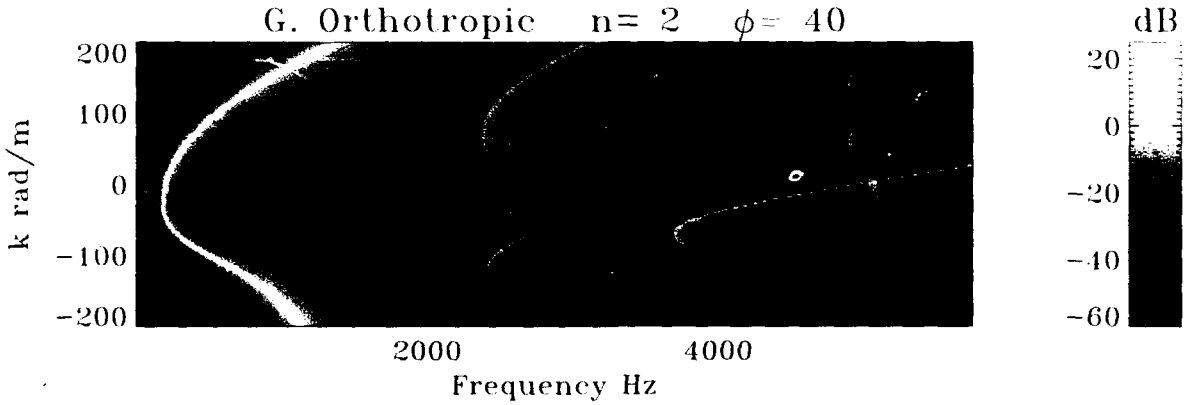

(c)

Figure 63. Bending Shell Transfer Surface (n = 2) for $0 \le \phi \le 90$; dB = $10\log((P_i(a/2)/P_o)^2)$

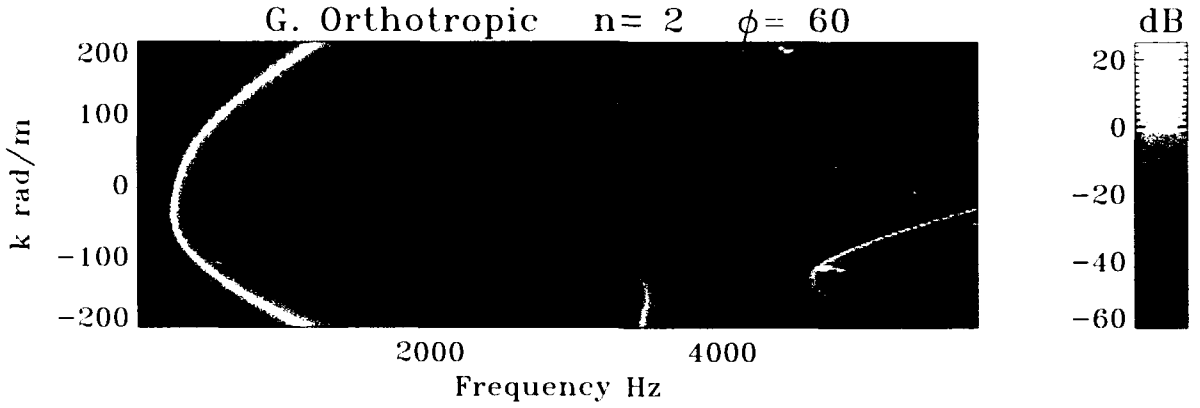

(d)

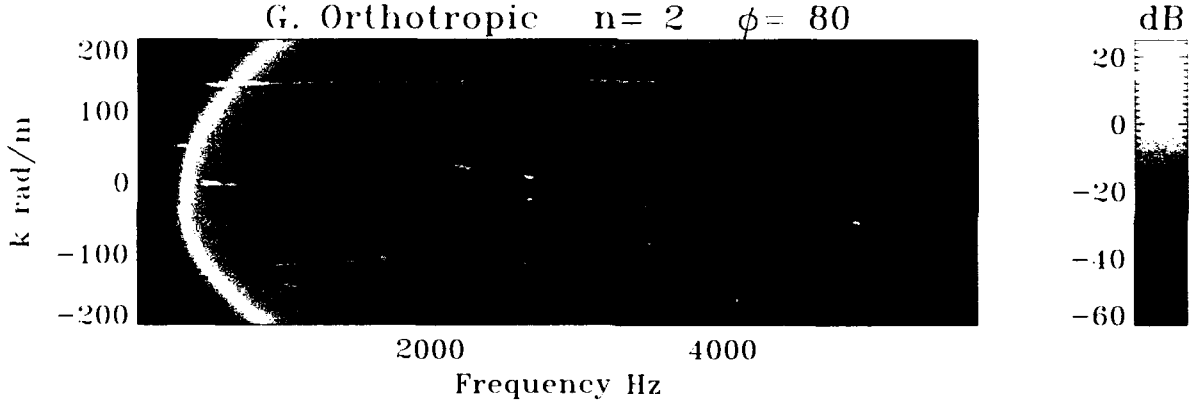

(e)

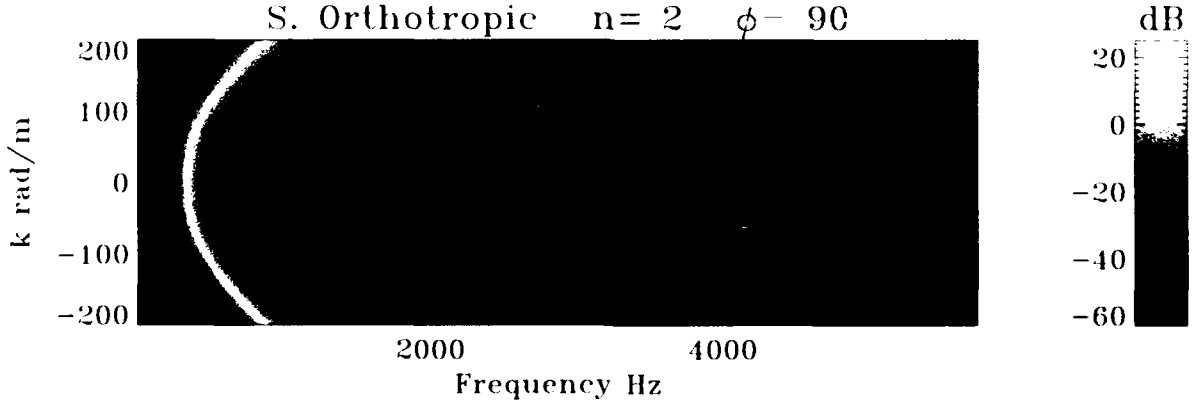

(f)

Figure 63. Bending Shell Transfer Surface (n = 2) for $0 \leq \phi \leq 90$; dB = $10\log((P_i(a/2)/P_o)^2)$ (Cont'd)

Interior Partial Cross Section Filling Core

In figures 64 and 65, we see the branch corresponding to the w component of mode $n = 0$. Since the branches are dispersive, we will describe their velocity by referring to the phase velocity at 45 rad/m. The phase velocity in figure 64 is 37 m/s and, in this case, the shell is fluid filled without an internal core. Let us now place a compressible infinitely long core into the shell; refer to figure C-1 in appendix C. The core has the following parameters:

$$r_c = 7.62 \times 10^{-3} \text{ m (0.3 inches)}$$

$$\nu_c = 0.45,$$

$$E_c = 1.5 \times 10^7 \text{ Pa}, \qquad \zeta_c = 0.01.$$

The transfer surface of figure 65 is computed by substitution of equations C-11 and C-12 for equations (54) and (55) when we evaluate equation (92) at $n = 0$. As seen in the development in appendix C, and now from figure 65, the effect of the core is to slow the phase velocity. The phase velocity from figure 65 at 45 rad/m is 28 m/s.

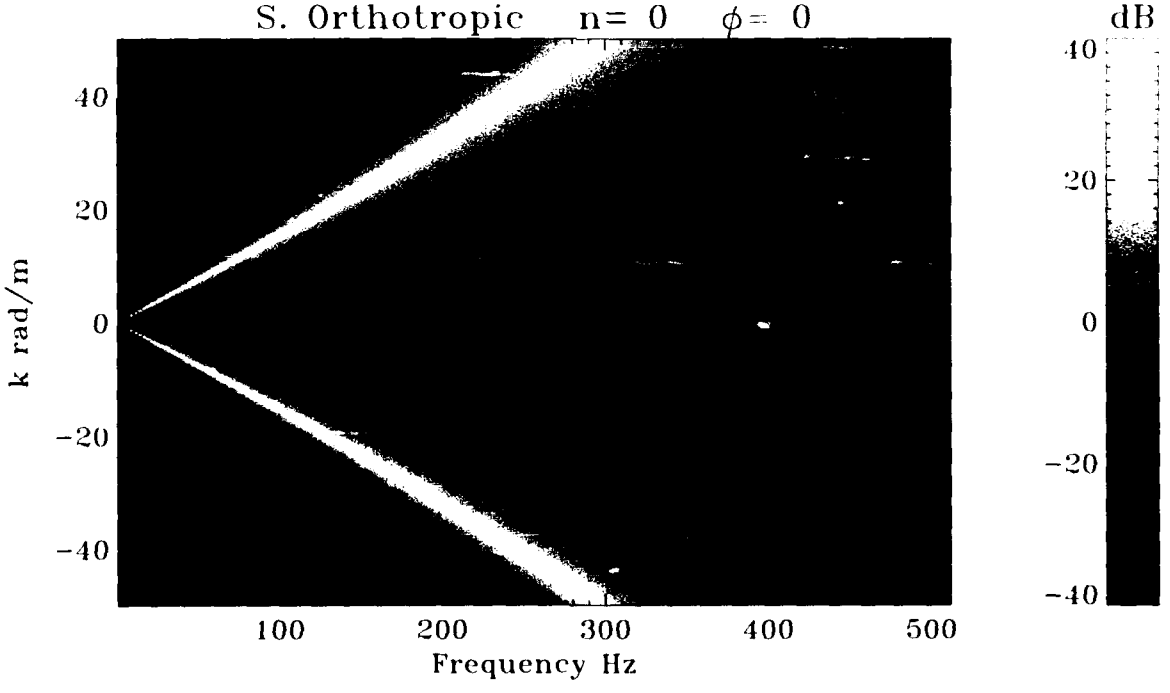

Figure 64. Bending Shell Transfer Surface Without Core; dB = 10log($(P_i(3a/4)/P_0)^2$)

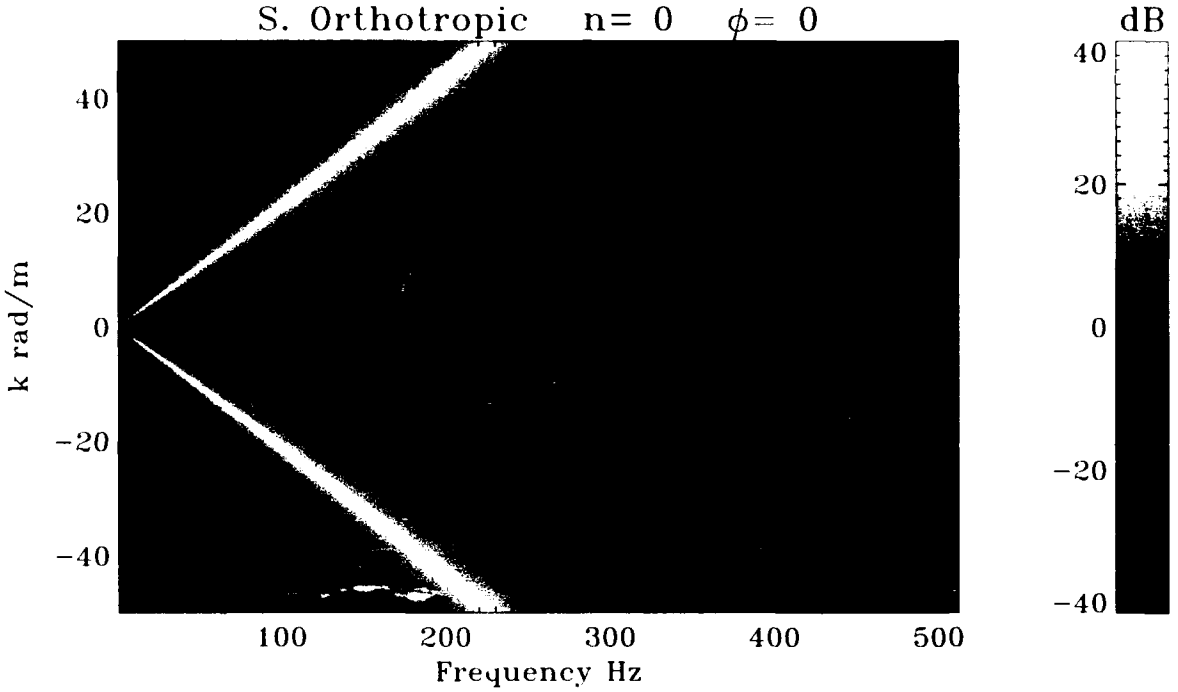

Figure 65. Bending Shell Transfer Surface With Core; dB = 10log($(P_i(3a/4)/P_o)^2$)

An extreme case of a compliant core is represented in figure 66. Material properties and dimensions of this core are

$r_c = 7.62 \times 10^{-3}$ m (0.3 inches),

$\nu_c = 0.45$,

$E_c = 1.0 \times 10^5$ Pa, $\quad \zeta_c = 0.01$.

This core is similar to soft foam rubber, where the fluid does not penetrate the foam. In this case, the phase velocity has slowed to 16 m/s. This very soft core gives rise to branches that bear a close resemblance to the air-backed case that we shall study in a later section.

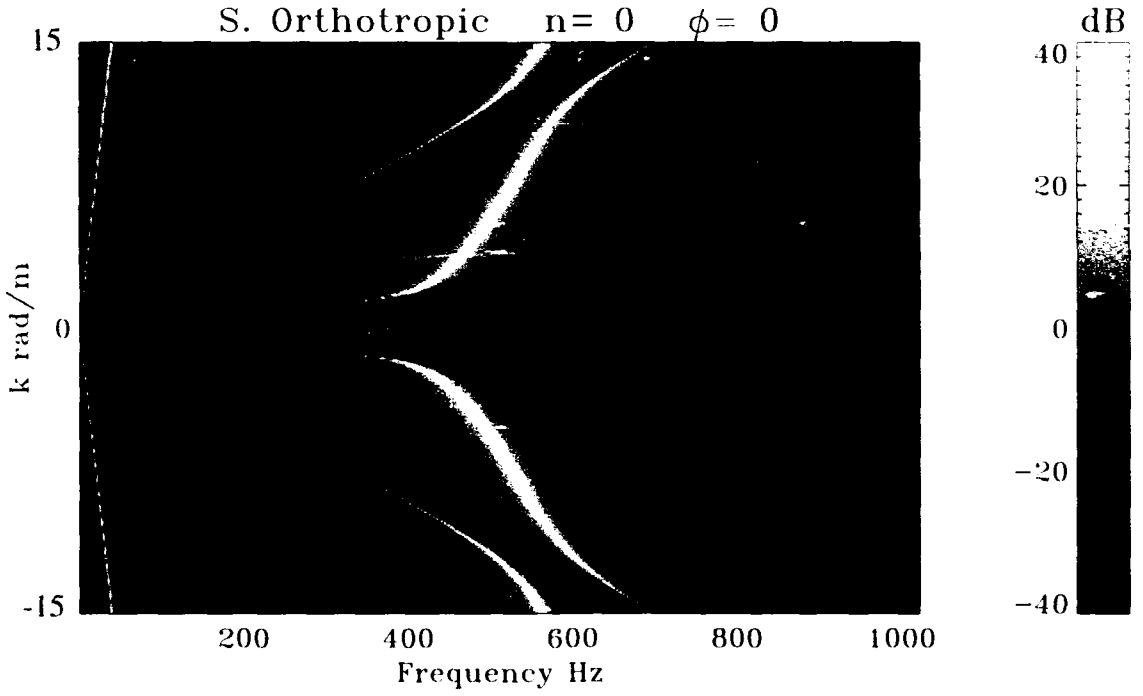

Figure 66. Bending Shell Transfer Surface With Soft Core; dB = 10log($((P_i(3a/4)/P_0)^2)$)

AXIAL SHEAR STRESS TRANSFER SURFACES

Bending Shell

In this section, we will explore the behavior of the branches for the first four modes of propagation from the transfer surfaces computed using equation (93). In this case, the shell is excited with a longitudinal shear stress.

The branches observed in figure 67(a) correspond, as before, to the w and u components of the $n = 0$ mode of propagation; the first (slower speed) branch represents the breathing wave and the second (faster) represents the extensional wave. Figure 67(a)-(c) should be compared with figure 56(a)-(c) to note the difference in structural response between an axial shear stress excitation and a normal pressure excitation. In figure 56(a)-(c), the extensional wave is barely excited, existing at a very low level. However, in figure 67(a)-(c), the extensional wave is strongly evident. The breathing wave is evident as well, but it is lower in level.

Of all the modes of propagation considered for the shell, the extensional wave is the most nondispersive, mainly because this mode engages the shell in minimum bending and very little interaction with the fluids. The addition of longitudinal reinforcement has increased the phase velocity from 138 m/s in the isotropic case of figure 67(a) to 295 m/s in the specially orthotropic case of figure 67(b). Phase and group velocities of the breathing wave have increased most noticeably for the high wavenumbers.

It is interesting to note the generally orthotropic case of figure 67(c), where another branch has appeared. The higher modes ($n = 1$ through $n = 3$) shown in figures 68 through 70, display the mode number, cutoff frequency, and group velocity characteristics that their counterparts did in figures 57 through 59.

Effects of Wrap Angle ϕ on the n = 0 Mode

Let us consider mode $n = 0$ and explore the effects of varying the angle of the reinforcement from 0 to 90 degrees. Figure 71 corresponds to this case. We begin with the breathing wave and extensional wave response for the specially orthotropic structure shown in figure 71(a). As wrap angle increases, we observe a slowing of the extensional wave phase velocity. The breathing wave phase velocity first decreases and then shows an increase, with the change occurring at approximately 45 degrees. This change in phase velocities corresponds to a shifting of stiffness from the longitudinal to the circumferential directions. Between the angles of 0 and 90 degrees, we see another branch developing and then almost disappearing at the 40-degree position, as its phase velocity at first increases to approximately the 45-degree point and then decreases after that.

This additional branch corresponds to the v component of the $n = 0$ mode of propagation, which only exists when the shell becomes generally orthotropic. Figure 37 illustrates the torsional motion of this mode, which occurs because there is coupling between the shear strain and the normal stresses (equation (7)).

Bending Shell Sequence

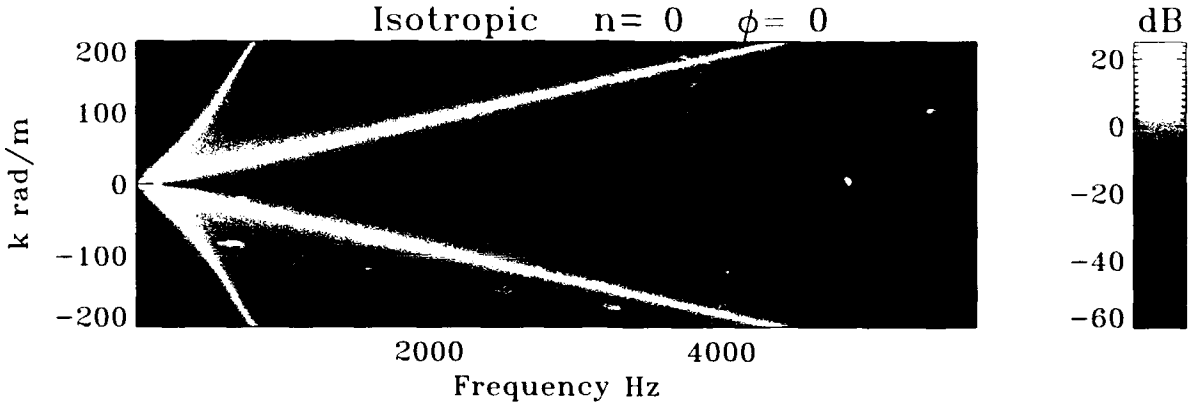

(a)

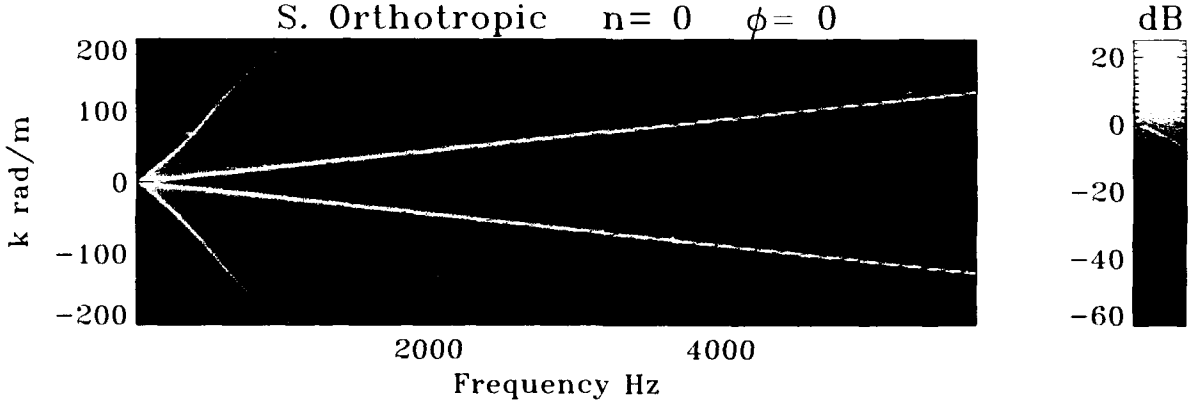

(b)

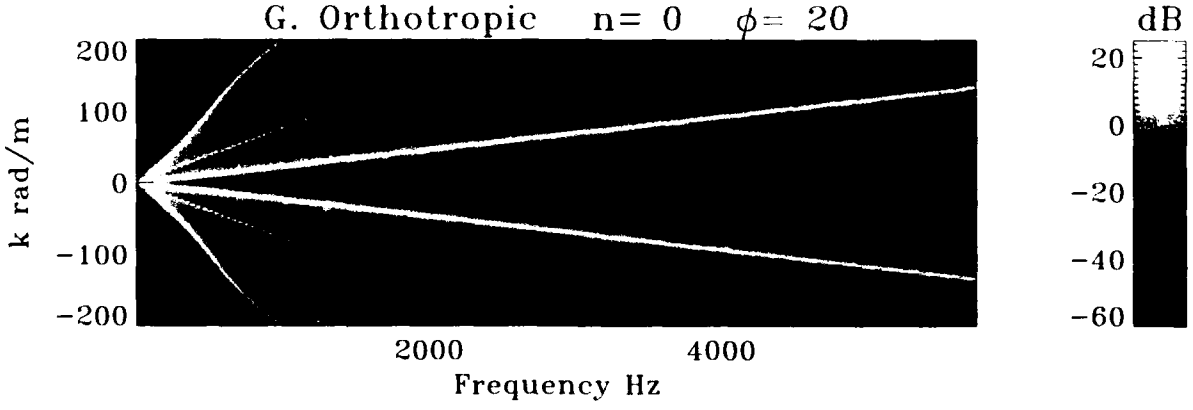

(c)

Figure 67. Bending Shell Transfer Surface (n = 0); dB = 10log($((P_i(a/2)/P_x)^2)$)

Bending Shell Sequence Continued

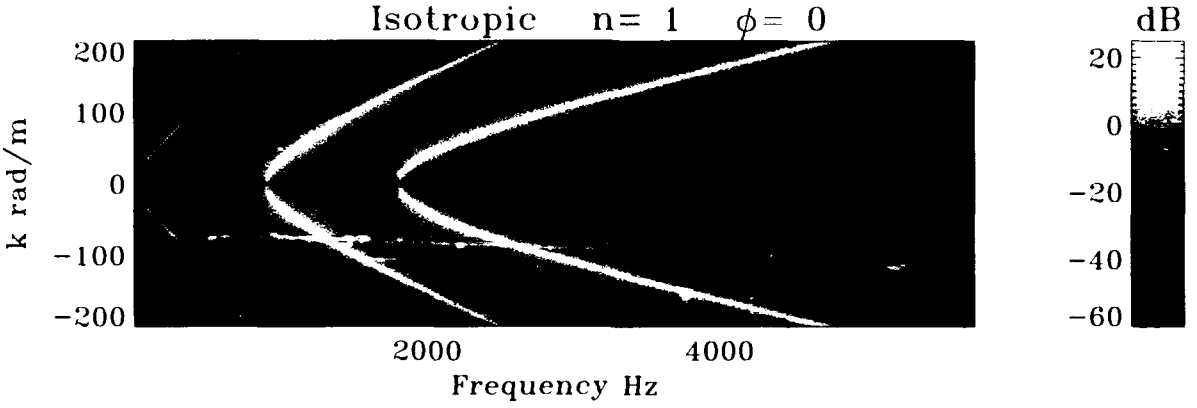

(a)

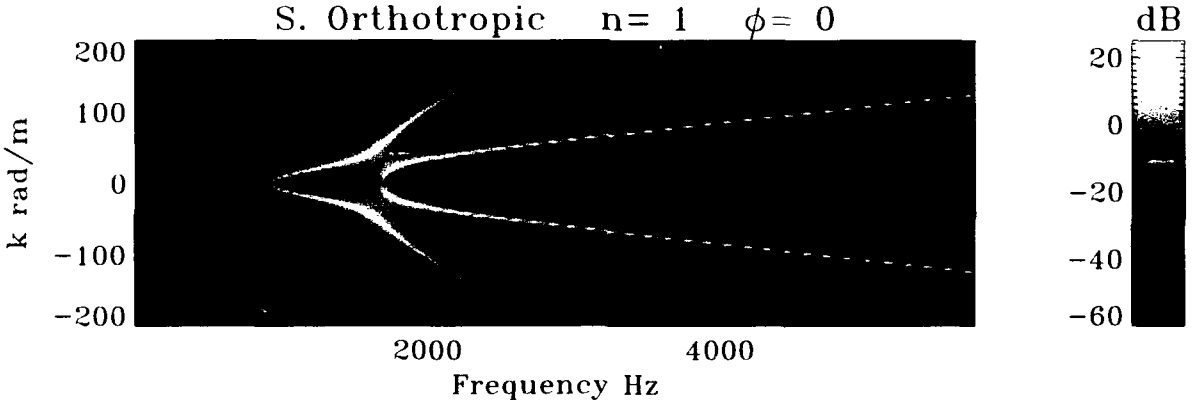

(b)

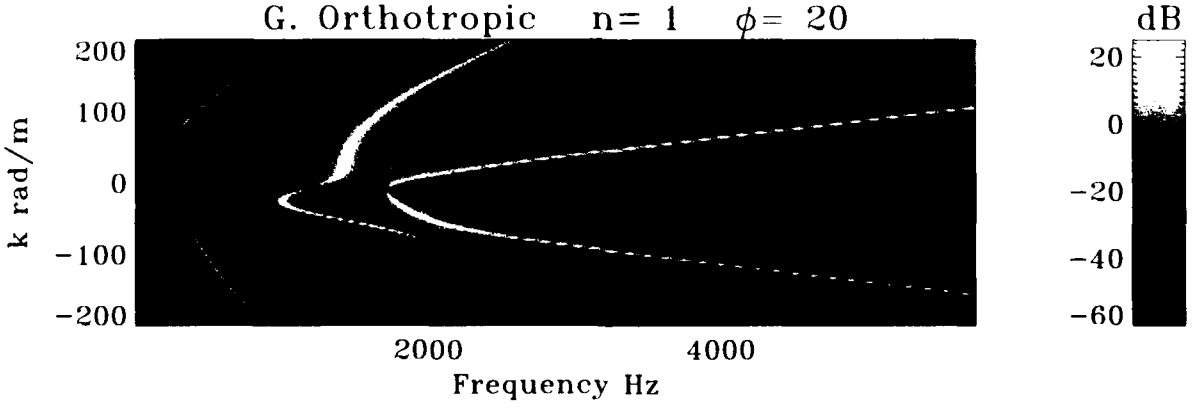

(c)

Figure 68. Bending Shell Transfer Surface (n = 1); dB = 10log($(P_i(a/2)/P_x)^2$)

Bending Shell Sequence Continued

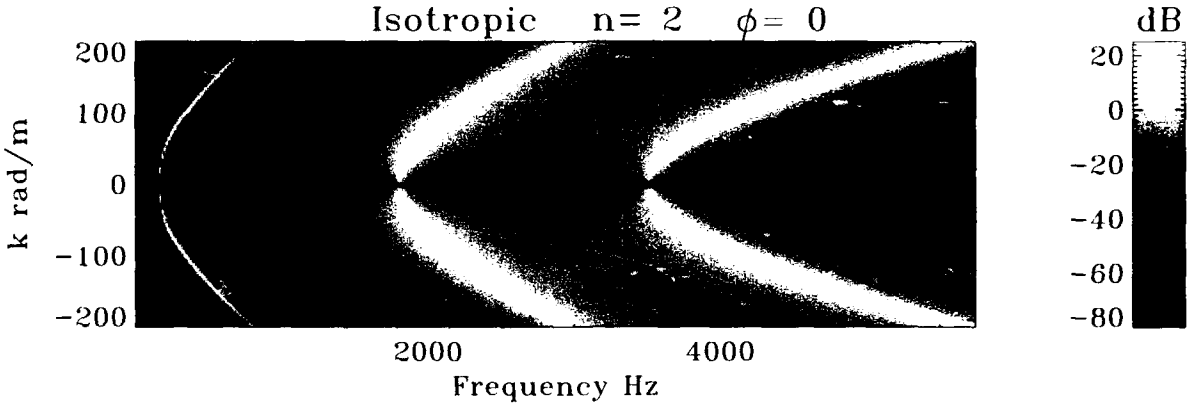

(a)

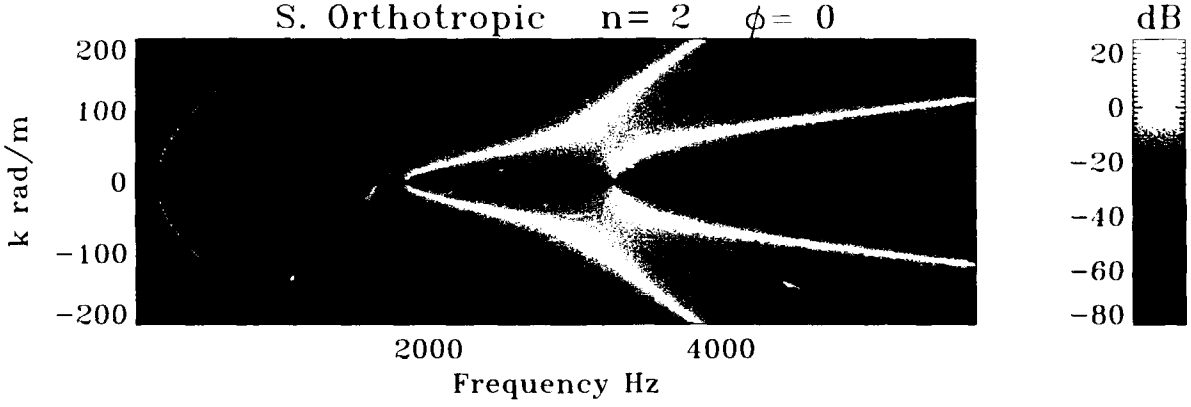

(b)

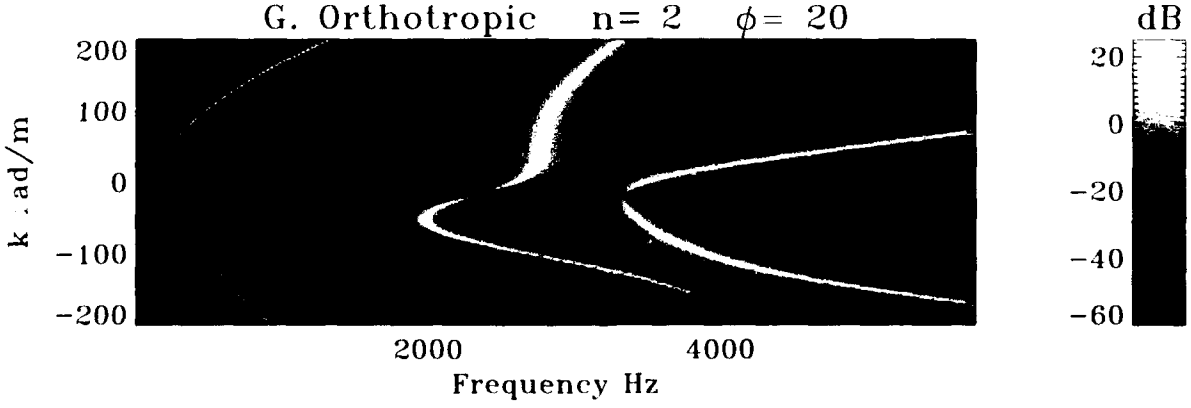

(c)

Figure 69. Bending Shell Transfer Surface (n = 2); dB = 10log($((P_i(a/2)/P_x)^2)$)

Bending Shell Sequence Continued

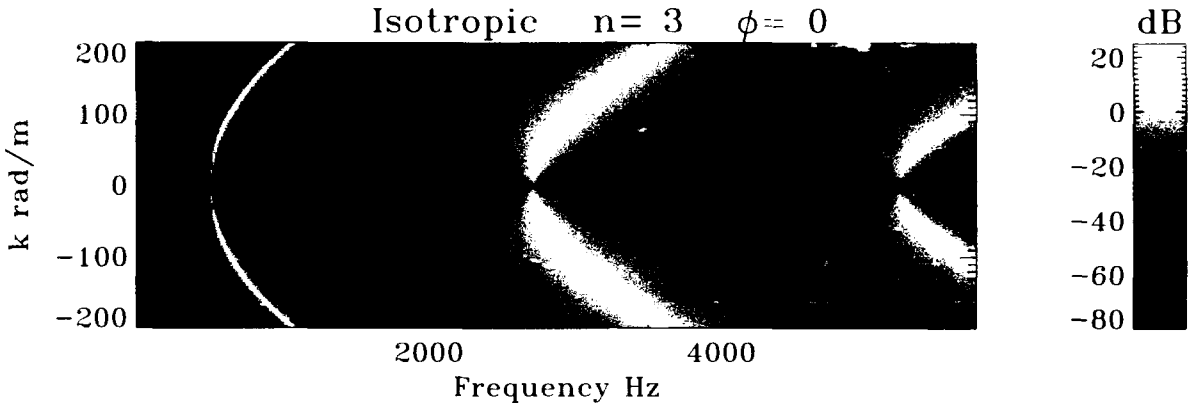

(a)

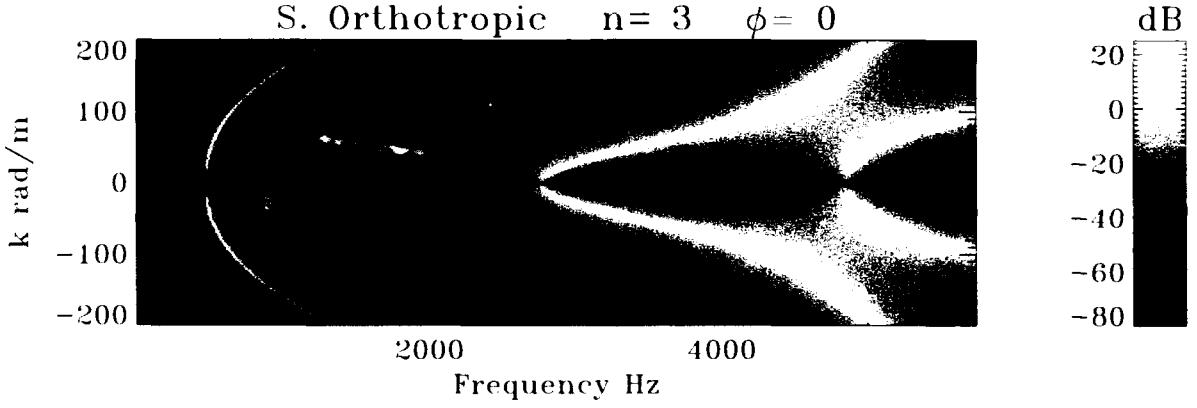

(b)

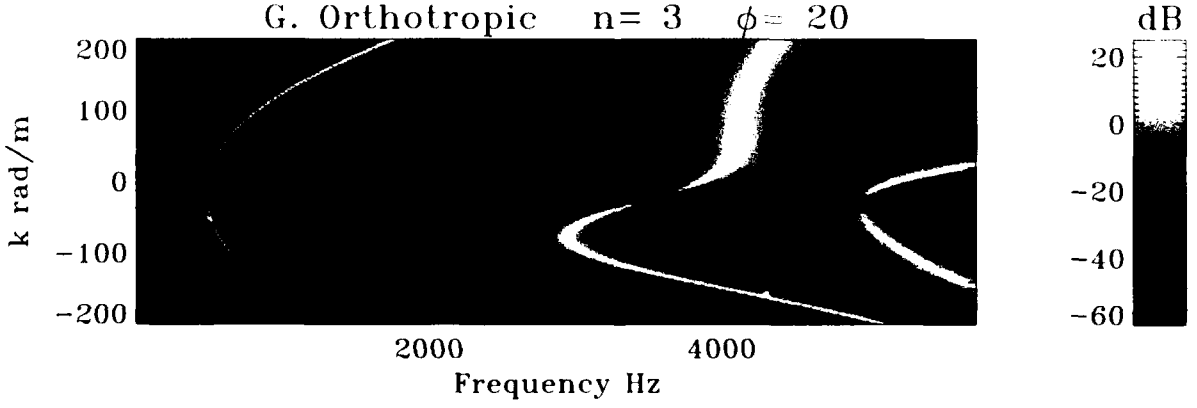

(c)

Figure 70. Bending Shell Transfer Surface (n = 3); dB = $10\log((P_i(a/2)/P_x)^2)$

Effects of Wrap Angle ϕ on the n = 0 Mode

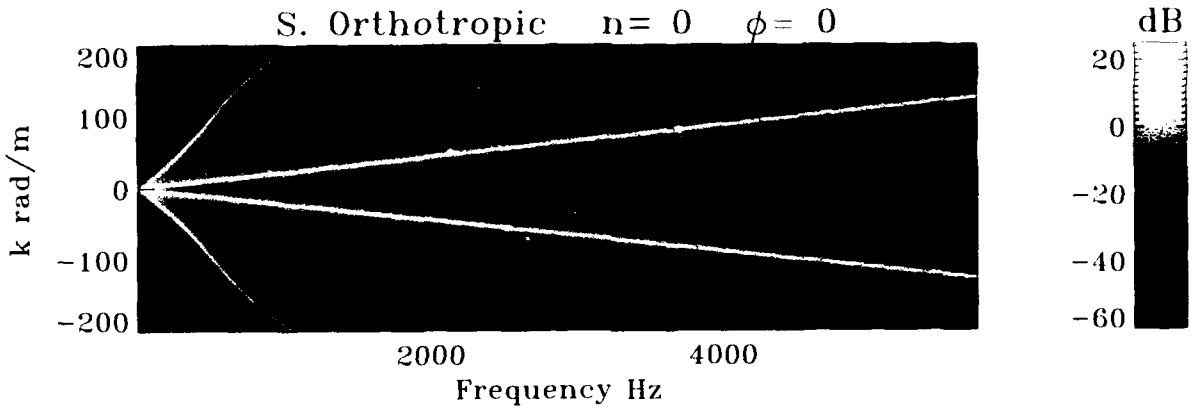

(a)

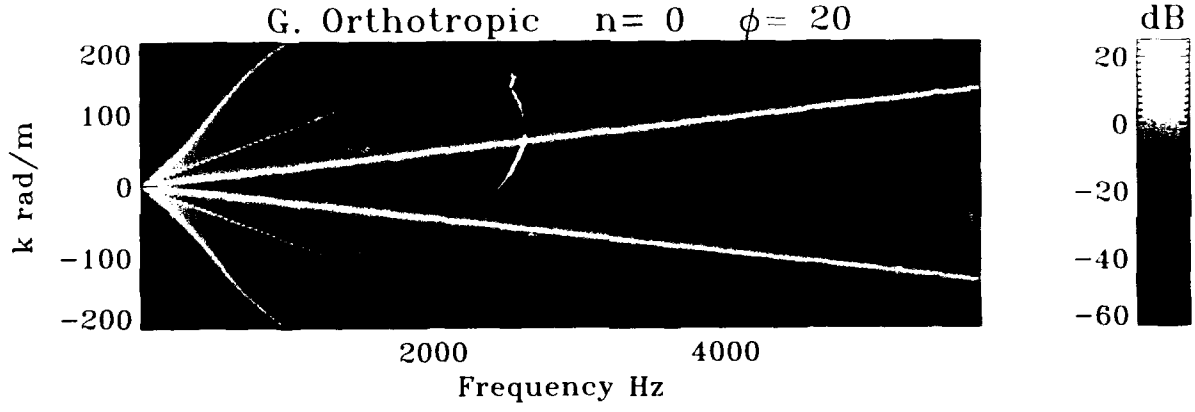

(b)

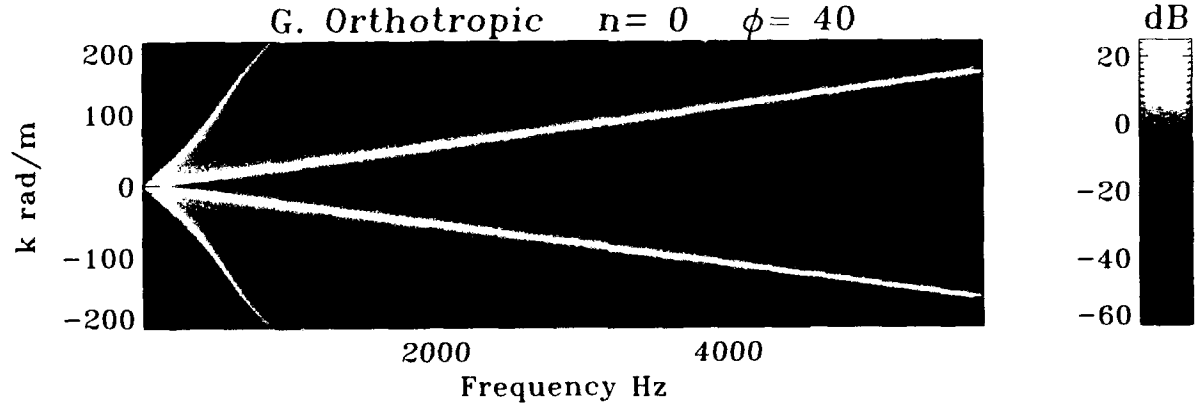

(c)

Figure 71. Bending Shell Transfer Surface (n = 0) for $0 \leq \phi \leq 90$; dB = $10\log((P_i(a/2)/P_x)^2)$

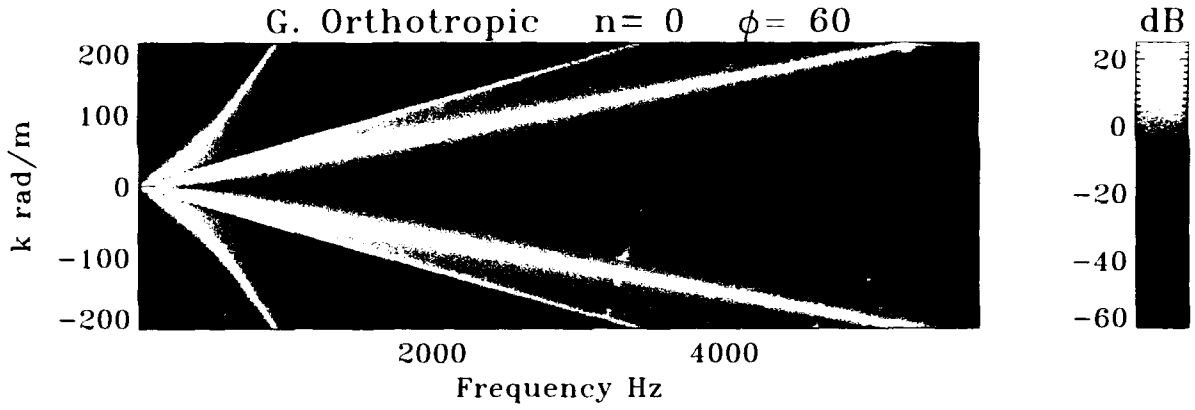

(d)

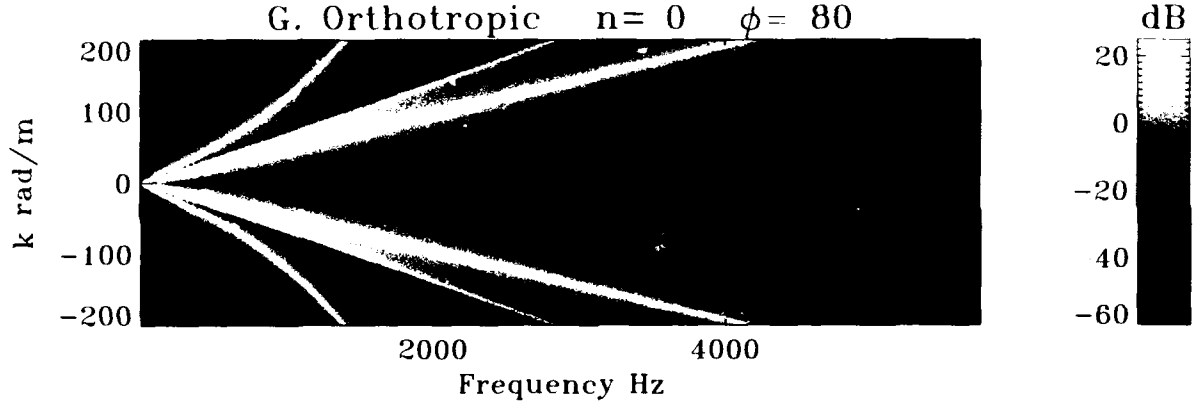

(e)

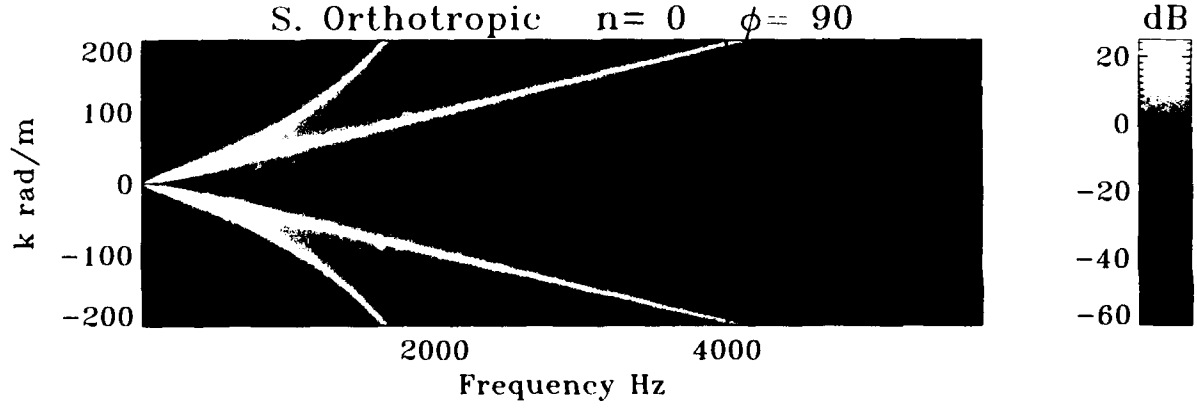

(f)

Figure 71. Bending Shell Transfer Surface (n = 0) for $0 \leq \phi \leq 90$; dB = $10\log((P_i(a/2)/P_x)^2)$ (Cont'd)

SHELL WALL STRAIN TRANSFER SURFACES

Thus far, we have considered responses in the inner fluid created principally by the displacement W. Let us now turn our attention to the shell and explore the strain occurring in the shell wall due to an applied radial pressure excitation from the outer fluid. Additional theoretical development is required to obtain equations for the strain in the shell from the displacement magnitudes, which are provided in equation (89).

Theoretical Development

From equation (89), the displacement magnitudes will be calculated from a P_o excitation only. The stress resultants, equation (13), will be calculated using the displacement magnitudes. The actual stresses will be calculated from the stress resultants. The strains will be calculated from the stresses and then rotated to the desired angle Ψ. It should be noted that Ψ does not have to equal ϕ but can be an independent angle of choice.

From equation (89), the displacement magnitudes of a point in the shell are

$$W = \frac{(S_{11}S_{22} - S_{21}S_{12})}{det[S]} P_o, \tag{96}$$

$$U = \frac{(S_{12}S_{23} - S_{13}S_{22})}{det[S]} P_o, \tag{97}$$

and

$$V = \frac{(-S_{11}S_{23} + S_{13}S_{21})}{det[S]} P_o. \tag{98}$$

The stress resultants needed to compose the stresses are N_{xx}, $N_{\theta\theta}$, $N_{x\theta}$, M_{xx}, $M_{\theta\theta}$, and $M_{x\theta}$. We will use the following linear relationship for the actual distribution of stress across the thickness of the shell:

$$\sigma_{xx} = \frac{N_{xx}}{h} - \frac{12M_{xx}z}{h^3}, \tag{99}$$

$$\sigma_{\theta\theta} = \frac{N_{\theta\theta}}{h} - \frac{12M_{\theta\theta}z}{h^3}, \tag{100}$$

$$\sigma_{x\theta} = \frac{N_{x\theta}}{h} - \frac{12M_{x\theta}z}{h^3}. \tag{101}$$

It should be noted that

$$\sigma_{x\theta} = \frac{N_{x\theta}}{h} - \frac{12M_{x\theta}z}{h^3} \qquad \text{and} \qquad \sigma_{\theta x} = \frac{N_{\theta x}}{h} - \frac{12M_{\theta x}z}{h^3} \tag{102}$$

will not necessarily yield identical results. There is, then, some objection to the assumed linear stress distribution. However, as Flugge[18] points out, the difference is usually small in thin shells and can be ignored. We should add that a better approach might be to take an average of the two shear stress equations in equation (102) rather than use equation (101) alone.

After the necessary derivatives of the displacements have been taken and inserted into equation (13), the stress resultants are written in terms of the displacement magnitudes as

$$N_{xx} = i\{U(D_{11}k + D_{16}\frac{n}{a}) + V(D_{12}\frac{n}{a} + D_{16}k + K_{16}\frac{k}{a^2})\} + W\{\frac{D_{12}}{a} + K_{11}\frac{k^2}{a} + K_{16}\frac{k}{a^2}\},$$

$$N_{\theta\theta} = i\{U(D_{12}k + D_{26}\frac{n}{a} + K_{26}\frac{n}{a^3}) + V(D_{22}\frac{n}{a} + D_{26}k)\}$$

$$+ W\{\frac{D_{22}}{a} + \frac{K_{22}}{a^3}(1-n^2) - K_{26}\frac{nk}{a^2}\},$$

$$N_{x\theta} = i\{U(D_{16}K + D_{66}\frac{n}{a}) + V(D_{26}\frac{n}{a} + D_{66}k + K_{66}\frac{k}{a^2})\} + W\{\frac{D_{26}}{a} + K_{16}\frac{k^2}{a} + K_{66}\frac{nk}{a}\},$$

$$M_{xx} = -i\{UK_{11}\frac{k}{a} + V(K_{12}\frac{n}{a^2} + 2K_{16}\frac{k}{a})\} + -W\{K_{11}k^2 + K_{12}\frac{n^2}{a^2} + 2K_{16}\frac{nk}{a}\},$$

$$M_{\theta\theta} = i\frac{K_{26}}{a^2}\{Un - Vka\} + W\{K_{22}\frac{(1-n^2)}{a^2} - K_{12}k^2 - 2K_{26}\frac{nk}{a}\},$$

$$M_{x\theta} = -i\{UK_{16}\frac{k}{a} + V(K_{26}\frac{n}{a^2} + 2K_{66}\frac{k}{a})\} - W\{K_{16}k^2 + K_{26}\frac{n^2}{a^2} + 2K_{66}\frac{nk}{a}\}. \tag{103}$$

Equations (99) through (101) are used to solve for the stresses. The final steps now involve the calculation of the strain. The strain-stress relations are then[19]

$$\begin{bmatrix} \varepsilon_{xx} \\ \varepsilon_{\theta\theta} \\ \varepsilon_{x\theta} \end{bmatrix} = \begin{bmatrix} \bar{S}m_{11} & \bar{S}m_{12} & \bar{S}m_{16} \\ \bar{S}m_{12} & \bar{S}m_{22} & \bar{S}m_{26} \\ \bar{S}m_{16} & \bar{S}m_{26} & \bar{S}m_{33} \end{bmatrix} \begin{bmatrix} \sigma_{xx} \\ \sigma_{\theta\theta} \\ \sigma_{x\theta} \end{bmatrix} . \tag{104}$$

The Sm and $\bar{S}m$ coefficients are given by

$$Sm_{11} = \frac{1}{E_1},$$

$$Sm_{12} = -\frac{\nu_{12}}{E_1},$$

$$Sm_{22} = \frac{1}{E_2},$$

$$Sm_{66} = \frac{1}{G_{12}},$$

$$\bar{S}m_{11} = Sm_{11}\cos^4\phi + (2Sm_{12} + Sm_{66})\sin^2\phi\cos^2\phi + Sm_{22}\sin^4\phi,$$

$$\bar{S}m_{12} = Sm_{12}(\sin^4\phi + \cos^4\phi) + (Sm_{11} + Sm_{22} - Sm_{66})\sin^2\phi\cos^2\phi,$$

$$\bar{S}m_{22} = Sm_{11}\sin^4\phi + (2Sm_{12} + Sm_{66})\sin^2\phi\cos^2\phi + Sm_{22}\cos^4\phi,$$

$$\bar{S}m_{16} = (2Sm_{11} - 2Sm_{12} - Sm_{66})\sin\phi\cos^3\phi + -(2Sm_{22} - 2Sm_{12} - Sm_{66})\sin^3\phi\cos\phi,$$

$$\bar{S}m_{26} = (2Sm_{11} - 2Sm_{12} - Sm_{66})\sin^3\phi\cos\phi + -(2Sm_{22} - 2Sm_{12} - Sm_{66})\sin\phi\cos^3\phi,$$

$$\bar{S}m_{66} = 2(2Sm_{11} + 2Sm_{22} - 4Sm_{12} - Sm_{66})\sin^2\phi\cos^2\phi + Sm_{66}(\sin^4\phi + \cos^4\phi) . \tag{105}$$

The strains in the shell coordinate system are then rotated to the desired angular position, ψ, using the rotation matrix given by equation (106):

$$\begin{bmatrix} \varepsilon_{1'1'} \\ \varepsilon_{2'2'} \\ \varepsilon_{1'2'} \end{bmatrix} = \begin{bmatrix} \cos^2\psi & \sin^2\psi & -2\sin\psi\cos\psi \\ \sin^2\psi & \cos^2\psi & 2\sin\psi\cos\psi \\ \sin\psi\cos\psi & -\sin\psi\cos\psi & \cos^2\psi - \sin^2\psi \end{bmatrix} \begin{bmatrix} \varepsilon_{xx} \\ \varepsilon_{\theta\theta} \\ \varepsilon_{x\theta} \end{bmatrix} . \tag{106}$$

The primes on the subscripts of the stresses refer to the coordinate system specified by the angle ψ, where ψ is measured as ϕ is (see figure 3). If $\psi = \phi$, then the following relation exists:

$$\begin{bmatrix} \varepsilon_{1'1'} \\ \varepsilon_{2'2'} \\ \varepsilon_{1'2'} \end{bmatrix} = \begin{bmatrix} \varepsilon_{11} \\ \varepsilon_{22} \\ \varepsilon_{12} \end{bmatrix} . \tag{107}$$

Transfer Surface ε_{11}/P_o

There is a large volume of data available to the analyst at this point. The wrap angle of the reinforcement ϕ can be varied. The strains are available at any angle, ψ, and at any location across the shell thickness from $-\frac{h}{2} \le z \le \frac{h}{2}$. The strain, ε_{11}, is the change in length per unit length of composite shell material when the stress is applied to the 1 face and in the 1 direction. The 1 direction corresponds to a principal material property direction.

We will consider the following restricted case consisting of ε_{11}/P_o, calculated at $z = h/2$, with the simplification that ψ will be chosen to be equal to ϕ. Therefore, we will be examining strains in the shell along the ϕ direction.

Liquid-Filled Shell

Let us begin by returning to the urethane shell with inner and outer fluids. In figure 72, the transfer surface for the longitudinal strain has been calculated. The two branches correspond to the breathing and extensional waves in an isotropic shell. Over this limited range of wavenumber, the slope of both branches is quite linear; at this point, the breathing wave has not become dispersive.

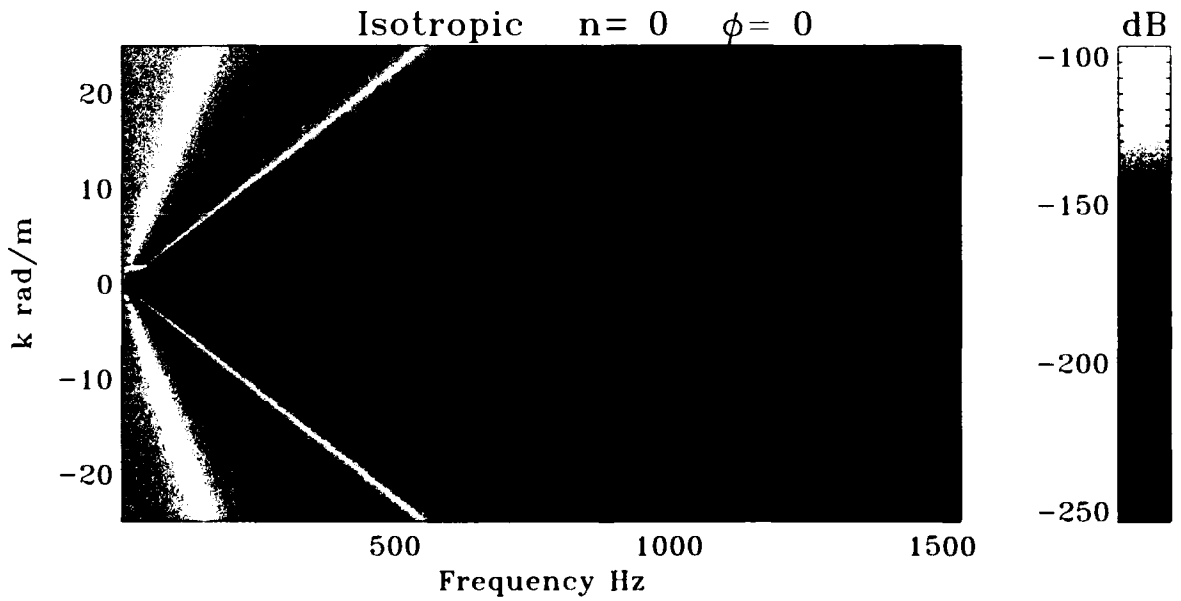

Figure 72. Bending Shell Transfer Surface (Liquid-Filled); dB = 10log($(\varepsilon_{11}(h/2)/P_0)^2$)

Air-Filled Shell

For the remainder of this discussion, we will change the properties of the inner fluid to those corresponding to air, results are presented as the stiffness of the shell and the reinforcing fiber are gradually increased for mode $n = 0$. The properties of the inner fluid are now

$$\rho_i = 1.2 \text{ kg/m}^3,$$

$$c_i = 343 \text{ m/s}.$$

We will begin with the transfer surface for the isotropic cylinder in figure 73. To provide an understanding of what type of wave propagation each branch represents, we plot the individual displacement magnitudes in figure 74 for $k = 9.15$ rad/m.

For the first resonant peak in figure 74, U exhibits the maximum displacement. The second and third resonant peaks are modes of propagation in w. We see coupling between the displacements as we did before in figure 46. There is also a strong similarity to figure 66, the case of the soft compliant core. The properties of the soft core are very similar to those of air. Therefore the internal stiffness of the system of figure 66 is governed by the core, and the effect of the inner fluid has been diminished.

In the circumferential direction, ε_{22}/P_o is plotted in figure 75. Figure 76 is a comparison of the longitudinal and circumferential strains at $k = 0.1$ rad/m. From this figure, we see, as expected, that the circumferential strain is some 20 dB larger than the longitudinal strain.

When longitudinal reinforcement is added, the branches reorient, as shown in figure 77. Again, we turn to analyzing the displacements corresponding to this specially orthotropic structure. The first resonance in figure 78 now corresponds to a mode of propagation in w, followed by a mode in u for the second resonance. The third resonance behaves as in figure 74, a mode in w. Increasing the shell stiffness in the longitudinal direction has increased the phase velocity of the u component of mode $n = 0$ (figure 77). The order of the branches, from left to right, now corresponds to w, u, w components of mode $n = 0$, respectively.

For the generally orthotropic shell (figures 79 and 80), we find the transfer surfaces to include a new branch, a v component of mode $n = 0$. The second, third, and fourth branches are now modes in which U is the maximum displacement (figure 80). Figures 74, 78, and 80 provide a very clear reminder that, for the $n = 0$ axisymmetric mode of propagation, $v = 0$ for isotropic and specially orthotropic shells. An $n = 0$ vibration only produces a v displacement in generally orthotropic shells.

Strain In The Shell

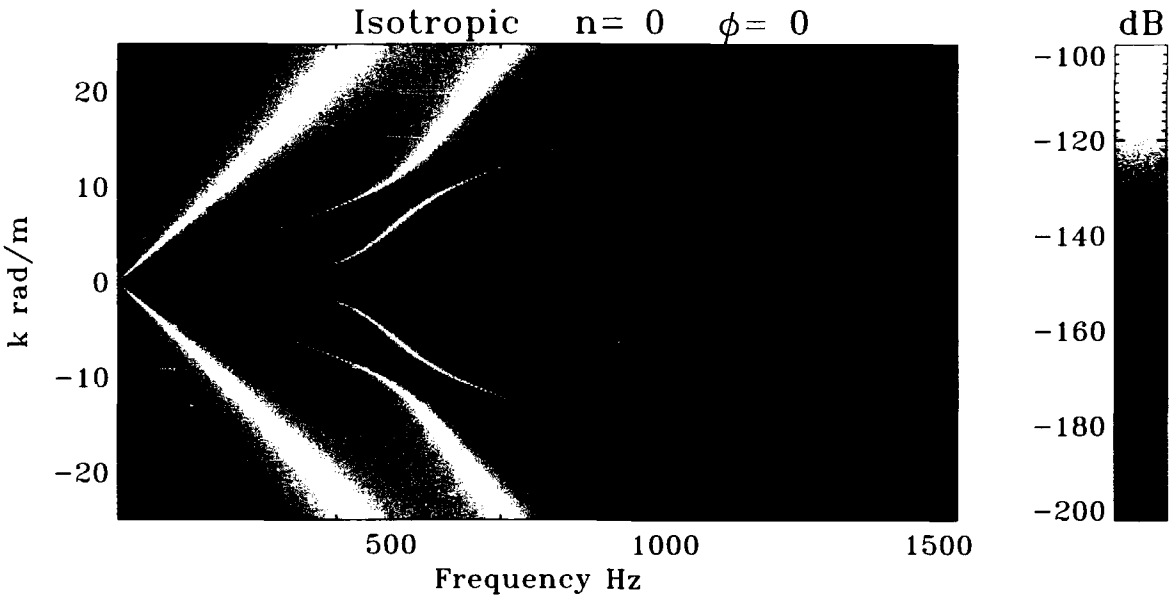

Figure 73. Isotropic Bending Shell Transfer Surface (Air-Filled); dB = 10log($(\varepsilon_{11}(h/2)/P_0)^2$)

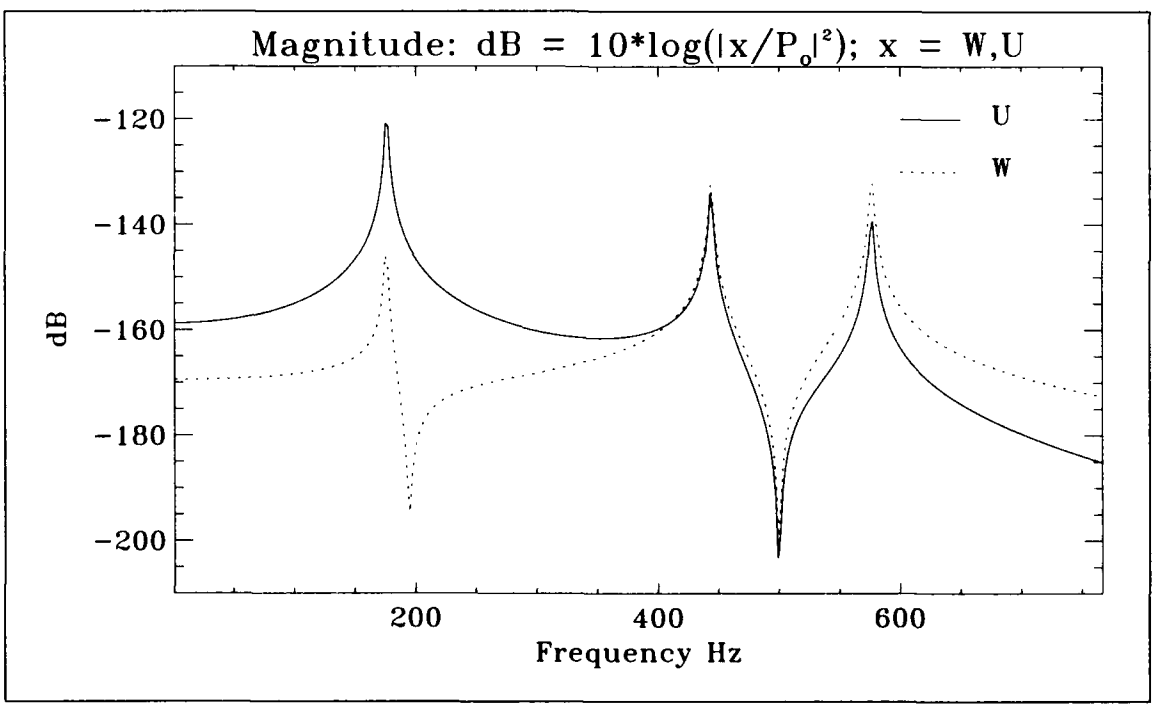

Figure 74. *U* and *W* Component Amplitudes at k = 9.15 rad/m From Figure 73

Strain In The Shell Continued

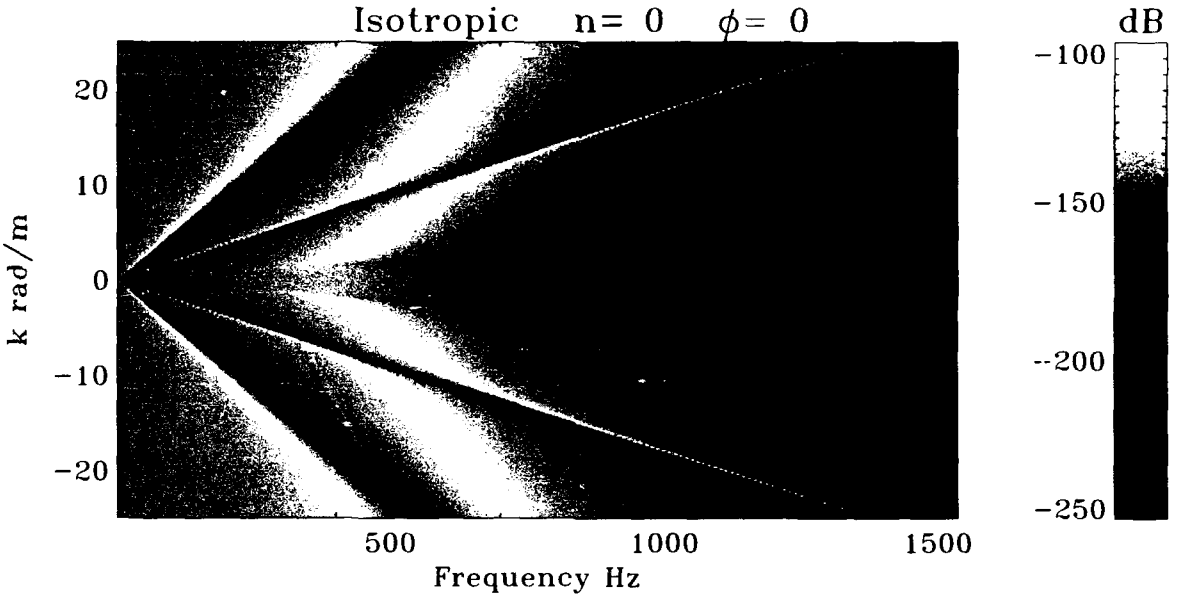

Figure 75. Isotropic Bending Shell Transfer Surface (Air-Filled); dB = 10log($(\varepsilon_{22}(h/2)/P_0)^2$)

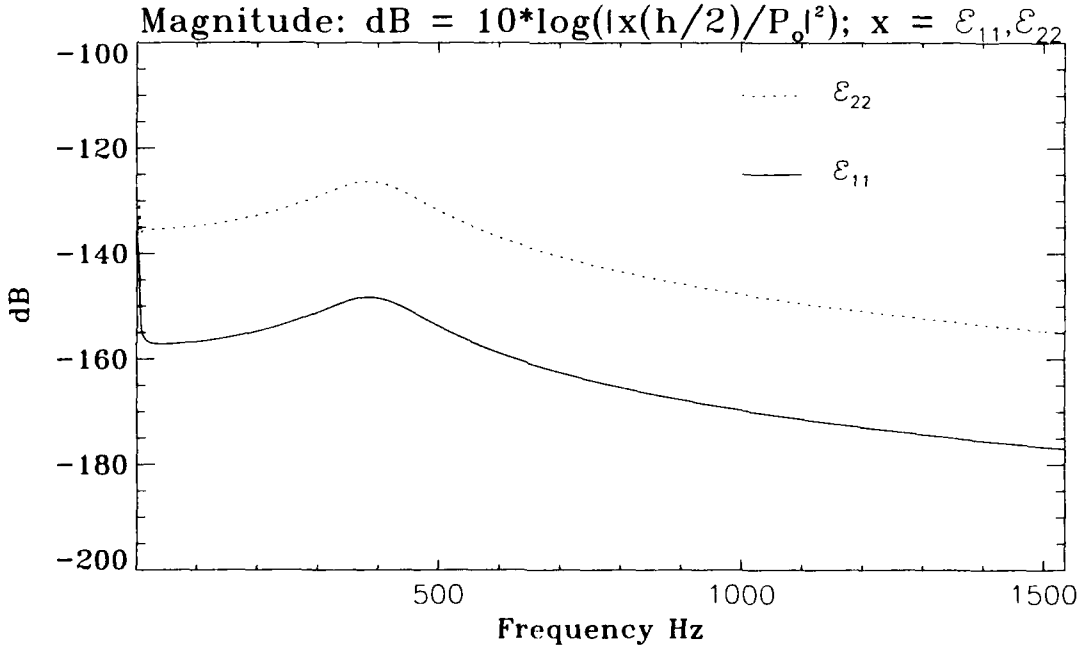

Figure 76. Strain Comparison at k = 0.1 rad/m From Figures 73 and 75

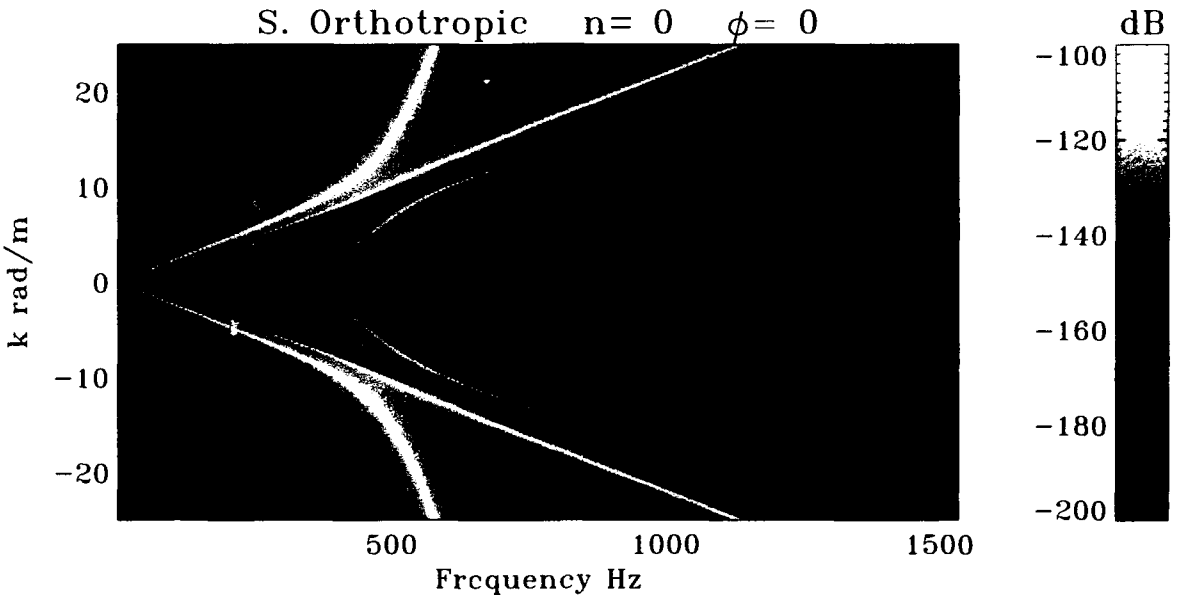

Figure 77. S. Orthotropic Bending Shell Transfer Surface (Air-Filled); dB = 10log($(\varepsilon_{11}(h/2)/P_o)^2$)

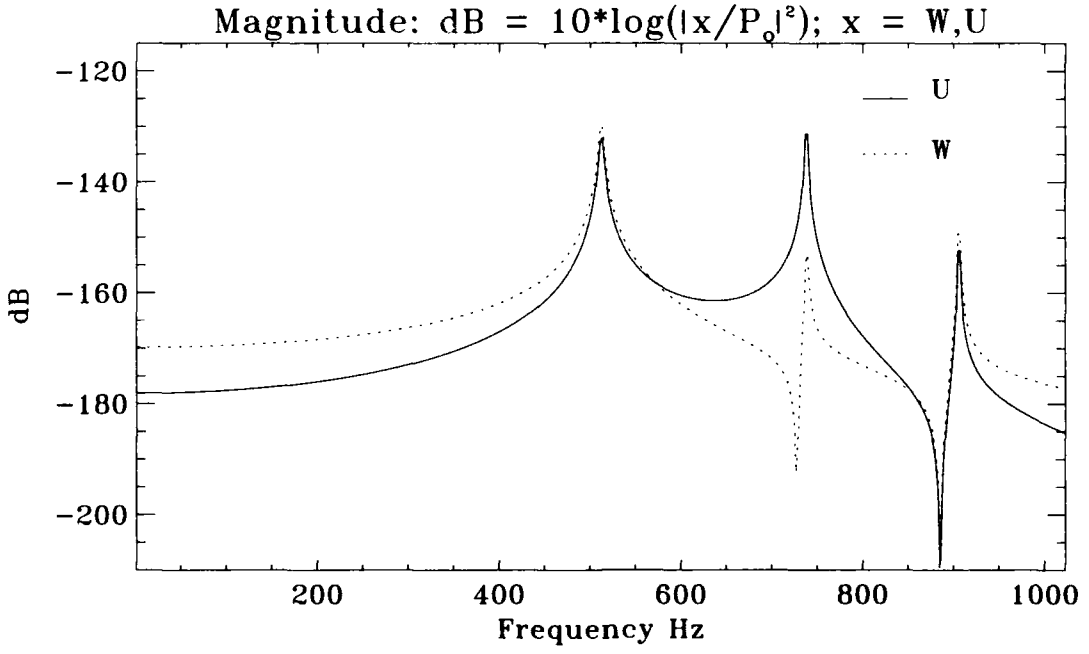

Figure 78. *U* and *W* Component Amplitudes at k = 16.2205 rad/m From Figure 77

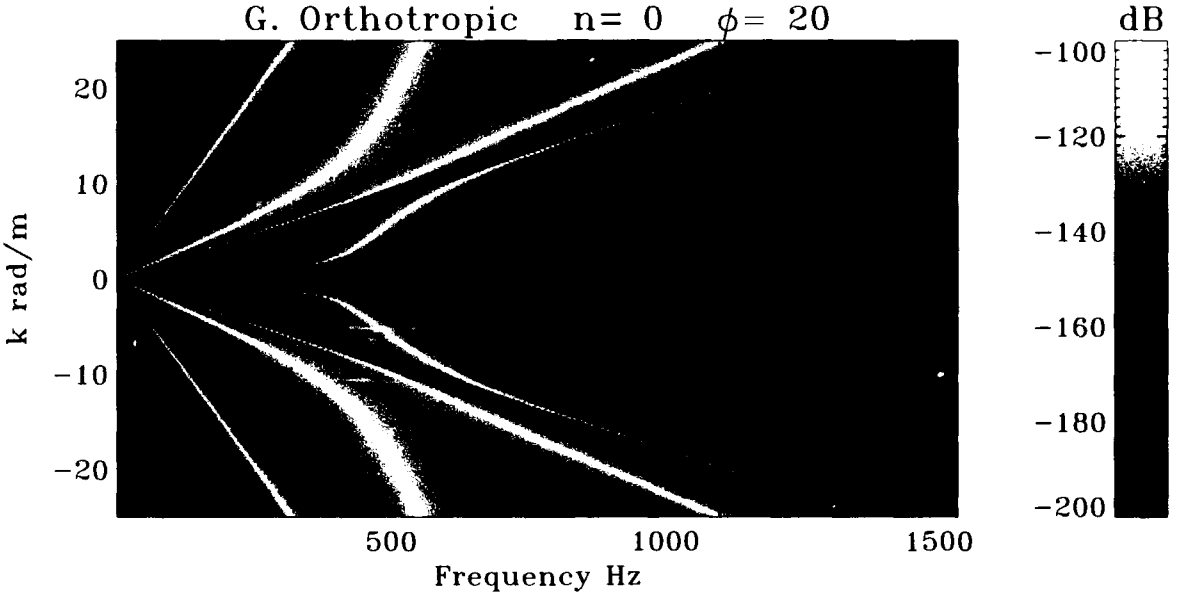

Figure 79. G. Orthotropic Bending Shell Transfer Surface (Air-Filled); dB = 10log($(\varepsilon_{11}(h/2)/P_0)^2$)

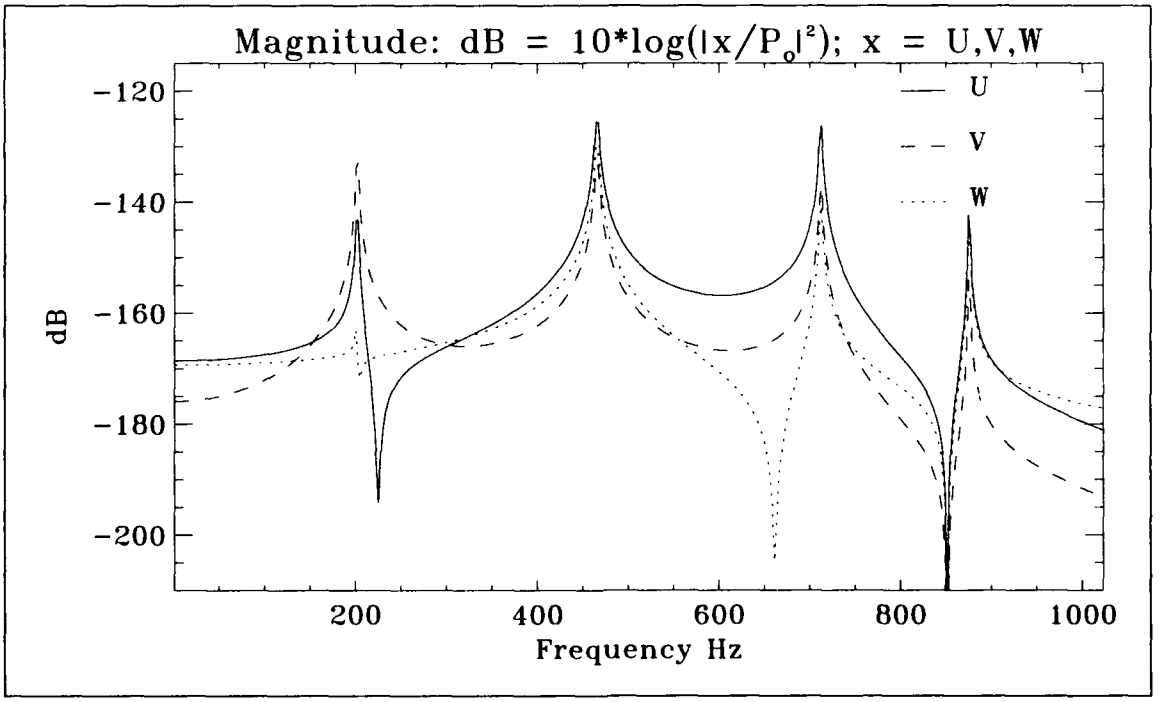

Figure 80. *U*, *V*, and *W* Component Amplitudes at k = 15.5905 rad/m From Figure 79

Air-Filled Shell of Increasing Stiffness

All the data presented thus far have been for the urethane shell. The modulus of elasticity for the shell matrix and reinforcement will be increased to the following values in figures 81 through 89. The shell will remain air backed while it is immersed in the outer fluid (whose properties are given with the data on the urethane shell).

Shell Data for Figure 81

$E_m = 1.5 \times 10^8$ Pa, $\zeta_m = 0.01$,

$\nu_m = 0.40$,

$E_f = 1.5 \times 10^{10}$ Pa, $\zeta_f = 0.0$,

$\nu_f = 0.15$.

Figures 82, 83, *and* 85 *Through* 89

$E_m = 2.5 \times 10^9$ Pa, $\zeta_m = 0.01$,

$\nu_m = 0.40$,

$E_f = 7.0 \times 10^{10}$ Pa, $\zeta_f = 0.0$,

$\nu_f = 0.15$.

Shell Data for Figure 84

$E_m = 2.5 \times 10^9$ Pa, $\zeta_m = 0.1$,

$\nu_m = 0.40$,

$E_f = 7.0 \times 10^{10}$ Pa, $\zeta_f = 0.0$,

$\nu_f = 0.15$.

Comparing figures 79, 81, and 82, we see all the branches becoming less dispersive as the stiffness of the shell is increased. The phase velocity increases as well with this progression in stiffness.

Figures 83 and 84 compare two levels of damping. Broadening of the width of the branches is obvious in figure 84. The resulting decrease in the peak level of the branches is most apparent in figure 85, where we compare a cut in wavenumber through both transfer surfaces.

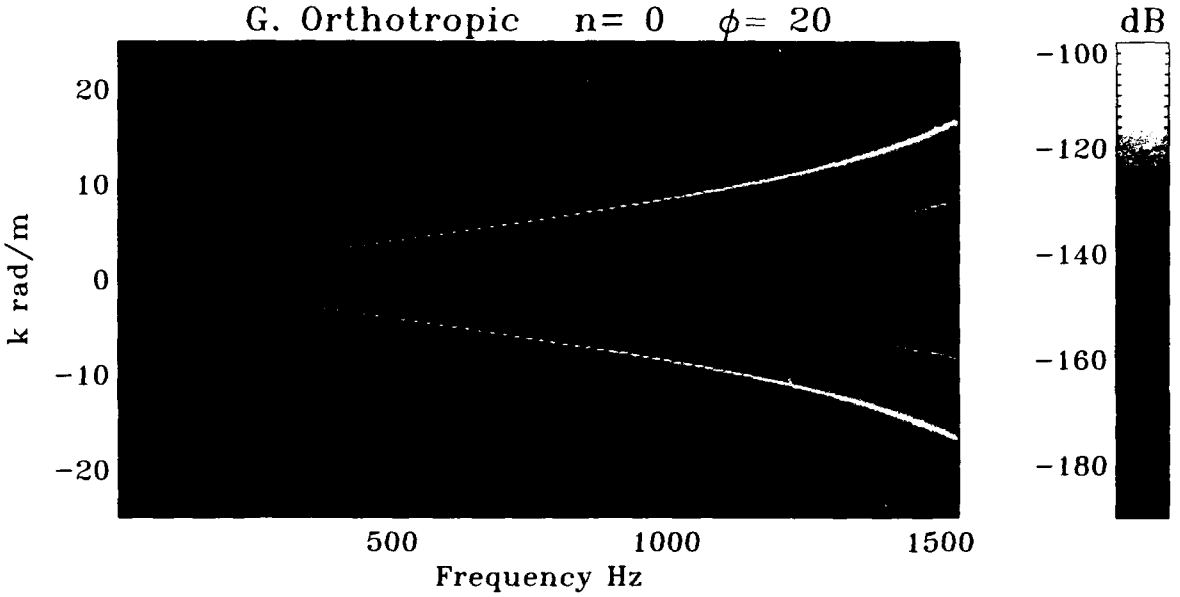

Figure 81. Transfer Surface (E_m = 1.5 X 10^9 Pa, E_f = 1.5 X 10^{10} Pa); dB = 10log(($\varepsilon_{11}(h/2)/P_o$)^2)

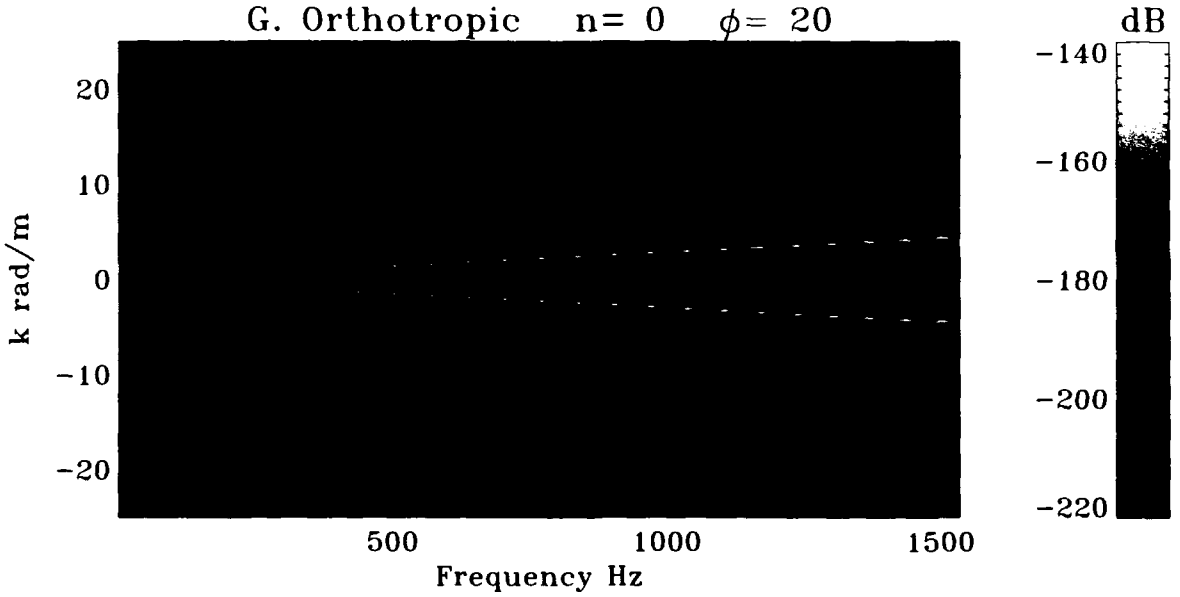

Figure 82. Transfer Surface (E_m = 2.5 X 10^9 Pa, E_f = 7.0 X 10^{10} Pa); dB = 10log(($\varepsilon_{11}(h/2)/P_o$)^2)

Extensional Waves

Returning to figure 83, we observe that the branches shown for this $n = 0$ mode are the least dispersive of all the cases presented. This shell is the best example of a fulfillment of the assumptions made when the simple expression for the phase velocity of the extensional wave given by equation (75) is derived. The effects of the fluids and bending stiffness were neglected in the derivation of equation (75) along with the frequency-dependent terms. The second branch in figure 83 corresponds to the u component of mode $n = 0$. From equation (75), a phase velocity of 2105 m/s is calculated. From figure 83, the reciprocal of the slope of the branch yields 2136 m/s. Both values are in very close agreement and provide a good example of the case where the simple expression is valid.

Expanding the frequency range to 11,500 Hz, we will look at transfer surfaces for the stiffest shell (figure 82) up to mode $n = 3$ as before. Once again, the strain plotted in the surface corresponds to the ϕ direction shown above each surface.

As frequency increases, the $n = 0$ modes become dispersive. Because of the extreme stiffness of this shell, only the first two components, w and u, of the $n = 1$ mode of propagation are visible within the frequency range chosen for display. Only the w component of the $n = 2$ and $n = 3$ modes appears in figures 88 and 89. The cutoff frequencies are extremely high for such stiff shells.

General observations concerning modes $n = 0$ through $n = 3$ reveal an increase in cutoff frequency with increasing mode number as well as decreasing phase and group velocity for a given component of a mode at a fixed wavenumber for a given category of shell stiffness (i.e., isotropic, specially orthotropic, or generally orthotropic). This means that energy propagates more slowly in the branches corresponding to a particular component of a mode as the mode number is increased for a fixed wavenumber.

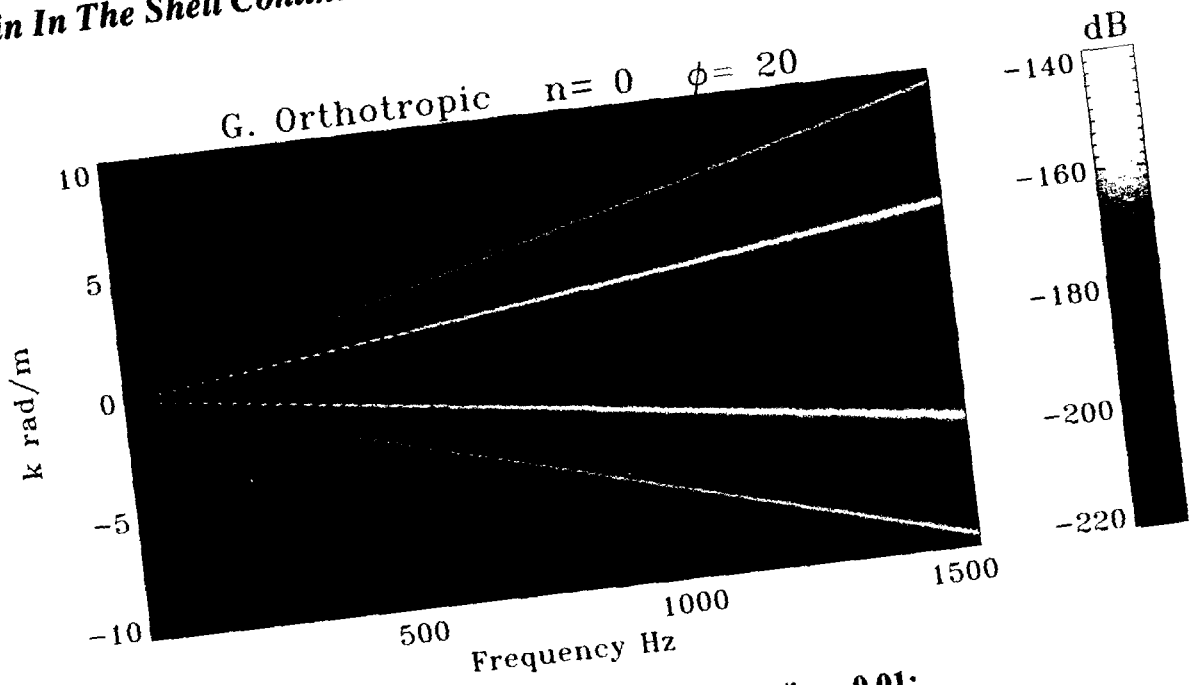

Figure 83. Transfer Surface with ζ_m = 0.01; dB = 10log($(\varepsilon_{11}(h/2)/P_o)^2$)

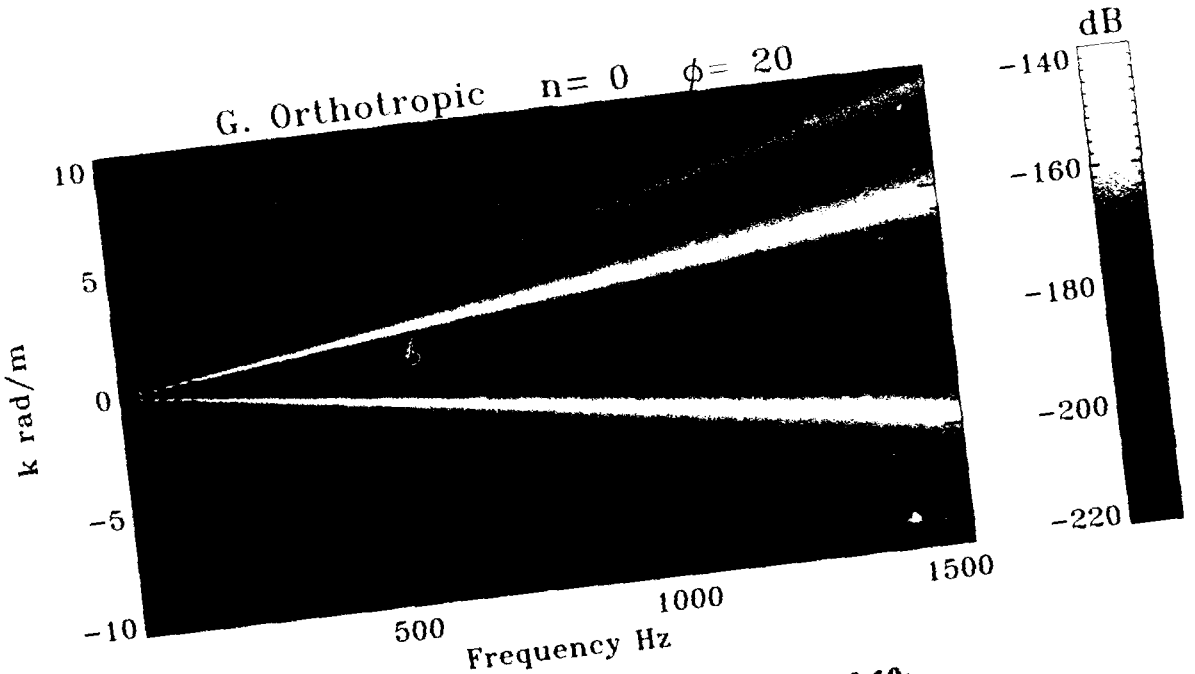

Figure 84. Transfer Surface with ζ_m = 0.10; dB = 10log($(\varepsilon_{11}(h/2)/P_o)^2$)

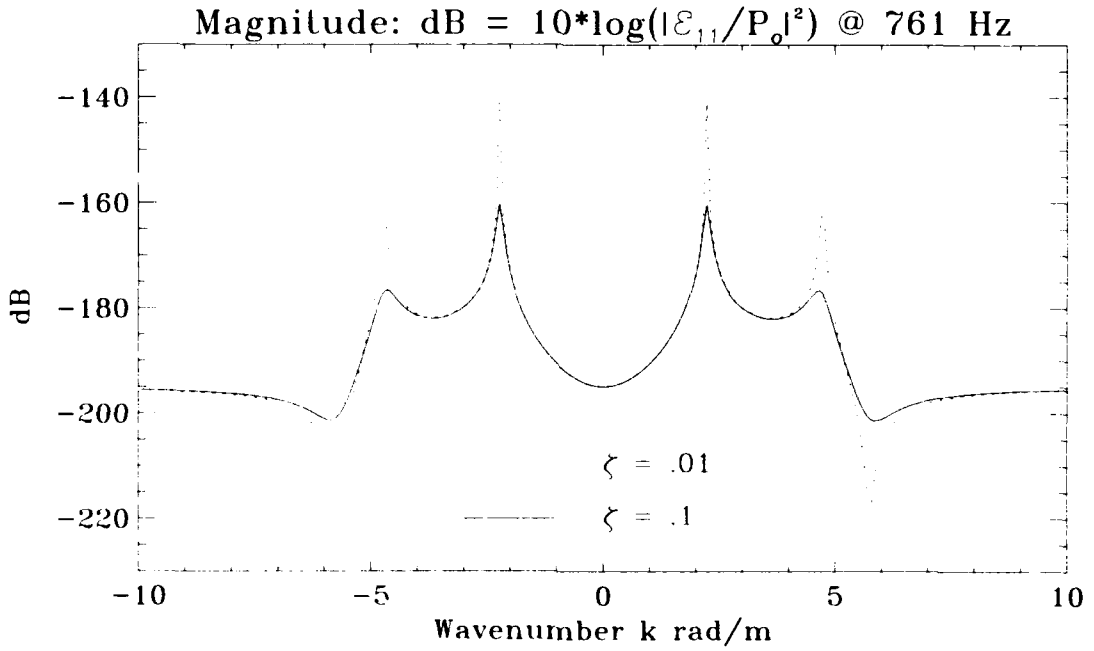

Figure 85. Comparison of a Cut Through Figures 83 and 84 at 761 Hz

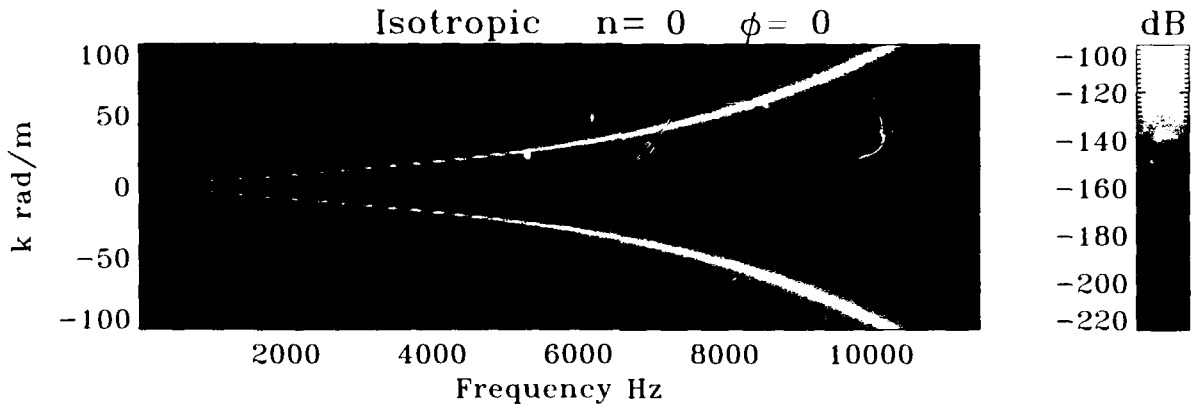

(a)

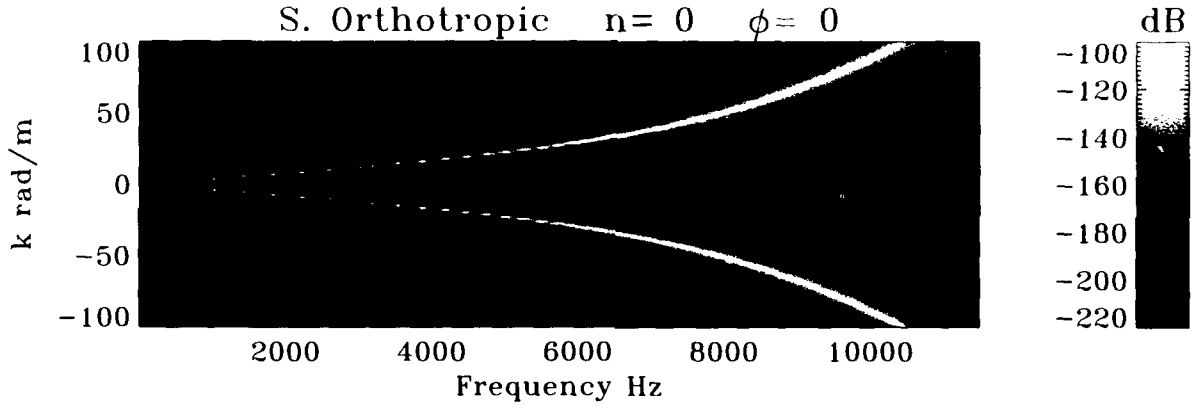

(b)

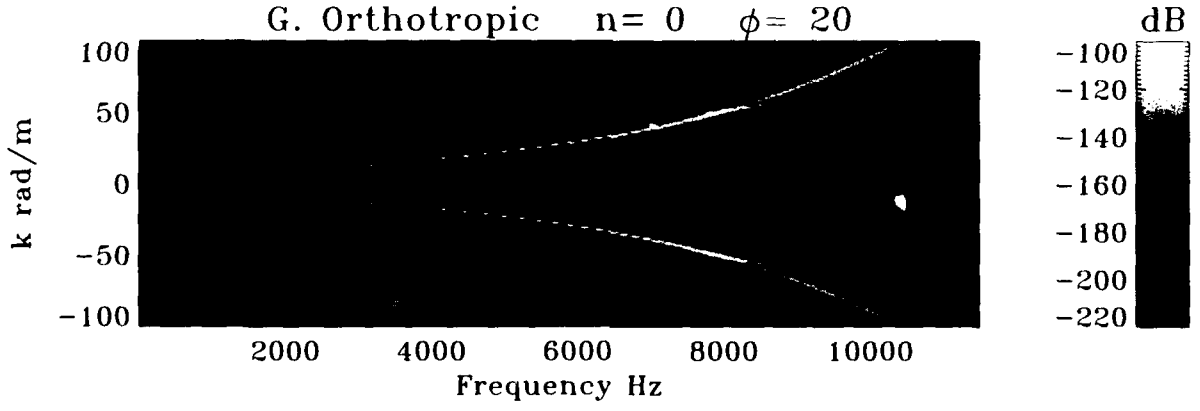

(c)

Figure 86. Transfer Surface (n = 0); dB = $10\log((\varepsilon_{11}(h/2)/P_0)^2)$

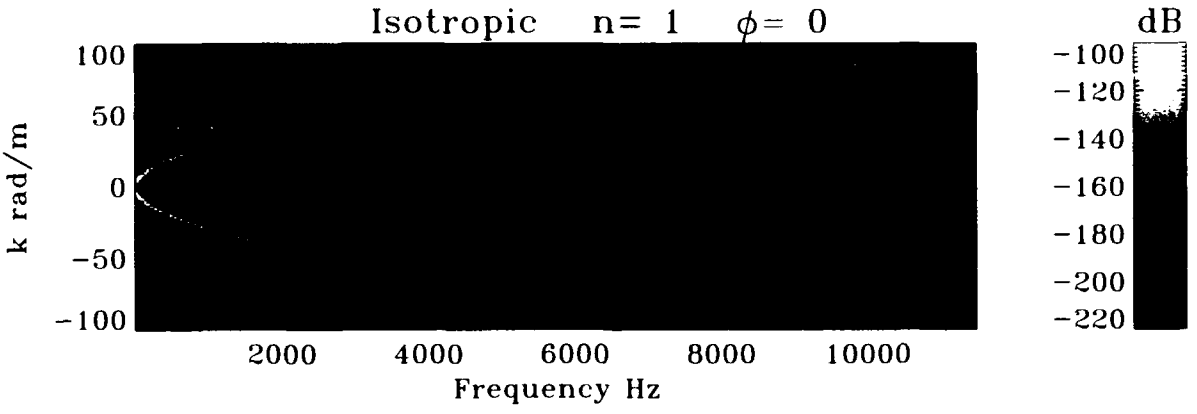

(a)

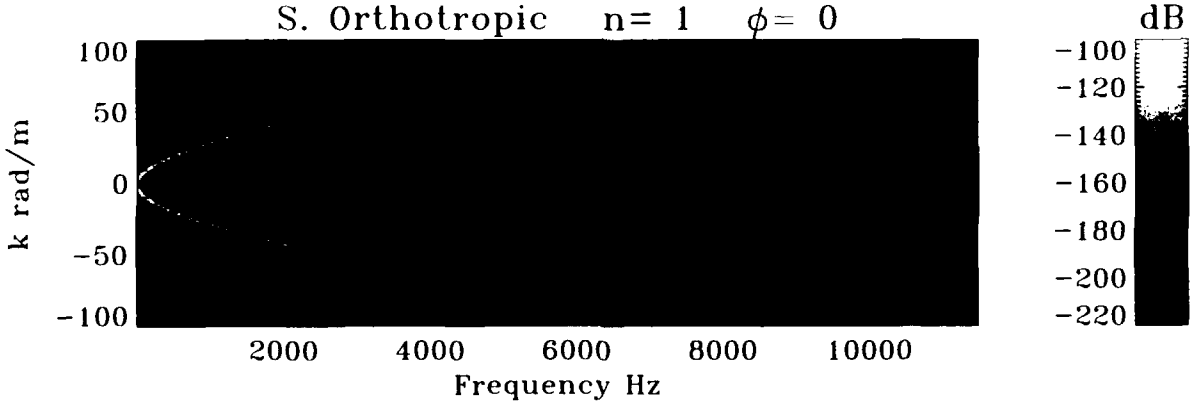

(b)

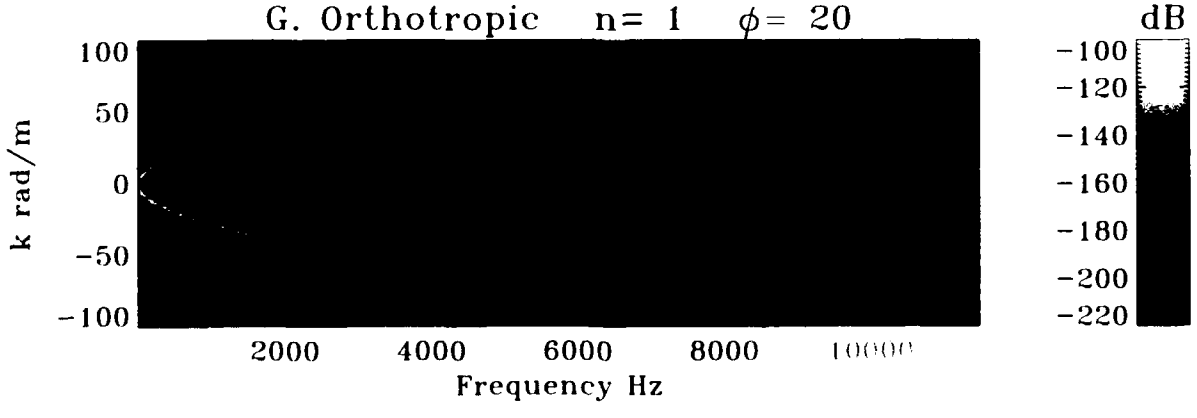

(c)

Figure 87. Transfer Surface (n = 1); dB = 10log(($\varepsilon_{11}(h/2)/P_o$)^2)

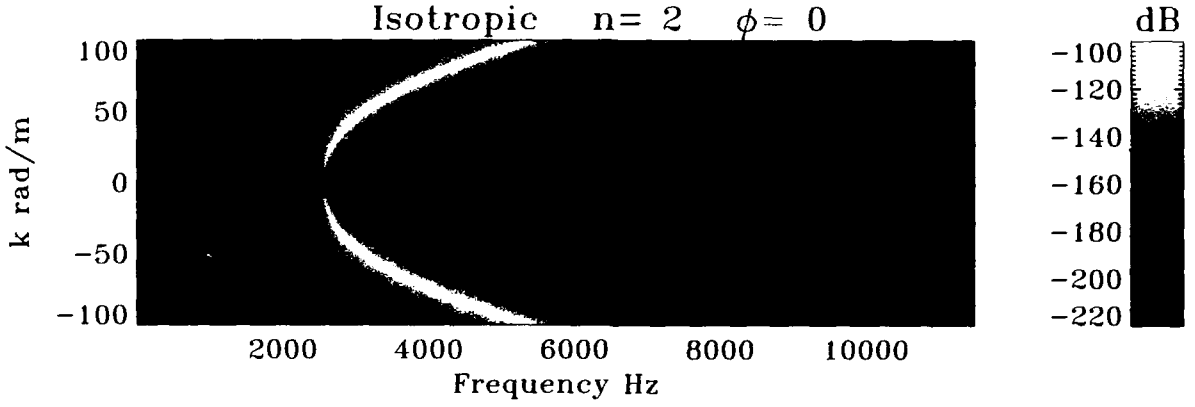

(a)

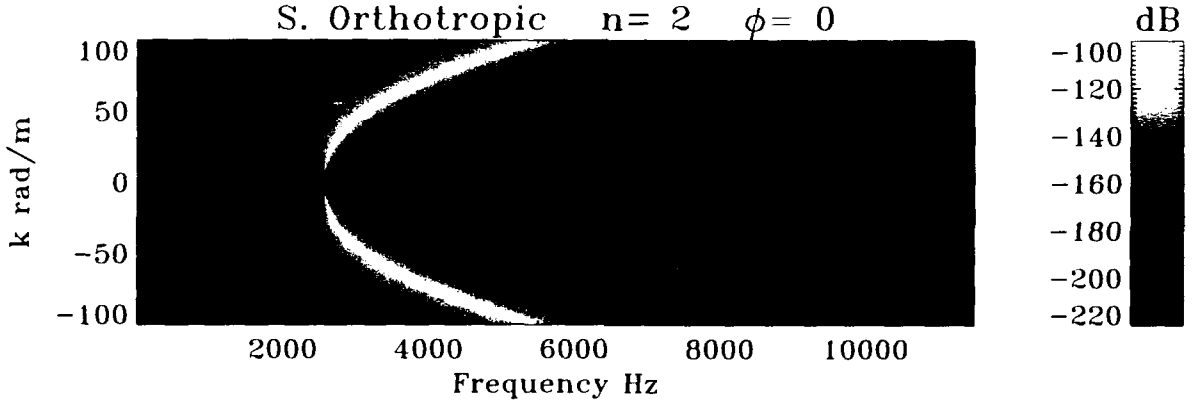

(b)

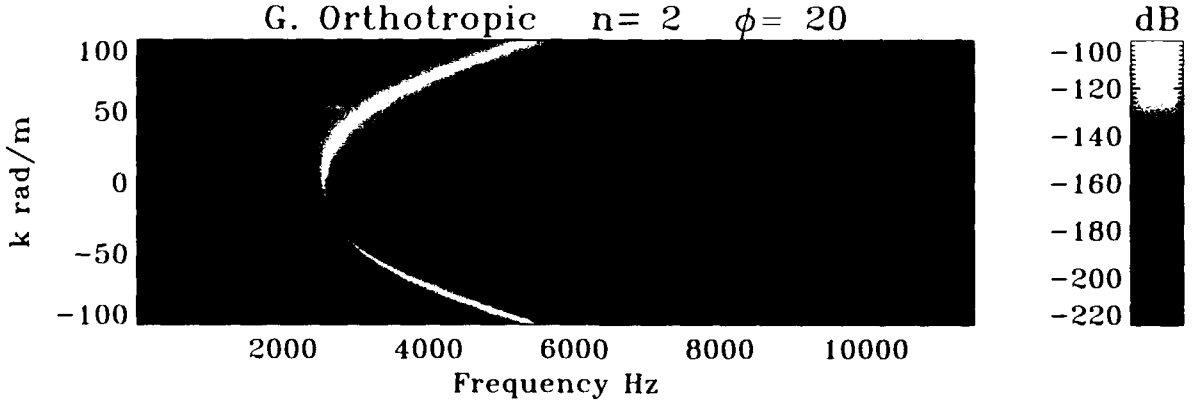

(c)

Figure 88. Transfer Surface (n = 2); dB = $10\log((\varepsilon_{11}(h/2)/P_0)^2)$

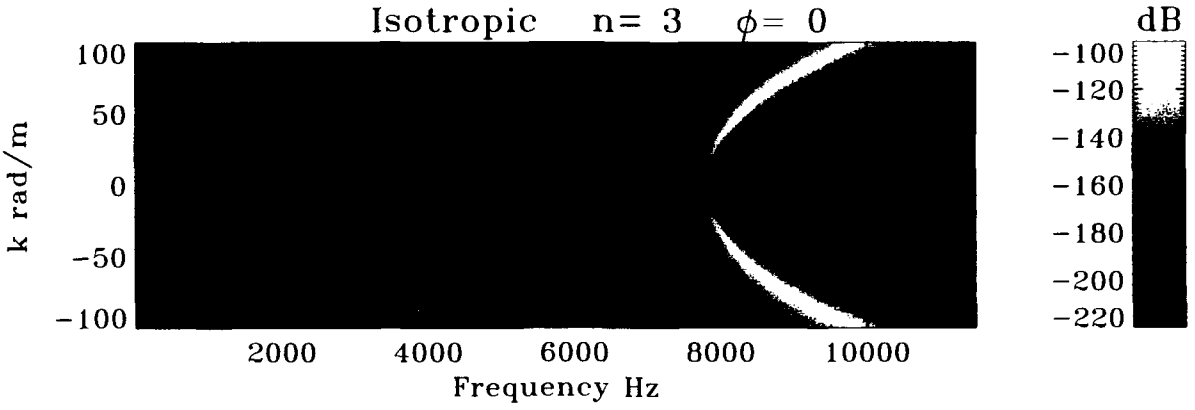

(a)

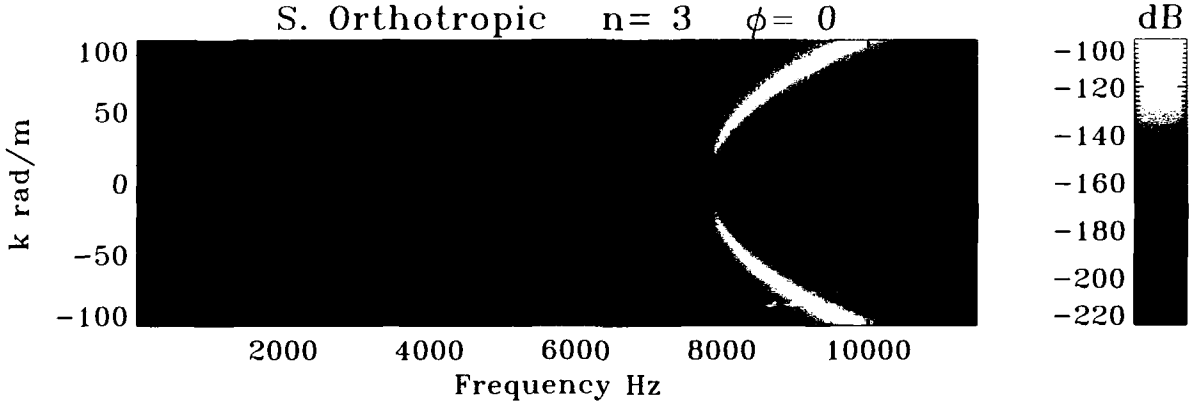

(b)

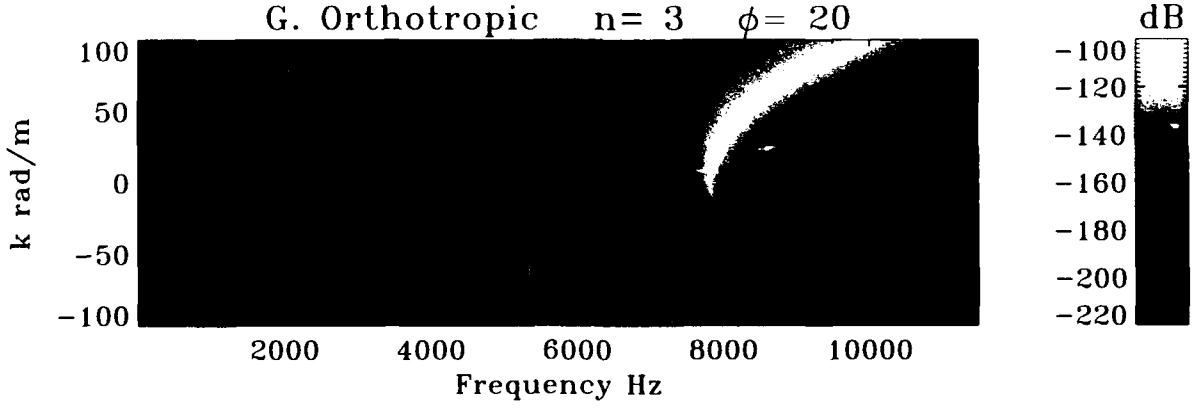

(c)

Figure 89. Transfer Surface (n = 3); dB = $10\log((\varepsilon_{11}(h/2)/P_o)^2)$

CONCLUSIONS

From first principals, we have formulated the equations of motion for a generally orthotropic cylindrical shell excited by a plane wave imparting either a normal, longitudinal, or circumferential stress to the surface of the shell. The shell itself can be prestressed in the axial direction by static tension. The shell is immersed in an outer fluid and contains an inner fluid; the two fluids need not be similar. The partial differential equations of motion are solved for the case of harmonic excitation in the x- and θ-directions. Harmonic solutions are considered for both a standing wave and a traveling wave in θ. Either is appropriate for the simpler cases of isotropic and specially orthotropic composite shell material. Only the traveling wave solution in θ is appropriate for the generally orthotropic shell. The resulting wave propagation is confined by the finite but continuous circumference of the shell to an integer number of wavelengths around the circumference, where the number of wavelengths is given by mode number n.

The shell exhibits coupling between the three displacements w, u, and v. For the isotropic and specially orthotropic shell, a radial excitation gives rise to coupled u displacement for the $n = 0$ mode of propagation, while for $n \geq 1$ both u and v coupled displacements occur. In the generally orthotropic shell, we find coupled u and v displacements for all modes ($n = 0$ included). The dynamic behavior of the isotropic and specially orthotropic shell is characterized by two branches for mode $n = 0$ and three branches for modes $n \geq 1$. In the generally orthotropic shell, there are three branches for any mode number.

Considering the magnitude of the shell response as a function of wavenumber and frequency for a fixed mode number, we see a number of branches exhibiting cutoff frequencies for modes $n \geq 1$. The cutoff frequency marks the onset of propagation for a given mode. At the cutoff frequency, the group velocity approaches zero and the phase velocity approaches infinity. Energy propagates at the group velocity; therefore, at cutoff, no energy propagates in that particular branch. Cutoff frequencies occur at zero wavenumber for the isotropic and specially orthotropic shell; for the generally orthotropic shell, there is an offset from zero wavenumber at the cutoff frequency. For a given component of a mode of propagation, the cutoff frequency increases with increasing mode number n. Bending stiffness also influences the cutoff frequency. The w component of modes 2 and 3 does not exhibit a cutoff frequency for the membrane case. The bending shell, however, does exhibit a cutoff frequency for this mode of propagation.

The transfer surfaces for the generally orthotropic shell are asymmetric with respect to the wavenumber axis. This shell presents a different stiffness to the excitation, depending on whether the excitation travels in the $+x$- or $-x$-direction. This difference in stiffness is responsible for the asymmetry that results in the wavenumber-frequency surface.

Imaginary wavenumbers used in the excitation and the solution for the shell response result in inhomogeneous vibrations. The amplitude decreases with increasing x, while it remains harmonic and homogeneous with respect to θ.

The vibration of the shell creates pressure fields in both fluids. For a given frequency, when the wavenumber of the vibration of the shell surface, k, is less than or equal to the propagation wavenumber in the medium, the pressure field propagates in the fluids. When the wavenumber

exceeds the propagation wavenumber in the medium, an evanescent pressure field results whose decay from the surface of the shell is functionally dependent on I_n in the inner fluid and K_n in the outer fluid. The effect of the outer fluid on the structure is to decrease the cutoff frequency, as was observed for the w component of the $n = 2$ mode. An internal core slows down the phase velocity for the w component of the $n = 0$ mode of propagation.

A normal pressure, P_O, excites a high level breathing wave and a weak extensional wave. The shear stress excitation, P_X, excites a high level extensional wave and a moderate level breathing wave. The extensional wave is the most nondispersive mode of propagation, as it engages the shell in a minimum amount of bending and very slight interaction with the fluids. For the w component of the $n = 0$ mode of propagation, as wrap angle increases, we observe a slowing of the extensional wave phase velocity and at first a decrease and then an increase in the phase velocity of the breathing wave, with the shift in speed occurring for a wrap angle of approximately 45 degrees. This characteristic corresponds to stiffness shifting from the longitudinal to circumferential directions.

When considering shell wall strain, the first step is to calculate the stress resultants from the displacement magnitudes. From the stress resultants, the stress distribution across the shell thickness is obtained based on the linear superposition of the normal and bending stress. The air-backed shell provides a good match for the simple linearized equation for the extensional wave speed (equation (75)). General observations concerning modes $n = 0$ through $n = 3$ reveal an increase in cutoff frequency with increasing mode number as well as decreasing phase and group velocity for a given component of a mode at a fixed wavenumber for a given category of shell stiffness (i.e., isotropic, specially orthotropic, or generally orthotropic). This means that energy propagates more slowly in the branches corresponding to a particular component of a mode as the mode number is increased for a fixed wavenumber.

At the time of this writing, the computation speed of workstations allows for the evaluation of the stresses and strains as a function of two independent variables. We have displayed the results of this study as grey-scale images or wire frame surfaces. Each image is composed of either 128 by 128 points (figure 47) or 256 by 256 points (figure 64). Currently, it is possible to exercise the solutions as a function of three independent variables, resulting in a volume rather than a surface representation. Such calculations are performed more expediently on supercomputers, although it is becoming possible to work with volume visualization on workstations.

REFERENCES

1. T. Young, "Hydraulic Investigations, Subservient to an Intended Croonian Lecture on the Motion of the Blood," *Philosophical Transactions of the Royal Society of London*, vol. 98, 1808, pp. 164-186.

2. R. Skalak, "Wave Propagation in Blood Flow, in Biomechanics," Proc. Symp. Appl. Mech. Div. of ASME, Y. C. Fung, Ed., New York, 1966, pp. 24.

3. H. Lamb, "On the Velocity of Sound in a Tube as Affected by the Elasticity of the Walls," *Manchester Literary and Philosophical Society*, Memoirs and Proceedings 42, 1898, pp. 1-16.

4. G. B. Warburton, "Vibration of a Cylindrical Shell in an Acoustic Medium," *Journal of Mechanical Engineering Science*, vol. 3, 1961, pp. 69-79.

5. D. G. Gazis, "Three Dimensional Investigation of the Propagation of Waves in Hollow Circular Cylinders," *Journal of the Acoustical Society of America*, vol. 31, no. 5, 1959, pp. 568-578.

6. J. E. Greenspon, "Vibration of Thick and Thin Cylindrical Shells Surrounded by Water," *Journal of the Acoustical Society of America*, vol. 33, no. 10, 1961, pp. 1321-1328.

7. W. Flugge, *Stresses in Shells*, Berlin, Springer - Verlag, 1960, p. 210.

8. W. Flugge, p. 9.

9. R. M. Jones, *Mechanics of Composite Materials*, Hemisphere Publishing Corporation, New York, 1975, p. 46.

10. W. Flugge, pp. 85-89, p. 130.

11. R. M. Jones, p. 51.

12. W. Flugge, p. 212

13. J. D. Achenbach, *Wave Propagation In Elastic Solids*, Elsevier Publishing Company, Inc., New York, 1990, p.78.

14. J. D. Achenbach, p. 78.

15. M. C. Junger and D. Feit, *Sound, Structures and Their Interaction*, Cambridge, Massachusetts, The MIT Press, 1986, p. 167.

16. M. Abramowitz and I. A. Stegun, *Handbook of Mathematical Functions*, Washington, D C, U.S. Government Printing Office, June 1964, p. 375, equation 9.6.4

17. M. R. Spiegel, *Advanced Mathematics for Engineers and Scientists*, McGraw-Hill Book Company, New York, 1971, p. 226.

18. W. Flugge, pp. 7-8.

19. R. M. Jones, p. 52.

APPENDIX A

STRESS RESULTANT INTEGRATION $N_{\theta\theta}$

The following integrals are necessary for the integration of $N_{\theta\theta}$:

$$\int \frac{x}{x+a} dx = x - a\log(x+a) \tag{A-1}$$

and

$$\int \frac{x^2}{ax+b} dx = \frac{x^2}{2a} - \frac{b}{a^2}x + \frac{b^2}{a^3}\log(ax+b) \tag{A-2}$$

Only the first two terms will be retained in the series expansion for the logarithm ratio, which results in

$$\log\left(\frac{1+\frac{h}{2a}}{1-\frac{h}{2a}}\right) \cong \frac{h}{a} + \frac{h^3}{12a^3} \tag{A-3}$$

The above simplification means we are neglecting terms of order $\frac{h^5}{a^5}$ and higher. Substituting equation (10) into (11) and then into the equation for $N_{\theta\theta}$ in equation (1), and using the following notation for the derivatives, yields

$$\frac{\partial}{\partial x}(\ ) = (\ )' \qquad \frac{\partial}{\partial \theta}(\ ) = (\ )^{\circ}, \tag{A-4}$$

resulting in

$$N_{\theta\theta} = \int_{-\frac{h}{2}}^{\frac{h}{2}} (\bar{Q}_{12}(u' - zw'') + \bar{Q}_{22}(\frac{1}{a}v^{\circ} - \frac{z}{a}\frac{w^{\circ\circ}}{(a+z)} + \frac{w}{a+z}) + \bar{Q}_{26}(\frac{u^{\circ}}{a+z} + \frac{a+z}{a}v' - w^{\circ\prime}(\frac{z}{a} + \frac{z}{a+z}))\, dz,$$

$$N_{\theta\theta} = \int_{-\frac{h}{2}}^{\frac{h}{2}} (\bar{Q}_{12}u' - \bar{Q}_{12}zw'' + \bar{Q}_{22}\frac{1}{a}v^{\circ} - \bar{Q}_{22}\frac{w^{\circ\circ}}{a}\frac{z}{a+z} + \bar{Q}_{22}\frac{w}{a+z} + \bar{Q}_{26}\frac{u^{\circ}}{a+z} + \bar{Q}_{26}v' + \bar{Q}_{26}\frac{v'z}{a} - \bar{Q}_{26}\frac{w^{\circ\prime}}{a}z - \bar{Q}_{26}w^{\circ\prime}\frac{z}{a+z})\, dz,$$

$$N_{\theta\theta} = [\bar{Q}_{12}u'z - \bar{Q}_{12}w''\frac{z^2}{2} + \bar{Q}_{22}v^{\circ}\frac{z}{a} - \bar{Q}_{22}w^{\circ\circ}\frac{z}{a} + \bar{Q}_{22}w^{\circ\circ}\log(a+z) + \bar{Q}_{22}w\log(a+z) + \bar{Q}_{26}u^{\circ}\log(a+z) + \bar{Q}_{26}v'z + \bar{Q}_{26}v'\frac{z^2}{2a} - \bar{Q}_{26}w^{\circ\prime}\frac{z^2}{2a} - \bar{Q}_{26}w^{\circ\prime}z + \bar{Q}_{26}w^{\circ\prime}a\log(a+z)\,]\Big|_{-\frac{h}{2}}^{\frac{h}{2}}. \qquad \text{(A-5)}$$

Evaluating at the limits $h/2$ and $-h/2$, the z^2 terms cancel out, which gives

$$(\bar{Q}_{12}u'\frac{h}{2}+\bar{Q}_{22}v^{\circ}\frac{h}{2a}-\bar{Q}_{22}w^{\circ\circ}\frac{h}{2a}+\bar{Q}_{22}w^{\circ\circ}\log(a+\frac{h}{2})$$

$$+\bar{Q}_{22}w\log(a+\frac{h}{2})+\bar{Q}_{26}u^{\circ}\log(a+\frac{h}{2})+\bar{Q}_{26}v'\frac{h}{2}$$

$$-\bar{Q}_{26}w^{\circ\prime}\frac{h}{2}+\bar{Q}_{26}w^{\circ\prime}a\log(a+\frac{h}{2}))+$$

$$(\bar{Q}_{12}u'\frac{h}{2}+\bar{Q}_{22}v^{\circ}\frac{h}{2a}-\bar{Q}_{22}w^{\circ\circ}\frac{h}{2a}-\bar{Q}_{22}w^{\circ\circ}\log(a-\frac{h}{2})$$

$$-\bar{Q}_{22}w\log(a-\frac{h}{2})-\bar{Q}_{26}u^{\circ}\log(a-\frac{h}{2})+\bar{Q}_{26}v'\frac{h}{2}$$

$$-\bar{Q}_{26}w^{\circ\prime}\frac{h}{2}-\bar{Q}_{26}w^{\circ\prime}a\log(a-\frac{h}{2}))\quad\cdot \tag{A-6}$$

Combining terms yields

$$N_{\theta\theta}=\left(\bar{Q}_{12}u'h+\bar{Q}_{22}v^{\circ}\frac{h}{a}-\bar{Q}_{22}w^{\circ\circ}\frac{h}{a}+\bar{Q}_{22}w^{\circ\circ}\log\left(\frac{a+\frac{h}{2}}{a-\frac{h}{2}}\right)+\bar{Q}_{22}w\log\left(\frac{a+\frac{h}{2}}{a-\frac{h}{2}}\right)\right.$$

$$\left.+\bar{Q}_{26}u^{\circ}\log\left(\frac{a+\frac{h}{2}}{a-\frac{h}{2}}\right)+\bar{Q}_{26}v'h-\bar{Q}_{26}w^{\circ\prime}h+\bar{Q}_{26}w^{\circ\prime}a\log\left(\frac{a+\frac{h}{2}}{a-\frac{h}{2}}\right)\right)\cdot \tag{A-7}$$

The log terms in equation (A-7) are simplified according to equation (A-3):

$$N_{\theta\theta} = \left(\bar{Q}_{12} u' h + \bar{Q}_{22} v^{\circ} \frac{h}{a} - \bar{Q}_{22} w^{\circ\circ} \frac{h}{a} + \bar{Q}_{22} w^{\circ\circ} \frac{h^3}{12a^3} \right.$$

$$+ \bar{Q}_{22} w \frac{h}{a} + \bar{Q}_{22} w \frac{h^3}{12a^3} + \bar{Q}_{26} u^{\circ} \frac{h}{a} + \bar{Q}_{26} u^{\circ} \frac{h^3}{12a^3} + \bar{Q}_{26} v' h$$

$$\left. - \bar{Q}_{26} w^{\circ\prime} h + \bar{Q}_{26} w^{\circ\prime} h + \bar{Q}_{26} w^{\circ\prime} a \frac{h^3}{12a^3} \right) . \qquad \text{(A-8)}$$

Collecting terms and simplifying equation (A-8), we arrive at the following expression for $N_{\theta\theta}$:

$$N_{\theta\theta} = \bar{Q}_{12} h u' + \bar{Q}_{22} \frac{h}{a} (v^{\circ} + w) + \bar{Q}_{26} \frac{h}{a} (u^{\circ} + a v') + \bar{Q}_{22} \frac{h^3}{12a^3} (w^{\circ\circ} + w)$$

$$+ \bar{Q}_{26} \frac{h^3}{12a^3} (u^{\circ} + a w^{\circ\prime}) \ . \qquad \text{(A-9)}$$

If the stiffnesses of equation (12) are applied along with a reversal of the shorthand notation in equation (A-4) to the above expression for $N_{\theta\theta}$, we will obtain the expression given in equation (13) for $N_{\theta\theta}$.

APPENDIX B

DETERMINATION OF THE COMPOSITE MATERIAL PROPERTIES E_1, E_2, ν_{12}, AND G_{12}

The determination of the composite material properties can be obtained by either experimental measurement or with an analytic model if both the properties of the matrix and the fiber are known. Presented here are two models for the composite properties: one based on the strength of materials approach (i.e., the rule of mixtures) and the other, on an elasticity approach.[1]

Rule of Mixtures

The most prominent assumption made for the mechanical behavior of the composite material is that strains in the fiber direction (the 1 direction) are the same in the fiber as in the matrix material. The volume fraction of fiber and matrix will be defined by the following equation:

$$V_f = \frac{A_f}{A}, \qquad V_m = \frac{A_m}{A} . \tag{B-1}$$

The composite modulus in the 1 direction can be expressed as

$$E_1 = E_f V_f + E_m V_m . \tag{B-2}$$

In the transverse direction, the same transverse stress is assumed to be applied to the fiber and the matrix, resulting in the following for E_2:

$$E_2 = \frac{E_f E_m}{V_m E_f + V_f E_m} . \tag{B-3}$$

The major Poisson ratio ν_{12} is given by

$$\nu_{12} = V_m \nu_m + V_f \nu_f . \tag{B-4}$$

The corresponding Poisson ratio, ν_{21}, is found from the condition of symmetry of the compliances to be

$$\nu_{21} = \nu_{12} \frac{E_2}{E_1} . \tag{B-5}$$

---

1. R. M. Jones, *Mechanics of Composite Materials*, Hemisphere Publishing Corporation, New York, 1975, pp. 90-114.

The assumption for the shear modulus, G_{12}, is that the shear stresses on the fiber and the matrix are the same, resulting in

$$G_{12} = \frac{G_m G_f}{V_m G_f + V_f G_m} \quad \text{(B-6)}$$

Elasticity

One very useful elasticity solution to the composite problem is presented by Tsai[2] for the case in which the composite is represented by a combination of fibers in contact with each other and by fibers interspersed uniformly in contact with the matrix. The two states are depicted in figure B-1. Most composites are a combination of both states and would be represented by a linear combination of the two solutions with the value of C ranging from 0 to 1.

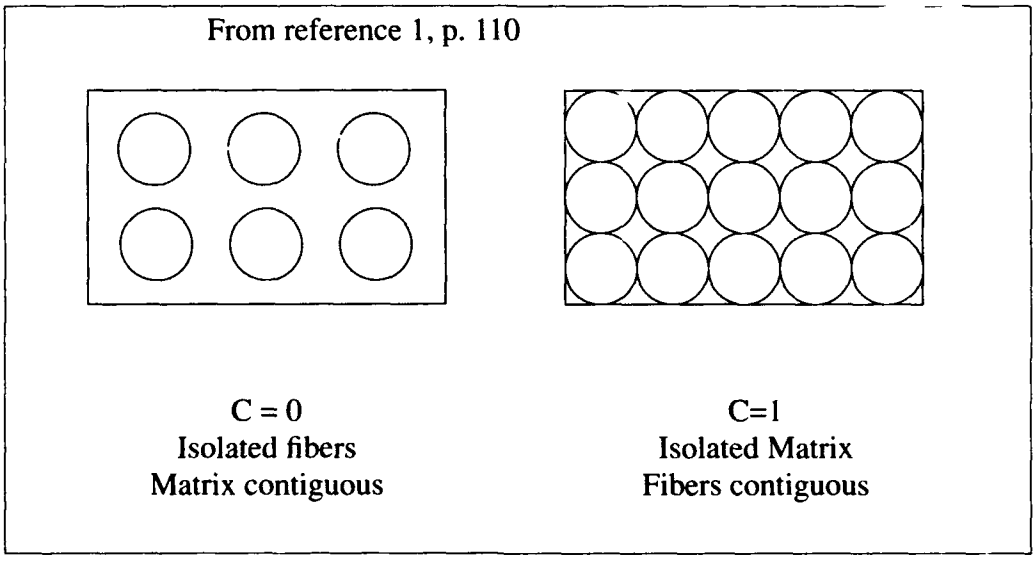

Figure B-1. Fiber Contiguity

2. S. W. Tsai, *Structural Behavior of Composite Materials*, National Aeronautics and Space Administration, CR-71, July 1964.

Tsai obtains the following elasticity solution to the problem when contiguity is considered:

$$E_2 = 2(1-\nu_f+(\nu_f-\nu_m)V_m)\left[(1-C)\frac{(K_f(2K_m+G_m)-G_m(K_f-K_m)V_m)}{(2K_m+G_m)+2(K_f-K_m)V_m}\right.$$

$$\left.+C\frac{(K_f(2K_m+G_f)+G_f(K_m-K_f)V_m)}{(2K_m+G_f)-2(K_m-K_f)V_m}\right] \qquad \text{(B-7)}$$

with

$$K_f = \frac{E_f}{2(1-\nu_f)}, \quad K_m = \frac{E_m}{2(1-\nu_m)}, \quad G_f = \frac{E_f}{2(1+\nu_f)}, \quad G_m = \frac{E_m}{2(1+\nu_m)}, \qquad \text{(B-8)}$$

$$\nu_{12} = (1-C)\frac{K_f\nu_f(2K_m+G_m)V_f+K_m\nu_m(2K_f+G_m)V_m}{K_f(2K_m+G_m)-G_m(K_f-K_m)V_m}$$

$$+C\frac{K_m\nu_m(2K_f+G_f)V_m+K_f\nu_f(2K_m+G_f)V_f}{K_f(2K_m+G_m)+G_f(K_m-K_f)V_m}, \qquad \text{(B-9)}$$

and

$$G_{12} = (1-C)G_m\frac{2G_f-(G_f-G_m)V_m}{2G_m+(G_f-G_m)V_m}+CG_f\frac{(G_f+G_m)-(G_f-G_m)V_m}{(G_f+G_m)+(G_f-G_m)V_m}. \qquad \text{(B-10)}$$

The modulus in the direction of the fibers is modified from the rule of mixtures to account for fiber misalignment. The misalignment factor, k_a, which varies from 0.9 to 1.0 and is dependent on the manufacturing process:

$$E_1 = k_a(V_fE_f+V_mE_m) \quad . \qquad \text{(B-11)}$$

APPENDIX C

EFFECTS OF AN ELASTIC SOLID CORE ON THE INNER PRESSURE FIELD, FOR THE AXISYMMETRIC CASE

Let us consider the interaction between the pressure field in the inner fluid and an elastic solid core. The core will be centered on the axis of the cylinder as depicted in figure C-1.

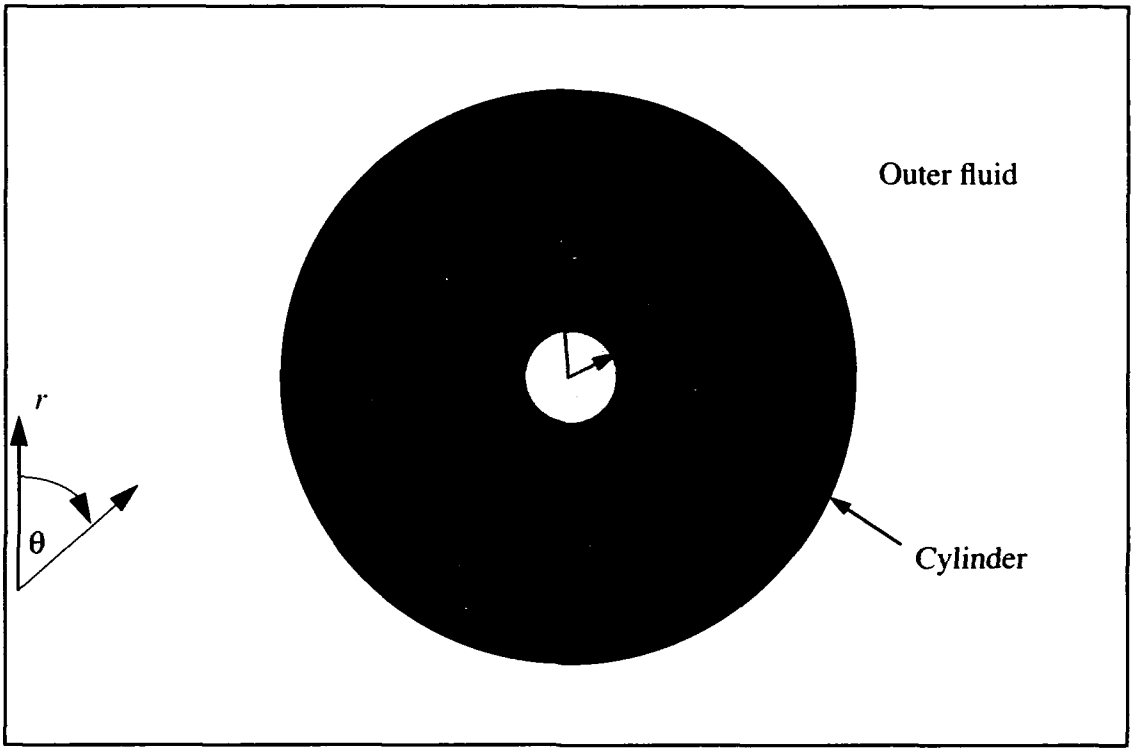

Figure C-1. Elastic Core Cross Section

The core radius is r_c with Young's modulus E_c and Poisson ratio ν_c. The core is modeled as a long thin cylinder using the plain strain approximation. The mass of the core will be neglected in this development and, as stated, the results will be limited to the axisymmetric case. The plane strain simplification is most appropriate here and will be used to describe the elastic behavior. Equation (C-1) shows the variation of the stresses with radius, and equation (C-2) defines the strain-stress and strain displacement relations:[1]

$$\sigma_r = 2C_2 + \frac{C_3}{r^2} \qquad \sigma_\theta = 2C_2 - \frac{C_3}{r^2} \tag{C-1}$$

and

1. C. Wang, *Applied Elasticity*, McGraw-Hill Book Company, New York, 1953, p. 55.

$$\varepsilon_r = \frac{1+\nu_c}{E_c}[(1-\nu_c)\sigma_r - \nu_c\sigma_\theta], \qquad \varepsilon_\theta = \frac{1+\nu_c}{E_c}[-\nu_c\sigma_r + (1-\nu_c)\sigma_\theta],$$

$$\varepsilon_r = \frac{du_c}{dr}, \qquad \varepsilon_\theta = \frac{u_c}{r} \quad . \tag{C-2}$$

For a solid cylinder, C_3 must be zero for the stresses to be finite at $r = 0$. Because C_3 is equal to zero, we find that $\sigma_r = \sigma_\theta = 2C_2 = C$. Together with equation (C-2), we have the following equation for the displacement in the r direction:

$$u_c = \frac{(1+\nu_c)(1-2\nu_c)rC}{E_c} \quad . \tag{C-3}$$

The velocity potential in the inner fluid will now contain both Bessel function terms. Referring back to equation (39), we have

$$\varphi_i = \{AJ_o(lr) + BY_o(lr)\}e^{i(kx-\omega t)},$$

$$l^2 = \frac{\omega^2}{c_i^2} - k^2 \qquad \text{for} \qquad k^2 < \frac{\omega^2}{c_i^2} \quad . \tag{C-4}$$

The velocity and pressure field for the fluid are given according to equations (36) and (37) and result in

$$\dot{w}_i = \{-lAJ_1(lr) - lBY_1(lr)\}e^{i(kx-\omega t)}, \quad p_i = i\omega\rho_i\{AJ_o(lr) + BY_o(lr)\}e^{i(kx-\omega t)} \quad . \tag{C-5}$$

The constant C is obtained by considering the boundary condition for radial stress at the surface of the core, $\sigma_r = -p$ at $r = r_c$. Because pressure is a compressive load applied to the core, its sign is negative, resulting in the following equation:

$$C = -i\omega\rho_i\{AJ_o(lr_c) + BY_o(lr_c)\}e^{i(kx-\omega t)}$$

$$\therefore \quad u_c = \left(-\frac{(1+\nu_c)(1-2\nu_c)r}{E_c}\right)i\omega\rho_i\{AJ_o(lr_c) + BY_o(lr_c)\}e^{i(kx-\omega t)}. \tag{C-6}$$

The velocity in the core is

$$\dot{u}_c = -\omega^2\rho_i r\frac{\nu_c}{\lambda_c}\{AJ_o(lr_c) + BY_o(lr_c)\}e^{i(kx-\omega t)}$$

$$\frac{\nu_c}{\lambda_c} = \frac{(1+\nu_c)(1-2\nu_c)}{E_c} \quad . \tag{C-7}$$

The condition of contact at the fluid-solid interface requires that the velocity of the core be equal to the velocity of the fluid at $r = r_c$. Equating equations (C-5) and (C-7) yields

$$A\{-\omega^2\rho_i r_c\frac{\nu_c}{\lambda_c}J_o(lr_c) + lJ_1(lr_c)\} + B\{-\omega^2\rho_i r_c\frac{\nu_c}{\lambda_c}Y_o(lr_c) + lY_1(lr_c)\} = 0 \quad . \tag{C-8}$$

Another equation containing the undetermined constants A and B results from equating the fluid and shell velocity at $r = a_i$. For this axisymmetric case, the displacement of the shell in the radial direction is given by equation (58); the magnitude of the shell velocity is then $\dot{w} = -i\omega W$, resulting in

$$-i\omega W = -AlJ_1(la_i) - BlY_1(la_i) \quad . \tag{C-9}$$

Configuring equations (C-8) and (C-9) into matrix form, we have

$$\begin{bmatrix} lJ_1(la_i) & lY_1(la_i) \\ \left[-\omega^2\rho_i r_c\frac{\nu_c}{\lambda_c}J_o(lr_c) + lJ_1(lr_c)\right] & \left[-\omega^2\rho_i r_c\frac{\nu_c}{\lambda_c}Y_o(lr_c) + lY_1(lr_c)\right] \end{bmatrix}\begin{bmatrix} A \\ B \end{bmatrix} = \begin{bmatrix} i\omega W \\ 0 \end{bmatrix} \quad . \tag{C-10}$$

Solving equation (C-10) for A and B and then substituting into equation (C-5) gives the following expression for the internal pressure field:

for the range $\dfrac{\omega^2}{c_i^2} > k^2$ with $l^2 = \dfrac{\omega^2}{c_i^2} - k^2$,

$$p_i(r) = \frac{\rho_i\omega^2\{\bar{C}Y_o(lr) - \bar{D}J_o(lr)\}We^{i(kx-\omega t)}}{l\{\bar{D}J_1(la_i) - \bar{C}Y_1(la_i)\}},$$

$$p_i(a_i) = \frac{\rho_i\omega^2\{\bar{C}Y_o(la_i) - \bar{D}J_o(la_i)\}We^{i(kx-\omega t)}}{l\{\bar{D}J_1(la_i) - \bar{C}Y_1(la_i)\}},$$

$$\alpha_i(r) = \frac{\rho_i\omega^2\{\bar{C}Y_o(lr) - \bar{D}J_o(lr)\}}{l\{\bar{D}J_1(la_i) - \bar{C}Y_1(la_i)\}}, \quad \alpha_i(a_i) = \frac{\rho_i\omega^2\{\bar{C}Y_o(la_i) - \bar{D}J_o(la_i)\}}{l\{\bar{D}J_1(la_i) - \bar{C}Y_1(la_i)\}},$$

$$\bar{C} = lJ_1(lr_c) - \frac{\omega^2\rho_i r_c\nu_c}{\lambda_c}J_o(lr_c), \qquad \bar{D} = lY_1(lr_c) - \frac{\omega^2\rho_i r_c\nu_c}{\lambda_c}Y_o(lr_c) \quad . \tag{C-11}$$

In a similar fashion, for the corresponding region of wavenumber

$$k^2 > \frac{\omega^2}{c_i^2} \qquad \text{with} \qquad m^2 = k^2 - \frac{\omega^2}{c_i^2},$$

$$p_i(r) = \frac{\rho_i \omega^2 \{\bar{H} I_o(mr) - \bar{G} K_o(mr)\} W e^{i(kx-\omega t)}}{m\{\bar{G} K_1(ma_i) + \bar{H} I_1(ma_i)\}},$$

$$p_i(a_i) = \frac{\rho_i \omega^2 \{\bar{H} I_o(ma_i) - \bar{G} K_o(ma_i)\} W e^{i(kx-\omega t)}}{m\{\bar{G} K_1(ma_i) + \bar{H} I_1(ma_i)\}},$$

$$\alpha_i(r) = \frac{\rho_i \omega^2 \{\bar{H} I_o(mr) - \bar{G} K_o(mr)\}}{m\{\bar{G} K_1(ma_i) + \bar{H} I_1(ma_i)\}}, \quad \alpha_i(a_i) = \frac{\rho_i \omega^2 \{\bar{H} I_o(ma_i) - \bar{G} K_o(ma_i)\}}{m\{\bar{G} K_1(ma_i) + \bar{H} I_1(ma_i)\}},$$

$$\bar{G} = m I_1(mr_c) + \frac{\nu_c}{\lambda_c} r_c \omega^2 \rho_i I_o(mr_c), \qquad \bar{H} = \frac{\nu_c}{\lambda_c} r_c \omega^2 \rho_i K_o(mr_c) - m K_1(mr_c) \cdot \tag{C-12}$$

The effect of the core is not easily understood from equation (C-12). Small argument approximations to the Bessel functions will be used to simplify the expression for α_i in order to observe the effect of the core on the breathing wave speed within certain limiting approximations. The small argument approximations are

$$I_o(x) \sim 1, \qquad K_o(x) \sim -ln(x) \sim 2,$$

$$I_1(x) \sim \frac{x}{2}, \qquad K_1(x) \sim \frac{1}{x} \cdot \tag{C-13}$$

Using equation (C-12), we arrive at the following simplification for $\alpha_i(a_i)$ for the case where $k \gg \frac{\omega}{c_i}$:

$$\alpha_i(a_i) = \frac{-\rho_i \omega^2 \{\frac{1}{r_c} + k^2 r_c\}}{k\{\frac{k(r_c^2 - a_i^2)}{2a_i r_c} + \frac{\nu_c}{\lambda_c} r_c \omega^2 \rho_i \left(\frac{1 + k^2 a_i^2}{k a_i}\right)\}} \cdot \tag{C-14}$$

Considering the case for a rigid core $\frac{\nu_c}{\lambda_c} = 0$, $\alpha_i(a_i)$, equation (C-14) reduces to

$$\alpha_i(a_i) = \frac{\rho_i \omega^2 a_i 2}{a_i^2 - r_c^2} \left(\frac{1}{k^2} + r_c^2\right) \cdot \tag{C-15}$$

Following the same development for the breathing wave speed that resulted in equation (70), we have the expression below for the case of a rigid core:

$$c_b = \sqrt{\frac{a_i^2 - r_c^2}{2\rho_i a^2 a_i}\left(C_{22} - \frac{C_{12}^2}{C_{11}}\right) - r_c\omega^2} \quad . \tag{C-16}$$

The specially orthotropic stiffness matrix in equation (4) simplifies equation (C-16) to the following expression, while making use of the symmetry property of equation (73):

$$c_b = \sqrt{\frac{hE_2}{2\rho_i a^2}\left(\frac{a_i^2 - r_c^2}{a_i}\right) - r_c\omega^2} \quad . \tag{C-17}$$

It is clearly seen that the presence of the core slows the breathing wave down relative to the result obtained in equation (74).

INITIAL DISTRIBUTION LIST

Addressee	No. of Copies
OFFICE OF NAVAL TECHNOLOGY [ONR 23 (CDR. G. Ramirez, T. Goldsberry)]	2
SBI [S. Berlin]	1
CAMBRIDGE ACOUSTICAL ASSOCIATES [J. Garrelick, J. Cole]	2
DTIC	12